Tuning cell fate with a toolbox of DoubleCatcher bispecific binder scaffolds



Claudia Louise Driscoll

Department of Biochemistry
St Hilda's College
University of Oxford

Trinity 2024

This thesis is submitted to the Department of Biochemistry, University of Oxford, in partial fulfilment of the requirements for the degree of Doctor of Philosophy.

Word count: 48,997

ABSTRACT

Molecular interactions underpin the regulatory networks of cells and biological systems. At the cell surface, differences in receptor-receptor interactions have profound consequences on cell behaviour and disease progression. Molecular bridges can be designed to replicate spatially sensitive biomolecular interactions, or to explore synergy arising from new interactions, and are emerging as promising tools in therapeutic discovery and synthetic biology. Bispecific binders, which bind simultaneously to two different targets, are an example of such a tool. Standard approaches for bispecific synthesis are limited by specialised binder formats or lack geometric tunability. Instead, I designed SpyMask: a platform for the modular, stepwise dimerisation of diverse ligands using SpyTag/SpyCatcher peptide-protein superglue. Mixing of SpyCatcher and SpyTag in solution results in spontaneous isopeptide bond formation between the pair. As such, SpyTag-bearing binders are covalently conjugated onto a tandem-SpyCatcher scaffold, here termed DoubleCatcher. To impart control into the platform, I engineered DoubleCatcher to possess one native, reactive Catcher and one whose reactivity is activated by a site-specific protease. I further designed a panel of DoubleCatcher scaffolds that are locked in distinct three-dimensional architectures, from which SpyTag-conjugated modules will project in different orientations. I assembled a matrix of anti-HER2 bispecific binders in parallel by coupling a panel of anti-HER2-binders to the DoubleCatcher toolbox in all possible permutations, using a simple and scalable protocol. Different modular combinations revealed anti-proliferative or pro-proliferative activity on HER2-addicted cancer cells. Crucially, activity depended on both the order of the binders within the assembly and the geometry of DoubleCatcher scaffolds. These findings emphasise the need for assembly and screening tools, such as SpyMask, for the combinatorial dimerisation of molecules in distinct geometries. Potential applications of SpyMask-discovered bispecifics range from interrogating cancer cell-surface receptor networks to fine-tuning chimeric antigen receptor-T cell responses.

DECLARATION OF AUTHORSHIP

I declare that the work described in this thesis is entirely my own, with any exceptions described below. This thesis has not been submitted for any other degree at the University of Oxford or any other institution.

Experiments performed by others:

Chapter 3:

- Intact protein mass spectrometry in Figure 3.5 was performed by Dr Anthony Tumber (Department of Chemistry, University of Oxford).

Chapter 4:

- Intact protein mass spectrometry in Figure 4.10A, B, D, E was performed by Dr Anthony Tumber (Department of Chemistry, University of Oxford).

Chapter 5:

- Intact protein mass spectrometry in Figure 5.3 was performed by Dr Anthony Tumber (Department of Chemistry, University of Oxford).
- Chemical compounds described in Figure 5.8 were synthesised by Dr Sona Krajcovicova and Thomas Warton (Department of Chemistry, University of Cambridge).
- Low resolution mass spectrometry performed in Figure 5.10A was performed by Dr Sona Krajcovicova (Department of Chemistry, University of Cambridge).
- Chemical re-bridging of Trastuzumab by TetraDVP-SpyTag003 and analysis by SDS-PAGE was performed by Thomas Wharton (Department of Chemistry, University of Cambridge).

Publications arising from this thesis are detailed below:

- Driscoll, C.L., Keeble, A.H., and Howarth, M.R. (2024). SpyMask enables combinatorial assembly of bispecific binders. Nat. Commun. *15*, 2403.
- Krajcovicova, S., Wharton, T., Driscoll, C.L., King, T.A., Howarth, R., Spring, D.R., Howarth, M.R., and Spring, D.R. (2024). All-At-Once Linkers for Single-Payload Bioconjugation to Native Antibodies. Manuscript Submitted
- Driscoll, C.L., Keeble, A.H., and Howarth, M. (2023). A bivalent polypeptide scaffold and uses thereof. United Kingdom Patent Application No. 2313175.8

ACKNOWLEDGEMENTS

I would like to express my sincere gratitude to my supervisor Prof Mark Howarth, for his endless creativity, guidance, and honest mentorship throughout this research. I deeply admire the research culture you have curated in your lab, which awards students with the independence to tackle diverse experimental endeavours, while encouraging discussion and providing direction whenever it is required. Thank you for granting me the opportunity to expand the SpyCatcher/SpyTag toolbox; it is a true honour to have contributed to such an impactful field of study. Plus, it makes for a great conversation starter at conferences.

A great thank you also to the Oxford Interdisciplinary Bioscience BBSRC DTP for providing me with many intellectual challenges and a brilliantly multi-talented cohort in my pandemic-clouded first term at Oxford. Not only did I gain skills and friendships during this time that shaped the following years of my DPhil, but I also met my best friend and life partner, Scott.

I wish to extend my thanks to my endlessly positive collaborators Dr Sona Krajcovicova and Thomas Wharton in the Department of Chemistry, University of Cambridge, without whom the chemical functionalisation of SpyMask would not have been possible.

I owe a genuine thanks to all my lab peers, past and present. The opportunity to work alongside some of the most driven, knowledgeable, innovative, and collaborative scientists has certainly been an experience I will treasure. I am particularly grateful for my colleagues who were in the lab when it relocated from Oxford to Cambridge; your companionship, support, advice, and impeccable satire made for a smooth transition. I wish you all the best of luck for the future and I hope our paths cross again in the future.

Finally, I am eternally thankful for my loving parents and sister, Honora, who remain my academic role models and moral exemplars. You provide me with a daily reminder of the impact that meaningful, persistent science has on our world. Of course, as such ambitious individuals, I can also always trust that you will put my challenges into perspective…

ABBREVIATIONS

ADCC	Antibody-dependent cellular cytotoxicity
ADCP	Antibody-dependent cell-mediated phagocytosis
Akt	A serine/threonine protein kinase (protein kinase B)
BCR	B-cell receptor
BiTE	Bispecific T-cell engagers
BLAST	Basic local alignment search tool
BRET	Bioluminescence resonance energy transfer
BSA	Bovine serum albumin
CAR	Chimeric antigen receptor
CDC	Complement-dependent cytotoxicity
CXCR7	C-X-C chemokine receptor type 7
CnaB2	Collagen adhesin domain
DARPin	Designed ankyrin repeat proteins
DART	Dual affinity retargeting
DBCO	Dibenzylcyclooctyne
DC	DoubleCatcher
DLS	Dynamic light scattering
DMEM	Dulbecco's modified Eagle's medium
DMSO	Dimethylsulfoxide
DTT	Dithiothreitol
DVD-Ig	Dual variable domain antibody
DVP	Divinylpyrimidine
ECD	Extracellular domain
EDTA	Ethylenediaminetetraacetic acid
EGFR	Epidermal growth factor receptor
ELISA	Enzyme linked immunosorbent assay
EpCAM	Epithelial cell adhesion molecule
EphA2	Ephrin type-A receptor 2
EpoR	Erythropoietin receptor
Fab	Fragment antigen binding region
FbaB	Fibronectin-binding protein
Fc	Fragment crystallisable
FcRn	Neonatal Fc receptor

FcγR	Fc gamma receptor
FGFR1	Fibroblast growth factor receptor 1
FLT3	FMS-like tyrosine kinase 3
FRET	Fluorescence resonance energy transfer
GAB1	GRB2-associated binding protein 1
GPCR	G protein-coupled receptors
GRB2	Growth factor receptor-bound 2
GRK	G protein–coupled receptor-kinases
HEPES	N-2-hydroxyethylpiperazine-N-2-ethane sulfonic acid
HER	Human epidermal growth factor receptor
HRP	Horseradish peroxidase
HSPC	Haematopoietic stem and progenitor cells
HuSA	Human serum albumin
IGF-2R	Insulin-like growth factor 2 receptor
IL-2R	Interleukin-2 receptor
IPTG	Isopropyl β-D-1-thiogalactopyranoside
JMD	Juxtamembrane domain
KD	Kinase domain
KiH	Knobs-into-holes
LC-MS	Liquid chromatography-mass spectrometry
LRP6	Low-density lipoprotein receptor-related protein 6
mAb	Monoclonal antibody
MAPK	Mitogen-activated-protein-kinase
MW	Molecular weight
MWCO	Molecular weight cutoff
NF-κB	Nuclear factor kappa B
NK	Natural killer
NTA	Nitrilotriacetic acid
PBS	Phosphate-buffered saline
PCR	Polymerase chain reaction
PD-L1	Programmed death-ligand 1
PDB	Protein Data Bank
PDGFRβ	Platelet-derived growth factor receptor β
PEG	Polyethylene glycol

Pert	Pertuzumab Fab
PI3K	Phosphoinositide 3-kinase
PIP_3	Phosphatidylinositol 3,4,5-trisphosphate
PLCγ	Phospholipase Cγ
PMSF	Phenylmethylsulfonylfluoride
PSMA	Prostate-specific membrane antigen
PTB	Phosphotyrosine binding
PTM	Post-translational modification
Ras	Rat sarcoma
RIPR	Receptor inhibition by phosphatase recruitment
RTK	Receptor tyrosine kinases
SC3	SpyCatcher003
scFv	Single chain variable fragment
SDS-PAGE	Sodium dodecyl sulfate-polyacrylamide gel electrophoresis
SEC	Size-exclusion chromatography
sfGFP	Superfolder green fluorescent protein
SH2	Src homology region 2
SOS	Sons of sevenless
SPAAC	Strain-promoted alkyne-azide cycloaddition
ST3	SpyTag003
STAT5	Signal transducer and activator of transcription 5
SUMO	Small ubiquitin modifier
TAA	Tumour-associated antigens
TCEP	Tris(2-carboxyethyl)phosphine
TCR	T-cell receptor
TEV	Tobacco Etch Virus
TMD	Transmembrane domain
TNF	Tumor necrosis factor
TNFR1	Tumor necrosis factor receptor 1
Tras	Trastuzumab Fab
Trk	Tropomyosin-related receptor kinase
VEGFR2	Vascular endothelial growth factor receptor 2

TABLE OF CONTENTS

ABSTRACT **1**

DECLARATION OF AUTHORSHIP **2**

ACKNOWLEDGEMENTS **3**

ABBREVIATIONS **4**

LIST OF FIGURES AND TABLES **10**

CHAPTER 1 – INTRODUCTION **12**

1.1 Bispecific antibodies 12
1.1.1 Bispecific antibody mechanisms of action 13
1.1.1.1 Effector retargeting (trans-acting) 13
1.1.1.2 Bridging at the cell surface (*cis*-acting) 15
1.1.1.3 Enhancing specificity 16
1.1.1.4 Transport across barriers 17
1.1.1.5 Induced proximity 18
1.1.2 Bispecific antibody format 19
1.1.3 Effect of bispecific antibody format on activity 22
1.1.4 Approaches for bispecific antibody synthesis for screening with increased throughput 25
1.2 The Human Epithelial Receptor 2 (HER2) receptor tyrosine kinase 32
1.2.1 HER2 signalling in breast cancer 33
1.2.2 Mechanism of HER2 signalling activation 36
1.2.3 Biased activation of HER-family receptors 38
1.3 Biased networking of biomolecules at the cell surface 40
1.3.1 Existing tools for controlling biomolecular interactions at the cell surface 44
1.3.1.1 DNA nanostructures 44
1.3.1.2 Bispecific antibodies 45
1.3.1.3 Designed proteins 47
1.3.1.4 Peptide dimers 48
1.4 Thesis objectives 49

CHAPTER 2 – METHODS **52**

2.1 Molecular Cloning 52
2.1.1 Gene and oligonucleotide synthesis 56
2.1.2 Polymerase Chain Reaction (PCR) 56
2.1.3 Agarose gel electrophoresis and gel extraction 57
2.1.4 Gibson assembly 57
2.1.5 E. coli transformation by heat shock 58
2.1.6 Plasmid purification 58
2.1.7 Plasmid sequencing 59
2.2 Protein expression and purification 59
2.2.1 Media and growth conditions 59
2.2.2 Protein expression 60
2.2.2.1 Bacterial expression 60
2.2.2.2 Mammalian expression 61
2.2.3 Ni-NTA purification of soluble proteins bearing a His6-tag 62
2.2.4 SpySwitch purification of soluble proteins bearing a SpyTag 63

2.2.5 Endotoxin depletion by phase separation 63
2.2.6 Size-exclusion chromatography....64
2.2.7 Quantification of protein concentration....64
2.3 Protein Characterisation....65
2.3.1 Polyacrylamide gel electrophoresis (PAGE)....65
2.3.2 Intact protein Mass Spectrometry....65
2.3.2.1 RapidFire....65
2.3.2.2 Liquid Chromatography-Quadrupole Time of Flight....66
2.3.3 Dynamic Light Scattering....67
2.3.4 Mass Photometry....68
2.3.5 Protein structural prediction and visualisation....69
2.4 Synthesis of immobilised covalent SpyCatcher003 for purification....70
2.5 Mammalian cell culture....70
2.6 Isopeptide bond reconstitution reactions....71
2.7 Assembly of dimeric molecules using DoubleCatcher....71
2.8 Design of DoubleCatcher disulfide-containing variants....72
2.9 Metabolic activity assay....73
2.10 ELISA on anti-HER2 molecule binding....74
2.10.1 Validation of binding of anti-HER2 binder panel to the HER2 ECD....74
2.10.2 Validation of nanoHER2 binding epitope on HER2 ECD....75
2.10.3 Validation of ABD035-DoubleCatcher binding to human serum albumin....75
2.11 Flow cytometry....76
2.12 Click conjugation of azide-modified oligonucleotides to DBCO-SpyTag003....77

CHAPTER 3 – DEVELOPMENT OF A BISPECIFIC ANTIBODY ASSEMBLY PLATFORM....79

3.1 Imparting protease activatability into SpyCatcher003 to generate Masked SpyCatcher003....82
3.1.1 Characterising reactivity of Masked SpyCatcher003 with SpyTag003 in the presence and absence of protease....83
3.2 Generation of DoubleCatcher from Masked SpyCatcher003....85
3.2.1 Characterising site-specific reactivity of DoubleCatcher with SpyTag003....86
3.2.2 DoubleCatcher-SpyTag003DX variants....87
3.2.3 DoubleCatcher linker variants....90
3.3 Development of SpyMask: a generalisable, one-pot protocol for dimerisation by DoubleCatcher....95
3.3.1 Optimization of Step 1: Saturation of N-terminal SpyCatcher003 of DoubleCatcher....96
3.3.2 Optimisation of Step 2: Unmasking and saturation of C-terminal SpyCatcher003 of DoubleCatcher....98
3.3.3 Optimization of Step 3: Purification of excess SpyTag-fused binder in reaction by immobilised SpyCatcher003....101
3.3.4 Monitoring reaction by mass photometry....105
3.3.5 Demonstrating generalisability of SpyMask protocol....108
3.4 Discussion....110

CHAPTER 4 – CONTROLLING HER2 DIMERISATION USING DOUBLECATCHER-ASSEMBLED ANTI-HER2 BISPECIFIC BINDERS....114

4.1 Identification and validation of panel of anti-HER2 binders targeting diverse epitopes on the HER2 extracellular domain....116

4.1.1 Epitope analysis of panel of anti-HER2 binders....117
4.1.2 Validation of reactivity of Fab with truncated linker to SpyTag....120
4.1.3 Validating mass of anti-HER2 binders by mass spectrometry....120
4.1.4 Validating binding activity of anti-HER2 binders on recombinant soluble HER2 extracellular domain by ELISA....124
4.1.5 Validating binding activity of anti-HER2 binders on HER2-overexpressing cells by flow cytometry....124
4.1.6 Elucidation of HER2 epitopes recognised by nanoHER2 by HER2:nanoHER2 complex prediction using AlphaFold2-multimer and competition ELISA....127
4.2 Assembly of matrix of anti-HER2 biparatopic binders using DoubleCatcher....130
4.2.1 Validation of bispecific assembly by SDS-PAGE and mass spectrometry....130
4.2.2 Effect on BT474 and SKBR3 cell proliferation using Resazurin assay....131
4.3 Bridging HER2 with other cell-surface receptors using SpyMask-assembled bispecifics....135
4.3.1 Validation of binders targeting alternative cell-surface receptors by mass spectrometry....137
4.3.2 Effect on SKBR3 cell proliferation using Resazurin assay....138
4.4 Discussion....142

CHAPTER 5 – DIVERSIFICATION OF THE SPYMASK PLATFORM....146

5.1 Designing DoubleCatcher structural variants....148
5.1.1 Tuning DoubleCatcher structure by varying linker....149
5.1.2 Tuning DoubleCatcher structure by introducing intramolecular disulfide bonds.150
5.1.3 Biophysical characterisation of DoubleCatcher structural variants....152
5.1.3.1 Monitoring intermolecular dimer formation by size-exclusion chromatography....152
5.1.3.2 Monitoring rigidity using dynamic light scattering....155
5.1.4 Validating reactivity of stable DoubleCatcher structural variants....155
5.1.5 Measuring the effect of DoubleCatcher architecture on activity of anti-HER2 bispecific antibodies....158
5.2 Extending the serum half-life of DoubleCatcher....162
5.3 Chemical functionalisation of SpyTag for diversifying SpyMask ligands....163
5.4 Generation of SpyTag003-fused small molecule ligands....168
5.4.1 Stability of the DBCO-SpyTag003 reagent....170
5.5 Chemical coupling of IgG1 to TetraDVP-SpyTag003 using selective disulfide re-bridging....172
5.5.1 Validation of assembly by MS and SDS-PAGE....172
5.5.2 Confirmation of IgG-SpyTag003-SpyCatcher003 reactivity and specificity....173
5.6 Discussion....177

CHAPTER 6 – SUMMARY AND GENERAL DISCUSSION....180

6.1 Resource requirements of SpyMask bispecific assembly....180
6.2 Rigidity of SpyTag-linked binders....183
6.3 Rigidity of the DoubleCatcher scaffold....187
6.4 Quantifying the architecture of different DoubleCatchers....188
6.5 Discerning relationships between the structure and activity of bispecific-induced dimers....190
6.6 Immunogenicity of the DoubleCatcher scaffold....194
6.7 Concluding summary....198

BIBLIOGRAPHY....200

LIST OF FIGURES AND TABLES

Figure 1.1 Common mechanisms of action of bispecific antibodies. 14
Figure 1.2. The anatomy of a bispecific antibody. 21
Figure 1.3. Mechanism of ligand-induced HER-family receptor activation. 35
Figure 1.4. Existing tools for controlling molecular geometry. 46
Figure 3.1. Masked SpyCatcher003 has protease-activatable reactivity. 84
Figure 3.2. Site-specific conjugation of Tagged proteins to DoubleCatcher is fast and site-specific. 88
Figure 3.3. Non-covalent SpyTag003 variants were assessed for SpyCatcher003 masking and unmasking activity. 91
Figure 3.4. The linker tethering SpyTag003DA mask to DoubleCatcher was varied and assessed for enhanced masking activity. 94
Figure 3.5. SpyMask enables one-pot dimerisation of two Tagged model proteins using DoubleCatcher, yet requires optimisation to minimise unwanted homodimer formation. 97
Figure 3.6. In Step 1 of SpyMask assembly protocol, Tagged binder must be in excess over DoubleCatcher to ensure saturation of its N-terminal SpyCatcher003. 99
Figure 3.7. Increased incubation time of Step 2 in SpyMask assembly eliminates formation of homodimeric byproducts. 100
Figure 3.8. Purification of excess SpyTag-linked proteins is most efficient after incubation with reactive SpyCatcher003-immobilised agarose beads. 104
Figure 3.9. Optimised and controlled stepwise conjugation of model proteins onto DoubleCatcher was monitored by mass photometry. 106
Figure 3.10. SpyMask protocol for one-pot combinatorial assembly of heterodimers is efficient with diverse pairs of Tagged proteins. 109
Figure 4.1. Panel of anti-HER2 binders spans epitopes across all four subdomains of the HER2 extracellular domain. 118
Figure 4.2. The reactivity of Tras Fab with DoubleCatcher is unaffected when the linker between the Fab and SpyTag003 is removed. 119
Figure 4.3. Mass spectrometry of HER2 binding proteins. 121
Figure 4.4. Without an upper-hinge region, the Pert-SpyTag003 Fab is post-translationally cysteinylated. 122
Figure 4.5. Validation of binder panel interaction with purified HER2 by ELISA. 123
Figure 4.6. Validation of binder panel interaction with HER2 on cells by flow cytometry. 126
Figure 4.7. Elucidation of nanoHER2 binding epitope on HER2 by complex prediction and competitive ELISA. 129
Figure 4.8. Purity of heterodimerisation by DoubleCatcher was validated by mass spectrometry. 131
Figure 4.9. SpyMask-assembled anti-HER2 bispecific binders exhibit a range of pro- or anti-proliferative activities in HER2-positive cancer cells. 133
Figure 4.10. Mass spectrometry of binders targeting alternative receptors for bridging to HER2. 139
Figure 4.11. Orientation of binders in SpyMask-assembled bispecific binders influences activity and potency. 141

Figure 5.1. DoubleCatcher architecture can be modified. 151
Figure 5.2. Analysis of the homogeneity of DoubleCatcher variants post-purification. 154
Figure 5.3. Complete oxidation of the five selected DoubleCatcher variants is confirmed by mass spectrometry. 156
Figure 5.4. Heterodimerisation of nanoHER2 and affiHER2 with the panel of DoubleCatcher variants is validated by mass spectrometry. 157
Figure 5.5. DoubleCatcher-heterodimerised anti-HER2 bispecific molecules harness a range of pro-proliferative and antiproliferative activities in HER2-positive cancer cells. 161
Figure 5.6. DoubleCatcher fused to the human serum albumin-binding protein ABD035 reacts efficiently with SpyTag-linked ligands to form bispecifics. 164
Figure 5.7. Diversification of the SpyMask-compatible ligand library. 166
Figure 5.8. Chemical structures of functionalised SpyTag003 molecules. 167
Figure 5.9. DBCO-SpyTag003 reacts with Azide-DNA to form SpyTagged DNA, which can be conjugated onto DoubleCatcher. 169
Figure 5.10. Degradation of DBCO-SpyTag003 after storage in DMSO. 171
Figure 5.11. The off-the-shelf IgG1 antibody Trastuzumab is selectively re-bridged with TetraDVP-SpyTag003. 175
Figure 5.12. Evaluation of SpyCatcher-reactivity and HER2-binding activity of Trastuzumab-tDVP-SpyTag003. 176
Figure 6.1. Bispecific antibody assembly by SpyMask with two-step purification. 182
Figure 6.2. Minimising flexibility in the hinge connecting the anti-HER2 Fab Tras to SpyTag003. 186

Table 1.1. Medium- to high-throughput methods for combinatorial bispecific antibody production. 27
Table 2.1. Plasmids used in this Thesis. 52

CHAPTER 1 – INTRODUCTION

1.1 Bispecific antibodies

Bispecific antibodies possess two different antigen-binding sites, enabling the simultaneous binding of two distinct epitopes by a single molecule. This property can be exploited to either bridge two cell types, or to engage two molecules on the same cell. Superior to single target binding, bispecific binding can lead to synergistic activity, decrease the chance of resistance emerging, or enable fine-tuning of signalling from multiple pathways (Chames et al., 2009; Morgillo and Lee, 2005). Single epitope-binding monoclonal antibodies (mAbs) have been at the forefront of targeted disease therapies for the last 35 years (Jin et al., 2022). The clinical success of mAbs is owed to the natural diversity of their antigen-binding sites that enable the antibodies to bind virtually any target with high affinity and specificity (Cochran, 2010; Lu et al., 2020; Runcie et al., 2018). Additionally, mAbs can trigger antibody-dependent cellular cytotoxicity (ADCC), antibody-dependent cell-mediated phagocytosis (ADCP), and complement-dependent cytotoxicity (CDC) mechanisms of the human immune response to eliminate the toxic entity (de Taeye et al., 2019). Nevertheless, mAbs frequently face shortcomings in their therapeutic efficacy arising from host acquired resistance. Often, the monospecific functionality of a mAb does not guard against the multifactorial nature of complex diseases that the antibody aims to treat, such as cancer and inflammatory diseases, which are driven by many signalling pathways which exhibit cross-talk, redundancy, and intricate mechanisms of regulation (Chames et al., 2009; Dong et al., 2011; Klein et al., 2024; Kontermann, 2012; Morgillo and Lee, 2005). Additionally, whilst they can induce multimerization/clustering of their target, mAbs are unable to exploit signalling outputs arising from the heterogeneous pairing of molecules or cells. Instead, bispecific binding moieties can address these shortcomings by targeting more than one disease-related pathway, as well as

bridging diverse target combinations to discover synergistic activities or novel biological activities (Gera, 2022).

1.1.1 Bispecific antibody mechanisms of action

Bispecific antibodies present the potential to improve the efficacy of antibody-based biologics by five leading obligate mechanisms, which will be summarised here, and depicted in Fig. 1.1.

1.1.1.1 Effector retargeting (trans-acting)

The archetypal application of bispecific antibodies is in the recruitment of effector cells (such as cytotoxic T cells, natural killer (NK) cells, granulocytes, neutrophils, or macrophages) to tumour cells (Husain and Ellerman, 2018) (Fig. 1.1A). Bispecifics recruiting T cells, known as bispecific T-cell engagers (BiTEs, or TCEs), are generally built as tandem single-chain variable fragments (scFvs), demonstrating high tissue penetration, excellent specificity, and potent anti-tumour activity at low concentrations (< 10 pg/ml) (Dreier et al., 2002; Mack et al., 1995; Moore et al., 2011). As of 2024, BiTE-functioning bispecifics constitute 32.9% of all solid tumour-targeted bispecifics in clinical development, and 9 of the 10 currently approved bispecifics for cancer therapy (Klein et al., 2024). BiTEs, and other immune cell engaging bispecifics, achieve their function by simultaneously targeting a tumour-associated antigen on a cancer cell (such as CD19/20/22/30/33 for haematological malignancies, or epithelial cell adhesion molecule (EpCAM), human epidermal growth factor receptor (HER2), programmed death-ligand 1 (PD-L1), or prostate-specific membrane antigen (PSMA) for solid tumours) and an effector cell (predominantly CD3ε, a component of the T-cell receptor (TCR), CD16 (FcγRIIIa) on NK cells, or CD89 (FcαRI) on neutrophils) (Demaria et al., 2019; Klein et al., 2024; Li et al., 2018). In the case of T-cell engagers, bringing the two cell types together induces the formation of an artificial immune synapse to trigger effector cell activation and cytotoxic

responses. However, engagement of activating Fc-receptors induces potent effector cell activation directly (Bryceson et al., 2006), and so NK cell or neutrophil-engaging bispecific antibodies act to bridge the target cell to an activated effector cell.

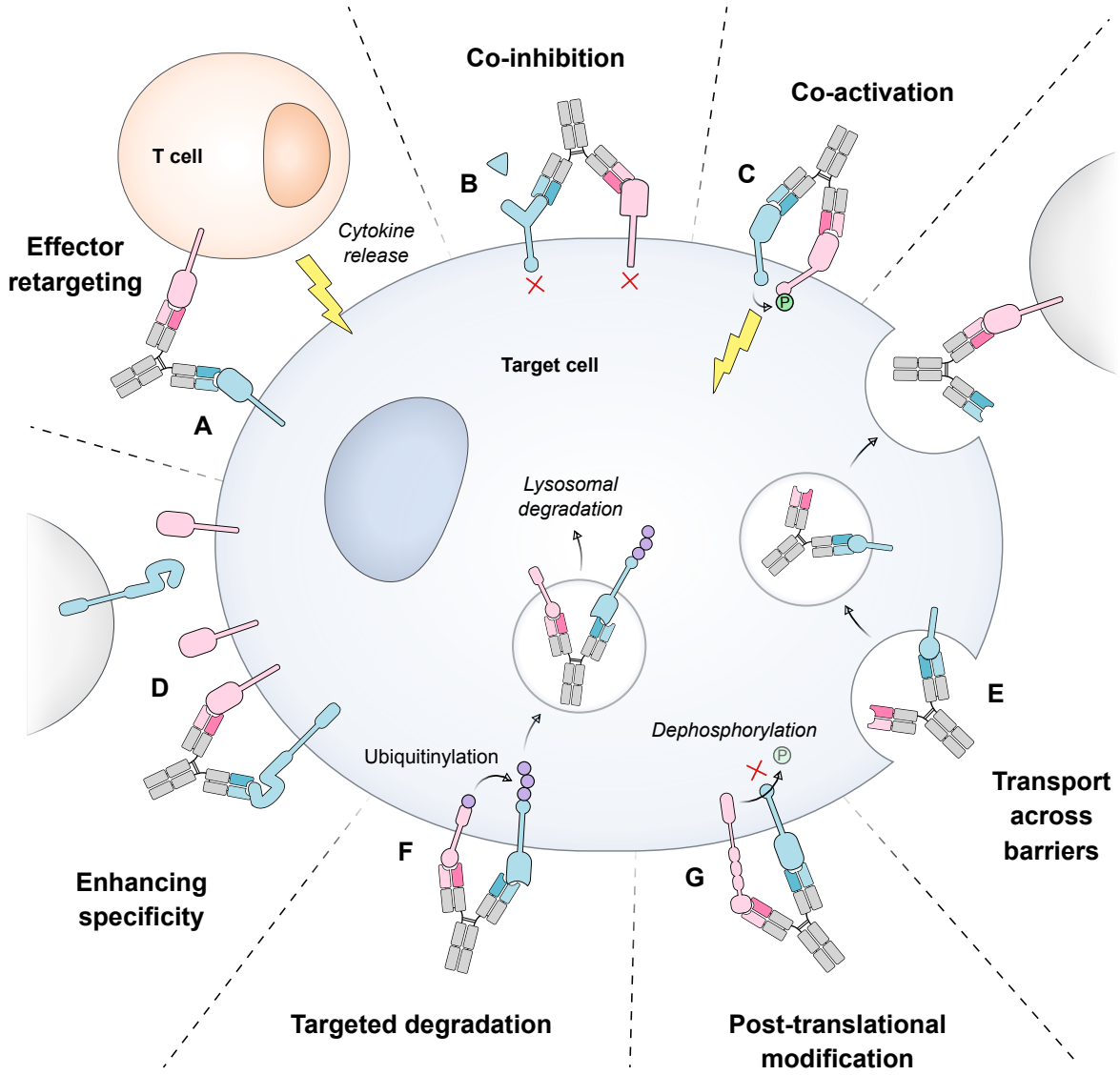


Figure 1.1 Common mechanisms of action of bispecific antibodies. Bispecific antibodies present novel biological activities by engaging two molecules simultaneously. Here, bispecific antibodies are represented as IgG-like molecules with constant domains in grey, and variable domains in pink (against the first target antigen) or blue (against the second target antigen). Target antigens are coloured to match the bispecific variable regions. (A) Bispecifics can function by binding molecules *in-trans*, for example to retarget effector cells or molecules. Alternatively, bispecific antibodies can act to bridge molecules on the surface of the same cell, *in-cis*, to simultaneously inhibit ligand binding or signal activation downstream of two receptors (B), or triggering signal activation of by inducing specific receptor dimerisation (C). (D) Bispecific antibodies can also act to enhance the specificity of a drug modality by co-targeting a cell- or tissue-specific antigen. (E) By taking advantage of native receptor internalisation or endosomal trafficking mechanisms, bispecific antibodies can also transport binding modalities across biological membranes or into specific cell compartments. Lastly, bispecific antibodies can function to induce proximity between two receptor types, such as to induce specific receptor ubiquitination to target it for lysosomal degradation (F), or receptor dephosphorylation to inhibit signal propagation (G).

The *trans*-acting bispecific mechanism remains one of the most widely exploited, and has been expanded for the recruitment of effector molecules, such as toxins, prodrug-converting enzymes, or cytokines (Kontermann, 2012; Runcie et al., 2018; Wang et al., 2019b; Zhang et al., 2017), to target cells.

1.1.1.2 Bridging at the cell surface (*cis*-acting)

While effector retargeting bispecifics account for almost half (49%) of all bispecifics in clinical development, over a third (36%) make up those that bridge two targets on the surface of the same cell, or 'in-*cis*' binding (Oslund et al., 2024). Within the pool of *cis*-acting bispecifics in the literature, a huge diversity in their modes of action has been described. Such diversity is reflected in the three clinically approved *cis*-acting bispecifics, which each function via a unique mechanism. For simplification, these bispecifics can be categorised into two mechanistic classes: those that induce target co-inhibition (Fig. 1.1B), or those that induce target co-activation (Fig. 1.1C).

Co-inhibiting bispecifics can act by blocking ligand-binding sites in receptors with compensatory or complementary signalling pathways, such as the 2021-approved epidermal growth factor receptor (EGFR)×hepatocyte growth factor receptor (MET)-binding bispecific Rybrevant (amivantamab), which was the first bispecific to simultaneously inhibit two receptor tyrosine kinases (Vijayaraghavan et al., 2020). Alternatively, bispecifics can block receptor multimerisation, such as between the growth factor receptors HER2 and HER3, which MCLA-128 (zenocutuzumab) aims to achieve in solid tumours possessing neuroregulin-1 gene fusions, which adventitiously induce HER2-HER3 heterodimer formation (Schram et al., 2022). In this way, the co-inhibitory class of *cis*-acting bispecifics function to target receptor redundancies (which typically emerge in the development of resistance) or signalling cross-talk, such as that

observed for cytokine and growth factor receptors (Kontermann, 2012; Labrijn et al., 2019). Importantly, it is not always the case that the co-inhibitory activity of these bispecifics can be matched by combinatorial treatment with monospecific counterparts (Jarantow et al., 2015). Instead, bispecifics often demonstrate synergistic inhibition, possibly due to enhanced receptor internalisation and degradation or enhanced receptor occupancy through avidity effects (Oslund et al., 2024).

On the other hand, bispecifics can take advantage of signalling activation mechanisms that require receptor oligomerisation, although these molecules are more challenging to develop. Unlike co-inhibitory bispecifics, which are typically functional as long as they bind their targets with high enough affinity to out-compete the native ligand, co-activating bispecifics must mimic more nuanced biological processes that may be sensitive to the precise geometry of the bridge, the duration of the interaction, or the conformational changes required for receptor activation (Madsen et al., 2024; Mayes et al., 2018; Yu et al., 2023). Nevertheless, effective co-activating bispecifics have been described; for example, a bispecific has been developed to mimic the hormone fibroblast growth factor 21 by bridging the fibroblast growth factor receptor 1 (FGFR1) and its co-receptor Klotho-β in adipose tissue, initiating mitogen-activated-protein-kinase (MAPK) signalling and energy expenditure (Kolumam et al., 2015). Similarly, the 2017-approved bispecific Hemlibra (emicizumab) acts to mimic the function of coagulation factor VIII, which is absent in haemophilia A patients, by co-engaging factors IXa and X (Kitazawa et al., 2012). Beyond inducing known biological pathways, bispecifics have the potential to introduce novel functionality by bridging new combinations of molecules at the cell surface (Labrijn et al., 2019).

1.1.1.3 Enhancing specificity

Many tumour-associated antigens (TAAs), whose activity a drug seeks to modulate, are expressed in various other tissues and the difference in expression between tumour and normal tissue may not be sufficient to generate a safe therapeutic index (Husain and Ellerman, 2018). Similarly, target molecules may be expressed weakly and difficult to target with a monospecific binder. Bispecifics, on the other hand, can leverage the binding of a tissue-specific target antigen, or one that is highly expressed, to kinetically favour engagement of the intended target via the second binding arm (Oslund et al., 2024) (Fig. 1.1D). As an example, specific binding and inhibition of low-density lipoprotein receptor-related protein 6 (LRP6) on tumour cells was facilitated by a bispecific co-targeting a second TAA displaying low or no expression in normal cells. Three different TAA co-targets were employed: ephrin type-A receptor 2 (EphA2), intercellular adhesion molecule 1 (ICAM-1), and activated leukocyte cell adhesion molecule (ALCAM) (Lee et al., 2018; Yang et al., 2021b). Relative to the activity of an LRP6 mAb, each bispecific combination enhanced Wnt signal inhibition by >100-fold. Additionally, the LRP6×ALCAM bispecific enhanced the receptor occupancy of LRP6 by 300-500-fold (Lee et al., 2018).

1.1.1.4 Transport across barriers

By the same principle as those designed to enhance tissue specificity, bispecifics can be employed to deliver a binder moiety to a restricted cellular compartment, such as into endosomal compartments (Wec et al., 2016) or across the blood-brain barrier to access the brain compartment (Labrijn et al., 2019; Yu et al., 2011) (Fig. 1.1E). The most widely explored application of these ‘piggybacking’ bispecifics is in crossing the blood-brain-barrier, whereby one binding arm targets a transcytosis-mediating receptor (such as the transferrin receptor, insulin receptor, the glucose transporter GLUT1, or the L-type amino acid transporter LAT1) (Pardridge, 2016). The second binding arm then targets the therapeutic protein of interest, such

as the enzyme β-secretase 1 which converts amyloid precursor protein to amyloid-β (Aβ) peptides associated with Alzheimer's disease (Yu et al., 2011). Blood-brain-barrier transversing bispecifics have been effective at increasing the brain-to-blood IgG concentration ratio from 0.1% to up to 3% (Thom et al., 2018).

1.1.1.5 Induced proximity

Besides controlling activation (or inhibition) of dimer-induced signalling pathways, proximity-inducing bispecifics have recently been applied to induce selective target degradation or post-translational modification (PTM) of a target ligand (Oslund et al., 2024). Inspired by the abundant successes of intracellular protein-degrading modalities (Liu and Ciulli, 2023), bispecific antibodies can be designed to bridge a cell-surface target antigen to a membrane-bound recycling receptor, where the target will be trafficked through early and late stage endosomes to the lysosome for protein degradation (Liu and Ciulli, 2023) (Fig. 1.1F). Thus far, proximity-induced targeted degradation of cell-surface proteins has been achieved by bispecific bridging to glycan-targeted recycling receptors, such as the cation-independent mannose 6-phosphate receptor (CI-M6PR) (Banik et al., 2020); transmembrane E3 ligases such as RNF43 or ZRNF3 (Cotton et al., 2021; Marei et al., 2022; Siepe et al., 2023); cytokine and growth factor recycling receptors, such as CXCR7 (Pance et al., 2023); the transferrin receptor (TfR) (Zhang et al., 2024a); integrins (Zheng et al., 2022); and insulin-like growth factor 2 receptor (IGF-2R), which is endocytosed upon rearrangement of the receptor's extracellular domains (Huang et al., 2024).

PTM of cell-surface receptors has also been demonstrated through the recruitment of membrane phosphatases, termed receptor inhibition by phosphatase recruitment (RIPR), using proximity-inducing bispecific nanobody-single chain variable fragment (scFv) fusions

(Fernandes et al., 2020) (Fig. 1.1G). By this approach, receptor signalling is inhibited intracellularly rather than indirectly through the inhibition of ligand binding, thus exhibiting immediate inhibition even when signalling persists in the absence of a ligand (tonic signalling).

1.1.2 Bispecific antibody format

The inception (Nisonoff et al., 1960) and first working design (Fudenberg et al., 1964) of a bispecific antibody described the inefficient recombination of two individually purified rabbit antigen-binding fragments targeting different antigens. Two decades later, the advent of hybridoma technology for the generation of monoclonal antibodies then permitted IgG-like bispecific generation through somatic fusion of two different hybridoma cells (Karpovsky et al., 1984; Köhler, G., Milstein, 1975; Perez et al., 1985), where the random pairing of heterologous immunoglobulin heavy and light chains (two of each type) from each parent cell produced the desired bispecific IgG molecule only 12.5% of the time (Milstein and Cuello, 1983; Wang et al., 2019b). Adventitious chain mispairing was first avoided by fusion of hybridomas from different species (Lindhofer et al., 1995); however, human anti-mouse and anti-rat IgG responses arose in patients receiving the drugs (Kontermann and Brinkmann, 2015; Wang et al., 2019b).

Reliable correct heavy-chain assembly was instead achieved through genetically engineering complementarity into the CH3 domains of the two different Fc domains (Fig. 1.2A, top). Termed the “knobs-into-holes” (KiH) method, a small amino acid is replaced with a larger, “knob” residue in the CH3 domain of one chain (T366W), while complementary small amino acid “hole” mutations (T336S, L368A, and Y407V) are introduced into the second heavy chain to replace large residues (Merchant et al., 1998; Ridgway et al., 1996; Shatz et al., 2013; Zhang et al., 2017). With additional stabilisation by an interdomain disulfide bond (S354C – Y349C

substitutions), KiH heterodimer formation is favoured over holes-holes homodimers > 95% of the time, and Fc-mediated effector functions are retained when the antibody chains are co-expressed in mammalian host systems (Brinkmann and Kontermann, 2017; Stutz and Blein, 2020). Heavy-chain heterodimerisation has also been achieved by engineering electrostatic, instead of steric, complementarity ('steering') into the CH3 interface, e.g. salt bridge-inducing K409D – D339K substitutions (Gunasekaran et al., 2010).

In parallel, multiple strategies for correct light-chain pairing have been developed, so that full bispecifics can be produced in a single host cell (Fig. 1.2A, bottom). The most frequently applied technique employs a common light chain (Merchant et al., 1998; De Nardis et al., 2017; Wang et al., 2019b). KiH and complementary electrostatic mutations have also been applied to light chains (Spiess et al., 2015). Through permutations of light-chain and heavy-chain pairing solutions, a creative array of Fc-containing bispecifics have emerged (Brinkmann and Kontermann, 2017; Klein et al., 2024; Kontermann and Brinkmann, 2015; Surowka and Klein, 2024). In general, the long serum half-life and other Fc-mediated properties of IgG-like bispecific formats come at the therapeutic cost of low tissue penetrability (Brinkmann and Kontermann, 2017).

In contrast, small recombinant bispecific antibodies that lack an Fc region, here termed 'fragment-based' bispecific antibodies, build upon a simple template whereby two antigen binding domains are genetically fused (Fig. 1.2B, top). Connecting linkers have ranged from flexible glycine-serine repeat linkers to rigid helical linkers or full-length Fc domains, and bridge the two binder domains in different orientations and stoichiometries (Brinkmann and Kontermann, 2017; Chen et al., 2021).

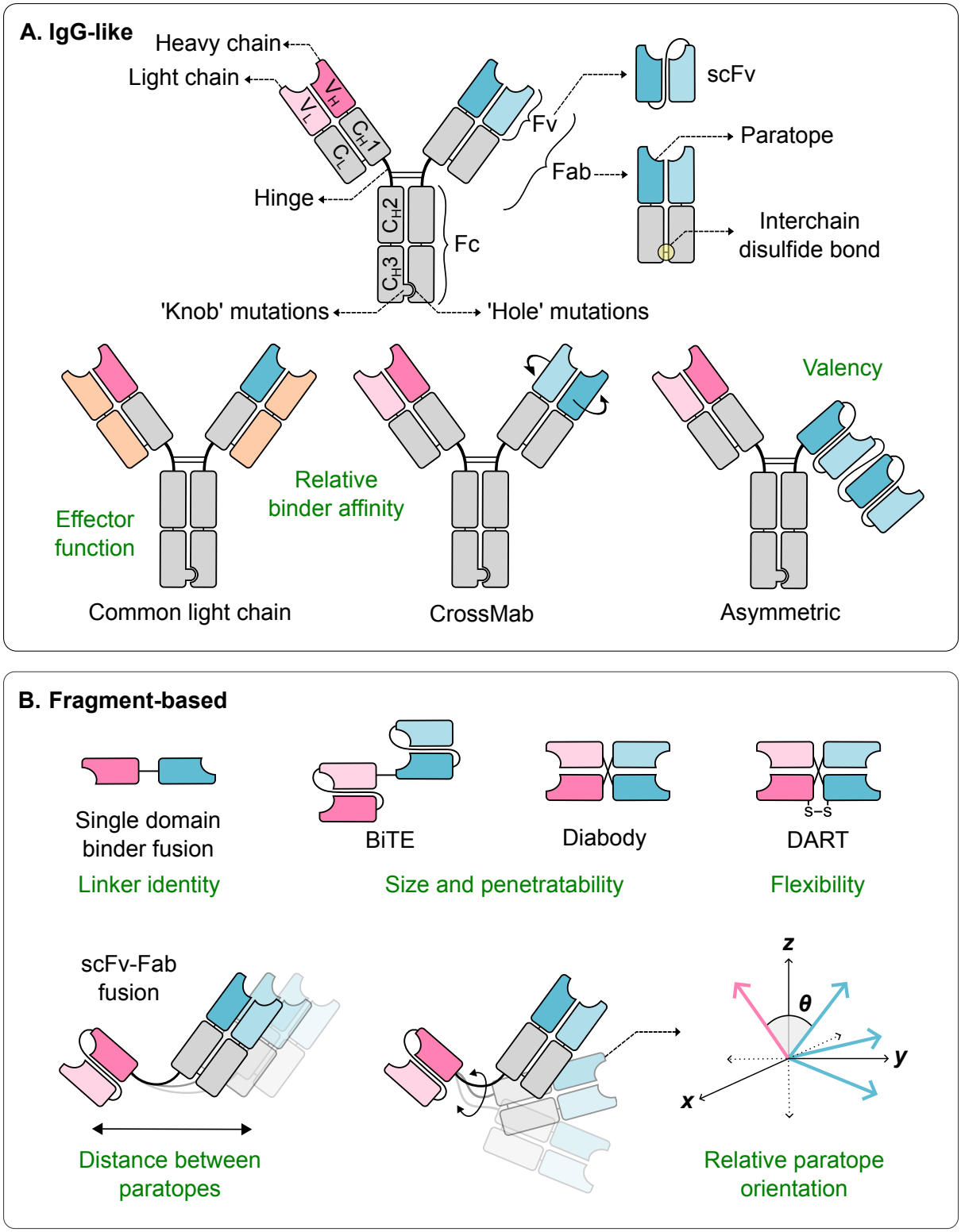


Figure 1.2. The anatomy of a bispecific antibody. Bispecific antibodies have been described in diverse formats to achieve their broad modes of action. The >100 different formats documented can be broadly classified into two groups: IgG-like, resembling a native IgG scaffold with an Fc-domain (top); or fragment-based, designed from antibody-derived fragments or synthetic binder domains (bottom). Exemplary common bispecific antibody formats within each category are depicted as cartoons and labelled in black. The format parameters of bispecifics that are subject to modification and optimisation during bispecific antibody are labelled in green. Fab, fragment antigen binding region; scFv, single chain variable fragment; BiTE, bispecific T cell engager; DART, dual-affinity retargeting.

As bispecific antibody technology platforms have evolved, over 100 unique bispecific antibody formats that vary in size, complexity, or similarity to native IgG antibodies have been described (Brinkmann and Kontermann, 2017; Labrijn et al., 2019; Ma et al., 2021; Zhang et al., 2017). It must be emphasised that the rich diversity of bispecific formats developed reflect the diverse mechanisms by which bispecifics must carry out their broad functions (Brinkmann and Kontermann, 2017; Dickopf et al., 2020; Klein et al., 2024). Each bispecific format accommodates modifications to different anatomical features of the molecule, which are defined in green text in Fig. 1.2 and will be referred to throughout this Thesis. Specifically, features include the relative affinity of the two binding motifs (paratopes), distance between paratopes, the relative orientation of the paratopes, valency, flexibility of the construct, size and penetrability, and effector function.

1.1.3 Effect of bispecific antibody format on activity

Each of the format parameters depicted in Fig. 1.2 contribute to the activity of a bispecific molecule. The following examples demonstrate the value of optimising each individual format parameter during bispecific discovery.

i) ***Relative binding affinity:*** As described in Section 1.1.1.3, one bispecific mode of action is to direct antibody binding to a specific cell or tissue-type. This mechanism is often achieved by tuning the affinities of the two binding moieties on the bispecific, with the tissue-specific antigen-binding arm possessing higher affinity for its target than the target antigen-binding arm. As such, IgG-like bispecific IBI319 was engineered to stimulate T cells only in PD-1-rich environments (i.e. those in tumours and tumour-draining lymph nodes) by reducing the potency of the anti-CD137 arm relative to the anti-PD-1 arm (Qiao et al., 2021). This

way, bispecific binding to CD137 was disfavoured until the bispecific engaged with PD-1, so the entropic penalty of binding was reduced.

ii) ***The distance between paratopes****:* A series of bispecific T cell engager (BiTE) molecules (Fig. 1.2B) with increasing inter-paratope distances (~3-15 nm) was synthesised to target CD3 on T cells and the tumour-associated antigen FMS-like tyrosine kinase 3 (FLT3), which possesses five extracellular domains that are increasingly membrane proximal (Chen et al., 2021). For each domain of FLT3 targeted, the ability of the T cell engager series to induce cytotoxicity and cytokine release differed, depending on the distance between two paratopes, which determined the size of the artificial immunological synapse induced.

iii) ***The relative paratope orientation:*** Diabodies are rigid bispecific scaffolds comprised of two single-chain variable fragments that are connected by short peptide linkers, with the heavy fragment of one scFv fused to the light fragment of the other, and vice versa (Fig. 1.2B). During the development of a diabody targeting the receptor tyrosine kinases EGFR and IGF-1R for their dual inhibition, the orientation of the scFvs was found to significantly influence the bispecific's ability to simultaneously engage both receptors (Lu et al., 2004), owing to their small size and steric limitations of bridging EGFR-IGF-1R.

iv) ***Valency of binding arms:*** One challenge in the development of T cell engaging bispecifics is increasing their size to reduce clearance, whilst ensuring T cell activation is minimised unless the bispecific is engaged with its tumour-associated antigen. As a solution, a bispecific was generated bearing three anti-EGFR nanobodies and only a single anti-CD3 nanobody (Harwood et al., 2018). Relative to an EGFR×CD3 bispecific with monovalent binding to both targets, the trivalent-monovalent bispecific demonstrated 15-to 20-fold ability to redirect T cells to EGFR-expressing cells, to upregulate activation markers, induce cytokine release, and induce cancer cell death.

v) ***Flexibility***: In a study disputing the traditional notion that T cell engaging bispecifics required substantial flexibility (Brinkmann and Kontermann, 2017; Hao et al., 2015), CD19×TCR or CD19×CD3 dual affinity retargeting (DART) bispecifics, which are synthesised by disulfide-stapling two scFv domains in a diabody (Fig. 1.2B), were significantly more potent than simple scFv-fusion equivalents (Moore et al., 2011). It was postulated that the flexible scFv fusion may require sampling of a number of conformations and orientations before adopting one that actively engages the T cell and tumour cell, while the rigid DART is fixed in this active structure. The sensitivity of bispecifics to flexibility was further demonstrated by the molecular optimisation of a dual variable domain antibody (DVD-Ig) targeting HIV gp120 and gp41, where target binding and cytotoxicity was enhanced with rigid helical linkers over short or flexible alternatives (Craig et al., 2012). A third example is in bispecifics which crosslink the B-cell receptor (BCR) with an inhibitory co-receptor, such as Fc gamma receptor II (FcγRII), to inhibit B cell proliferation as a treatment for inflammatory or autoimmune diseases (Smith and Clatworthy, 2010). Importantly, B cell inhibition is dependent on the BCR crosslinking with inhibitory receptors on the same cell, rather than on adjacent cells. As such, BCR×FcγRII DARTs were synthesised to achieve *cis*-bridging of its target (Veri et al., 2010)

vi) ***Size and penetrability****:* The small size (~ 55 kDa) of the canonical tandem scFv format of BiTEs is advantageous due to high tissue penetrability in solid tumours. However, the size lies below the glomerular filtration threshold of 50-60 kDa, leading to rapid clearance of tandem scFvs (Klinger et al., 2012). While short plasma half-life (~1.25 h) is appropriate for imaging applications, frequent intravenous infusion of the binder is required for use as a therapeutic. As a solution, BiTEs have been fused to Fc domains, with reported half-life of ~210 h (Lorenczewski et al., 2017).

vii) ***Effector function****:* The Fc domain in IgG-like bispecific formats imparts an antibody effector functions through FcγR binding and complement-binding to activate cytotoxicity, as well as extending its serum half-life via binding to the neonatal Fc receptor (FcRn) (Galvez-Cancino et al., 2024). However, complement-mediated cell lysis is not always desirable, for example in cofactor mimetic bispecifics or brain compartment-targeted bispecifics (Couch et al., 2013; Kontermann and Brinkmann, 2015). Therefore, through sophisticated antibody engineering efforts, the native Fc domains can be replaced with Fc variants which have modified (or removed) effector functions, while retaining their long half-life (Nimmerjahn et al., 2023; Wang et al., 2018).

viii) ***Linker identity:*** In drug development, linker regions are generally optimised for length and amino acid composition to reduce the aggregation tendency of scFvs or other Fc-less architectures (Labrijn et al., 2019; Schanzer et al., 2011), or to improve solubility (Whitlow et al., 1993). Linker domains additionally have the potential to fine-tune the bispecific architecture, yet linker properties are rarely explored beyond 'flexible' (i.e. Gly/Ser repeats) or 'rigid' (i.e. single α-helix).

1.1.4 Approaches for bispecific antibody synthesis for screening with increased throughput

As alluded to in Section 1.1.2, substantial research in the bispecific field has been dedicated to minimising the technical challenges that arise during bispecific assembly, i.e. their 'developability'. The term developability encompasses manufacturing considerations (correct chain pairing, yield, stability, and solubility), as well as therapeutic potential (format, immunogenicity, and on-target activity) (Kreudenstein et al., 2013). It is widely accepted that the biological activity of a bispecific antibody is not equivalent to the sum of its monospecific counterparts (Dickopf et al., 2020; Lee et al., 2018; Lu et al., 2004; Nielsen et al., 2000; Yumura

et al., 2017). The maturation of a bispecific therefore requires unbiased, empirical optimisation of the different format parameters. Variation of a single parameter alone can generate hundreds to thousands of variants which need to be synthesised and screened for desired activity; for the identification of the factor VIII mimetic bispecific emicizumab, 40,000 bispecific variants were generated with variation in their factor IX or X-binding Fab arms, of which only ~0.3% displayed factor VIII mimetic activity (Kitazawa et al., 2012). Thus, when varying more than one format parameter simultaneously, the combinatorial format space rapidly becomes too expansive to search using conventional methods. Thus, it is necessary to employ high-throughput screening strategies that may be facilitated through automation. In Table 1.1, efficient methods amenable to medium- to high-throughput bispecific antibody production will be summarised, which are optimised to ensure the processes of cloning, protein expression, protein purification, and biophysical validation can be conducted in a single workflow.

Table 1.1. Medium- to high-throughput methods for combinatorial bispecific antibody production. The activity of a bispecific antibody is not equal to the sum of its monospecific counterparts and is instead influenced by multiple different format parameters. Therefore, bispecific discovery generally requires many different bispecific candidates, which vary in one or more format parameters, to be screened for desired activity. To conduct bispecific assembly and screening at scale, multiple successful bispecific production workflows which have demonstrated, or have the potential for, increased throughput have been described. These methods are summarised in the table with their key features.

Class	Method	Brief description	Format	Parameters varied	Scale	Limitation	Reference
Bioconjugation	Split intein	Single Fab-Fc fragments are synthesised with a C-terminal intein fragment in place of the second Fab, whilst Fabs are synthesised with an N-terminal intein fragment. When the Fab-Fc and Fab fragments are mixed, the inteins recombine by post-translational trans-splicing, which excises the intein fragments.	IgG	Binder affinity	>384	Most inteins require reducing agent, not permissible to modification of bispecific geometry	(Hofmann et al., 2020a)
	Sortase A	One binder bears the terminal sortase A (SrtA) recognition peptide LPETG. SrtA cleaves the Thr-Gly bond to yield a covalent acyl-enzyme intermediate, which is reactive with the N-terminal glycine of a Gly_5-peptide-fused to the second binder. Upon formation of a new Thr-Gly bond, SrtA is released.	Fab-Fab, scFv-scFv, DARPin-DARPin	Target, epitope, binder orientation	441	Requires enzyme, each binder must be cloned with terminal peptides	(Andres et al., 2020)
	SpyCatcher/ SpyTag	Candidate binder arms are fused to SpyCatcher or SpyTag peptide, for spontaneous reconstitution when mixed. Alternatively, a tandem SpyCatcher construct has been designed with one reactive Catcher, and one containing an S-thiolated cysteine which is only activated in the presence of reducing agent. SpyTagged binders can then be sequentially coupled onto the tandem Catcher.	Fab-Fab	Binder affinity, valency	<36	Not permissible to modification of bispecific geometry, leaves potentially immunogenic ‘scar’; Requires reducing agent	(Akiba et al., 2020; Hentrich et al., 2024; Yumura et al., 2017)

Redox chain-exchange	Format chain exchange (FORCE)	Each parental antibody (each containing knob or hole mutations) is first expressed with a Fab-less 'dummy' Fc chain containing the identical mutations, and a LC. When the two monovalent parental antibodies are mixed with reducing agent (to separate the half antibodies from the dummy chains), the knob-hole half antibodies will associate to form bispecific antibodies.	IgG-like or IgG-Fab	Target epitopes, binder affinity, distance between paratopes, valency, size of bispecific	>>144	Requires redox control; geometries explored are restricted to IgG-like format	(Dengl et al., 2020)
	DuoBody	Two parental antibody panels, which contain one of two complementary mutations in their CH3 domains, are expressed separately. When mixed in a 1:1 ratio with mild reducing agent, the heavy chains of each antibody homodimer will dissociate and pair with a complementary heavy chain from the other antibody panel to form a stable heterodimer.	IgG-like	Binder paratope	~1,920	Not permissible to modification of bispecific geometry	(Barron et al., 2024; Labrijn et al., 2013; Neijssen et al., 2021)
Complementary chain pairing	Knobs-into-holes with modified light chain	The heavy chain for one half of the bispecific contains 'hole' mutations (T366S, S368A, Y407V) and the heavy chain for the second half of the bispecific contains a 'knob' mutation (T366W). To ensure correct heavy chain-light chain pairing, light chains may be orthogonal (κ/λ), one Fab may contain an alternate disulfide bond, or one Fab may have charge pair mutations in their constant domains. Heavy and light chain plasmids are transfected into a single host for their coexpression.	IgG-like	Binder target, binder affinity	~100	Can be low yielding, typically requires multiple purification steps; not permissible to modification of bispecific geometry	(Dillon et al., 2017; Fischer et al., 2015; Joshi et al., 2019; Lewis et al., 2014; Mazor et al., 2015; Shatz et al., 2016)
	Knobs-into-holes with common light chain	Bispecifics are synthesised from parental antibodies (containing knobs or holes mutations in their CH3 domains) which share common light chains, so that when they are	IgG-like	Binder affinity	545	Not permissible to modification of bispecific geometry; one	(Geuijen et al., 2018; Gong et al., 2021)

		paired the risk of light chain mispairing is eliminated.				parental antibody requires discovery through phage display transgenic animals with limited light chain diversity	
	CrossMab	CrossMabs are formed through crossover of domains within one arm of the bispecific; either the heavy and light chains of the entire Fab arm are switched, the V_H and V_L domains only, or the CH1/C_L domains only (Fig. 1.2B). Co-expression of all four bispecific chains allows bispecific production.	IgG-like	Binder affinity	~100	Typically requires multiple purification steps; not permissible to modification of bispecific geometry	(Klein et al., 2019; Schaefer et al., 2011)
	Bipod	One half of the antibody comprises a Fab linked to a CH2-CH3 heavy chain with T350V, T366L, K392L, T394W mutations. The second half-antibody comprises an scFv linked to a CH2-CH3 heavy chain with complementary T350V, L351Y, F405A, Y407V mutations. Cells are transfected with a DNA ratio of 2:1 scFv:Fab half antibody, and assembled bispecifics are purified by their CH1 domain.	Fab-scFv on Fc	Target epitopes, binder affinity	112	Each binder must be cloned and expressed in two different formats; not permissible to modification of bispecific geometry	(Nesspor et al., 2020)
Non-covalent plug-and-play	Antibody-peptide pair	For each Fab binder arm, two libraries were synthesised and expressed: one with a GCN4 peptide fused to the CH1 domain, and the other with an anti-GCN4 scFv fused to the CH1. When peptide-bearing libraries are mixed with scFv-bearing libraries, Fabs will form strong-affinity heterodimers.	Fab-Fab	Binder epitope, binder affinity, relative binder orientation	450,000	High flexibility, not permissible to modification to bispecific geometry	(Bhatta et al., 2021)

DNA library synthesis	Single-cell-based bispecific library expression and screening	HEK293 cell lines are integrated with a single copy of "attP" attachment site specific to BxB1 recombinase, and a target 'A' protein expression cassette. These cells are transfected with a BxB1 recombinase expression plasmid, and a library of donor plasmids containing BiTE variants and an "attB" donor site. The BiTE gene will thus incorporate into the host genome. Library cells are then mixed with reporter T cells expressing target 'B', which will fluoresce if activated by BiTE-mediated library cell engagement.	BiTE (scFv fusion)	Binder affinity, epitope, linker identity, relative binder orientation	22,300	Restricted to single-chain binder domains, high resource requirements (robotics, software, and data storage)	(Segaliny et al., 2023)
	In-silico DNA cassette design and combinatorial assembly	Libraries of heavy chain and light chains for cross-over are generated *in silico* to vary in their variable domains and linker sequences, before DNA cassettes are synthesised for assembly into vectors by restriction cloning. Heavy and light chain plasmid libraries are then mixed combinatorially for transfection of mammalian cells, protein expression, and purification.	IgG-like with each 'Fab' displaying two scFvs	Binder affinity, linker identity, relative binder orientation	>25,000	Not permissible to modification to bispecific geometry, high resource requirements (robotics, software, and data storage)	(Furtmann et al., 2021)
	Cytokine agonists	A subset of nanobodies and scFvs against different epitopes on two targets of interest are genetically dimerised in a combinatorial fashion via linkers of varying length.	V_{HH}-V_{HH} or scFv-V_{HH}	Binder orientation, binder type, binder affinity, distance between paratopes	60	Not permissible to modification to bispecific geometry, restricted to single-chain binder domains	(Yen et al., 2022)

Chemical conjugation	Bis-maleimide crosslinked 'bisFabs'	Digestion of murine IgGs with isotype-specific proteases followed by complete reduction yields Fab fragments. Mild re-oxidation of the inter-chain disulfide bond in the Fab with dehydroascorbic acid (as well as an intra-hinge disulfide bond in isotypes with three hinge cysteines) yield Fabs with one free cysteine. For IgG isotypes containing two hinge cysteines, one is capped with N-ethylmaleimide. Re-oxidised Fab molecules against the first target are then reacted with a bis-maleimide cross-linker. Activated Fabs are finally mixed with re-oxidised Fab against the second target to produce the desired bispecific.	Fab-Fab	Binder orientation, binder affinity	>10	High flexibility; not permissible to modification to bispecific geometry; complicated by disulfide scrambling during reoxidation; labile thiosuccinimide linkage limits serum half-life; low-throughput SEC purification	(Patke et al., 2017)
	Next-generation maleimide disulfide rebridging	scFv and Fab constituents are incubated with reducing agent to reduce inter-chain disulfide bonds. Reduced binders are incubated sequentially with an e.g. bis-dibromomaleimide cross-linker which rebridges their disulfides connect the two moieties as a bispecific. This method can be extended to couple two Fab or IgG2 moieties, by rebridging one Fab with dibromomaleimide azide and a second Fab with dibromomaleimide-strained alkyne. Subsequent mixing of the two rebridged binders enables click conjugation and bispecific generation.	Fab-scFv, Fab-Fab, IgG2-IgG2	Binder orientation, binder identity, binder type, linker length	Not yet scaled	Challenging to modify bispecific geometry	(Hull et al., 2014; Patterson et al., 2017b, 2017a)
	Pyridazine-dione disulfide rebridging	Linkers bearing a pyridazinedione group at one end and either an azide or a strained alkyne group at the other are synthesised, and Fabs are mildly reduced. Analogous to the above approach, pyridazinedione-rebridged Fabs are dimerised by click conjugation.	Fab-Fab	Binder orientation, binder identity, linker length and identity	Not yet scaled	Challenging to modify bispecific geometry	(Maruani et al., 2020; Szijj et al., 2023; Thoreau et al., 2023)

1.2 The Human Epithelial Receptor 2 (HER2) receptor tyrosine kinase

The human growth factor signalling system consists of a highly interconnected network of at least 11 growth factor ligands and four receptor tyrosine kinases (RTKs) – EGFR (ErbB1), HER2 (ErbB2), HER3 (ErbB3), and HER4 (ErbB4) (Yarden and Sliwkowski, 2001) – which interact combinatorially to drive intricately linked survival, metabolism, proliferation, and differentiation responses in normal physiological conditions (Dent, 2002). The four HER-family RTKs share a structurally conserved frame, consisting of an amino-terminal extracellular ligand-binding domain (comprised of four subdomains), a single transmembrane helix connected via a cytoplasmic juxtamembrane helical linker to a tyrosine kinase domain, and a carboxy-terminal tail.

Each of the four HER-family receptors require dimerisation for activation (Yarden and Sliwkowski, 2001), through which large-scale rearrangements of their extracellular, transmembrane, and juxtamembrane domains drive transphosphorylation of their carboxy-terminal tails (Zhang et al., 2006). In general, ligand binding to the extracellular domain (ECD) of a HER-family receptor initiates the formation of homodimers or heterodimers with another HER-family receptor, depending on the identity of both the receptor and ligand. There are two exceptions to this rule: HER3, which possesses an inactive kinase domain (Hynes and Lane, 2005; Yarden and Sliwkowski, 2001), requires heterodimerisation for activation; and HER2, which does not possess ligand-binding activity (Garrett et al., 2003) and is able to dimerise in the absence of a ligand. Regardless, a total of 614 unique possible signalling-active receptor-ligand combinations have been documented for this family (Roskoski, 2014), to predominantly bring about signalling via phosphoinositide 3-kinase (PI3K)/protein kinase B (Akt), rat sarcoma (Ras)/MAPK, and phospholipase Cγ (PLCγ) axes, albeit with intricate cross-talk and redundancy (Moasser, 2007).

1.2.1 HER2 signalling in breast cancer

Aberrant expression of the HER2 receptor, by *ERBB2* gene amplification or transcriptional deregulation, leads to a 40- to 100-fold increase in the number of HER2 copies on the cell surface (Moasser, 2007). This overexpression of HER2 is found in 25-30% of breast and ovarian cancers (Slamon et al., 1987), and around 20% of gastric cancers (Lucas and Cristovam, 2016). Whilst *ERBB2* dysregulation is an early event in tumorigenesis, this status is retained throughout progression to invasive disease and metastasis (Carlsson et al., 2004).

As evidenced by the inability of the HER2 ECD to dimerise in solution (Arkhipov et al., 2013a), the low (~40 μM) ECD self-association affinity measured by analytical ultracentrifugation (Alvarado et al., 2009), and the resulting lack of apo-HER2-HER2 homodimer crystal structures (Ferguson et al., 2000; Hu et al., 2015), it is understood that HER2 only forms signalling-active homodimers when overexpressed (Garrett et al., 2003), or mutated in its transmembrane domain (Fleishman et al., 2002). The C-terminal tails of HER2 possess at least four independent tyrosyl phosphorylation sites which bind the adaptor protein Shc and one which binds growth factor receptor-bound 2 (GRB2) (Nami et al., 2018). Both Shc and GRB2 recruit the guanine nucleotide exchange factor sons of sevenless (SOS) to HER2, which catalyses the conversion of Ras-GDP to Ras-GTP for Ras activation (Ghosh et al., 2011). Once activated, Ras triggers a phosphorylation cascade down multiple MAPK effectors (Raf, MEK, MAPK), culminating in upregulation of cell proliferation and differentiation responses (Schlessinger, 2000).

However, HER-family homodimers are not as potent signalling activators as heterodimers (Yarden and Sliwkowski, 2001). Instead, HER2 is the favoured dimerisation partner for each

of the other three HER-family receptors (Graus-Porta et al., 1997; Tzahar et al., 1996), albeit with graded degrees of dimer stability (Duneau et al., 2007). The receptor which binds HER2 with the highest affinity to form the most potent signalling dimers is HER3 (Lee-Hoeflich et al., 2008), which is known to be an obligate partner for tumorigenesis in HER2-overexpressing cancers (Baselga and Swain, 2009; Holbro et al., 2003). The HER2-HER3 heterodimer predominantly activates the PI3K-Akt pathway to promote tumour cell survival and anti-apoptotic signalling. HER2, like EGFR, is able to recruit PI3K via the adaptor proteins GRB2 and GRB2-associated binding protein 1 (GAB1) but does not bind PI3K directly. Meanwhile, HER3 possesses seven phosphotyrosine motifs in its C-terminal tail that interact directly with the p85 subunit of PI3K (Moasser, 2007), allowing the phosphorylation of membrane-bound phosphatidylinositol 4,5-bisphosphate (PIP_2) to form phosphatidylinositol 3,4,5-trisphosphate (PIP_3), to which Akt is then recruited and phosphorylated. Subsequent phosphorylation of downstream effector proteins by Akt results in their activation (NF-κB, GSK3β, and mTOR), or suppression (p27, BAD), for transcriptional regulation of genes associated with cell survival, suppression of apoptosis, and cell cycle control (Baselga and Swain, 2009).

Conversely, the second most potent heterodimer, HER2-EGFR, drives activation of the invasive phenotype through activation of the Ras/MAPK pathway (Harada et al., 2022). HER2 association drives autophosphorylation of C-terminal tyrosines in EGFR at the binding sites for GAB1, which then recruits phosphatase SHP2 to downregulate inhibition of the GTPase Ras (Montagner et al., 2005). Similarly, GAB1 recruits PLCγ which acts to activate Ras via protein kinase C activation (Roskoski, 2014). Simultaneously, binding of GRB2 to the EGFR and HER2 C-terminal binding sites recruits SOS for the direct activation of Ras (Hartman et al., 2013), effecting a strong Ras/Raf/MEK/MAPK-driven proliferative phenotype similar to that of the activated HER2 homodimer.

HER4, whose expression is relatively lower than the other members of its family (Sweeney et al., 2000), can still form dimers with HER2 with appreciable affinity to activate signal transducer and activator of transcription 5 (STAT5) through the JAK-STAT pathway (Duneau et al., 2007; Kaushansky et al., 2008). In contrast to the proliferative and pro-survival phenotypes driven by activation of other HER2-containing dimers, STAT5 is associated with growth inhibition and differentiation (Feng et al., 2007). However, considering the ability of HER4 to directly bind PI3K and activate Akt-regulated signalling, the role of HER2-HER4 dimer formation in tumorigenesis is not well defined (Baselga and Swain, 2009).

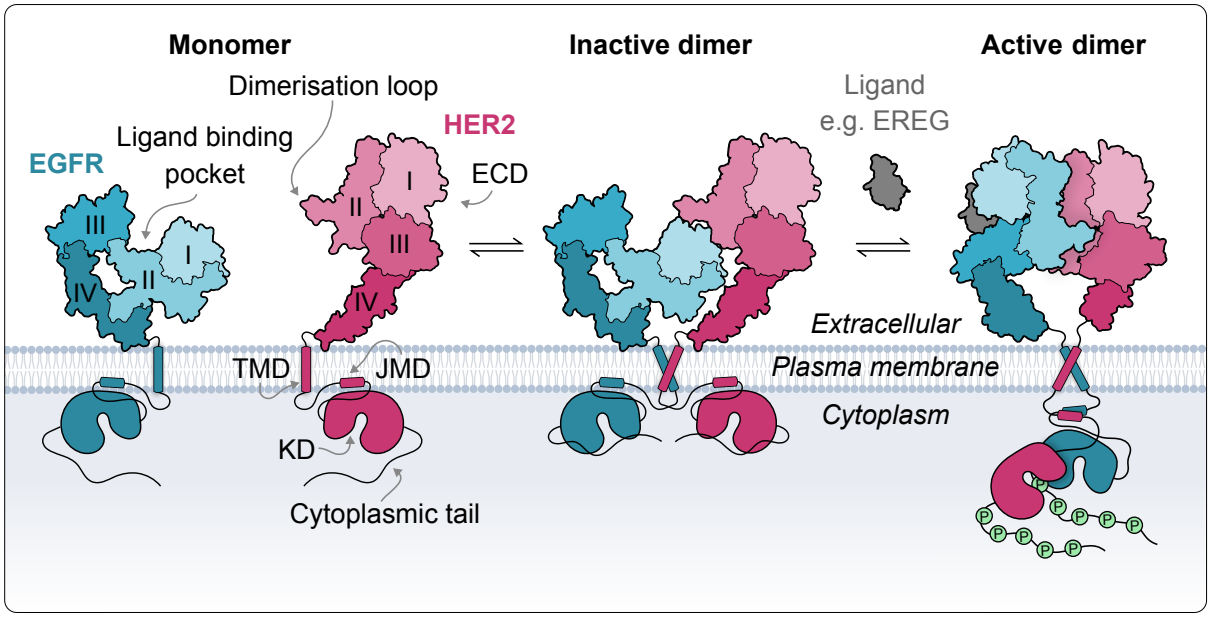


Figure 1.3. Mechanism of ligand-induced HER-family receptor activation. HER-family receptors (EGFR, HER2, HER3, and HER4) require dimerisation for activation and signal propagation. The proposed activation mechanism for an EGFR-HER2 dimer (PDB 8HGP) driven by epiregulin (EREG) binding is illustrated, with EREG in grey (PDB 8HGP), EGFR in blue (PDB 5XWD), and HER2 in pink (PDB 1N8Z). The subdomains of the receptor extracellular domains (ECD) are coloured in different shades and outlined. In the absence of ligand, the EGFR ECD (like HER3 and HER4) adopts a 'closed', inactive state, with its subdomain II dimerisation loop buried (left). Conversely, the HER2 ECD permanently adopts an 'open', dimerisation loop-exposed conformation. HER-family receptors can form signalling-inactive 'pre-dimers', in which their transmembrane domains (TMD) form a distinct coiled-coil, and their intracellular domains do not form active dimers (centre). Upon ligand binding to EGFR (or HER3/HER4), its ECD rotates substantially to expose the subdomain II dimerisation loops for stable dimer formation (right). The extracellular conformational changes are translated through the TMD, which adopts a different coiled-coil, to the juxtamembrane domain (JMD), which dimerises with the JMD of the second receptor. The distinct TMD and JMD dimer that forms is dependent on the bound ligand and the dimerisation partner. Finally, the intracellular kinase domains (KDs) of the receptors form asymmetric dimers which are poised for autophosphorylation of the respective C-terminal tails, resulting in adaptor protein recruitment and signalling activation.

1.2.2 Mechanism of HER2 signalling activation

Distinct from other HER family of receptors, the monomeric, apo-form of the HER2 ECD exists in a constitutively active 'open' conformation, which structurally mimics the conformation of the active, ligand-bound EGFR receptor (Alvarado et al., 2009; Cho et al., 2003; Garrett et al., 2002) (Fig. 1.3). The open conformation of HER-family receptors describes an elongated hairpin arrangement of the four subdomains (I-IV) of their ECD, stabilised by direct (in the case of HER2) or ligand-mediated (in the case of EGFR, HER3, and HER4) contacts between subdomains I and III, but an absence of interactions between subdomains II and IV. As a result of the hairpin conformation, subdomain II is forced into a bent orientation, exposing a protruding 18-residue loop from the centre of the domain which is responsible for mediating dimerisation with HER-family receptors predominantly via the equivalent domain II dimerisation loop (Garrett et al., 2002; Ogiso et al., 2002).

Early X-ray crystallographic work described a simple model by which ligand binding to 'closed', inactive ECD of monomeric EGFR, HER3, or HER4 drove a conformational change that permitted dimerisation with itself or HER2 and, as a result, transactivation of their kinase domains (KDs) (Cho et al., 2003; Ferguson et al., 2000; Lemmon, 2009). However, scrutiny of this model over the subsequent two decades uncovered two significant features of HER-family receptor behaviour that disfavoured such a simple binary switch: first, that all HER-family receptors have been found to form ligand-independent, signalling-inactive dimers (Tao and Maruyama, 2008); and second, that synthetic dimerisation and phosphorylation of EGFR does not induce ERK, Ras, or Akt signalling (Liang et al., 2018). As a result, the mechanism by which HER-family receptors decode ligand-induced conformational changes in their extracellular domain into the signal propagation has emerged as complex system with multiple layers of regulation (Kovacs et al., 2022; Westerfield and Barrera, 2020).

In their ligand-free state, HER-family receptors exist in equilibrium between monomeric and inactive dimeric states (Bragin et al., 2016; Macdonald-Obermann and Pike, 2014) (Fig. 1.3, left). In the first step of activation, growth factor ligands bind to the receptors in either oligomeric state, driving large-scale structural reorganisation of subdomains I-III of the ECD to expose the dimerisation loop of domain II for 'active' dimer formation (Fig. 1.3, centre). These conformational changes are propagated to the transmembrane domain (TMD) via subdomain IV, which adopts a different orientation depending on the bound ligand (Doerner et al., 2015; Scheck et al., 2012; Sinclair et al., 2018). As the C-terminus of subdomain IV directly connects to the transmembrane helix, spatial reorganisation of subdomain IV results in re-positioning of the transmembrane domains.

The single helix transmembrane domains of EGFR, HER2, and HER4 each contain a conserved GxxxG-like dimerisation motif at both termini, while the same motif is found at only the C-terminus of the HER3 TMD (Samna Soumana et al., 2008). Indeed, NMR structural elucidation and subsequent molecular dynamics simulations unveiled two distinct TMD dimer conformations (Bocharov et al., 2008; Fleishman et al., 2002). The first TMD dimer, mediated by the C-terminal GxxxG motif, was observed only in signalling-inactive dimers (Fig. 1.3, centre). In such dimers, the positively-charged residues connecting the C-terminus of the TMD to the adjacent juxtamembrane domains (JMD) are brought in spatial proximity, and their resulting repulsion drives embedding of the JMDs into the anionic lipid bilayer (Arkhipov et al., 2013b). The second dimer is instead established via a distinct hydrogen bond network between the N-terminal dimerisation motifs within the TMD helices and is associated with the active receptor dimer (Fig. 1.3, right). Formation of the N-terminal dimer drives the C-termini of the TMD apart, allowing the JMDs to dissociate from the membrane and form stable

antiparallel helical dimers (Sinclair et al., 2018). Importantly, JMD dimer formation is translated directly to the contiguous KDs.

Directly mirroring the two TMD dimerisation states, two distinct dimeric structures of the intracellular KDs of HER-family receptors EGFR and HER2 have been elucidated (Macdonald-Obermann et al., 2012; Zhang et al., 2006). The current convention therefore suggests a switch-like mechanism within TMD helix dimers upon ligand binding to the receptor, by which their conformational rearrangement is translated to the KDs via JMDs (Bocharov et al., 2008). In the inactive state, a symmetric 'back-to-back' dimer is formed and stabilised by the electrostatically and geometrically-complementary C-terminal tails of the receptor which dock tightly onto the KDs (Landau et al., 2004). Here, the ATP-binding site in the KD is partially blocked by the C-terminal tail, rendering it inactive for autophosphorylation. However, the kinase dimer associated with the active state of the HER receptor is asymmetric, with the C-terminal tails detached (Zhang et al., 2006). Thus, in the final activation step, the structural reorganisation of the KDs liberates the receptor C-terminal tails for autophosphorylation and association with proteins containing Src homology region 2 (SH2)- or phosphotyrosine binding (PTB)-domains for the intracellular transmission of the signal (Yarden and Sliwkowski, 2001).

1.2.3 Biased activation of HER-family receptors

A consequence of the highly coordinated, multi-domain conformational coupling mechanism of HER-family receptors is that subtle, ligand-induced changes in the ECD will be translated across the whole dimer architecture. Consequently, HER-family receptor activation can be biased towards activation of a certain signalling outcome, depending on the bound ligand

(Wilson et al., 2009). Three key origins of ligand discrimination will be discussed here: dimer stability, juxtamembrane domain orientation, and C-terminal phosphorylation patterns.

In the first case, a profound difference in signalling output has been observed for high affinity ligands relative to low affinity ligands. For example, the high-affinity EGFR ligands TGFα and EGF induce transient ERK signalling associated with cell proliferation, while the lower-affinity ligands epigen and epiregulin cause sustained ERK activation and induction of cell differentiation by adipogenesis (Freed et al., 2017). Importantly, these signalling nuances were attributed to the stability and longevity of the activated dimers. Generally, high-affinity ligands induce strong, symmetric ECD dimer formation (Garrett et al., 2002), and low-affinity ligands induce weak, asymmetric ECD dimers, with prolonged autophosphorylation and signalling (Freed et al., 2017). The somewhat counter-intuitive relationship between dimer strength and sustained signalling may result from the accessibility to tyrosine phosphatases of long-lived dimers (Eden et al., 2010), or differential patterns of phosphorylated tyrosines in the receptor C-termini (Salazar-Cavazos et al., 2020).

To understand how subtle changes in ECD architecture influence intracellular domains, the mechanism of TMD helix conformational switching was revisited (Doerner et al., 2015; Mozumdar et al., 2020; Sinclair et al., 2018). Briefly, cysteine residues were introduced into the TMD or JMD helices of EGFR or HER2, so that either disulfide or tetracysteine motifs will form upon dimerisation. Then, by either detecting disulfide crosslinking, or monitoring fluorescence after addition of a tetracysteine-binding dye ReAsH, the dimer architecture could be interpreted. In the revised model of activation, conformational distinctions in the ligand-bound ECD are directly encoded in the N-terminal TM helix dimers. Two groups of coiled-coil TM helices were deduced: one with large (~36°) cross-angles centred at the start of the TM

helix, and a second with smaller (~27°) cross-angles centred at the start or middle of the TM helix (Sinclair et al., 2018). Through their direct fusion, the TM helix shapes are proposed to induce anti-parallel JMD coiled coil architectures that fall into one of three distinct orientations (Doerner et al., 2015), for further signal propagation into the KDs and C-terminal tails. However, it is important to highlight that the proposed mechanism for the observed ligand-induced JMD rotation is based on molecular dynamics simulations, and further work is required to support a model of dimer architecture in which each receptor domain is rigidly linked (Karl et al., 2020).

Finally, comprehensive analysis of the C-terminal phosphorylation patterns in differentially activated EGFR (Salazar-Cavazos et al., 2020), HER2 (Scheer et al., 2012), HER3 (Van Lengerich et al., 2017), and HER4 (Kaushansky et al., 2008) receptors have revealed a clear basis for signalling disparities. Each of the four HER-family receptors possess multiple cytoplasmic tyrosines sites within their C-terminal tail, which are phosphorylated by their own or their dimerisation partner's KDs to then recruit a specific signalling effector protein to effect intracellular signal propagation (Wilson et al., 2009). The potential for a site to become phosphorylated in a ligand-bound HER dimer depends on multiple factors, including dimer conformation and dimer lifetime (Sinclair et al., 2018). Whilst the specific complement of signalling proteins recruited to the dimer depend on the phosphorylated sites, recruitment is also affected by steric hinderance from proximally bound adaptors and the relative abundance of adaptor proteins (Salazar-Cavazos et al., 2020). Thus, each ligand-bound HER-family homo- or hetero-dimer engages a different set of signalling proteins for signal propagation, which are guided by unique C-terminal phosphorylation arrays (Macdonald-Obermann and Pike, 2014).

1.3 Biased networking of biomolecules at the cell surface

Proteins in natural biological systems exist in a precise spatial relationship with their subunits or multimerisation partners (e.g. receptors) (Papaleo et al., 2016; Thirumalai et al., 2019). The HER-family receptor tyrosine kinases exemplify a system which can result in biased signalling, or the selective activation of certain signalling pathways over others. The proposed mechanisms influencing biased signalling in the HER-family described above – ligand-dependent domain rotation, dimer stability, phosphorylation profiles, and dimerisation partner – are emerging as common driving forces behind biases in many different receptor systems, both within receptor tyrosine kinase families and across other receptor classes (Karl et al., 2020; Smith et al., 2018).

An example of a second family of receptor tyrosine kinases that demonstrates biased signalling arising from dimer stability is the tropomyosin-related receptor kinase (Trk) family of neurotrophin receptors (Ahmed et al., 2020, 2021). Notably, the binding of different endogenous ligands to both Trk types A (TrkA) and B (TrkB) was found to stabilise homodimers with different conformations and thermodynamic stabilities, resulting in engagement of different signalling cascades. Through stable dimers, neuron survival and growth was promoted, while weaker dimers were only associated with axon growth (Ahmed et al., 2021). Conversely, the mechanism by which signalling bias has been observed for the insulin receptor (IR) and IGF-1R describes ligand-determined phosphorylation of distinct intracellular tyrosines, rather than different durations of phosphorylation (Jensen et al., 2007; Yunn et al., 2023). In the case of the ephrin (Eph) receptor EphA2, which belongs to the largest class of RTKs, biased ligands induce distinct oligomeric structures with varying levels of separation (Singh et al., 2018). It has been proposed that differential C-terminal phosphorylation drives the differences in signalling (Gomez-Soler et al., 2022), and increased

spacing between EphA2 monomers results in different extents of phosphorylation (Shaw et al., 2014), but the mechanism of biased activation is yet to be fully elucidated.

Investigations into biased signalling of receptor tyrosine kinases were pioneered by the equivalent phenomenon in G protein-coupled receptor (GPCR) signalling. Ligand bias in GPCR systems has been extensively studied, with three dominant driving mechanisms which converge with those attributed to RTK signalling bias. Ligand binding to GPCR extracellular loops induces specific conformational changes that result in the PTM (such as phosphorylation and ubiquitinylation) of the C-terminus and intracellular loops of the receptor. Together, the ligand-induced conformational changes and PTMs result in the coupling of three classes of transducers: heterotrimeric G proteins, G protein–coupled receptor-kinases (GRKs), and β-arrestins. The prevailing explanation for biased activation is the ability of different ligands to stabilise multiple different conformations in the cytoplasmic ends of GPCR helices (Seyedabadi et al., 2019). Of particular relevance is the chemokine signalling system, where 20 chemokine receptors respond to 50 ligands by inducing multiple subtle conformational changes (Smith et al., 2018), such as CCR5 which signals through distinct ligand-specific G protein subtypes (Kufareva et al., 2017; Zheng et al., 2017). Analogous to RTK bias, different biased ligands have also been shown to induce different phosphorylation signatures, leading to coupling of specific transducer combinations, with the β_2-adrenergic receptor as a leading example (Nobles et al., 2011; Reyes-Alcaraz et al., 2018). Lastly, ligand-induced homo- or hetero-dimerisation of GPCRs has been attributed to biased signalling outcomes, as observed in dopamine D2 receptor signalling (Fuxe et al., 2014; Lane et al., 2014).

Keeping a focus on systems that exhibit dimer-dependent signalling biases, attention is drawn to cytokine receptors, which are activated upon ligand-induced dimerisation. It has long been

known that the proximity and relative orientation of the two erythropoietin receptor (EpoR) domains, D1 and D2, in ligand-bound EpoR homodimers can greatly influence signalling output (Ballinger and Wells, 1998; Syed et al., 1998). However, only recently has the mechanism by which dimer geometries influence signalling been elaborated (Kim et al., 2017). It has been proposed that the topological reorganisation in the ECD of EpoR upon ligand binding influences the orientation of JAK2 kinases associating with the intracellular domain. In turn, the ability of JAK2 kinases to transphosphorylate each other within the EpoR dimer is altered, resulting in altered phosphorylation and activation of downstream effector proteins such as STAT1 and STAT5 (Kim et al., 2017; Mohan et al., 2019). It may also be the case that ligand-induced EpoR dimers with more extreme topologies (i.e., a greater angle between domains), which are more strained, do not form as readily as unstrained dimers, which could disproportionally reduce activation of some effectors over others (Mohan et al., 2019).

Approaches to understand and exploit signalling biases and synergies are of growing clinical interest. The ability to fine-tune responses to therapeutics has long been desired in basic and synthetic biology, so that the activity of a drug or tool can be tailored to different environments, and its beneficial effects can be maximised whilst its adverse activities are minimised (Rajagopal et al., 2010; Ritter and Hall, 2009). For example, the anti-tumour activity of chimeric antigen receptor (CAR) T-cells must be balanced against toxicities arising from high inflammatory cytokine release, which is often achieved through tuning the molecular properties of the CAR (Burton et al., 2023; Elazar et al., 2022). Similarly, knowledge of different signalling outcomes arising from distinct receptor dimers can facilitate the discovery of binding moieties that induce the formation of dimers with favourable phenotypes, for example apoptosis-inducing HER3 homodimers (Jay et al., 2011). Therefore, there exists a need for molecular tools that induce changes to cell-surface receptor complexes with spatial and

temporal precision, both for mechanistic studies of natural or novel receptors and for engineering drugs to exploit receptor interactions.

1.3.1 Existing tools for controlling biomolecular interactions at the cell surface

1.3.1.1 DNA nanostructures

Currently, the leading technology for spatial programming of molecules on a nanoscale is DNA-based scaffold design, owing to the superior programmability of single stranded (ss) or double-stranded (ds) DNA secondary and tertiary structures (Park et al., 2005; Sun et al., 2023; Yang et al., 2020). Indeed, an impressive array of sophisticated DNA nanostructures has been described, which aim to fine-tune or bias signalling pathways through spatial redistribution of different receptor targets at the cell surface. The first of these approaches attach ligands to DNA nanotemplates with user-defined distributions, valencies, and stoichiometries. These ligands may be proteins, such as the EphA2-binding protein ephrin-A5 (Shaw et al., 2014). Ephrin-A5 dimer architectures with precise spacing between paratopes (101 nm or 43 nm apart), assembled by conjugation of the ligand onto dsDNA 'nanocalipers' at fixed positions along the structure, were found to simultaneously tune the activation level of EphA2 and the cell invasion response (Shaw et al., 2014). Alternatively, DNA-templated ligands may be DNA aptamers (Wang et al., 2022). For example, DNA-origami templates were designed to position 1-8 mesenchymal−epithelial translation factor (Met)-binding aptamers. The differently distributed ligands were able to program the oligomerisation of the RTK to switch epithelial cells to mesenchymal-like cells (Wang et al., 2022). More straightforward bridging of aptamers directly, using designed, rigid dsDNA spacers, has also generated bispecific molecules that effectively control receptor distribution (Miao et al., 2021; Sun et al., 2024; Wang et al., 2019a, 2023); aptamers binding the Met receptor and transferrin receptor were bridged with a series of DNA linkers ranging from 9 nt to 80 nt in length in order to identify the optimal ligand

distance to inhibit Met phosphorylation (Wang et al., 2019a) (Fig. 1.4A). However, nucleotide-based therapeutics have limited applicability owing to their low stability in physiological conditions, potential immunogenicity, and high surface charge, resulting in an additional challenge of exploring routes for delivery and extended half-life (Keller and Linko, 2020).

1.3.1.2 Bispecific antibodies

Instead, bispecific antibodies offer great potential for precise spacing of their targets, with favourable pharmacokinetic properties. While the importance of geometric constraints in bispecific design is beginning to be discussed (Dickopf et al., 2020; Madsen et al., 2024; Romei et al., 2024), bispecifics have seldom been designed with defined architectures to fine-tune signalling. As a pertinent example, matrices of bispecifics were synthesised by combinatorially fusing nanobodies or scFvs targeting the cytokine receptors interleukin-2 receptor β (IL-2Rβ) and IL-2Rγ_C (Fig. 1.4B), which are normally dimerised by IL-2 induce proliferation and survival of T cells, NK cells, and B lymphocytes (Yen et al., 2022). Within the panel of bispecifics synthesised, the linkers, binder epitopes, binder affinities, and relative binder orientations were varied. Relative to the native ligand IL-2, the bispecific fusion variants were found to induce graded or differential (biased) phosphorylation of STAT5, ERK, and Akt, resulting in preferential memory T cell expansion and survival, and NK cell cytotoxicity over T cells. Bispecific activity was found to depend on which target epitopes were bridged and binder orientation, which both determined the geometry of the IL-2Rβ–γ_C dimer that formed (Yen et al., 2022). A second study built a comprehensive array of anti-PD-L1×anti-HER2 symmetric small domain antibody (sdAb)-IgG bispecific fusions, by fusing sdAbs to either termini of the heavy or light chains of a native IgG (Madsen et al., 2023).

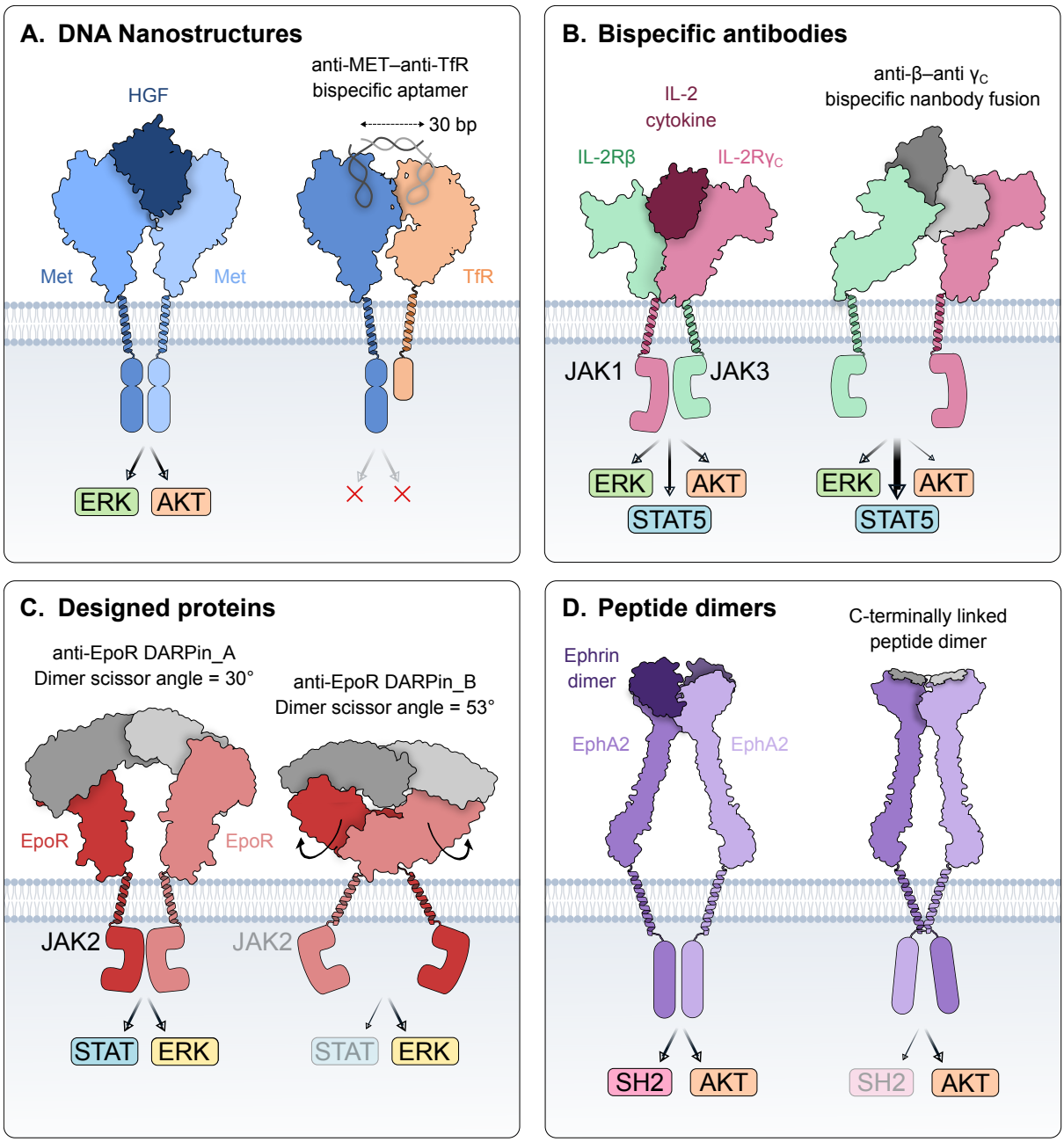


Figure 1.4. Existing tools for controlling molecular geometry. Protein-protein interactions at the cell surface, such as ligand-induced receptor dimers, are exquisitely sensitive to the geometry of the interaction. Small changes in the arrangement of interacting molecules can exert large or biased effects on intracellular signalling. To investigate such interactions, molecular caliper-like tools have been designed, whose architectures can be controlled. These tools include DNA nanostructures (A), bispecific antibodies (B), *de novo* designed proteins (C), or stapled peptide dimers (D). The specific examples illustrated here are described in the main text. Interacting receptor extracellular domains, ligands, and molecular spacers are shown as silhouettes of their structures with surface representation, from the following crystal structures: Mesenchymal-epithelial transition factor receptor (Met) and hepatocyte growth factor (HGF), PDB 1SHY; Transferrin receptor (TfR), PDB 1SUV; Interleukin-2 receptor (IL-2R) β, IL-2Rγ_C, and IL-2, PDB 2B5I; nanobody and IL-2Rβ, PDB 7S2S; nanobody and IL-2Rγ_C, PDB 7S2R; Erythropoietin receptor (EpoR) and designed ankyrin repeat protein A (DARPin_A), PDB 6MOK; EpoR and DARPin_B, PDB 6MOJ; Ephrin-A receptor 2 (EphA2) and Ephrin, PDB 3MX0.

Therefore, depending on the bispecific generated, the IgG-bound target epitopes will have different spatial orientations with respect to the sdAb epitopes. While different constructs were found to show varied *in vitro* stabilities and target binding activities, their cellular effects were not studied, which will be necessary to understand the relationship between binder architecture and signalling. As a third example, bispecific Fab-fusions that crosslink CD79 (which forms a complex with the BCR) and CD22 (an inhibitory co-receptor of the BCR) on the B cell surface were found to display an orientation dependence on B cell inhibitory signalling (Bhatta et al., 2021). Interestingly, B cells treated with the bispecifics constructed in both orientations (CD22×CD79 or CD79×CD22) displayed similar increase in inhibition of phosphorylated Akt, p38, and NF-κB, but differential inhibition of phospho-PLCγ2.

1.3.1.3 Designed proteins

Owing to the lack of geometric control in scFv-fusions and antibodies that act as surrogate cytokine agonists, but the knowledge that cytokine dimer geometry influences signalling (Moraga et al., 2015), Mohan *et al.* designed a series of bivalent designed ankyrin repeat protein (DARPin) binders against the erythropoietin receptor (EpoR) (Mohan et al., 2019). The bivalent panel induced systematic variations in the angle (38–72°), distance (30–73 Å), and curvature between EpoR monomers within a dimer (Fig. 1.4C). Their efforts yielded a binder panel that was able to rigidly dimerise EpoR in distinct geometries, inducing full, partial, or biased agonism of EpoR signalling. The phosphorylation state of multiple signalling effectors, such as STAT1/3/5 and ERK, varied in a graded or biased manner in primary human erythroid cells treated with each bivalent scaffold, and in haematopoietic stem and progenitor cells (HSPCs). As a result, differentiation of HSPCs to erythroid cells was activated at different stages of maturation. These results have been monumental in signifying the importance of dimer geometry in modulation of signalling outputs, and have largely influenced the design of

protein tools for exploiting receptor signalling, such as bispecific antibodies, in the years since their publication (Alvarez et al., 2020; Arber et al., 2017; Moraga et al., 2017; Ullrich et al., 2023; Yen et al., 2022). A second application of designed protein architectures for control over molecular organization at the cell surface is *de novo* design of geometrically tunable cyclic oligomers from repeat protein subunits (Edman et al., 2024). When FGFR binders were fused to the termini of monomers from cyclic 2-, 4-, 6-, or 8-mer scaffolds, the binding structures were able to bias the fate of human induced pluripotent stem cells to an arterial-like endothelial or perivascular state. While new approaches and improved methods for *de novo* protein design are emerging at a near exponential rate (Kortemme, 2024), vast computational resources are required, and a low 'hit rate' of soluble and functional binders from initial designs has still been quoted as a bottleneck in the design-selection process (Krishna et al., 2024; Pan and Kortemme, 2021; Zhang et al., 2024b).

1.3.1.4 Peptide dimers

Methods for *de novo* design of peptide ligands are also evolving rapidly (Bryant and Elofsson, 2023; Wu et al., 2023). Considering >30% of class A GPCRs bind peptides (Davenport et al., 2020), peptide-based molecular tools may be desirable for organising GPCRs at the cell surface. Additionally, peptide ligands bind their targets with high specificity, high affinity, and are cheap to synthesise. Peptide ligands targeting the GPCR bombesin BB_2 receptor that were separated by 10, 20, or 30 Å with rigid oligoproline linkers demonstrated a biased ability to induce Gαq, β-arrestin-1/2, and GRK2/3/5 recruitment to the receptor, as different dimer architectures were induced (Romantini et al., 2021). Beyond GPCRs, peptide-based tools have also been used to induce biased signalling of the EphA2 receptor (Gomez-Soler et al., 2022). By stapling EphA2-binding peptides into different configurations, using disulfide or click linkages, distinct EphA2 dimer geometries were induced and linked to biased changes in

ligand-induced phosphorylation of a SH2-recruiting tyrosine on EphA2 and phosphorylation of Akt (Fig. 1.4D).

1.4 Thesis objectives

Bispecific antibodies have the potential to bridge any two molecular targets of interest, with tailored biophysical properties and defined molecular geometries. However, existing platforms for bispecific discovery are limited to a fixed format, challenging to scale, or require substantial resources for reagent synthesis. The primary aim of this Thesis was therefore to design and validate a simple and generalisable methodology for the combinatorial dimerisation of ligands to produce bispecific binders. I describe a modular assembly protocol that is comprised of a core, tandem SpyCatcher003 dimerisation module, onto which complementary SpyTag-fused ligands can be site-specifically conjugated. The SpyCatcher/SpyTag protein/peptide pair was originally engineered by the Howarth group by genetically splitting an intramolecular isopeptide bond between Lys31 and Asp117 within the collagen adhesin domain (CnaB2) of the *Streptococcus pyogenes* fibronectin-binding protein (FbaB) (Zakeri et al., 2012). When the two components are mixed, the covalent isopeptide bond spontaneously reconstitutes. Through rational engineering and evolution by phage display, the reaction kinetics of SpyCatcher/SpyTag were enhanced 400-fold, close to the limit of diffusion, to generate SpyCatcher003/SpyTag003. Unique from other bioconjugation approaches to high-throughput bispecific assembly, including those which have employed SpyCatcher/SpyTag (Akiba et al., 2020; Mei et al., 2022; Yumura et al., 2017), it was important that the designed platform employed ligands in a common format (SpyTag-fused), to minimise size of the ligand library. Furthermore, SpyCatcher003 and SpyTag003 demonstrate salt-, temperature-, redox-, and pH-stability (Keeble et al., 2022), lack cysteine residues that could complicate functionality with antibody fragments, and are not restricted to the termini of the proteins to be coupled (Keeble

and Howarth, 2020; Zakeri et al., 2012). Additionally, as binding components possessing a SpyTag peptide, the SpyMask platform is compatible with one-step affinity purification for the recovery of the target molecule.

Secondly, this Thesis aimed to exemplify an application of the SpyMask platform in the assembly and screening of bispecific antibodies in medium-throughput. I therefore identified a panel of anti-HER2 binders, which targeted unique epitopes on the HER2 extracellular domain with varied affinities. I then applied SpyMask to the rapid combinatorial assembly of anti-HER2 biparatopic binders in 96-well plate format, and directly screened the purified constructs their effect on the metabolic activity of HER2-addicted cancer cells. Intriguingly, the activity of anti-HER2 bispecifics was found to depend on the HER2 epitopes targeted, and the order in which the ligands are displayed on the final bispecific.

The modular nature of the proposed bispecific assembly platform invites customization of each constituent, for facile modification of multiple different bispecific format parameters. Thus, the third aim of this Thesis was focussed on engineering a panel of DoubleCatcher variants which possess distinct geometries and validating these architectures for their compatibility with the SpyMask platform. Anti-HER2 biparatopic binders assembled using the full panel of DoubleCatcher variants were tested for their effect on the metabolic activity of HER2-overexpressing cells. Importantly, activity was dependent not only on the identity and orientation of ligands on the bispecific scaffold, but also the geometry of the scaffold itself.

The fourth and final aim of this Thesis sought to expand the functionality of the SpyMask toolbox further. The signalling activity of cell-surface receptors is regulated or can be modified with diverse ligand types, including small molecules, peptides, full-length IgGs, carbohydrates,

or DNA. Therefore, bispecific assembly with single-chain or fragment-based protein binding modules limits the targets that can be investigated. Instead, I demonstrated approaches to generate SpyTagged small molecules, full-length IgGs, and oligonucleotides, to be compatible with the SpyMask bispecific assembly platform. This way, in theory, diverse pairs of ligands can be combined in varied, defined geometries to bridge any two targets of interest to exploit existing or novel biological activities.

CHAPTER 2 – METHODS

2.1 Molecular Cloning

The constructs designed or described within this Thesis are summarised in Table 2.1. All constructs were cloned into standard bacterial (pET28a, pET21, pDEST14) or mammalian (pHL, pTT3, pcDNA3.1) expression vectors by Gibson assembly for recombinant protein production (Gibson et al., 2009).

Table 2.1. Plasmids used in this Thesis. Plasmids encoding proteins described throughout this Thesis are listed with the following information: name of backbone vector and protein construct, description of the protein sequence from its N- to C-terminus, Addgene and GenBank deposition reference numbers, and the sequence or plasmid source.

Backbone and construct	Description (N- to C-terminus)	Addgene Plasmid ID	GenBank Accession no.	Source
pET28a-SpyTag003-MBP	Maltose binding protein (MBP)-SpyTag003-His_6 tag	133450	MN433888	(Keeble et al., 2019)
pET28-SpyTag003-mClover3	SpyTag003-mClover3-His_6 tag	133453	–	(Keeble et al., 2019)
pET28a-SUMO-SpyTag003	His_6 tag-Small ubiquitin modifier (SUMO) protein-SpyTag003	216282	PP341235	(Driscoll et al., 2024)
pET28a-SnoopTag-AffiHER2-SpyTag	His_6 tag–SnoopTag–anti-HER2 Affibody–SpyTag	216280	KU296975	(Brune et al., 2017)
pET28a-SnoopTag-SpyTag-$(AffiHER2)_3$	His_6 tag–SnoopTag–anti-HER2 Affibody–SpyTag	216281	KU296976	(Veggiani et al., 2016)
pET21-MBP_X-MBP_X-SpyTag003	His_6-MBP A312V I317V Δ172 -173 Δ175-176 (MBP_X)-MBP_X-SpyTag003	216291	PP341236	Cloned by Dr Henry Wood (University of Oxford)
pET28-MBP-superTEV	MBP-G-His_7 tag-Tobacco Etch Virus (TEV) protease C19V C110V C130S V219D	171782	–	(Keeble et al., 2022)
pET28a-SpyCatcher002-MBP	His_6 Tag-TEV protease cleavage site-SpyCatcher002 MBP	216295	PP341225	Cloned by Dr Anthony Keeble (University of Oxford)
pDEST14-SpyCatcher003	His_6 Tag-TEV protease cleavage site-SpyCatcher003	133447	MN433887	(Keeble et al., 2019)
pDEST14-SpyCatcher003 S49C	His_6 tag-TEV protease cleavage site-SpyCatcher003 S49C	133448	–	(Vester et al., 2022)
pDEST14-SpyCatcher003 S49C E77A	His_6 tag-TEV protease cleavage site-SpyCatcher003 S49C E77A	–	–	This Thesis

pDEST14-SpyCatcher003 S49C S59T E77A	His_6 tag-TEV protease cleavage site-SpyCatcher003 S49C S59T E77A	–	–	This Thesis
pDEST14-SpyCatcher003 S49C E77A V94I	His_6 tag-TEV protease cleavage site-SpyCatcher003 S49C E77A V94I	–	–	This Thesis
pDEST14-SpyCatcher003-TEVs-SpyTag003DA	'Masked SpyCatcher0003'; His_6 tag-SpyCatcher003-TEV protease cleavage site-SpyTag003 D117A	216283	PP341217	Cloned by Dr Anthony Keeble (Driscoll et al., 2024)
pDEST14-DoubleCatcher	DoubleCatcher; His_6 tag-TEV site-SpyCatcher003-$(GSG)_3$ spacer-SpyCatcher003-TEV site-SpyTag003 D117A	216284	PP341218	(Driscoll et al., 2024)
pDEST14-DoubleCatcher SpyTag003DX variants	His_6 tag-TEV site-SpyCatcher003-$(GSG)_3$ spacer-SpyCatcher003-TEV site-SpyTag003 D117X (X = V, S, T, or E)	–	–	This Thesis
pDEST14-DoubleCatcher S59T V94I	His_6 tag-TEV site-SpyCatcher003-$(GSG)_3$ spacer-SpyCatcher003 S59T V94I-TEV site-SpyTag003 D117A	–	–	This Thesis
pDEST14-DoubleCatcher ΔRGV	His_6 tag-TEV site-SpyCatcher003-$(GSG)_3$ spacer-SpyCatcher003-TEV site-SpyTag003 ΔRGV D117A	–	–	This Thesis
pDEST14-DoubleCatcher PGP	His_6 tag-TEV site-SpyCatcher003-$(GSG)_3$ spacer-SpyCatcher003-G-TEV site-GPGP-SpyTag003 D117A	–	–	This Thesis
pDEST14-DoubleCatcher BeforeTEV	His_6 tag-TEV site-SpyCatcher003-$(GSG)_3$ spacer-SpyCatcher003-G-TEV site-GGSG-SpyTag003 D117	–	–	This Thesis
pDEST14-DoubleCatcher AfterTEV	His_6 tag-TEV site-SpyCatcher003-$(GSG)_3$ spacer-SpyCatcher003-GSSGS-TEV site-G-SpyTag003 D117	–	–	This Thesis
pDEST14-DoubleCatcher-H-Lock	His_6 tag-TEV site-SpyCatcher003-Helical linker-SpyCatcher003-TEV site-SpyTag003 D117A	216285	PP341219	(Driscoll et al., 2024)
pDEST14-DoubleCatcher-α-Lock	His_6 tag-TEV site-SpyCatcher003 S77C-$(GSG)_3$-SpyCatcher003 S199C-TEV site-SpyTag003 D117A	216286	PP341220	(Driscoll et al., 2024)
pDEST14-DoubleCatcher-β-Lock	His_6 tag-TEV site-SpyCatcher003 L31C-$(GSG)_3$-SpyCatcher003 S163C-TEV site-SpyTag003 D117A	216287	PP341221	(Driscoll et al., 2024)

pDEST14-DoubleCatcher-γ-Lock	His_6 tag-TEV site-SpyCatcher003 G39C-$(GSG)_3$-SpyCatcher003 G200C-TEV site-SpyTag003 D117A	216288	PP341222	(Driscoll et al., 2024)
pDEST14-DoubleCatcher-δ-Lock	His_6 tag-TEV site-SpyCatcher003 Y96C-$(GSG)_3$-SpyCatcher003 Y219C-TEV site-SpyTag003 D117A	216289	216288	(Driscoll et al., 2024)
pDEST14-DoubleCatcher-ε-Lock	His_6 tag-TEV site-SpyCatcher003 K79C-$(GSG)_3$-SpyCatcher003 H211C-TEV site-SpyTag003 D117A	216290	PP341224	(Driscoll et al., 2024)
pDEST14-DoubleCatcher[2]	His_6 tag-TEV site-SpyCatcher003 G42C-$(GSG)_3$-SpyCatcher003 D231C-TEV site-SpyTag003 D117A	–	–	This Thesis
pDEST14-DoubleCatcher[4]	His_6 tag-TEV site-SpyCatcher003 G88C-$(GSG)_3$-SpyCatcher003 G210C-TEV site-SpyTag003 D117A	–	–	This Thesis
pDEST14-DoubleCatcher[6]	His_6 tag-TEV site-SpyCatcher003 D87C-$(GSG)_3$-SpyCatcher003 H211C-TEV site-SpyTag003 D117A	–	–	This Thesis
pDEST14-DoubleCatcher[8]	His_6 tag-TEV site-SpyCatcher003 D87C-$(GSG)_3$-SpyCatcher003 K201C-TEV site-SpyTag003 D117A	–	–	This Thesis
pDEST14-ABD035-SpyCatcher003-TEVs-SpyTag003DA	His_6 tag-ABD035-SpyCatcher003-$(GSG)_3$-SpyCatcher003-TEV site-SpyTag003 D117A	–	–	This Thesis
pET28a-nanoHER2-SpyTag003	Anti-Human epidermal growth factor receptor (HER)2 nanobody-SpyTag003-His_6 tag	216312	PP341234	Nanobody sequence from (Verheije et al., 2013)
pET28a-SnoopTagJr-affiHER3-SpyTag003	His_6-SnoopTagJr-Affibody against HER3-SpyTag003	–	–	Affibody sequence from (Malm et al., 2013), previously cloned by Irsyad Khairil Anuar
pET28a-SnoopTagJr-affiEGFR-SpyTag003	His_6-SnoopTagJr-Affibody against epidermal growth factor receptor (EGFR)-SpyTag003	–	–	Affibody sequence from (Friedman, 2008), previously

				cloned by Irsyad Khairil Anuar
pET28a-SnoopTagJr-affiPDGFRβ-SpyTag003	His_6-SnoopTagJr-Affibody against platelet-derived growth factor receptor β (PDGFRβ)-SpyTag003	–	–	Affibody sequence from (Lindborg et al., 2011), previously cloned by Irsyad Khairil Anuar
pET28a-SnoopTagJr-affiVEGFR2-SpyTag003	His_6-SnoopTagJr-Affibody against vascular endothelial growth factor receptor 2 (VEGFR2)-SpyTag003	–	–	Affibody sequence from (Frejd et al., 2016), previously cloned by Irsyad Khairil Anuar
pET28a-SnoopTagJr-nanoTNFR1-SpyTag003	His_6-SnoopTagJr-nanobody against tumor necrosis factor receptor 1 (TNFR1)-SpyTag003	–	–	Nanobody sequence from (Steeland et al., 2015), previously cloned by Irsyad Khairil Anuar
pHL-HER2	Endogenous HER2 signal peptide-HER2 extracellular domain (ECD)-human IgG Fc domain fusion-His_6 tag	–	–	Cloned previously by Dr Jayati Jain (University of Oxford).
pTT3-ALB-bio-His	Human Serum albumin precursor ectodomain-rat CD4d3+4 tag-biotinylation sequence-His_6 tag	52176	–	Fab sequence from (Sun et al., 2015)
pcDNA3.1-Tras heavy chain-GSG-SpyTag003	pHLsec signal peptide-hu4D5 D102W Heavy-GSG-SpyTag003-His_6 tag. With Tras light chain, forms Tras-SpyTag003.	216292	ON131076	Cloned previously by Jamie Lam (University of Oxford) from similar constructs in pOPIN which have been described (Vester et al., 2022).
pcDNA3.1-Tras heavy chain-SpyTag003	pHLsec signal peptide-hu4D5 D102W Heavy-SpyTag003-His_6 tag. With Trastuzumab (Tras) light chain, Tras NoLink-SpyTag003	216293	PP341237	
pcDNA3.1-Tras light chain	pHLsec signal peptide-hu4D5 V_L– Human kappa C_L	216294	ON131084	
pcDNA3.1-39S Heavy chain-SpyTag003	pHLsec signal peptide-39S V_H-Human IgG1 CH1-SpyTag003-His_6 tag	216296	PP341226	Fab sequence from (Oganesyan et al., 2018)
pcDNA3.1-39S Light chain	pHLsec signal peptide-39S V_L-Human kappa C_L	216297	PP341227	
pcDNA3.1-MF3958 Heavy chain-SpyTag003	pHLsec signal peptide-MF3958 V_H-Human IgG1 CH1-SpyTag003-His_6 tag	216303	PP341228	Fab sequence from (Geuijen et al., 2018)
pcDNA3.1-MF3958 Light chain	pHLsec signal peptide-MF3958 V_L-Human kappa C_L	216304	PP341229	

pcDNA3.1-H2-18 Heavy chain-SpyTag003	pHLsec signal peptide-H2-18 V_H-Human IgG1 CH1-SpyTag003-His_6 tag	216307	PP341230	Fab sequence from (Hu et al., 2015)
pcDNA3.1-H2-18 Light chain	pHLsec signal peptide-H2-18 V_L-Human kappa C_L	216308	PP341231	
pcDNA3.1-Pert Heavy chain-SpyTag003	pHLsec signal peptide-Pertuzumab (Pert) V_H-Human IgG1 CH1-SpyTag003-His_6 tag	216309	PP341232	Fab sequence from (Gennaro et al., 2014)
pcDNA3.1-Pert Light chain	pHLsec signal peptide-Pert V_L-Human Kappa C_L	216310	PP341233	
pcDNA3.1-RNF43-90 Heavy chain-SpyTag003	pHLsec signal peptide-RNF43-90 V_H-Human IgG1 CH1-SpyTag003-His_6 tag	–	–	Fab sequence from (Agard et al., 2022), previously cloned by Qize Yang (Howarth group, University of Cambridge)
pcDNA3.1-RNF43-90 Light chain	pHLsec signal peptide-RNF43-90 V_L-Human IgG1 kappa light domain	–	–	

2.1.1 Gene and oligonucleotide synthesis

DNA oligonucleotide primers and gene fragments were designed in Benchling (https://www.benchling.com/). Desiccated oligonucleotides and a gBlock gene fragment encoding DoubleCatcher were obtained from Integrated DNA Technologies (IDT, Leuven, Belgium). Gene fragments encoding the variable heavy and variable light chains of anti-HER2 Fabs 39S, MF3958, HFS2, H2-18 and Pert; and anti-RN43 Fab RNF43-90 were obtained from Twist Bioscience. Oligonucleotides were resuspended in nuclease-free water (Promega) to obtain a DNA concentration of 100 µM and gene fragments were resuspended to a concentration of 100 ng/µL.

2.1.2 Polymerase Chain Reaction (PCR)

PCR reactions were performed with Q5 High-Fidelity 2× Master mix (NEB), with the following composition: 5 ng of template DNA, 0.5 µM forward and reverse primers, 25 µL 2×Q5 High-Fidelity master mix, made up to a total volume of 50 µL with nuclease-free water (Promega). A C1000 Thermal Cycler (Bio-Rad) was used with the following thermocycling

settings: initial denaturation at 95 °C for 60 s followed by 32 cycles of denaturation at 95 °C for 30 s, primer annealing at 60-68 °C for 30 s and elongation at 72 °C for 40 s per kb, and one final elongation step at 72 °C for 5 min.

2.1.3 Agarose gel electrophoresis and gel extraction

PCR reaction mixtures of 50 µL total volume were mixed with 10 µL of 6× DNA loading dye (10 mM Tris-HCl pH 7.4, 0.15% (w/v) orange G, 60% (v/v) glycerol, 60 mM EDTA) and loaded on 0.7-1.4% (w/v) agarose gels, according to the expected amplicon size, containing 0.007% (v/v) SYBR Safe (Thermo Fisher Scientific). Gels were run at 130 V for 45 min in TAE buffer (40 mM Tris base, 20 mM acetic acid, 1 mM EDTA pH 8.0). Agarose gels were imaged using a ChemiDoc XRS+ Imager (Bio-Rad) with an XcitaBlue Conversion Screen and Filter (Bio-Rad), or iBright FL1500 imaging system (Thermo Fisher). Bands of the correct size were excised and amplicon DNA was extracted using the Wizard SV Gel and PCR Clean-Up Kit (Promega). DNA concentrations were determined using a NanoDrop ND-1000 or NanoDrop One Spectrophotometer (Thermo Fisher).

2.1.4 Gibson assembly

PCR fragments were assembled into a circular plasmid according to the standard Gibson assembly protocol (Gibson et al., 2009), using a 2× Gibson assembly master-mix made in house according to the original protocol. To assemble the reaction mixture, Phusion-like DNA polymerase (Wang et al., 2004) and Taq DNA ligase were cloned, expressed, and purified by Karl Brune (Howarth group, University of Oxford), and T5 exonuclease was purchased from New England Biolabs (NEB). For standard insertion of a gene into a vector, gel-purified PCR products were mixed in a 3:1 mass ratio (450 fmol insert:150 fmol backbone vector) and made up to a volume of 10 µL with nuclease-free water on ice. 10 µL of the 2× Gibson assembly

master-mix was then added, and reactions were incubated for 2 h at 50 °C in a pre-heated C1000 Thermal Cycler (Bio-Rad).

2.1.5 E. coli transformation by heat shock

50 µL chemically competent NEB Turbo *E. coli* cells (New England Biolabs), *E. coli* DH5α (Life Technologies), or XL1-Blue cells (Agilent) were thawed on ice for 10-20 min, to which 8 µL of Gibson assembly reaction mixture, or 1 µL of supercoiled purified plasmid, was then added. Tubes containing cells and DNA were flicked to ensure sufficient mixing, and incubated on ice for another 20 min. Cells were then heat-shocked by placing tubes in a 42 °C water bath for 45 s, and quickly transferring them back on ice for 2 min. Cells were recovered by the addition of 300 µL Super Optimal broth with Catabolite repression (SOC) outgrowth media (2% (w/v) Tryptone, 0.5% (w/v) Yeast extract, 10 mM NaCl, 2.5 mM KCl, 10 mM $MgCl_2$, 10 mM $MgSO_4$, 20 mM Glucose, in Milli-Q water). Cells transformed with ampicillin-resistant plasmids were incubated at 25 °C for 5-10 min, before plating directly onto ampicillin (100 µg/mL)-containing LB agar plates. Cells transformed with kanamycin-resistant plasmids were incubated at 37 °C for 1 h, before plating onto plates containing 50 µg/mL kanamycin. All agar plates containing bacterial transformants were incubated at 37 °C for 16-18 h.

2.1.6 Plasmid purification

11 mL aliquots of LB media (high salt for ampicillin; low salt for kanamycin) supplemented with 100 µg/mL ampicillin or 50 µg/mL kanamycin were inoculated with single colonies from transformed bacteria on selection plates. NEB Turbo Competent *E. coli* cells (New England Biolabs) were grown for 4-6 h at 37 °C in a shaking incubator, while *E. coli* DH5α and *E. coli* XL1-Blue cells were grown for 16-18 h at 37 °C, before cells were pelleted by centrifugation (4,000 *g*, 10 min, 4 °C). Plasmid DNA was extracted from the cells using the GeneJET Plasmid

Miniprep Kit (Thermo Fisher). For the preparation of purified plasmid DNA for Expi293 transfection, 200 mL of culture was grown from a single transformant colony and pelleted at 4000 *g* for 10 min at 4 °C, from which plasmid was extracted using the PureLink Fast Low-Endotoxin Midi Plasmid Purification Kit (Invitrogen). The concentration of purified plasmid DNA was quantified using the NanoDrop ND-1000 or NanoDrop One (Thermo Fisher).

2.1.7 Plasmid sequencing

All plasmid constructs described in this Thesis were validated by Sanger sequencing by Source BioScience (Cambridge, UK), or Genewiz (Leipzig, Germany), followed by sequence alignment with the predicted sequence using Nucleotide BLAST (NCBI).

2.2 Protein expression and purification

2.2.1 Media and growth conditions

E. coli growth media was first obtained from the Media Glassware Sterilisation Laboratory of the Department of Biochemistry, University of Oxford, and then from the Media Kitchen of The Gurdon Institute, University of Cambridge. Low salt LB media was composed of 5 g tryptone, 5 g yeast extract, and 10 g NaCl dissolved in Milli-Q water to a final volume of 1 L and then adjusted to pH 7.0. Addition of a further 5 g NaCl to this mixture produced high salt LB media. 2×TY was composed of 16 g tryptone, 10 g yeast extract, and 5 g NaCl, dissolved in Milli-Q water to a final volume of 1 L and pH-adjusted to 7.0. All media were subjected to sterilisation by autoclaving at 121 °C for 20 min and stored at 25 °C thereafter. Cells were grown in an Infors Multitron shaker (Infors HT) with a 2.5 mm throw at 200 rpm.

Expi293F mammalian cells were cultured in Expi293 Expression Medium (Thermo Fisher) supplemented with 50 U/mL penicillin and 50 µg/mL streptomycin and grown in a humidified

Multitron Cell incubator (Infors HT) at 37 °C with 8% (v/v) CO_2 and shaking at 125 rpm in 125 mL flasks (Corning). Cells were routinely grown to a density of 3-5×10^6 cells/mL and passaged to a density of 0.3-0.5×10^6 cells/mL. For protein expression, transfected cells were grown under the same conditions, unless expression was performed in 50 mL mini bioreactor tubes (Corning), when they were grown with shaking at 240 rpm.

2.2.2 Protein expression

2.2.2.1 Bacterial expression

pDEST14 constructs were transformed into chemically competent *E. coli* C41 (DE3), gifted by Anthony Watts (University of Oxford), except for the pDEST14-SpyCatcher003-SpyCatcher003-TEV site-SpyTag003DA disulfide-containing mutants ('DoubleCatcher disulfide-Lock' variants), which were transformed into chemically competent *E. coli* T7SHuffle (NEB). pET21 and pET28a constructs were transformed into chemically competent *E. coli* BL21 (DE3) (Agilent Technologies), with the exception of pET28a-SnoopTag-AffiHER2-SpyTag, which was transformed into chemically competent *E. coli* T7 Express (NEB). Colonies were picked into 10 mL LB containing either 100 μg/mL ampicillin (pDEST14) or 25-50 μg/mL kanamycin (pET28a/pET21), and grown at 37 °C at 200 rpm for 4-16 h. Starter cultures were diluted 100-fold into either 1 L LB supplemented with appropriate antibiotic and 0.8% (w/v) glucose (C41, BL21 (DE3)), 1 L LB supplemented with antibiotic alone (T7 Express only), or 2×TY supplemented with antibiotic and 0.5% (w/v) glycerol (T7SHuffle only), and grown at 37 °C with shaking at 200 rpm. Culture OD_{600} was monitored by spectrophotometry until OD_{600} 0.5-0.6 was reached, at which point expression was induced with 0.42 mM isopropyl β-D-1-thiogalactopyranoside (IPTG; Fluorochem). pDEST14-transformed cultures were incubated for 4 h at 30 °C and 200 rpm, while all other cultures were

incubated for 16 h at 18 °C and 200 rpm post-induction. Cells were harvested by centrifugation at 4,000 *g* for 15 min at 4 °C, and pellets were stored at -80 °C until purification.

2.2.2.2 Mammalian expression

Proteins encoded in pcDNA3.1 or pOPIN vectors were expressed by transient transfection in suspension Expi293 cells (Thermo Fisher), using the ExpiFectamine 293 Transfection Kit (Thermo Fisher), following the manufacturer's protocol. Briefly, the day before transfection (and after ≥ 3 passages since thawing), cells were diluted to 2.5-3×10^6 cells/mL and grown overnight at 37 °C with 8% (v/v) CO_2 and shaking at 200 rpm. The following day, cells were pelleted by centrifugation (300 *g* for 5 min) and resuspended in antibiotic-free Expi293 Expression Medium to a final density of 3×10^6 cells/mL, before being transfected with a 1:2 mixture of midiprepped Fab heavy chain plasmid DNA (0.5 µg DNA/mL culture volume):Fab light chain plasmid DNA (1 µg DNA/mL culture volume) pre-incubated with ExpiFectamine 293 reagent. For the expression of HER2-Fc, a plasmid concentration of 1 µg DNA per mL culture volume was used for transfection. Cells were then grown at 37 °C with 8% (v/v) CO_2 and shaking as described in Section 2.2.2.1. ExpiFectamine 293 Transfection Enhancers 1 and 2 were added 20 h post transfection and cultures were incubated for 5 days post-transfection, until cell viability fell below 50%. For harvesting protein, cell supernatants were supplemented with cOmplete, Mini, EDTA-free Protease Inhibitor Cocktail (Roche) and clarified by centrifugation at 4,000 *g* at 4 °C, followed by filtration through a 0.22 µm syringe filter (Thermo Fisher). One tenth supernatant volume of Ni-NTA wash buffer (50 mM Tris-HCl pH 7.8, 300 mM NaCl, 10 mM imidazole) was added to filtered supernatant, which was then pH-adjusted to pH 7.6 using 1 M Tris-HCl pH 8.0. Supernatants were stored at -80 °C until purification.

2.2.3 Ni-NTA purification of soluble proteins bearing a His6-tag

After thawing, bacterial cell pellets were resuspended in 1×Ni-NTA buffer (50 mM Tris-HCl pH 7.8, 300 mM NaCl), supplemented with cOmplete, Mini, EDTA-free Protease Inhibitor Cocktail (Roche) and 1 mM phenylmethylsulfonyl fluoride (PMSF), and lysed by sonication on ice (60 s with a 50% duty cycle at 30%-40% output, repeated 3-5 times) using a Sonics Vibra-Cell sonicator (Ultrasonic Processor). SpyCatcher003 S49C variants and DoubleCatcher disulfide-Lock variants were further supplemented with 10 mM 2-mercaptoethanol to reduce any disulfide bonds to other proteins. Clarified cell lysates were centrifuged at 30,000 *g* for 30 min at 4 °C and adjusted to pH 7.6, using 1 M Tris-HCl pH 8.0, before purification by Ni-NTA affinity chromatography (Qiagen), using 0.5 mL Ni-NTA resin per 1 L expression culture. From this point onwards, clarified mammalian supernatants and bacterial lysates were purified identically. Elution of all proteins was performed in the absence of 2-mercaptoethanol. For all protein preparations that will be used for mammalian cell treatment, including SpyTagged binding molecules, DoubleCatcher variants, MBP-SuperTEV, and SpyCatcher003 S49C variants, the following washes were performed directly prior to elution: 50 column volumes (CV) wash buffer (50 mM Tris-HCl pH 7.8, 300 mM NaCl, 10 mM imidazole) + 0.1% (v/v) Triton X-114, followed by 10 CV wash buffer. Eluted proteins were dialysed three times against phosphate buffered saline (PBS; 137 mM NaCl, 2.7 mM KCl, 10 mM Na_2HPO_4, 1.8 mM KH_2PO_4) pH 7.4 in 3.5 kDa molecular weight cut-off (MWCO) Spectra/Por tubing (Spectrum Labs) at 4 °C. SpyCatcher003 S49C variants to be coupled to resin were instead dialysed into their size-exclusion chromatography running buffer (50 mM Tris-HCl pH 8.5 (25 °C), 5 mM EDTA, 1-2 mM tris(2-carboxyethyl)phosphine (TCEP)). Protein concentrations were determined from A_{280} using extinction coefficients predicted from ExPASy ProtParam. If necessary, purified proteins were concentrated using a pre-washed centrifugal concentrator (GE Healthcare).

2.2.4 SpySwitch purification of soluble proteins bearing a SpyTag

E. coli cell pellets from MBP_X-MBP_X-SpyTag003 or $AffiHER2_3$-SpyTag expressions were lysed and clarified as outlined above, except thawed pellets were resuspended in SpySwitch buffer (50 mM Tris-HCl pH 7.5, 300 mM NaCl). SpySwitch purifications were performed at 4 °C, as described (Vester et al., 2022). Briefly, SpySwitch resin (0.75 mL per 1 L bacterial culture) was equilibrated with 2×10 CV SpySwitch buffer, prior to addition to clarified cell lysate and incubation on an end-over-end rotator for 1 h at 4 °C, after which resin was washed with 4×10 CV SpySwitch buffer. pH-dependent elution was performed by six cycles of resin incubation with 1.5 CV SpySwitch elution buffer (50 mM acetic acid, 150 mM NaCl, pH 5.0) for 5 min each, passing the flow-through directly into 0.3 CV aliquots of 1 M Tris pH 8.0 for immediate neutralisation. Proteins were subsequently dialysed into PBS pH 7.4 as for Ni-NTA-purified samples.

2.2.5 Endotoxin depletion by phase separation

Prior to assembly of bispecific molecules with DoubleCatcher for mammalian cell treatment, any protein preparations that had not been subjected to Triton X-114-containing washes during purification were purified from endotoxin by phase separation with Triton X-114 (Aida and Pabst, 1990). Purified protein samples were aliquoted into 1.5 mL endotoxin-free microcentrifuge tubes (StarLab, cat. E1415−1510), to which 1% (v/v) Triton X-114 was added. Samples were incubated on ice for 5 min, until all Triton X-114 was dissolved. Samples were then incubated at 37 °C for 5 min and centrifuged for 1 min at 16,000 *g* at 37 °C. The supernatant was removed by pipetting, and the entire procedure was repeated twice. Endotoxin concentrations of all protein samples that were to be added to mammalian cells were determined using the Limulus amebocyte lysate (LAL) Chromogenic Endotoxin Quantitation

Kit (Thermo Fisher) according to the manufacturer's instructions, which confirmed the endotoxin level to be below 1 endotoxin unit/mL.

2.2.6 Size-exclusion chromatography

Ni-NTA- or SpySwitch-purified protein samples were injected onto a HiLoad 16/600 Superdex 200 pg column (DoubleCatcher variants; GE Healthcare), or a HiLoad 16/600 Superdex 75 pg column (SpyCatcher003 S49C variants, SpyTag003-linked non-antigen binding proteins, nanobodies, and affibodies; GE Healthcare). Columns were pre-equilibrated with running buffer (PBS pH 7.4 for all samples except SpyCatcher003 S49C variants, whose running buffer was 50 mM Tris-HCl pH 8.5 (25 °C), 5 mM EDTA, 1-2 mM TCEP). Samples were run on an ÄKTA Pure 25 (GE Healthcare) fast protein liquid chromatography instrument with a flow rate of 0.5–1 mL/min in PBS pH 7.4 at 4 °C. Before SpyCatcher003 S49C variants were loaded onto to the column, samples were spiked with 2 mM TCEP to reduce the formation of disulfide-linked dimers. The absorbance of column elutions was recorded at 230 nm, 260 nm, and 280 nm. Each column was calibrated using 660 kDa to 1.35 kDa molecular weight protein standards (thyroglobulin, IgG, ovalbumin, myoglobin, and vitamin B12) (Bio-Rad). Following A_{280} peak analysis by SDS-PAGE, fractions containing purified protein at the expected molecular weight were pooled and, if necessary, concentrated using Vivaspin 20 centrifugal filters (Cytiva) at 4 °C, before long-term storage at -80 °C.

2.2.7 Quantification of protein concentration

Protein concentrations were estimated using their absorbances at 280 nm measured by a NanoDrop ND-1000 or NanoDrop One Spectrophotometer (Thermo Fisher) Spectrophotometer. The extinction coefficient of proteins were predicted by ExPASy ProtParam (Wilkins et al., 1999).

Typical yield for SpyCatcher003-containing protein constructs was 10-25 mg per L of culture. A typical yield for affibody expression was ~3 mg per L of culture and 30 mg per L for nanobody expressions. Expression of SpyTag003-fused, non-antigen binding proteins yielded 5-15 mg protein per L of culture, while expression of SpyTag003-fused Fabs from mammalian culture ranged from 6 to 156 mg per L of culture.

2.3 Protein Characterisation

2.3.1 Polyacrylamide gel electrophoresis (PAGE)

SDS-PAGE was performed using 8, 10, 12, 14, or 16% Tris-glycine polyacrylamide gels or precast 4-12% NuPAGE Bis-Tris gradient gels (Thermo Fisher) in XCell SureLock Mini-cell gel chambers (Thermo Fisher). Before loading onto gels, samples were mixed with 6×SDS loading buffer (0.23 M Tris-HCl pH 6.8, 24% (v/v) glycerol, 120 µM bromophenol blue, 0.23 M SDS) and boiled at 99 °C for 3 min. For reducing samples, 10-100 mM 1,4-dithiothreitol (DTT) was added to samples prior to boiling. Tris-glycine gels were run at 200 V in 25 mM Tris-HCl pH 8.5, 192 mM glycine, 0.1% (w/v) SDS, while Bis-Tris gels were run in 1×NuPAGE MOPS SDS Running Buffer (Thermo Fisher). Gels were stained with Coomassie Brilliant Blue G-250 for 2-16 h and destained with Milli-Q H_2O prior to imaging on a ChemiDoc XRS+ imager. ImageLab 6.1.0 software (Bio-Rad) was used for densitometric quantification of bands, with background subtraction at 1.2 mm disk size. For imaging on an iBright FL1500 imaging system (Invitrogen), analysis was performed using iBright Analysis Software (Thermo Fisher).

2.3.2 Intact protein Mass Spectrometry

2.3.2.1 RapidFire

Intact protein mass spectrometry in positive ion mode was performed using a RapidFire 365 jet-stream electrospray ion source (Agilent) coupled to a 6550 Accurate-Mass Quadrupole Time-of-Flight (Q-TOF) (Agilent) mass spectrometer. Mass spectrometry experiments were performed by Dr Anthony Tumber (Department of Chemistry, University of Oxford). 50 µL protein samples at 10 µM in PBS pH 7.4 were prepared on a 384-well polypropylene plate (Greiner). Samples were acidified to 1% (v/v) formic acid, before aspiration under vacuum for 0.4 s and loading onto a C4 solid-phase extraction cartridge. Samples were washed with 0.1% (v/v) formic acid in water (1.5 mL/min flow rate for 5.5 s), before being eluted to the Q-TOF detector with deionised water containing 85% (v/v) acetonitrile and 0.1% (v/v) formic acid (1.25 mL/min flow rate for 5.5 s). The cartridge was equilibrated with deionised water for 0.5 s. Nitrogen drying gas for the ionisation source was operated at 780 L/h at 225 °C, with a jet stream sheath gas flow-rate of 12 L/min at 350 °C, and a nozzle voltage of 1,500 V. Data were analysed using Mass Hunter Qualitative Analysis software B.07.00 (Agilent). Expected molecular weights for full-length proteins were calculated using the ExPASy ProtParam tool, with the N-terminal fMet (bacterial expression) or signal peptide sequence (mammalian expression) removed. Signal peptide cleavage sites were predicted using SignalP 6.0 (Nielsen et al., 2019). Minor +178 Da peaks are observed where spontaneous post-translational gluconoylation has occurred, which is common in proteins overexpressed in *E. coli* BL21 (Geoghegan et al., 1999). A mass difference of -2 Da was predicted for the formation of each disulfide bond.

2.3.2.2 Liquid Chromatography-Quadrupole Time of Flight

DoubleCatcher γ-Lock, SpyTag-(AffiHER2)$_3$, Pert-SpyTag003, RNF43-90 Fab-SpyTag003, AffiEGFR-SpyTag003, Trastuzumab, and all DoubleCatcher-assembled bispecific molecules were analysed using an UPLC system (Aquity) with an UPLC BEH300 C4 column (1.7 µm,

2.1 × 50 mm; Acquity) coupled to a Xevo G2-S Q-TOF (Waters Corporation) mass spectrometer. 30 µL protein samples at 1 µM in PBS pH 7.4 were prepared in UPLC autosampler vials (Fisher Scientific). Samples were run with a flow rate of 0.2 mL/min with a mobile phase constituted of water with 0.1% (v/v) formic acid (aq.) (Solvent A) and 95% (v/v) acetonitrile with 5% (v/v) water with 0.1% (v/v) formic acid (aq.) (Solvent B). The following gradient was executed: 95% (v/v) A for 0.93 min, then a gradient to 100% (v/v) B over 4.28 min, then 100% B for 1.04 min, then finally a gradient to 95% A over 1.04 min for elution to the Q-TOF detector. Nitrogen desolvation gas for the ionisation source was operated at 850 L/h, with the nozzle operating at a capillary voltage of 2,000 V and a cone voltage of 190 V. Data were processed using MassLynx software V4.2 SCN 971 (Waters) for Waters mass spectrometry systems; protein ionisation data were processed using Waters' maximum entropy deconvolution algorithm (MaxEnt 1), analysing only the region of the total ion chromatogram containing protein signals. For DoubleCatcher-assembled bispecific molecules, the loss of two water molecules (-36 Da) was factored into the calculation to account for formation of two isopeptide bonds. Trastuzumab-containing samples were deglycosylated with PNGase F (NEB) prior to analysis by LC-MS, by 20 µg protein sample with 2,500 units PNGase for 24 h at 37 °C, as per the manufacturer's protocol.

2.3.3 Dynamic Light Scattering

Aggregates were removed from size-exclusion chromatography-purified protein samples by centrifugation at 16,900 *g* for 30 min at 4 °C. First, samples were filtered through 0.33 mm diameter sterile syringe filters with a 0.22 µm hydrophilic polyvinylidene difluoride (PVDF) membrane (Sigma-Aldrich). Immediately after filtration, samples were diluted to a final concentration of 25 µM for protein samples > 35 kDa, or 75 µM for samples < 35 kDa into sterile filtered PBS pH 7.4. 20 µL diluted sample was loaded into a reusable quartz cuvette,

allowed to acclimatise to 20 °C, and measurements (10 scans of 10 s each) were recorded using a Viscotek 802 (Viscotek) at 20 °C. Data were analysed using OmniSIZE 3.0 software (Viscotek), by normalising the intensity of the size distribution to the main peak and calculating the mean and standard deviation from the multiple scans.

2.3.4 Mass Photometry

Microscope coverslips (24 × 50 mm; Menzel Gläser) and silicone gaskets (6 mm × 1 mm, GBL103280; Grace Bio-Labs) were cleaned by sequential sonication, first in 50% (v/v) isopropanol, and then Milli-Q water (5 min each), and dried under a clean nitrogen stream before assembly into flow chambers as described (Young et al., 2018). Data were acquired on a Refeyn TwoMP mass photometer (Refeyn Ltd). Immediately prior to mass photometry measurements, protein samples were diluted into freshly prepared and degassed sample buffer (PBS pH 7.4, 300 mM NaCl, 0.5% (v/v) glycerol, 1 mM NaN_3), that had been sterile filtered through a 0.22 μm pore-size syringe filter (Thermo Fisher). Before measurements were taken from a new coverslip, a dynamin protein mass standard (MS1000 20-40×), diluted into sample buffer, was used to calibrate the mass photometer (Foley et al., 2021). The focal position of the microscope was found in flow chambers containing 20 μL sample buffer, from which 0.5-10 μL was then replaced with an equivalent volume protein sample to achieve a final working concentration of 2-50 nM, to account for differences in the dissociation characteristics of different proteins. After ≤ 10 s, images were acquired for 60 s at 331 Hz; each sample was measured at least twice independently. Data were processed using DiscoverMP v1.2.3 (Refeyn Ltd) (Foley et al., 2021). Masses were plotted as mass histogram (bin width = 2.5 kDa), before fitting to Gaussian non-linear regression curves in GraphPad Prism 9 (GraphPad Software). Gaussian fitting extracts the mean masses of each protein subpopulation within the heterogeneous sample. Expected molecular weights for protein constituents were calculated

using ExPASy ProtParam, with the N-terminal fMet (bacterial expression) or signal peptide sequence (mammalian expression) removed.

2.3.5 Protein structural prediction and visualisation

PyMOL (version 2.5.4, Schrödinger) was used for the visualisation of protein structures. The structure of HER2 was reconstructed in PyMOL from PDB ID 1N8Z (extracellular domain) (Cho et al., 2003), 2KS1 (transmembrane domain) (Mineev et al., 2010), and 3PP0 (kinase domain) (Aertgeerts et al., 2011) by manually connecting the termini of adjacent domains as previously (Goodsell, 2022). With the exception of HFS2 and nanoHER2, the anti-HER2 binders had previously resolved crystal structures: Tras, PDB ID 1N8Z (Cho et al., 2003); Pert, PDB ID 1S78 (Franklin et al., 2004); 39S, PDB ID 6ATT (Oganesyan et al., 2018); MF3958, PDB ID 5O4G (Geuijen et al., 2018); H2-18, PDB ID 3WLW (Hu et al., 2015); and AffiHER2, PDB ID 3MZW (Eigenbrot et al., 2010). All structures displayed for DoubleCatcher variants were initially predicted using ColabFold versions 1.3 and 1.5.2 (Mirdita et al., 2022), and validated using AlphaFold version 2.3.1 (Jumper et al., 2021; Zhong et al., 2022) or AlphaFold version 3 (Abramson et al., 2024) for the generation of structures shown in this Thesis. Twenty five structural models for HER2 ECD in complex with nanoHER2 were predicted using AlphaFold-multimer (Evans et al., 2022; Jumper et al., 2021; Zhong et al., 2022). Docking predictions were performed using the full-length protein sequence.

For all AlphaFold2/3-simulated structures of the DoubleCatcher variants, the model predicted with the highest confidence is presented. To simulate vectors that depict the docking site and directionality of SpyTag003 within DoubleCatcher variants, the modevectors PyMOL Plugin was used to linearly connect Ser57 to His53 (N-terminal SpyCatcher003) and Ser179 to His175 (C-terminal SpyCatcher003) by their carbonyl main-chain oxygens (Law, 2020)

(DoubleCatcher numbering). The vector arrowhead represents the N-terminus of the SpyTag003 peptide. As such, a ligand with a C-terminal SpyTag003 would project from the arrowhead of the vector when coupled to DoubleCatcher.

2.4 Synthesis of immobilised covalent SpyCatcher003 for purification

SpyCatcher003 S49C-derived variants were attached to SulfoLink Coupling Resin (Thermo Fisher) according to the manufacturer's instructions, with the following changes: SpyCatcher003 S49C variants in coupling buffer were concentrated to ≥ 20 mg/mL using a Vivaspin 20 5 kDa MWCO centrifugal filter at 4 °C, then reduced with 1 mM TCEP for 30 min at 25 °C before incubation with SulfoLink Coupling Resin at a concentration of 20 mg reduced protein/mL packed resin. Additionally, following washes with 1 M NaCl, the coupled resin was washed with 2 CV TP buffer (25 mM orthophosphoric acid adjusted to pH 7.0 with Tris base) to remove any SpyCatcher003 S49C-derived variant that had bound non-covalently to the resin. Lastly, coupled resin was stored in 20% (v/v) ethanol in PBS pH 7.4 at 4 °C for ≤ 3 months.

2.5 Mammalian cell culture

SKBR3 cells (HTB-30; a HER2-positive breast cancer cell line) and MDA-MB-468 (HTB-132; a HER2-negative breast cancer cell line) were purchased from ATCC. BT474 cells were from Cancer Research UK, Lincoln's Inn Fields. SKBR3 and MDA-MB-468 cells were grown in complete Dulbecco's Modified Eagle Medium–high glucose (DMEM) (DMEM supplemented with 10% (v/v) fetal bovine serum (FBS), 100 U/mL penicillin and 100 µg/mL streptomycin (1 × pen/strep; Sigma-Aldrich), 1% (v/v) GlutaMAX (Thermo Fisher)) at 37 °C and 5% (v/v) CO_2. BT474 cells were grown in complete RPMI (RPMI-1640 supplemented with 10% FBS, 1 × pen/strep, and insulin (5 µg/mL; Sigma-Aldrich)) at 37 °C and 5% (v/v)

CO_2. Cells were passaged at 70-80% confluency and were sub-cultured for fewer than 3 months. All cell-lines were validated as mycoplasma-negative by PCR.

2.6 Isopeptide bond reconstitution reactions

All reactions between SpyCatcher002/3, SpyCatcher002/3-conjugates, Masked SpyCatcher003, or DoubleCatcher and SpyTag/003-linked protein were carried out in triplicate in PBS pH 7.4, and repeated at least once under similar or identical reaction conditions. At each time-point or end-point indicated, reactions were quenched by adding 6×SDS loading buffer (0.23 M Tris-HCl pH 6.8, 24% (v/v) glycerol, 120 μM bromophenol blue, 0.23 M SDS), with subsequent heating at 95 °C for 5 min in a pre-heated C1000 Thermal Cycler (Bio-Rad). Reactions were analysed by SDS-PAGE with Coomassie staining and the depletion of SpyCatcher003-derived reactant over time was quantified by densitometry when required. For time-course reactions, the extent of reaction between binding partners at each time point is defined as 100 × [SpyCatcher003-derived reactant / average density of SpyCatcher003-derived reactant in triplicate control lanes]. The control lanes contain SpyCatcher003-containing partner alone. To quantify the extent of disulfide-bond formation within DoubleCatcher disulfide-Lock variant monomers, densitometry was applied to calculate the relative density of the 'oxidised monomer' as a percentage of the sum of densities of oxidised monomer and reduced monomer in that lane.

2.7 Assembly of dimeric molecules using DoubleCatcher

With the exception of time-course assays, the assembly of bispecific molecules from two SpyTag(003)-linked ligands of interest, '**A'** and '**B**', was performed in 100-300 μL total volume per well in 96-well Nunclon Delta-Treated, Flat-Bottom cell culture plates (Thermo Scientific, cat. 167008). All reactions were carried out in PBS pH 7.4 as follows: Step 1) DoubleCatcher

variant with concentration *N* (here, *N* = 1–20 μM) was first mixed with 1.25 × *N* **A**-SpyTag003 for 2 h at 37 °C with shaking at 550 rpm in a Thermomixer C (Eppendorf); Step 2) 5 × *N* **B**-SpyTag003 and 1/12 × *N* MBP-SuperTEV were added to the reaction mixture simultaneously and incubated for 4 h at 34 °C with shaking at 550 rpm; Step 3) 40 μL packed SulfoLink resin coupled to SpyCatcher003 S49C (washed thrice in PBS pH 7.4) per 1 mg unreacted SpyTag003-linked protein was added directly to the reaction mixture and incubated for 16 h at 4 °C with shaking at 550 rpm, to remove excess unreacted SpyTag003-linked binders from solution. For the removal of MBP-SuperTEV from solution, 330 mL packed Amylose Resin (NEB, cat. E8021S; thrice washed in PBS pH 7.4) per milligram of MBP-SuperTEV was added to the reaction mixture and incubated at 16 h at 4 °C. Plates were finally centrifuged at 1,000 *g* for 5 min, so the supernatant containing purified bispecific reaction mixtures could be separated from resin by aspiration and stored at -80 °C, if long-term storage was required.

2.8 Design of DoubleCatcher disulfide-containing variants

Original ColabFold version 1.3 predictions for the structure of DoubleCatcher generated five output structures. In each model, both SpyCatcher003 domains were consistently well-folded with high confidence (predicted local distance difference test (pLDDT) > 80), with structures that aligned near-identically to the X-ray crystal structure of SpyCatcher (PDB ID 4MLI (Li et al., 2014)). However, owing to the low certainty (pLDDT = 22-25) in the predicted structure of the flexible $(GSG)_3$ linker separating the two SpyCatcher003 moieties, the relative position of the C-terminal Catcher with respect to the N-terminal Catcher varied considerably across the five models. As the average pLDDTs for each structure showed minimal variation (pLDDT range = 60.1-54.9), it was not possible to assign one model to the orientation of DoubleCatcher in solution with high confidence, but instead it is concluded that each conformation may be sampled with a similar probability. Therefore, for the introduction of an intramolecular

disulfide bond within DoubleCatcher, I identified two unique pairs of residues for cysteine substitution from each of the five ColabFold models to generate two disulfide-Lock DoubleCatcher variants per model (except model_3, which yielded one disulfide variant). Within each pair, one residue was from the N-terminal Catcher, and the other was from the C-terminal Catcher. Pairs of residues were selected if they were proximal (< 1.5 nm between alpha carbons), resided in loops (ideally near the terminus of a loop to prevent substantial movement around the disulfide bond), and did not contribute to the enhanced reactivity of SpyCatcher003 fold for SpyTag (Keeble et al., 2019). Therefore, DoubleCatcher model_1 resulted in DoubleCatcher disulfide-Lock variants [1] and [2], model_2 yielded [3] and [4], model_3 yielded [5], model_4 yielded [6] and [7], and model_5 yielded [8] and [9]. Cysteine substitution mutations for DoubleCatcher disulfide-Lock variants were designed into primers and variants were subsequently cloned from pDEST14-DoubleCatcher by 3-part Gibson assembly.

2.9 Metabolic activity assay

One day prior to treatment, BT474 or SKBR3 cells were seeded into 96-well plates at 1.25 × 10^4 cells per well and grown in DMEM supplemented with 0.5% (v/v) FBS, 1% (v/v) GlutaMAX, 50 U/mL penicillin and 50 µg/mL streptomycin (0.5×pen/strep) at 37 °C for 24 h. Bispecific molecules were prepared in 125 µL DMEM with 0.1% (v/v) FBS, 1% (v/v) GlutaMAX, and 0.5×pen/strep to a working concentration of 100 nM, from which subsequent serial dilutions were prepared if required. Spent media was removed from cells and protein solutions were added to cells. DoubleCatcher, SpyTagged binder, or MBP-superTEV alone were also applied to cells at the same concentrations as in the bispecific mixture, to control for their effect on cell proliferation. Cells were treated for 96 h at 37 °C with 5% (v/v) CO_2. 0.15 mg/mL Resazurin (Alamar Blue; Sigma-Aldrich) solution was prepared in PBS pH 7.4 and

sterile-filtered through a 0.22 μm pore-sized membrane filter, and 40 μL was then added directly to each well. Plates containing Resazurin were incubated for 4 h at 37 °C with 5% (v/v) CO_2, before detecting fluorescence (λ_{ex} 544 nm, λ_{em} 590 nm) from each well using a FLUOstar Omega plate reader (BMG Labtech). Fluorescence from each plate was measured three times, and the mean fluorescence was calculated. The fluorescence of wells containing cells grown in DMEM + 1% (v/v) FBS, 0.5×pen/strep alone, without treatment ('untreated cells') was also measured. The fluorescence intensity of 125 μL treatment media, without cells, containing Resazurin ('background') was subtracted from each measurement. The percent metabolic activity of treated cells relative to untreated cells was then defined as 100×(fluorescence of treated cells – fluorescence of background)/(fluorescence of untreated cells – fluorescence of background).

2.10 ELISA on anti-HER2 molecule binding

2.10.1 Validation of binding of anti-HER2 binder panel to the HER2 ECD

To validate binding activity of anti-HER2 binders to the HER2 extracellular domain (ECD), 80 nM SpyCatcher002-MBP in PBS pH 7.4 was adsorbed onto clear Nunc Maxisorp 96-Well flat-bottom plates (Thermo Fisher, cat. 442404) for 16-18 h at 4 °C. Wells were washed three times with PBS pH 7.4 with 0.1% (v/v) Tween-20 (PBS-T), before blocking in PBS pH 7.4 with 5% (w/v) bovine serum albumin (BSA) (blocking buffer) for 1 h at 25 °C. After three more washes with PBS-T, 80 nM of SpyTag-coupled anti-HER2 binder (Tras, 39S, MF3958, H2-18, nanoHER2, Tras NoLink, affiHER2, Pert, or HSF2) or SpyTag003-MBP (as a non-specific control) in blocking buffer was added to wells and incubated for 1 h at 25 °C. Blocking buffer alone was added to 'no binder' control wells. Wells were washed three times with PBS-T, after which serial dilutions of HER2 ECD-Fc (1 μM – 1 pM) in blocking buffer were incubated with binder-coated wells for 1 h at 25 °C. Wells were washed three more times with

PBS-T, before incubating with 1:5,000 mouse anti-human IgG Fc conjugated with HRP (GenScript, cat. A01854) in blocking buffer for 1 h at 25 °C. Six final washes were performed with PBS-T, following which 50 µL 1-Step Ultra TMB-ELISA Substrate Solution (Thermo Fisher) was added to the wells and left to stand for 5 min. Reactions were quenched with 50 µL 1 M HCl and A_{450} was measured using a FLUOstar Omega plate reader (BMG Labtech). All ELISA experiments were performed in triplicate.

2.10.2 Validation of nanoHER2 binding epitope on HER2 ECD

The epitope on the HER2 ECD recognized by nanoHER2 was elucidated by a competitive ELISA, which was performed as described in the previous section, with the following changes: 80 nM nanoHER2 in blocking buffer for 1 h at 25 °C was added to wells coated with SpyCatcher002-MBP. During this incubation step, 10 nM HER2 ECD-Fc was incubated with serial dilutions (3.16 µM – 1 pM monomer) of each anti-HER2 binder (except nanoHER2 and HFS2) in blocking buffer for 1 h at 37 °C with shaking at 600 rpm. Wells were then washed three times with PBS-T, and the HER2 ECD-Fc/binder mixtures were added to wells for 1 h at 25 °C. After three more washes with PBS-T, wells were incubated with 1:5,000 mouse anti-human IgG Fc conjugated with HRP and nanoHER2-HER2 ECD-Fc binding was detected as described.

2.10.3 Validation of ABD035-DoubleCatcher binding to human serum albumin

Validation of binding of ABD035-DoubleCatcher to human serum albumin (HuSA) was achieved by an ELISA performed exactly as described in Section 2.10.1, with the following changes: wells were coated with 80 nM SpyTag003-MBP in PBS pH 7.4 for 16-18 h at 4 °C, washed and blocked as described, and incubated with 80 nM ABD035-DoubleCatcher in blocking buffer for 1 h at 25 °C. For the ‘No SpyTag003-MBP’ control, wells were incubated

with PBS pH 7.4 alone prior to washing and blocking, and for the 'DoubleCatcher' control, SpyTag003-MBP coated wells were incubated with 80 nM DoubleCatcher instead of the ABD035-fusion. Wells were washed three times with PBS-T, before the addition of 0.2 μg/mL HuSA in blocking buffer that was previously expressed, purified, and biotinylated with BirA by Rory Hills (Howarth group, University of Oxford/Cambridge). Wells were incubated with biotinylated HuSA for 1 h at 25 °C, washed three times in PBS-T, and then incubated with 1:5,000 Pierce High Sensitivity Streptavidin-HRP conjugate (Thermo Fisher, cat no. A16160) in blocking buffer for 30 min at 25 °C. After six final washes with PBS-T, 50 μL 1-Step Ultra TMB-ELISA Substrate Solution was added to wells, and a FLUOStar Omega plate reader was used to monitor A_{652} over time (one measurement per minute) until the signal from the wells with the strongest colour change became saturated.

2.11 Flow cytometry

SpyTag-linked anti-HER2 binder (2 μM) was first incubated with SpyCatcher002-sfGFP (2 μM) in HEPES Buffered Saline (HBS; 50 mM HEPES + 150 mM NaCl) pH 7.2 supplemented with 10% (v/v) FBS at 37 °C for 1 h. As controls for background signal, SpyTagged binders or SpyCatcher002-sfGFP alone were incubated in HBS + 10% (v/v) FBS at 2 μM. HER2-positive SKBR3 and HER2-negative MDA-MB-468 cells were grown in complete DMEM until 80% confluency, when they were detached by trypsinisation and resuspended in HBS pH 7.2 + 10% (v/v) FBS to a final concentration of 4×10^6 cells/mL. Cells were aliquoted into 96-well V-bottom plates (Corning, cat no. 3894) (50 μL, $2x10^5$ cells, per well) and pelleted by centrifugation at 125 *g* at 4 °C for 3 min, before resuspension in 50 μL of the indicated pre-incubated binder:SpyCatcher002-sfGFP mixture. 'Unstained' cells were resuspended in HBS + 10% (v/v) FBS alone. Cells were incubated with binder-fluorophore mixtures for 30 min at 37 °C and 5% (v/v) CO_2, and then washed twice by centrifugation at 125 *g* at 4 °C for 3 min

and resuspending in 200 µL HBS, except for the final wash step when cells were resuspended in 150 µL FACS buffer (HBS + 1% (w/v) BSA + 0.1% (w/v) sodium azide). Cells were kept on ice and 5 minutes prior to flow cytometric analysis, 2.5 µL eBioscienceTM 7-AAD Viability Staining Solution (Invitrogen, Cat no. 00-6993-50) per million cells was added to each well to exclude non-viable cells from analyses.

A CytoFLEX LX flow cytometer (Beckman Coulter) was used to analyse labelled cells by flow cytometry, with at least 10,000 events acquired per sample. To compensate for the small overlap of sfGFP and 7-AAD fluorescence spectra, compensation matrices were calculated from unstained or single-stained compensation controls: unstained cells, heat-treated (70 °C, 30 min) cells stained with eBioscienceTM 7-AAD Viability Staining Solution, and cells incubated with 2 µM pre-incubated nanoHER2-SpyTag003:SpyCatcher002-sfGFP only. Compensation matrices were calculated by the CytExpert software (Beckman Coulter) and applied to sample data. FCS data files were subsequently analysed using FlowJo v10.10.0 software (BD Biosciences).

2.12 Click conjugation of azide-modified oligonucleotides to DBCO-SpyTag003

All ligation reactions between Dibenzocyclooctyne (DBCO) and azide groups by strain-promoted alkyne-azide cycloaddition (SPAAC) were carried out in PBS pH 7.4. DBCO-SpyTag003 was synthesised by Sona Krajcovicova (Department of Chemistry, University of Cambridge) and kindly gifted to me as a white amorphous solid. DBCO-SpyTag003 solid was solubilised in dimethylsulfoxide (DMSO) to a final concentration of 2 mg/mL, and aliquoted into 50 µL aliquots for long-term storage at -80 °C. Lyophilised azide-modified oligonucleotides (DNA-1 and DNA-2) were ordered from ELLA Biotech GmbH (Fürstenfeldbruck, Germany) and resuspended in nuclease-free water to a final concentration

of 100 µM. 50 µM Azide-DNA was then incubated with 5-fold excess DBCO-SpyTag003 for 16 h at 37 °C, with shaking at 600 rpm. Before conjugation of DNA-SpyTag003 onto SpyCatcher003 or DoubleCatcher, unreacted DBCO-SpyTag003 was separated from the reaction mixture by buffer-exchange 3-4 times into PBS pH 7.4 using Vivaspin 500 Centrifugal Concentrators (Satorius) with a MWCO of 5 kDa.

2.1 Chemical coupling of IgG with SpyTag003-tetraDVP using selective disulfide rebridging

Chemical rebridging of Trastuzumab IgG1 was performed by Thomas Wharton (Department of Chemistry, University of Cambridge), following the protocol described (Krajcovicova et al., 2024). Briefly, 5 mM TCEP was added to a 2.5 mg/mL solution of trastuzumab (F. Hoffmann-La Roche AG) in Tris-buffered saline (TBS; 25 mM Tris-HCl, 25 mM NaCl, 0.5 mM EDTA, pH 8.3, 100 µL) and incubated for 1 h at 37 °C with shaking at 400 rpm. 2.5 mM TetraDVP linker in DMSO was then added to the partially-reduced antibody and the reaction mixture was incubated for 23 h at 37 °C with continued shaking at 400 rpm. The stepwise process of Trastuzumab reduction followed by TetraDVP linker addition was then repeated exactly as described twice more, resulting in a total reaction time of 72 h. The final reaction solution was filtered through a Zeba Spin desalting column with a 40 kDa MWCO (Thermo Fisher) pre-equilibrated into PBS pH 7.4, and buffer-exchanged into PBS using an Amicon-Ultra 15 spin-concentrator with a 10 kDa MWCO (Merck Millipore) to yield a final antibody-conjugate concentration of up-to 100 µM.

CHAPTER 3 – DEVELOPMENT OF A BISPECIFIC ANTIBODY ASSEMBLY PLATFORM

For the assembly of bispecific antibodies, it is desirable to design a platform for heterodimerisation of binders that exist in the same format. Then, combinatorial dimerisation of all possible binders with all other binders within a given library would mean binders do not need to be cloned, expressed, purified, and validated into two or more different, complementary formats. Assembly of bispecific antibodies by simple reduction and chain switching of unmodified IgGs or IgG-derived antibody fragments is generally avoided in the field owing to the well-known challenges with chain mispairing and downstream purification (Ridgway et al., 1996), as discussed in Chapter 1. Instead, a modular approach can be adopted, where two binders that exist in an identical format are dimerised via a central bridging module. Such tri-modular platforms for bispecific antibody assembly have seldom been described.

However, innovative and broadly-functional chemical cross-linker scaffolds have been developed for the chemical conjugation of native antibody fragments in a modular manner (Szijj and Chudasama, 2021). Chemical linkers typically include maleimide- or next-generation maleimide-based linkers for maleimide-thiol click chemistry. Maleimide-derived linkers offer the benefit of coupling full-length IgG or IgG-derived antibody fragments that exist in identical formats. Bis-maleimide conjugates, such as *ortho*-phenylenedimaleimide (*o*-PDM), have been developed to bridge free cysteines on Fabs by forming thiosuccinimide linkages (Glennie et al., 1987; Scheer et al., 2012). Free cysteines are generated either by partial reduction/oxidation of antibody fragments with odd numbers of cysteines (Patke et al., 2017), or introduction of an unpaired cysteine (Junutula et al., 2008). However, thiol cross-linking is not site-specific, so the conjugation of any two free cysteines on two Fabs/scFvs could take place, ultimately leading to reduced heterodimer purity and additional purification

requirements (Patke et al., 2017; Szijj and Chudasama, 2021). Additionally, low serum stability of thiosuccinimide linkers have been reported (Szijj et al., 2018), where a retro-Michael deconjugation reaction can lead to the loss of cargo and reattachment to serum thiols, which is undesirable for bispecific antibodies that are to be used as therapeutics (Szijj and Chudasama, 2021). Instead, more stable disulfide rebridging linkers have proven effective for stepwise conjugation of Fabs, scFvs, of full-length IgGs. Such linkers include the bis-sulfone crosslinker in which two bis-sulfone molecules are attached to a large polyethylene glycol (PEG) bridge (Khalili et al., 2013), or next-generation maleimide crosslinkers such as dihalomaleimides (Hull et al., 2014; Patterson et al., 2017a), which are maleimide derivatives that possess two halogen leaving groups (Schumacher et al., 2013). However, bis-sulfone linkers only yield ~18% desired dimer (Khalili et al., 2013), and dihalomaleimide junctions are limited by a competing dihalomaleimide hydrolysis reaction, although a 64% dimer conversion is still achieved (Hull et al., 2014). More recently, bispecific conversion by rebridging Fab interchain disulfides was achieved with pyridazinedione scaffolds which harbour complementary click handles for subsequent heterodimerisation (Maruani et al., 2020). This controlled bioconjugation yielded up to 85% bispecific with a single purification step. Importantly, the modular format permits modification of linker lengths and flexibility or Fc attachment, albeit with reduced yields (Thoreau et al., 2023). Clearly, chemical conjugation approaches for bispecific synthesis present great potential for combinatorial assembly of many binders during screening stage of bispecific discovery (Fawcett et al., 2024; Thoreau and Chudasama, 2022; Thoreau et al., 2023), However, the scalability of chemically-conjugated bispecifics to medium- or high-throughput is yet to be investigated (Fawcett et al., 2024; Szijj et al., 2023; Thoreau et al., 2023), and control of bispecific geometry will require substantial linker design (Zografou-Barredo et al., 2023).

An alternative approach for the modular conjugation of two molecules in a common format is to employ a tandem SpyCatcher003 dimerisation scaffold onto which any two SpyTag-linked binders can be covalently conjugated. Binders are often expressed with a SpyTag for purification (Keeble and Howarth, 2020; Khairil Anuar et al., 2019; Vester et al., 2022), conjugation to imaging probes for labelling and detection (Alam et al., 2019; Zakeri et al., 2012), or multimerization (Bruun et al., 2018; Khairil Anuar et al., 2019). Therefore, the SpyCatcher/SpyTag pair are a convenient system to exploit for bispecific assembly. The expansive HuCAL recombinant Fab-SpyTag002 generation service offered by Bio-Rad will further increase the number of SpyTag-fused antigen binding molecules available to the research community (Hentrich et al., 2021; Kellmann et al., 2023). However, in order to ensure site-specific conjugation of each SpyCatcher moiety within a tandem Catcher construct, the reactivity of at least one SpyCatcher within the module must be controlled.

Switchable reactivity of the SpyCatcher/SpyTag system has been imparted previously in response to changes in pH (Cao et al., 2017; Che et al., 2024; Vester et al., 2022), redox (Wu et al., 2018), temperature (Vester et al., 2022), or light (Hartzell et al., 2021; Rahikainen et al., 2023; Ruskowitz et al., 2023; Yang et al., 2023). Low-to-moderate reaction efficiency is maintained in most switchable Catcher/Tag systems, yet some systems display incomplete switching or a substantially destabilised SpyCatcher protein, thus limiting its utility. Furthermore, these switches are limited to applications which can tolerate the chemical or physical changes that are necessary to control SpyCatcher reactivity. As such, a redox-switchable variant of SpyCatcher would not be appropriate for use in bispecific assembly owing to the redox sensitivity of IgG-derived binder constituents. Indeed, the SpyLock approach adopted by Bio-Rad describes the stepwise assembly of SpyTag-linked Fabs onto a tandem SpyCatcher003 construct (Hentrich et al., 2024), where the reactivity of one Catcher is

redox-controlled. As a result, this approach favours the dimerisation of Fabs that do not contain inter-chain disulfide bonds (Hentrich et al., 2021), which introduces the possibility of light chain mispairing in the final bispecific molecule.

3.1 Imparting protease activatability into SpyCatcher003 to generate Masked SpyCatcher003

Instead of engineering switchable reactivity into the SpyCatcher003 protein itself, Dr Anthony Keeble (Howarth group) fused SpyCatcher003 to the previously engineered non-reactive SpyTag003 D117A (SpyTag003DA) mutant (Keeble et al., 2019) via a flexible linker that harbours a Tobacco Etch Virus (TEV) protease recognition site (ENLYFQ↓G, where ↓ denotes the cleavage site; Fig. 3.1A). This construct is termed 'Masked SpyCatcher003' throughout. SpyTag003DA peptide binds tightly to SpyCatcher003 (K_D = 21 nM for the non-linked pair (Keeble et al., 2019)). Thus, in the absence of TEV protease, SpyTag003DA of the Masked Catcher construct will bind to and mask the reactive Lys31 of SpyCatcher003 (Fig. 3.1A). The intramolecular interaction between SpyCatcher003 and SpyTag003DA should be entropically favoured over a competing intermolecular interaction with SpyTag003 in solution (Fig. 3.1A, blue shaded box). Incubation of Masked SpyCatcher003 with TEV protease will facilitate site-specific cleavage, so that the SpyTag003DA peptide will be free to dissociate from SpyCatcher003, unmasking Lys31 for reaction with SpyTag003. Unique to allosteric, electrostatic, redox, or post-translational modification-induced control of protein reactivity, proteolytic activation is irreversible. Thus, uses of Masked SpyCatcher003 are not restricted to specific reaction conditions following proteolysis by TEV. Indeed, the SpyCatcher/SpyTag pair and its variants have demonstrated rapid and efficient reactivity under a broad range of temperatures, pH values, detergents and buffers (Keeble et al., 2017, 2022; Zakeri et al., 2012).

3.1.1 Characterising reactivity of Masked SpyCatcher003 with SpyTag003 in the presence and absence of protease

The extent to which the reactivity of the Masked SpyCatcher003 construct was muted was investigated by incubating equimolar amounts of the construct with a model SpyTag003 fusion protein, SpyTag003-Maltose Binding Protein (MBP) (depicted in the schematic in Fig. 3.1A). The disappearance of Masked SpyCatcher003 over time was monitoring by SDS-PAGE with Coomassie staining followed by densitometry (Fig. 3.1B (top), E). The reaction was carried out at 37 °C to accelerate the disassembly of any non-covalent dimer present, as dimer dissociation has a larger temperature dependence than intramolecular SpyCatcher003-SpyTag003DA association. Under these conditions, 3.7 ± 0.63 % (mean ± 1 s.d., n = 3) reaction of Masked SpyCatcher003 with SpyTag003-MBP was observed after 60 min, supporting near-complete silencing of SpyCatcher003 reactivity.

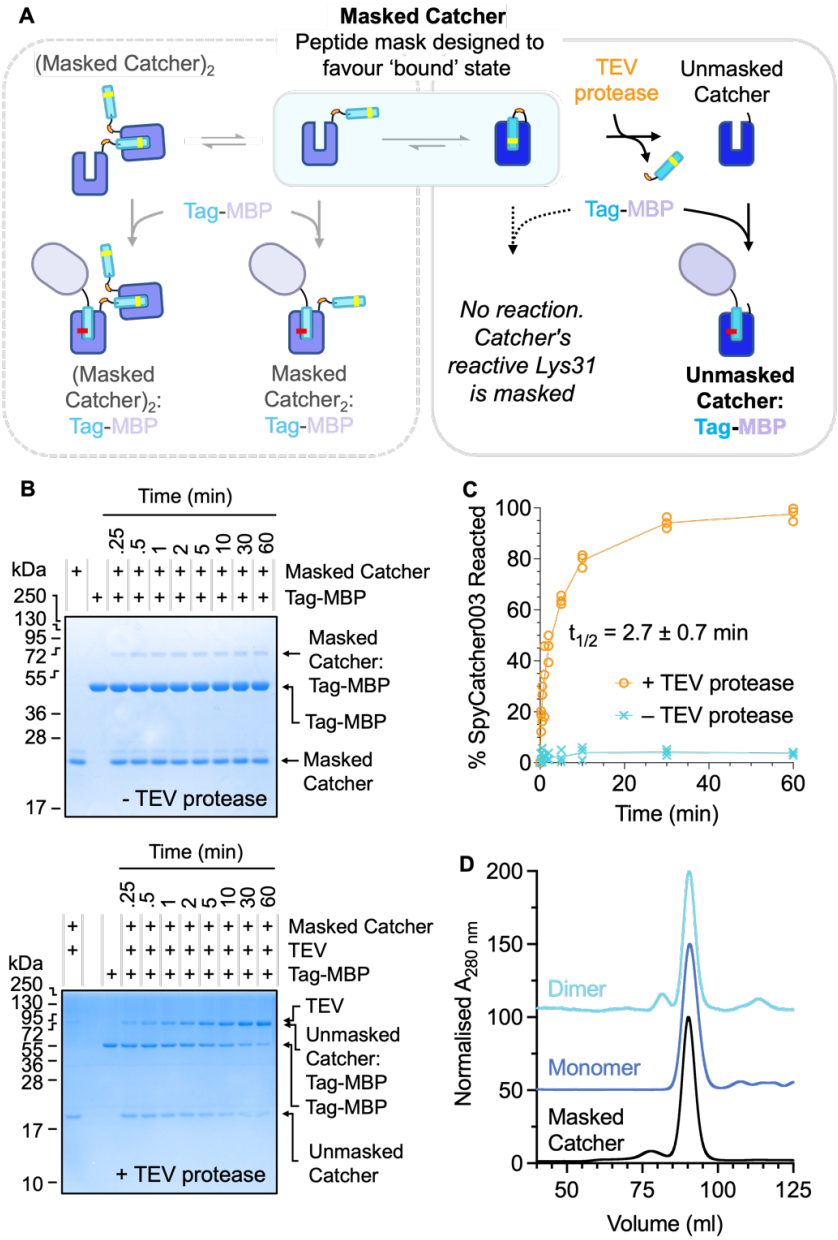


Figure 3.1. Masked SpyCatcher003 has protease-activatable reactivity. (**A**) Cartoon of Masked SpyCatcher003 ('Catcher') is displayed in the blue shaded box (centre). The reactive Lys31 of SpyCatcher003 is sterically blocked by the genetically tethered SpyTag003DA peptide 'mask', which docks non-covalently onto SpyCatcher003. SpyCatcher003 is represented in dark blue, SpyTag003 peptide in cyan with the D117A in yellow, Maltose Binding Protein (MBP) in lilac, and isopeptide bond in red. A colon indicated covalently linked products. Intended protease-controlled unmasking of Masked Catcher is displayed in the solid-outlined box (left). The possible undesired side-products are depicted in the dotted-outlined box. (**B**) Minimal reactivity of Masked SpyCatcher003 with SpyTag003-MBP (both partners at 5 μM) is detected after 60 min at 37 °C, as determined by SDS-PAGE with Coomassie staining (top). After incubation of Masked SpyCatcher003 with TEV protease, equimolar (5 μM) amounts of Unmasked Catcher and SpyTag003-MBP reacted efficiently to near-completion in 60 min at 37 °C, as determined by SDS-PAGE/Coomassie and quantified by densitometry (**C**) (individual replicates with means connected, $n = 3$), indicating the mean half-time of reaction, $t_{1/2}$ (shown ± 1 s.d., $n = 3$). (**D**) Size-exclusion chromatography (SEC) of Ni-NTA-purified Masked SpyCatcher003 (black line, $n = 1$) at 4°C in PBS pH 7.4 confirmed the presence of two species, which were each re-analysed by SEC ('Monomer' fractions in dark blue, and 'Dimer' fractions in light blue).

Trace reactivity may be attributed either to the fraction of Masked SpyCatcher003 in an 'open conformation' (with SpyTag003DA dissociated; blue shaded box, Fig. 3.1A) that exists in dynamic equilibrium with Masked SpyCatcher003 in a 'closed conformation', or to residual dimer formation (Fig. 3.1A). To support this hypothesis, Masked SpyCatcher003 was analysed for intermolecular SpyTag003DA-SpyCatcher003 by size-exclusion chromatography (SEC) following expression in *E. coli* C41 and purification by Ni-NTA (black curve, Fig, 3.1D). Two peaks were identified in the SEC chromatogram, confirming ~92% of protein exists in its monomeric state (~90-110 mL elution volume, Fig. 3.1D), while ~8% of protein forms non-covalent timers or higher-order multimers (~70-90 mL elution volume, Fig. 3.1D). Multimer formation was supported by the observation that fractions from both peaks ran as equivalent molecular weights by SDS-PAGE. Furthermore, when the fractions from the two main $A_{280\ nm}$ peaks in the elution profile were subjected to a second round of size-exclusion chromatography, the protein re-equilibrated into a major peak and a minor peak at equivalent elution volumes as in the initial spectrum (dark blue and light blue curves, Fig. 3.1D).

Following incubation of Masked SpyCatcher003 with superTEV protease (2 h, 34 °C), Masked SpyCatcher003 reacts with SpyTag003-MBP (Fig. 3.1A), to > 99% completion in 30 min, with a half-life of reaction ($t_{1/2}$) of 2.7 ± 0.7 min (mean ± 1 s.d., n = 3) (Fig. 3.1B (bottom), C). To reduce the extent to which SpyTag003DA dissociation limits the rate of reaction between TEV-cleaved Masked SpyCatcher003 ('Unmasked Catcher') with SpyTag003-MBP, the temperature of reaction was maintained at 37 °C. SuperTEV protease was chosen due to its efficient activity in the absence of reductant (Correnti et al., 2018), therefore rendering the enzyme compatible with reactions involving redox-sensitive binder moieties.

3.2 Generation of DoubleCatcher from Masked SpyCatcher003

My aim was to design a platform that facilitates the conjugation of any two SpyTagged binder molecules in a controlled, site-specific manner. Therefore, Masked SpyCatcher003 was genetically fused to the C-terminus of a native SpyCatcher003 protein via a flexible Gly/Ser linker. This dimerisation scaffold was termed DoubleCatcher (Fig. 3.2A). DoubleCatcher expressed to high yields in *E. coli* (~ 20 mg per L of culture).

3.2.1 Characterising site-specific reactivity of DoubleCatcher with SpyTag003

The reactivity of each SpyCatcher003 moiety within the DoubleCatcher construct was determined sequentially, by monitoring the reaction of DoubleCatcher with SpyTag-linked model proteins before and after cleavage of the SpyTag003DA peptide mask by MBP-superTEV protease. First, DoubleCatcher was incubated with 2-fold molar excess of the green fluorescent protein mClover3 fused to SpyTag003 in the absence of superTEV protease (Fig 3.2A, B). After 1 h, 91% reactivity of the N-terminal Catcher moiety of DoubleCatcher was observed, with a half life of reaction ($t_{1/2}$) of 0.58 ± 0.05 min (mean ± 1 s.d., n = 3) (Fig. 3.2C).

To determine the reactivity of the C-terminal Catcher, DoubleCatcher was first incubated with 2-fold molar excess of SpyTag003-MBP for 2 h (37 °C), to saturate the N-terminal SpyCatcher003 moiety as established previously. Unreacted SpyTag003-MBP was sequestered from the reaction mixture by incubation with bead-immobilised SpyCatcher003 for 16 h at 4 °C, before addition of superTEV-protease to the singly-saturated DoubleCatcher:SpyTag003-MBP sample (2 h, 34 °C) to induce cleavage of the peptide mask from the C-terminal SpyCatcher003 moiety (Fig. 3.2D). The cleaved construct was then mixed with a 5-fold molar excess of Small Ubiquitin-like Modifier (SUMO) conjugated to SpyTag003, and the reaction was monitored over time by SDS-PAGE and densitometry (Fig. 3.2E, F). Reactivity of the unveiled C-terminal Catcher with Tag was rapid with a $t_{1/2}$ of 3.6 ± 0.7 min (mean ± 1 s.d., n =

3), proceeding to > 95% saturation in 60 min. The efficient coupling of Tag to the unmasked Catcher affirms that the reactivity of the second Catcher is not impeded by the steric bulk of an adjacent Catcher coupled to a protein payload.

3.2.2 DoubleCatcher-SpyTag003DX variants

It was observed in Section 3.2.1 that the SpyTag003DA peptide mask of Masked Catcher was 96% effective at preventing reaction to SpyTag003 after 60 min at 37 °C, with slight 'leaky' reactivity arising due to temporary SpyTag003DA unbinding and intermolecular docking of SpyTag003DA to another Masked Catcher construct. To test whether the masking activity of the non-covalent SpyTag003 peptide, I designed four DoubleCatcher variants which harbour an alternative point mutation at the reactive D117 residue of SpyTag003 peptide mask: D117V, D117E, D117S, or D117T. These residues were selected for substitution based on their similarity to the native Asp in size, charge, or hydrogen bonding ability (Kang and Baker, 2011), to minimise disruption of SpyTag003DX (where X = V, E, S, T) mutant docking to the C-terminal SpyCatcher003.

DoubleCatcher-SpyTag003DX variants were initially tested for their ability to mask the reactivity of the C-terminal Catcher moiety in the absence of TEV protease. DoubleCatcher variants (10 μM) were reacted with 5-fold excess SpyTag003-MBP (50 μM) in triplicate for 4 h at 37 °C in PBS pH 7.4. Reaction products were then analysed (Fig. 3.3A) and the relative amount of DoubleCatcher-SpyTag003DX coupled to a single SpyTag003-MBP (DC:ST3-MBP, 'Monosaturated DoubleCatcher') was quantified as a percentage of all reaction products (Fig. 3.3B).

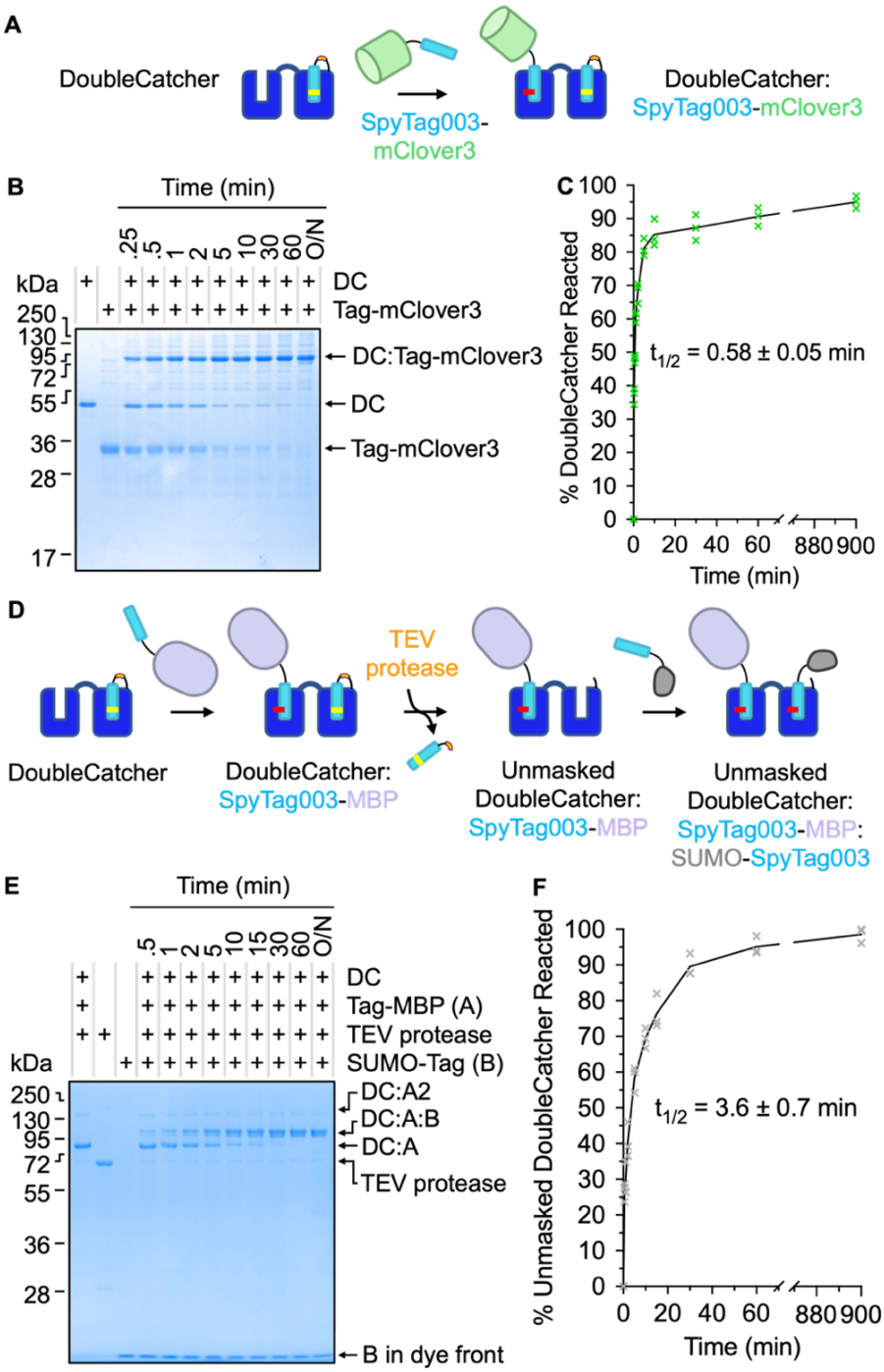


Figure 3.2. Site-specific conjugation of Tagged proteins to DoubleCatcher is fast and site-specific. (**A**) Schematic depicting covalent conjugation of SpyTag003-mClover3 (Tag-mClover3) to the reactive N-terminal Catcher of DoubleCatcher. (**B**) Time-course of reaction between DoubleCatcher (DC; 2.5 µM) and SpyTag003-mClover3 (Tag-mClover3; 5 µM) was analysed by SDS-PAGE with Coomassie staining (n = 3). (**C**) Depletion of unreacted DoubleCatcher over the course of reaction was quantified by densitometry, following (B) ($t_{1/2}$ mean ± 1 s.d., n = 3). (**D**) Schematic illustrating unmasking and conjugation of the C-terminal Catcher of DoubleCatcher. (**E**) Reaction at the unmasked Catcher of DoubleCatcher. Following saturation of the N-terminal Catcher of DoubleCatcher (DC) with SpyTag003-MBP (A), the sample was incubated with TEV protease for 2 h at 34 °C. The resulting unmasked DoubleCatcher:SpyTag003-MBP (2 µM) was then reacted with SUMO-SpyTag003 (B; 10 µM) over the time indicated, before SDS-PAGE/Coomassie (n = 3 reaction). (**F**) Quantification of reaction at the unmasked Catcher of DoubleCatcher, based on (E). All triplicate data points are shown, with the line connecting the mean. ($t_{1/2}$ mean ± 1 s.d., n = 3).

For each variant, no residual unreacted DoubleCatcher was detected, allowing the relative formation of monosaturated product to be fairly compared between variants. Under these conditions, the previously characterized DoubleCatcher-SpyTag003DA variant reacted to produce 75.9 ± 4.2% (mean ± s.d., $n = 3$) monosaturated product over disaturated homodimer. Intriguingly, DoubleCatcher-SpyTag003DS improved upon this masking ability, producing 83.3 ± 2.2% monosaturated DoubleCatcher.

For the DoubleCatcher-SpyTag003DS variant to be useful as a dimerisation tool, it is imperative that peptide mask can be cleaved off to enable saturation of the C-terminal Catcher. I therefore subjected DoubleCatcher-SpyTag003DA ('DC-ST3DA' in Fig. 3.3C) or DoubleCatcher-SpyTag003DS ('DC-ST3DS') (both at 2.5 μM) to reaction with 2-fold excess SpyTag003-MBP ('A') (5 μM; 4 h, 37 °C), followed by co-incubation with MBP-superTEV protease (0.21 μM) and 5-fold excess MBP_X-MBP_X-SpyTag003 ('B') (12.5 μM; 2 h, 34 °C). To remove unreacted, excess SpyTag003-fusion from the reaction mixture, immobilised SpyCatcher003 was incubated with the crude mixture (4 °C, 16 h). Each step of the reaction process was monitored (Fig. 3.3C). For both DoubleCatcher variants, control reactions were conducted with A alone, A + TEV, or B + TEV were also analysed by SDS-PAGE, to aid the identification of DC:A, DC:A_2, or DC:B_2 bands.

Relative to native DoubleCatcher ('DC-ST3DA'), the C-terminal SpyCatcher003 moiety of DoubleCatcher-SpyTag003DS ('DC-ST3DS') mutant reacts to a lesser extent following cleavage of the peptide mask by TEV protease. The addition of TEV protease alone to the DC-ST3DS + A reaction mixture resulted in a mass shift of the DC-ST3DS:A band, as well as the formation of a band corresponding to DC-ST3DS:A_2 homodimer product (Fig. 3.3C). This

confirms successful TEV cleavage of this mutant. However, following co-incubation of DC-ST3DS:A with TEV and B, the unmasked DC-ST3DS:A band (highlighted in a blue box in Fig. 3.3C) is not fully depleted. Since the unmasked monosaturated product band is absent from the equivalent lane from the DC-ST3DA reaction, it is suspected that after TEV cleavage the SpyTag003DS mask dissociates with an off-rate that is too slow to allow for saturation of the C-terminal Catcher after 4 h at 34 °C. To minimise the time required for bispecific assembly, the original DC-ST3DA construct was taken forward for further optimisation.

3.2.3 DoubleCatcher linker variants

ColabFold version 1.3 was used to model the structure of DoubleCatcher (Mirdita et al., 2022). Upon inspection of the five highest-confidence ColabFold-predicted structures of DoubleCatcher, it was observed that three of the five models predict the SpyTag003DA mask to dock parallel to β-strand 1 of the C-terminal SpyCatcher003 (Li et al., 2014), while the other two structures show SpyTag003DA docked in the opposite orientation, anti-parallel to β-strand 1. The X-ray crystal structure of CnaB2 (PDB 2X5P (Oke et al., 2010)), from which SpyCatcher/SpyTag pair was derived, and SpyCatcher/SpyTag (PDB 4MLI (Li et al., 2014)) confirm the parallel alignments of β-strand 1 and SpyTag (β-strand 9 in CnaB2), with an extensive parallel hydrogen bond network and electrostatic interactions bringing the two strands together. A representative ColabFold-predicted structure exemplifying the ‘correct’ docking of SpyTag003DA to C-terminal Catcher is displayed in Fig. 3.4A, and a model displaying ‘incorrect’ docking is shown in Fig. 3.4B. The reactivity silencing mutation is highlighted in yellow. Considering the addition of only one or two additional point mutations to SpyTag003DA were shown to vary 50-fold in affinity for SpyCatcher003 by surface plasmon resonance (Keeble et al., 2019), it is unlikely that an incorrectly oriented SpyTag003DA will dock with sufficient affinity to mask SpyCatcher003 reactivity.

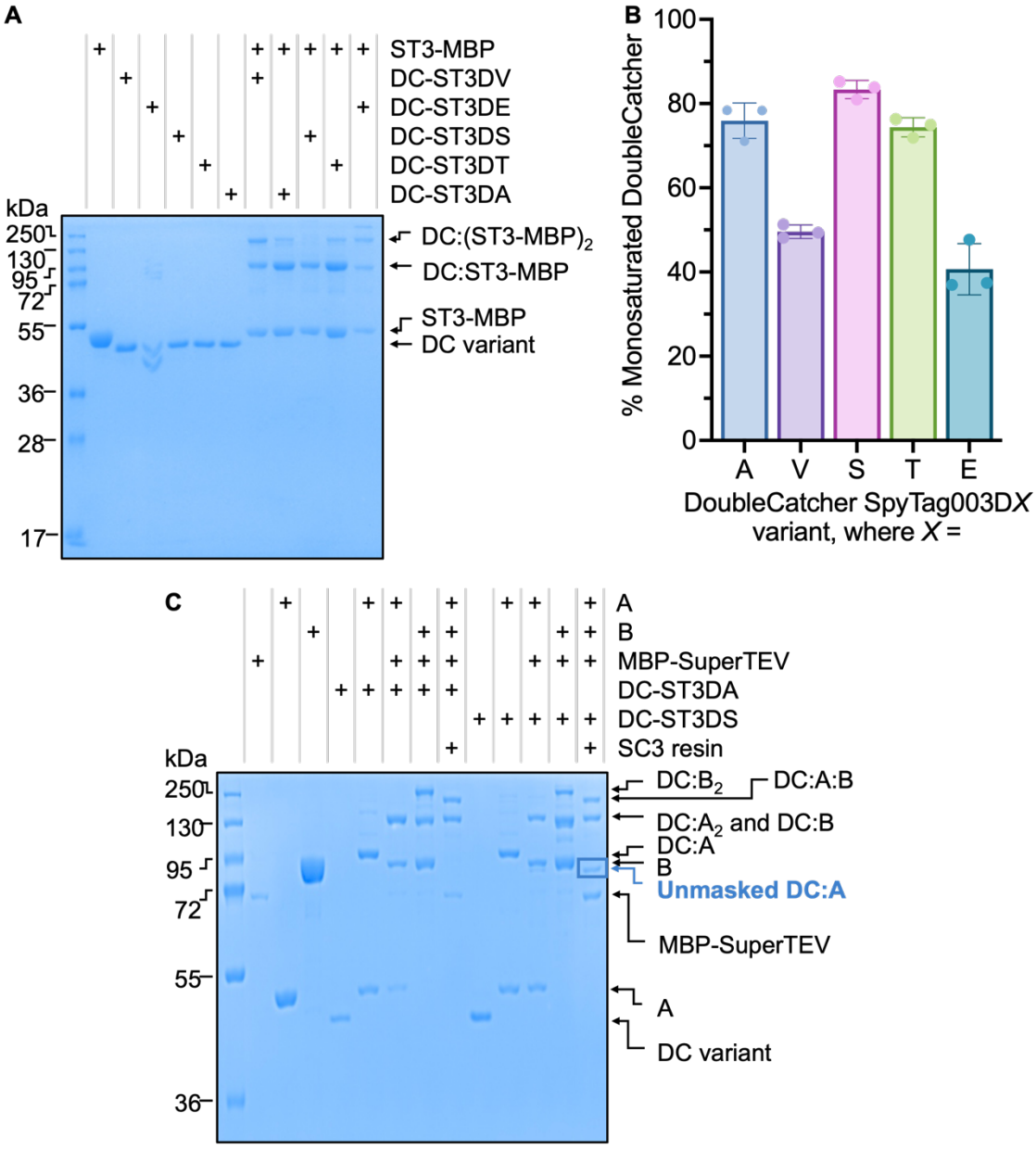


Figure 3.3. Non-covalent SpyTag003 variants were assessed for SpyCatcher003 masking and unmasking activity.(**A**) Variants of DoubleCatcher with alternative substitution mutations in the reactive D117 residue were assessed for their ability to mask the reactivity of the C-terminal SpyCatcher003. 10 µM of each DoubleCatcher variant (abbreviated to DC-ST3DX, where X = V, E, S, T, or A) was incubated with 50 µM SpyTag003-MBP (ST3-MBP) for 4 h at 37 °C, and reactions were monitored by SDS-PAGE with Coomassie staining. The formation of homodimer (DC:ST3-MBP) relative to all the products in the reaction mixture was quantified by densitometry, and presented as a percentage in (**B**) (n = 3). DoubleCatcher variants with a strong peptide mask will have a high relative proportion of monosaturated product over doubly-saturated product, as the reactivity of the second SpyCatcher003 moiety will be tightly silenced. (**C**) Unmasking and reactivity of the C-terminal Catcher of the two best-performing mask variants, DoubleCatcher-SpyTag003DS and DoubleCatcher003-DA was tested. Each DoubleCatcher was reacted with SpyTag003-MBP ('A') (5 µM; 4 h, 37 °C), followed by co-incubation with MBP-superTEV protease (0.21 µM) and 5-fold excess MBP_X-MBP_X-SpyTag003 ('B'), and each step of the reaction was monitored by SDS-PAGE/Coomassie. The enhanced masking activity of SpyTag003DS was disadvantageous for heterodimer assembly, as the peptide mask was too slow to dissociate from DoubleCatcher following TEV cleavage, hindering the reactivity of the C-terminal Catcher.

I therefore designed a series of DoubleCatcher variants with affinity-enhancing mutations or alternative linkers between the C-terminal SpyCatcher003 and SpyTag003DA, with the goal of driving docking of SpyTag003DA to SpyCatcher003 in the correct orientation. The sequences of the DoubleCatcher linker variants are listed in Fig. 3.4C, where 'WT' corresponds to native DoubleCatcher. The following variants were designed as follows (nomenclature follows Fig. 3.4C):

1. **S59T V94I**: The S59T and V94I mutations were identified in phage display screens that led to the engineering of the pH- and temperature-switchable SpyCatcher variant SpySwitch, and are hypothesised to improve non-covalent association with SpyTag003 (Vester et al., 2022). Therefore, these mutations were made to increase association of SpyTag003DA with the C-terminal SpyCatcher003 moiety within DoubleCatcher.
2. **ΔRGV**: The ΔRGV variant possesses a deletion of the three N-terminal-most residues of SpyTag003DA mask. These variants were designed to test the effect of shortening the chain length between the TEV recognition site at the masking peptide.
3. **PGP**: The substitution of the GSG preceding the SpyTag003DA mask with PGP tripeptide was made to staple the peptide mask onto the Catcher; the pyrrolidine ring of proline gives rise to fixed φ and ψ angles, resulting in reduced conformational freedom of the peptide backbone.
4. **BeforeTEV**: A substitution of the GSSGS flexible linker that precedes the TEV protease recognition site for a single glycine was made to decrease the length of the linker separating the peptide mask from the Catcher. For the mask to dock onto the Catcher in the incorrect orientation, the mask's N-terminus is ~ 4Å from the C-terminus of the fused Catcher. Therefore, if the linker is not of a sufficient length, docking may be favoured in the correct orientation.

5. **AfterTEV**: In the same way as for the BeforeTEV linker variant, the GGSG linker following the TEV cleavage site was substituted for a single glycine to shorten the linker between the peptide mask and the C-terminal Catcher.

Similarly to DoubleCatcher-SpyTag003DX variant analysis in Section 3.2.2, DoubleCatcher linker variants (10 μM) were reacted with 5-fold excess SUMO-SpyTag003 (50 μM) for 4 h at 37 °C (PBS pH 7.4; Fig. 3.4D). To compare the masking functionality of each DoubleCatcher linker variant, densitometry was used to quantify the amount of DoubleCatcher saturated to a single SUMO-SpyTag003 (DC:SUMO-SpyTag003) as a percentage of all reaction products (Fig. 3.4E).

However, none of the designed DoubleCatcher linker variants substantially reduced the dissociation of SpyTag003DA from the C-terminal Catcher. While S59T V94I (78.2 ± 4.9% monosaturated DoubleCatcher formed) and BeforeTEV (77.3 ± 2.3%) variants performed marginally better than native DoubleCatcher ('WT'; 76.4 ± 2.0%), their improvements were within the error for WT (all data are mean ± 1 s.d., n = 3). Therefore, the native DoubleCatcher construct was taken forwards for further optimisation.

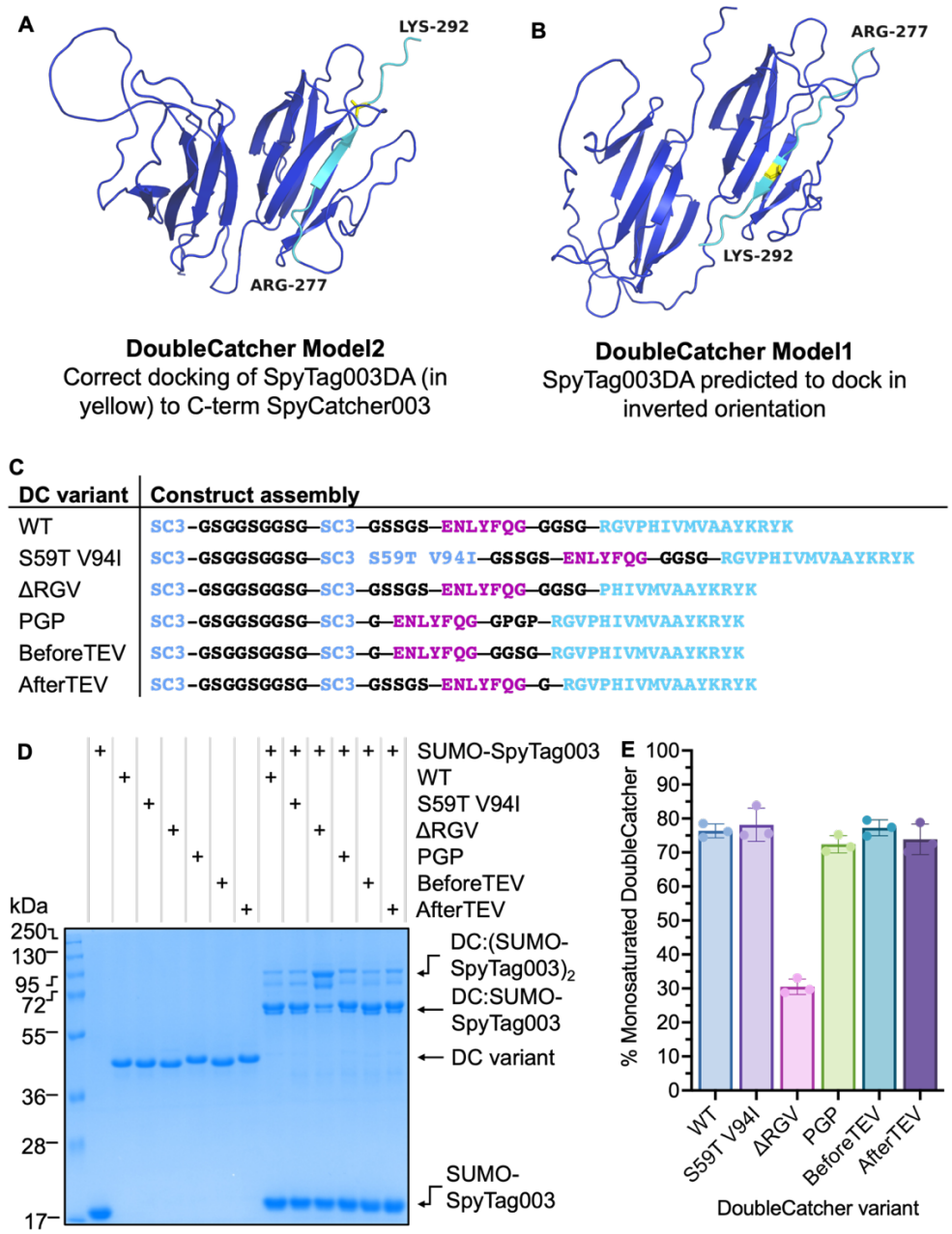


Figure 3.4. The linker tethering SpyTag003DA mask to DoubleCatcher was varied and assessed for enhanced masking activity. (**A**) Three of the five highest-confidence ColabFold-modelled structures of DoubleCatcher (DC) predict the SpyTag003 peptide mask to dock onto β-strand 1 of the C-terminal Catcher in a parallel orientation, shown here for Model2. SpyCatcher003 moieties are represented as dark blue cartoons, SpyTag003DA in cyan with the D117A reactivity silencing mutation shown as yellow sticks. The N- and C-terminal residues of SpyTag003DA are labelled in black. (**B**) The other two highest-confidence predicted structures of DoubleCatcher predict SpyTag003DA to dock in an inverted orientation, anti-parallel to β-strand 1 of the C-terminal Catcher, shown here for 'Model1'. The C-terminal Catcher is aligned identically to that in (A). (**C**) Sequences of DoubleCatcher variants that were designed to facilitate correct docking of the SpyTag003DA mask onto its adjacent SpyCatcher003 within DoubleCatcher. (**D**) 10 μM of each DoubleCatcher variant (labelled as in (C)) were incubated with 50 μM SUMO-SpyTag003 for 4 h at 37 °C and analysed by SDS-PAGE/Coomassie. The relative proportion of DoubleCatcher:SUMO-SpyTag003 formed over DoubleCatcher:SUMO-SpyTag003$_2$ was quantified by densitometry (**E**). Individual data points are shown, with bars connecting the mean (n = 3, ± 1 s.d)

3.3 Development of SpyMask: a generalisable, one-pot protocol for dimerisation by DoubleCatcher

A bispecific antibody assembly platform that is generally-applicable and compatible with high-throughput screening applications requires a simple, scalable methodology that accommodates any combination of starting molecules. I therefore sought to optimise a multi-step, single-pot reaction in which any two SpyTag-linked binders can be consecutively coupled to a selected DoubleCatcher scaffold. The protocol is outlined in Fig. 3.5A: the first SpyTag-linked protein is conjugated to the N-terminal Catcher of DoubleCatcher (*Step 1*), before simultaneous addition of superTEV protease and the second SpyTag-linked protein to saturate the C-terminal Catcher (*Step 2*). Any unreacted, excess SpyTag-linked binder is then depleted from the reaction mixture by incubating the crude mixture with SpyCatcher003 (*Step 3*).

For optimisation of each step of the bispecific assembly protocol, I used SDS-PAGE to monitor the conjugation of two model SpyTagged ligands onto DoubleCatcher: SpyTag-AffiHER2-AffiHER2-AffiHER2 ('SpyTag-AfiiHER2$_3$', abbreviated to ligand A throughout this section and in Fig. 3.5A) and MBP$_X$-MBP$_X$-SpyTag003 ('(MBP$_X$)$_2$-SpyTag003', abbreviated to ligand B). These ligands were selected as they do not contain free cysteines (which may form inter-ligand disulfides that complicate analyses) and have sufficient differences in M_W that permit unambiguous detection of reactant and product bands by SDS-PAGE. The masses of purified reactants were validated by electrospray-ionisation mass spectrometry (Fig. 3.5B).

In the first step of the assembly reaction (*Step 1* in Fig. 3.5A), DoubleCatcher was initially reacted with an equimolar quantity of ligand A for 2 h at 37°C. However, SDS-PAGE followed by densitometric analysis revealed the reaction mixture to contain only 76% of the desired DC:A product ('DC + A' lane in Fig. 3.5C). The major contaminant was residual, unreacted

DoubleCatcher (21%), and the minor contaminant was DoubleCatcher bound to two A molecules, DC:A_2 (5%). The identity of this by-product was corroborated by the increase in the density of the band corresponding to DC:A_2 homodimer in a control reaction containing twice the concentration of A, as well as superTEV protease ($1/12^{th}$ molar equivalents) ('DC + A + TEV + A' lane in Fig. 3.5C).

3.3.1 Optimisation of Step 1: Saturation of N-terminal SpyCatcher003 of DoubleCatcher

To ensure negligible unreacted DoubleCatcher remained in solution after *Step 1*, the assembly reaction was repeated with 1.25 molar excess of ligand A. This change is highlighted in green in the schematic in Fig. 3.6A. The reaction was monitored by SDS-PAGE and densitometry as previously (Fig. 3.6B). Pleasingly, excess ligand A ensured DoubleCatcher was depleted from the reaction mixture after *Step 1* ('DC + A' lane in Fig. 3.6B), to form 91% DC:A desired product and only 4% of DC:A_2 homodimer (with 5% residual ligand A), in accordance with the Masked SpyCatcher003 reactivity assays described in Section 3.1.

To monitor the subsequent unmasking and saturation of the C-terminal SpyCatcher003 moiety of DoubleCatcher, superTEV protease ($1/12^{th}$ molar equivalent) and ligand B (5-fold molar excess) were added to the singly saturated DoubleCatcher simultaneously, and reaction proceeded for 2 h at 34 °C (*Step 2*, Fig. 3.6A). Thus, immediately upon cleavage of SpyTag003DA, ligand B will be at a 20-fold higher concentration than residual, unreacted ligand A and so DC:A_2 homodimer formation is minimised.

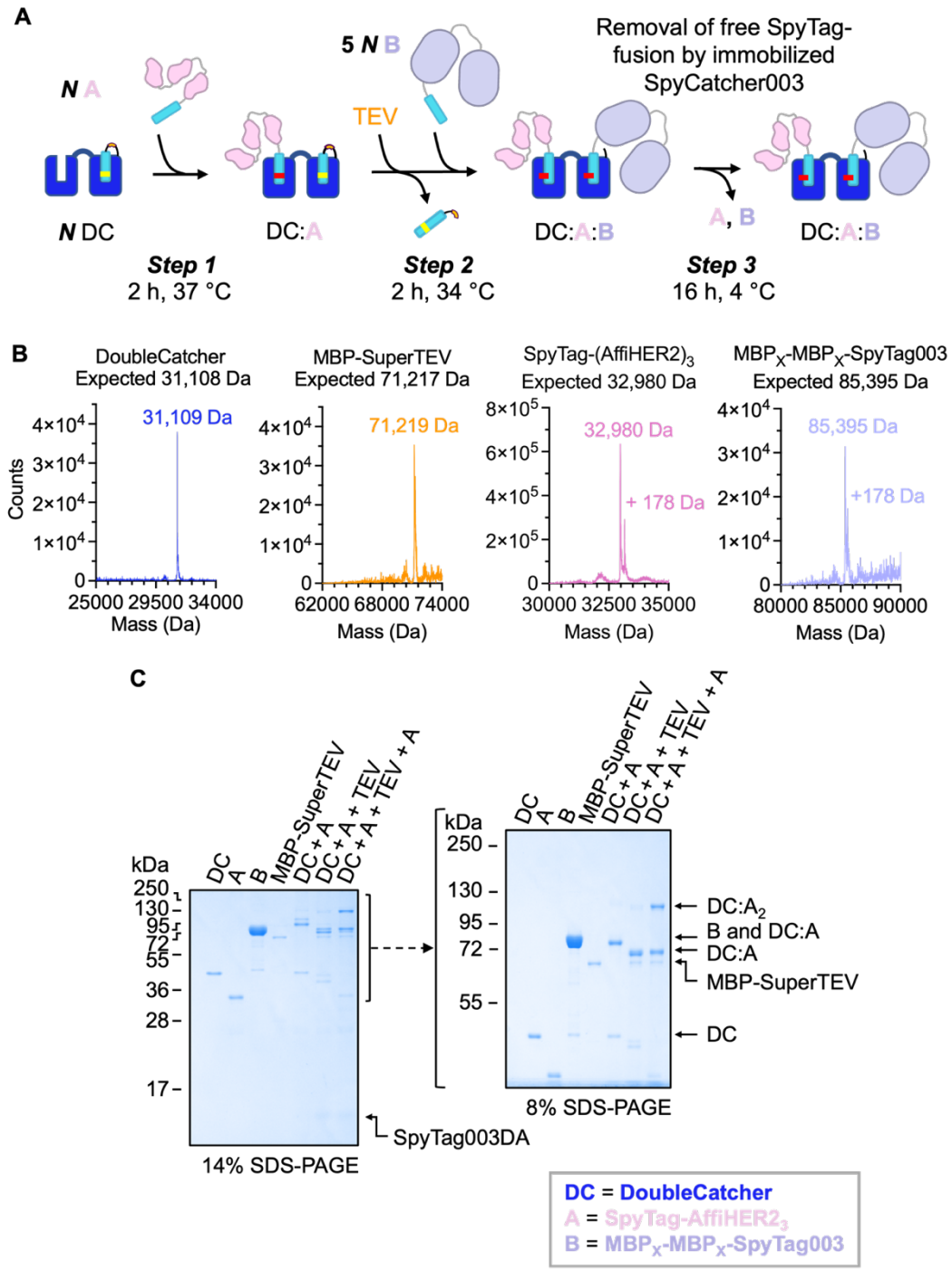


Figure 3.5. SpyMask enables one-pot dimerisation of two Tagged model proteins using DoubleCatcher, yet requires optimisation to minimise unwanted homodimer formation. (**A**) Schematic depicting the SpyMask protocol for assembly of ligand A (SpyTag-AffiHER2$_3$; pink) and ligand B (MBP$_X$-MBP$_X$-SpyTag003; purple) onto DoubleCatcher (DC, blue). *N* represents the concentration of DoubleCatcher (*N* = 5 μM in this reaction). A colon indicated covalently linked products. Immobilized SpyCatcher003 allows excess, unreacted Tagged proteins to be removed from solution into the solid-phase, leaving the desired heterodimeric product in solution. (**B**) Purified model proteins used for optimisation of the SpyMask protocol were analysed by intact electrospray-ionisation mass spectrometry. (**C**) In *Step 1* of panel (A), equimolar amounts of DoubleCatcher and ligand A were incubated for 2 h at 37 °C, and the reaction was monitored by SDS-PAGE with Coomassie staining. To aid the identification of by-product bands from the desired DoubleCatcher:A (DC:A) product band, a control reaction of DoubleCatcher incubated with MBP-superTEV and twice the concentration of ligand A ('DC + A + TEV + A' lane) was also analysed.

Indeed, AffiHER2$_3$ homodimer still accounted for only 3% of the total species in the reaction mixture ('DC + A + TEV + B' in Fig. 3.6B). Surprisingly, negligible formation of DoubleCatcher conjugated to two B molecules (DC:B$_2$) was observed by SDS-PAGE; the band corresponding to the DC:B$_2$ species was identified by reacting DoubleCatcher, TEV, and B alone ('DC + B + TEV + B' lane in Fig. 3.6B) and noting the formation of the DC:B and DC:B$_2$ conjugation product bands. However, the major contaminant in the reaction mixture after *Step 2* was unreacted, unmasked DC:A (55%). While 2 h incubation of TEV with singly-saturated DoubleCatcher was sufficient for its complete cleavage and subsequent reactivity in Fig. 3.1A, ligand A is larger and contains more unfolded, flexible linkers than SpyTag003-MBP, so it is not unlikely that MBP-superTEV was more sterically occluded from its recognition site in DC:A, resulting in incomplete cleavage.

3.3.2 Optimisation of Step 2: Unmasking and saturation of C-terminal SpyCatcher003 of DoubleCatcher

To optimise cleavage of the C-terminal Catcher's peptide mask, the model heterodimerisation reaction was repeated, with the *Step 2* increased to 4 h (highlighted in green in Fig. 3.7A). The conditions of *Step 1* were unchanged, and so efficient assembly of DC:A (97%, with only 3% DC:A$_2$ formation; 'DC + A' lane in Fig. 3.7B) was observed as in Fig. 3.6B. Upon addition of MBP-superTEV and 5-fold excess ligand B, the desired DC:A:B heterodimer was formed, with no further formation of DC:A$_2$ observed. Trace (3%) formation of ligand B homodimer (DC:B$_2$) was detected by SDS-PAGE, validated by the formation of a band of equivalent mobility in a control reaction with DoubleCatcher, TEV, and excess ligand B ('DC + B + TEV + B' lane in Fig. 3.7B).

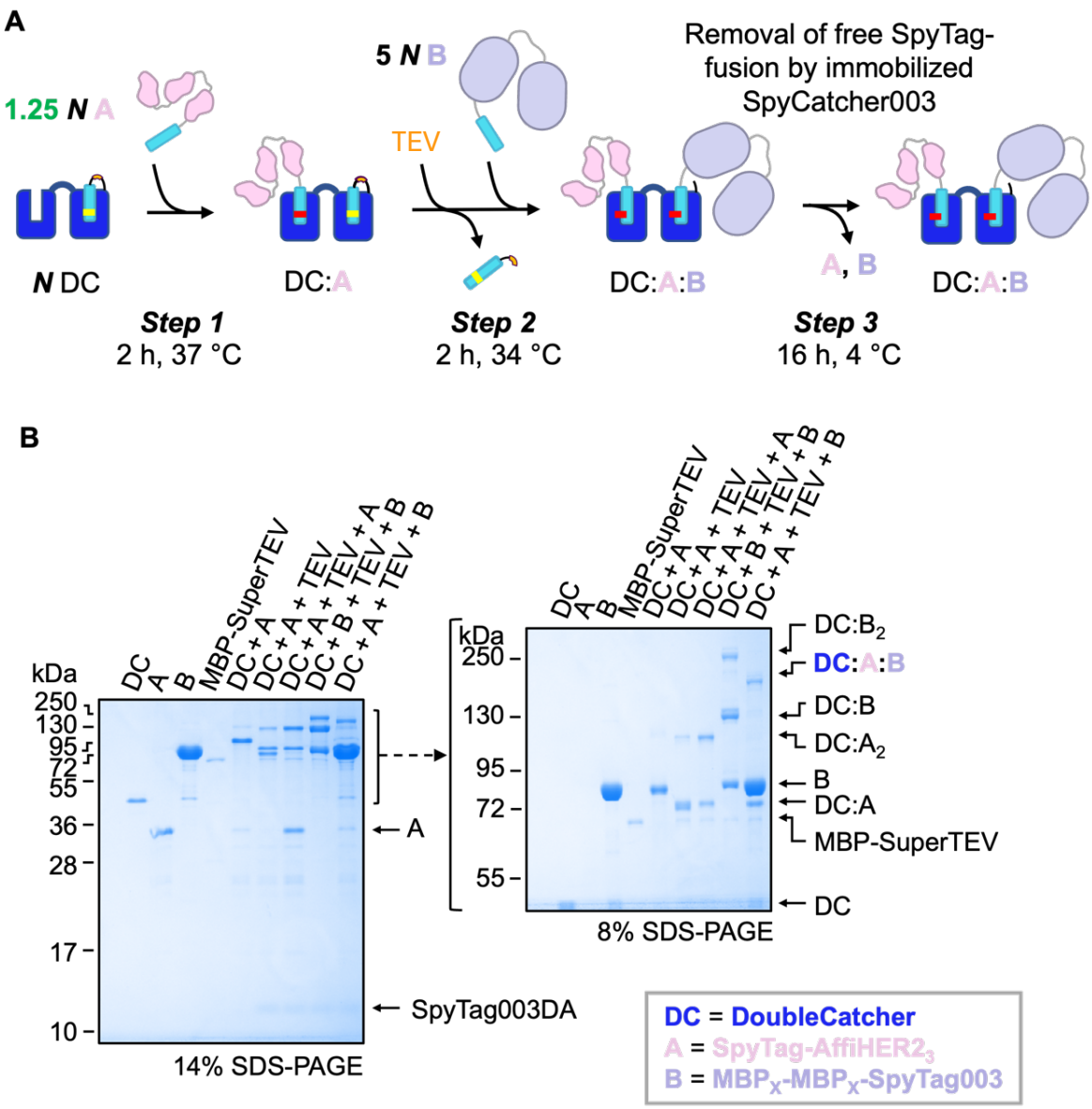


Figure 3.6. In Step 1 of SpyMask assembly protocol, Tagged binder must be in excess over DoubleCatcher to ensure saturation of its N-terminal SpyCatcher003. (**A**) Schematic depicting model heterodimerisation reaction of ligand A (SpyTag-AffiHER2$_3$; pink) and ligand B (MBP$_X$-MBP$_X$-SpyTag003; purple) onto DoubleCatcher (DC, blue). Reaction conditions that were changed from Fig. 3.5A for optimisation are highlighted in green. Colon indicates covalently linked products. *N* represents the concentration of DoubleCatcher; here $N = 5$ µM. (**B**) *Step 1* and *Step 2* of the assembly reaction depicted in (A) were conducted before analysis by SDS-PAGE/Coomassie. The identification of desired heterodimer (DC:A:B) product bands, and undesired homodimer (DC:A$_2$ or DC:B$_2$) or unreacted (DC:A) bands were facilitated by control reactions that aimed to drive the formation of these undesired products.

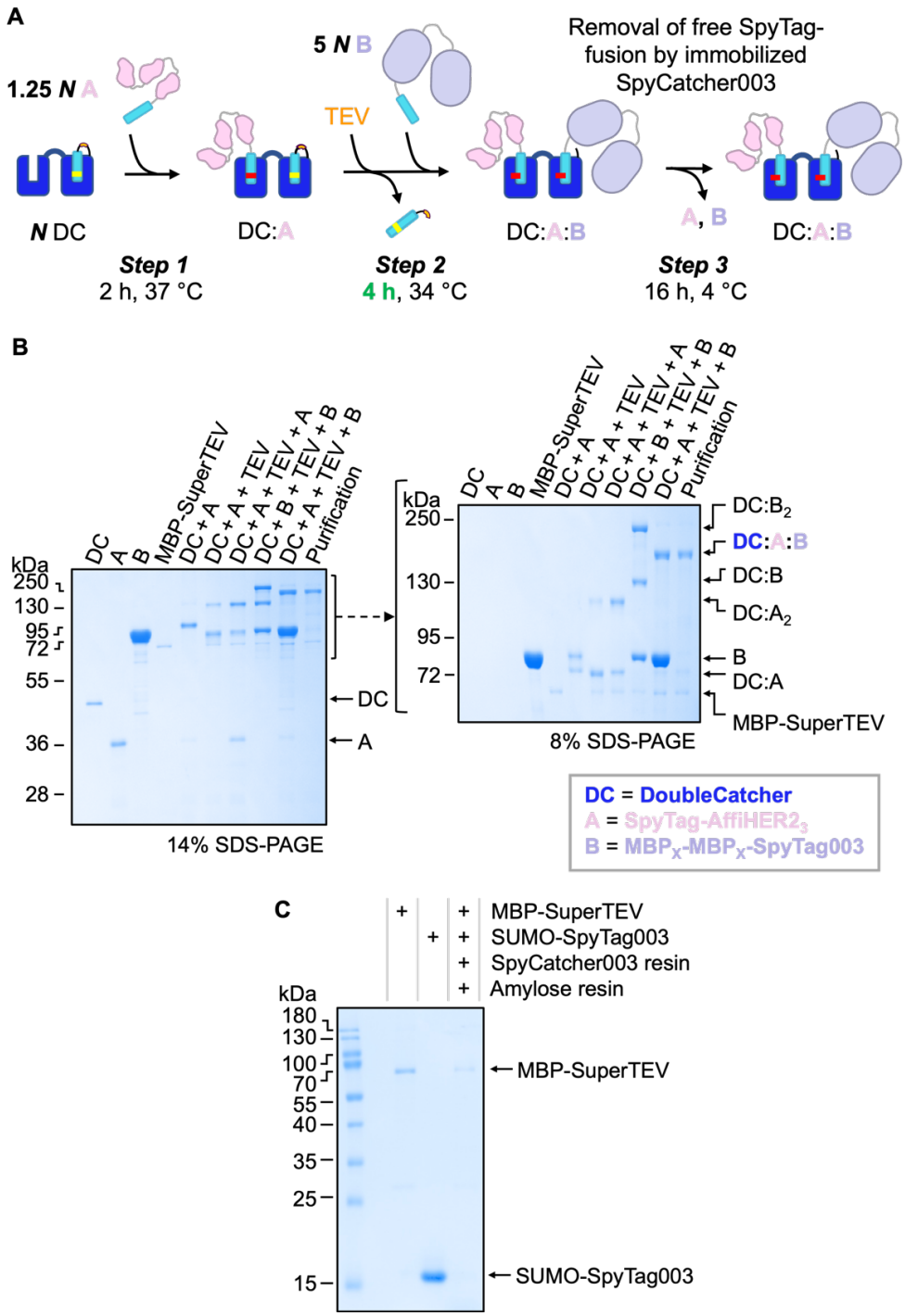


Figure 3.7. Increased incubation time of Step 2 in SpyMask assembly eliminates formation of homodimeric byproducts. (**A**) Schematic depicting optimised SpyMask protocol for stepwise and site-specific conjugation of Tagged proteins onto DoubleCatcher (DC; blue). Model proteins SpyTag-AffiHER2$_3$ (ligand A; pink) and MBP$_X$-MBP$_X$-SpyTag003 (ligand B; purple) were used for optimisation. Reaction conditions that differ from Fig. 3.6A are highlighted in green. Colon indicates covalently linked products, and *N* represents the concentration of DoubleCatcher. Here, $N = 2.5$ µM. (**B**) The heterodimerisation of ligands A and B using DoubleCatcher was performed and analysed by SDS-PAGE/Coomassie. The 'Purification' lane analyses the supernatant after incubation of the reaction mixture with agarose bead-immobilised SpyCatcher003 for 16 h at 4 °C (*Step 3*). (**C**) Co-incubation of a reaction mixture containing both MBP-superTEV and a SpyTag003-linked model protein (SUMO-SpyTag003) with a slurry of amylose agarose beads and SpyCatcher003 beads (16 h, 4 °C) allowed for depletion of both reagents from solution, as confirmed by SDS-PAGE/Coomassie.

To enrich the desired heterodimer product, the crude reaction mixture was incubated with bead-immobilised SpyCatcher003 (16 h, 4 °C) (*Step* 3, Fig. 3.7A), to deplete excess and unreacted SpyTag-linked binders from solution. As intended, SDS-PAGE confirmed the loss of the band corresponding to ligand B following purification, and densitometry revealed the purity of DC:A:B to be 95%, if excluding MBP-superTEV ('Purification' lane in Fig. 3.7B). The predominant contaminant in the reaction mixture was identified as MBP-superTEV (71 kDa, Fig. 3.7B). TEV protease has an excellent specificity for its recognition sequence, which is not found in the human proteome, and has been expressed without effect on cells (Gray et al., 2010). Therefore, TEV protease was not removed from heterodimer in this study.

However, if removal of TEV protease were to be desired, I showed that MBP-superTEV sequestration was possible in parallel with SpyTag-ligand depletion by incubating the crude reaction mixture with a mixture of immobilised SpyCatcher003 and immobilised amylose, which binds to the MBP-superTEV fusion (Fig. 3.7C).

3.3.3 Optimization of Step 3: Purification of excess SpyTag-fused binder in reaction by immobilised SpyCatcher003

Bead-immobilised SpyCatcher003 was added to bispecific assembly reaction mixtures for the removal of unreacted SpyTag-linked binders as described in the preceding Sections and is summarised in Fig. 3.8A. This resin was generated using iodoacetyl-sulfhydryl chemistry to anchor the SpyCatcher003 to agarose beads via a surface-exposed cysteine, introduced by an S49C mutation that has been used previously for site-specific fluorophore labelling and anchoring to resin (Dovala et al., 2016; Khairil Anuar et al., 2019; Vester et al., 2022). After initial coupling of SpyCatcher003 S49C to amylose beads, the binding capacity of the resin was tested by incubating titrated volumes of resin (in a 1:1 slurry in PBS pH 7.4) with 30 μM

SpyTag003-MBP at 4 °C, which was the optimal temperature for SpyTag binding by both SpyDock and SpySwitch non-covalent Catcher variants (Khairil Anuar et al., 2019; Vester et al., 2022). Since SpyCatcher003 S49C reacts irreversibly to SpyTag, binding capacity was tested after incubating resin and SpyTag003-MBP for 2 h, as well as overnight (16 h). Following incubation, samples were centrifuged (1 min, 10,000 *g*), and the supernatant was analysed by SDS-PAGE (Fig. 3.8B). Depletion of SpyTag003-MBP from solution was quantified by densitometry, as a percentage of SpyTag003-MBP in the control lane with no resin added (Fig. 3.8C). Whilst near-complete depletion of SpyTag003-MBP was achieved after incubation with 45 µL immobilised SpyCatcher003 slurry for 2 h (0.87% Tag remaining), only 15 µL resin slurry was required to achieve the same extent of SpyTag003-MBP depletion (0.35% Tag remaining) after 16 h. Therefore, overnight incubation of the reaction mixture was preferred going forward.

In addition to a minimised resin volume, scaling up of bispecific binder assembly using SpyMask would ideally include a purification step that utilises regeneratable resin, as the generation of immobilised SpyCatcher003 resin can become costly and time consuming in high quantities. The SpyCatcher003 residues that are essential for isopeptide bond formation with SpyTag are the reactive K31 and catalytic E77. It has been shown previously that mutation of either residue is detrimental to covalent reactivity (Hagan et al., 2010), but it is important to note that reactive D117 residue of SpyTag forms electrostatic interactions with the ε-amino group of SpyCatcher K31 prior to isopeptide bond formation, likely contributing to its binding affinity. Thus, careful rational engineering to generate the tight and reversible SpyTag binder SpyDock identified E77A as the most suitable mutation to inhibit covalent reactivity, whilst maintaining tight binding between the modified Catcher and its Tag (Khairil Anuar et al., 2019).

Therefore, I immobilised the SpyCatcher003 S49C E77A non-covalent variant to agarose beads following an identical protocol as used for SpyCatcher003 S49C coupling, to eliminate differences in coupling efficiency resulting from protein concentration, coupling time, and volumes of washes. I then tested the resin's binding capacity at 4 °C by incubating 30 μM SpyTag003-MBP with titrated volumes of resin slurry for 16 h, and analysing supernatant by SDS-PAGE (top, Fig. 3.8D). With 15 μL resin slurry, which was required for SpyCatcher003 S49C resin to deplete > 99% of SpyTag003-MBP, SpyCatcher003 S49C E77A resin only depleted 82.2% of Tag (light green line in Fig. 3.8C). Instead, to achieve the same extent of depletion, 90 μL resin slurry was required. Incubation at 25 °C did not improve purification capacity; after 16 h incubation with 90 μL of resin slurry, 5.3% of SpyTag003-MBP remained in solution (light blue line in Fig. 3.8C).

The previously described SpyCatcher003 mutations S59T and V94I (Vester et al., 2022), which are expected to enhance association between SpyCatcher003 and SpyTag003, were then each introduced into the SpyCatcher003 S49C E77A scaffold. Both variants – SpyCatcher003 S49C E77A S59T and SpyCatcher003 S49C E77A V94I – were immobilised to agarose beads and 30 μM SpyTag003-MBP was titrated against resin in a 1:1 slurry for 16 h. The supernatant was then analysed by SDS-PAGE (Fig. 3.8D). The improvement in depletion activity at 4 °C was marginal when S59T was introduced (0.69% Tag remaining with 90 μL resin slurry) (orange line in Fig. 3.8C), but was substantially greater in the V94I-containing variant (0.78% Tag remaining with 30 μL resin slurry) (line Fig. 3.8C, D). At 25 °C, the binding activity of both Catcher variants was reduced. However, even the best performing non-covalent variant (SpyCatcher003 S49C E77A V94I) required 90 μL resin slurry to match the activity of 15 μL SpyCatcher003 S49C resin. For the low- to medium-scale bispecific assemblies performed in this project, the covalent SpyCatcher003 resin was used for purification throughout.

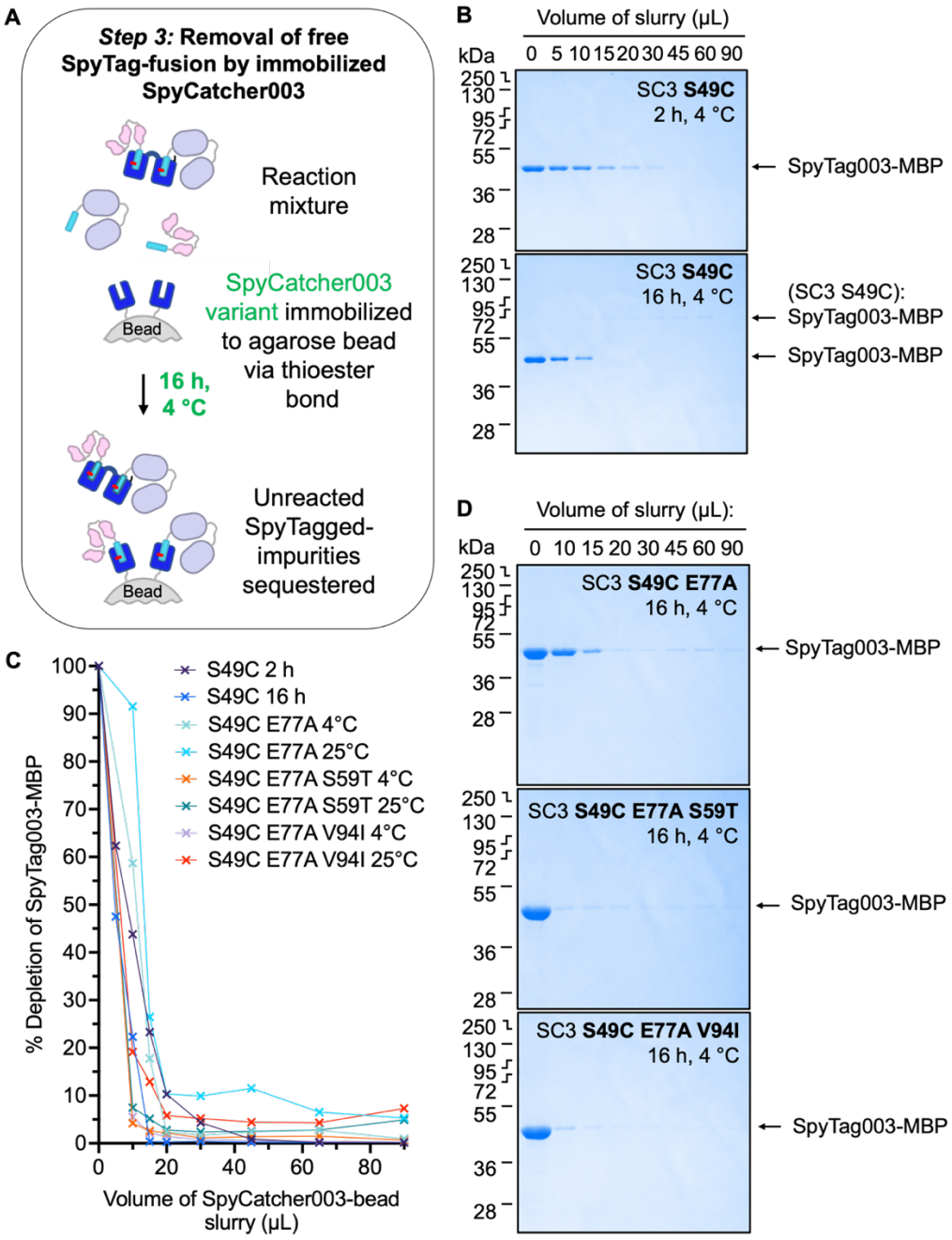


Figure 3.8. Purification of excess SpyTag-linked proteins is most efficient after incubation with reactive SpyCatcher003-immobilised agarose beads. (**A**) Schematic illustrating the purification of excess, unreacted SpyTag-linked proteins from solution by immobilised SpyCatcher003 in *Step 3* of the reaction in Fig. 3.7A. SpyTagged proteins are represented in purple or pink, with their SpyTag in cyan. DoubleCatcher is shown in blue. The reaction conditions in green were subject to optimisation. (**B**) SpyCatcher003 (SC3) was conjugated to agarose beads via a surface-exposed S49C mutation, using iodoacetyl-sulfhydryl chemistry. The efficiency of SpyTag003 depletion from solution by bead-immobilised SpyCatcher003 was tested by titrating SpyTag003-MBP (30 µM) with beads in a 1:1 slurry in PBS pH 7.4 for 2 h or 16 h at 4 °C. Supernatant was analysed by SDS-PAGE/Coomassie and the depletion of SpyTag003-MBP over time was quantified by densitometry and plotted in (**C**) (n = 1). (**D**) Substitution of the catalytic E77 residue in SpyCatcher003 to an alanine generates a variant of SpyCatcher003 that binds non-covalently to SpyTag, and S59T or V94I mutations are activity enhancing. As in (A), the depletion of SpyTag003-MBP (30 µM) with titrated volumes of resin-immobilised SpyCatcher003 E77A variant was monitored at either 4 °C or 25 °C for 16 h was monitored by SDS-PAGE/Coomassie followed by densitometry. Results are plotted in (C) (n = 1).

3.3.4 Monitoring reaction by mass photometry

The stepwise conjugation of SpyTag-AffiHER2$_3$ and MBP$_X$-MBP$_X$-SpyTag003 to DoubleCatcher using optimised reaction conditions, summarised in Fig. 3.7A, was further evaluated by mass photometry. Mass photometry is a biophysical technique that calculates the exact masses (with less than ± 5% error) of individual protein molecules in solution (Young et al., 2018). When a beam of light is used to illuminate proteins present in solution within a well on a glass coverslip, some light is reflected by the coverslip itself, and some light is scattered each time a molecule comes into contact with the coverslip surface (Asor and Kukura, 2022). The interference between reflected and scattered light –the molecule's 'shadow' – is then measured.

As the density and optical properties of all folded proteins are very similar, biomolecules scatter light at an intensity that it is directly proportional to its mass (Young et al., 2018). Therefore, accurate masses can be calculated for each individual molecule that collides with the coverslip in a single mass photometry experiment. Mass distribution histograms are then fit to Gaussian curves to extract the peak median and standard deviation (Wu and Piszczek, 2021). Therefore, mass photometry is an appropriate tool for complementing SDS-PAGE data, which provide information on relative shifts in molecular weight but cannot be used for accurate molecular weight characterisation of all proteins due to differences in their interaction with SDS (Guan et al., 2015).

Each step of the assembly reaction in Fig. 3.7B, including the control reactions, was analysed by mass photometry. As DoubleCatcher (31.1 kDa) and ligand A (33.1 kDa) are below the mass photometry limit of detection of 40 kDa (Wu and Piszczek, 2020, 2021), accurate mass distribution profiles for these controls could not be obtained.

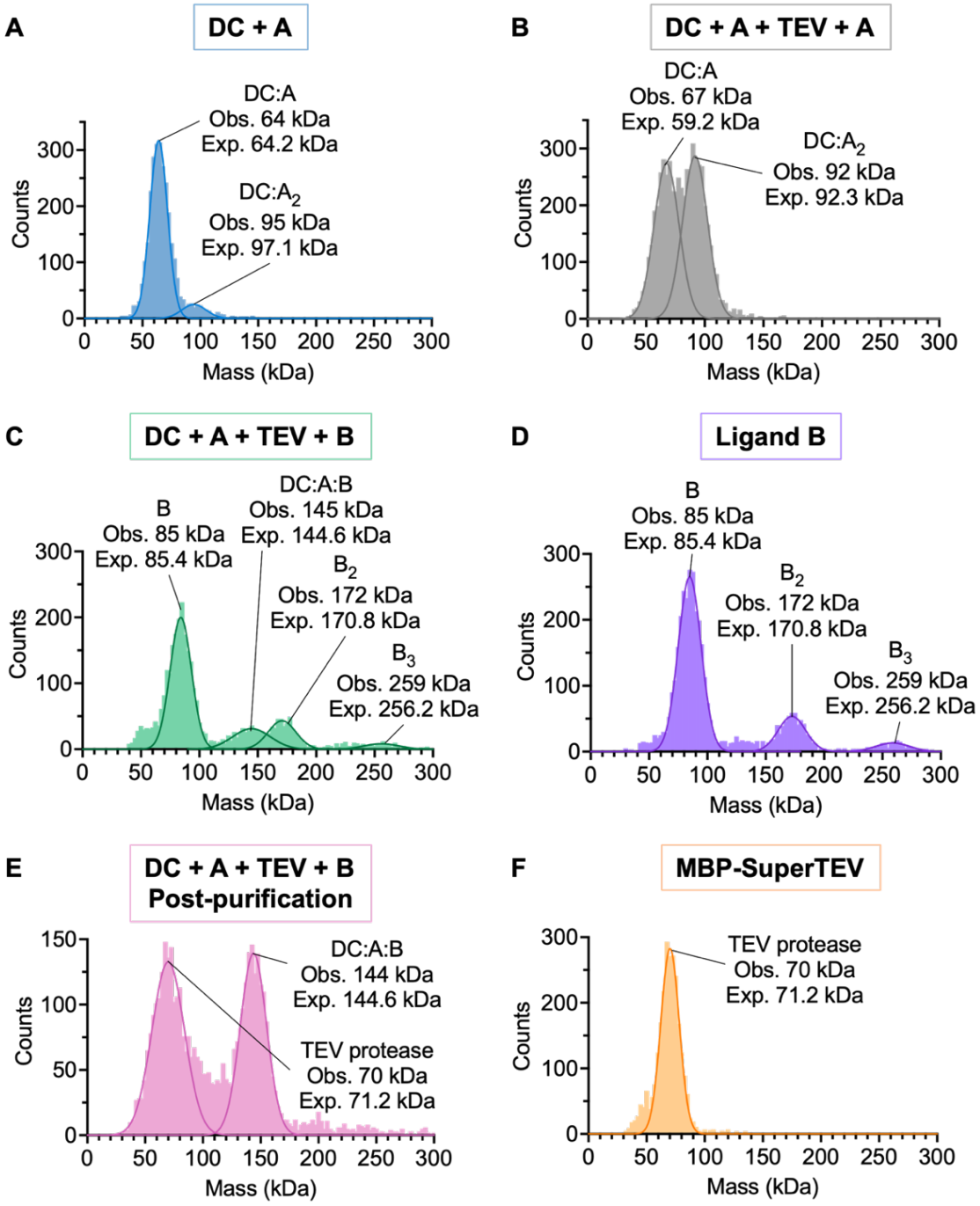


Figure 3.9. Optimised and controlled stepwise conjugation of model proteins onto DoubleCatcher was monitored by mass photometry. The stepwise conjugation of the model proteins A (SpyTag-AffiHER2$_3$) and B (MBP$_X$-MBP$_X$-SpyTag003) to DoubleCatcher (DC) as optimised in Fig. 3.7 was monitored by mass photometry. The Gaussian-determined median and standard deviation of each peak, corresponding to the mass of molecules in that subpopulation, is indicated under the peak labels in black with the expected masses. (**A**) Mass distribution of DC (5 µM) reacted with A (6.25 µM) (2 h, 37 °C; *Step 1* in Fig. 3.7A). (**B**) Incubation of the reaction mixture in (A) with MBP-superTEV protease (0.42 µM; 4h, 34 °C) and a greater excess of A (12.5 µM total) facilitated identification of the (DC:A$_2$) peak in panel (A) (**C**). Incubation of (A) with an excess of ligand B (22.5 µM) and MBP-superTEV (0.42 µM) (4 h, 34 °C; *Step 2* in Fig. 3.7A) resulted in the desired formation of the DC:A:B heterodimer. Unreacted ligand B and its non-covalent multimers were detected (**D**). (**E**) Incubation of the reaction mixture in (C) with bead-immobilised SpyCatcher003 (*Step 3* in Fig. 3.7A), resulted in the loss of peaks corresponding to excess, unreacted SpyTag(003)-linked binders. The predominant contaminant within the purified reaction mixture aligns with the of MBP-superTEV peak (**F**).

In *Step 1*, DC was incubated with a small excess (1.25-fold) of ligand A, to produce DC:A, which was validated by the peak at 64 kDa (Fig. 3.9A). In accordance with the SDS-PAGE result, a minor impurity in the reaction mixture was the formation of DC:A_2 homodimer, identified by mass photometry as a peak at 93 kDa.

Upon addition of superTEV protease and twice the concentration of ligand A to the reaction mixture, the amplitude and relative quantity of this peak in the reaction increased (Fig. 3.9B), confirming its identity as DC:A_2. I note that the observed mass of cleaved DC:A species (67 kDa) is greater than the expected mass (59.2 kDa), even when considering the expected 5% error, due to overlap with the peak corresponding to the DC:A_2 species.

In *Step 2*, superTEV protease and excess ligand B are added to the reaction mixture containing DC:A, to cleave the masking SpyTag003DA peptide from the C-terminal SpyCatcher003 moiety of DoubleCatcher and activate its reactivity. In agreement with SDS-PAGE analysis of this reaction ('DC + A + TEV + B' in Fig. 3.7B), mass photometry reveals the formation of the heterodimer (DC:A:B) at the expected molecular weight of 145 kDa (Fig. 3.9C), as well as a dominant peak at 85 kDa corresponding to unreacted B. However, the mass distribution profile also revealed peaks at 172 kDa and 259 kDa that did not correspond to bands on SDS-PAGE. As these species are multiples of 85 kDa, they were suspected to be non-covalent multimers of ligand B. To validate this hypothesis, ligand B alone control was analysed by mass photometry, revealing the identical laddering of peaks (Fig. 3.9D).

Finally, the success of purification by immobilised SpyCatcher003 in *Step 3* of the assembly reaction was corroborated by mass photometry, which showed the loss of peaks at 85 kDa, 172 kDa, and 259 kDa that were attributed to ligand B and its multimers, and a corresponding

enrichment of the peak at the expected mass (DC:A:B, 144 kDa, Fig. 3.9E). In the 'Purification' lane in Fig. 3.7B, MBP-superTEV was proposed as the only measurable contaminant present in the reaction mixture, and a peak at the expected molecular weight (70 kDa, Fig. 3.9E, F) was clearly resolved in the mass distribution profile.

3.3.5 Demonstrating generalisability of SpyMask protocol

It was important to demonstrate translatability of the optimised SpyMask reaction to the assembly of any two pairs of SpyTagged proteins, as combinatorial assembly in higher throughput should avoid the need for the assembly protocol to be optimised for each pair of binders. Therefore, I applied the SpyMask protocol to two other pairs of SpyTag-fused proteins, monitored heterodimer formation by SDS-PAGE and quantified purity by densitometry. As previously, the first binder was abbreviated to ligand A, and the second binder to ligand B. The first reaction coupled AffiHER2-SpyTag (A) and SUMO-SpyTag003 (B) to DoubleCatcher, to form DC:A:B with 88% purity, excluding TEV protease (Fig. 3.10A). In the second assembly, αDR5-SpyTag003 (A; a nanobody against Death Receptor 5, DR5) and Tras-SpyTag003 (B; a Fab against the Human Epidermal Growth Factor Receptor, HER2) were conjugated onto DoubleCatcher as exemplary binders that could be used for bispecific assembly (Fig. 3.10B). In this case, heterodimer was formed with 89% purity (excluding TEV protease). Interestingly, in both cases, the major contaminant besides MBP-superTEV in the final reaction mixture was the DC:A species, as was the case in Fig. 3.6 and resolved by increasing the incubation time in *Step 2* of the assembly reaction from 2 h to 4 h. Therefore, incubation longer than 4 h for *Step 2* may be necessary for the conjugation of larger binders that may hinder the access of TEV protease to its cleavage site, or sterically occlude a second SpyTag-binder from the C-terminal Catcher.

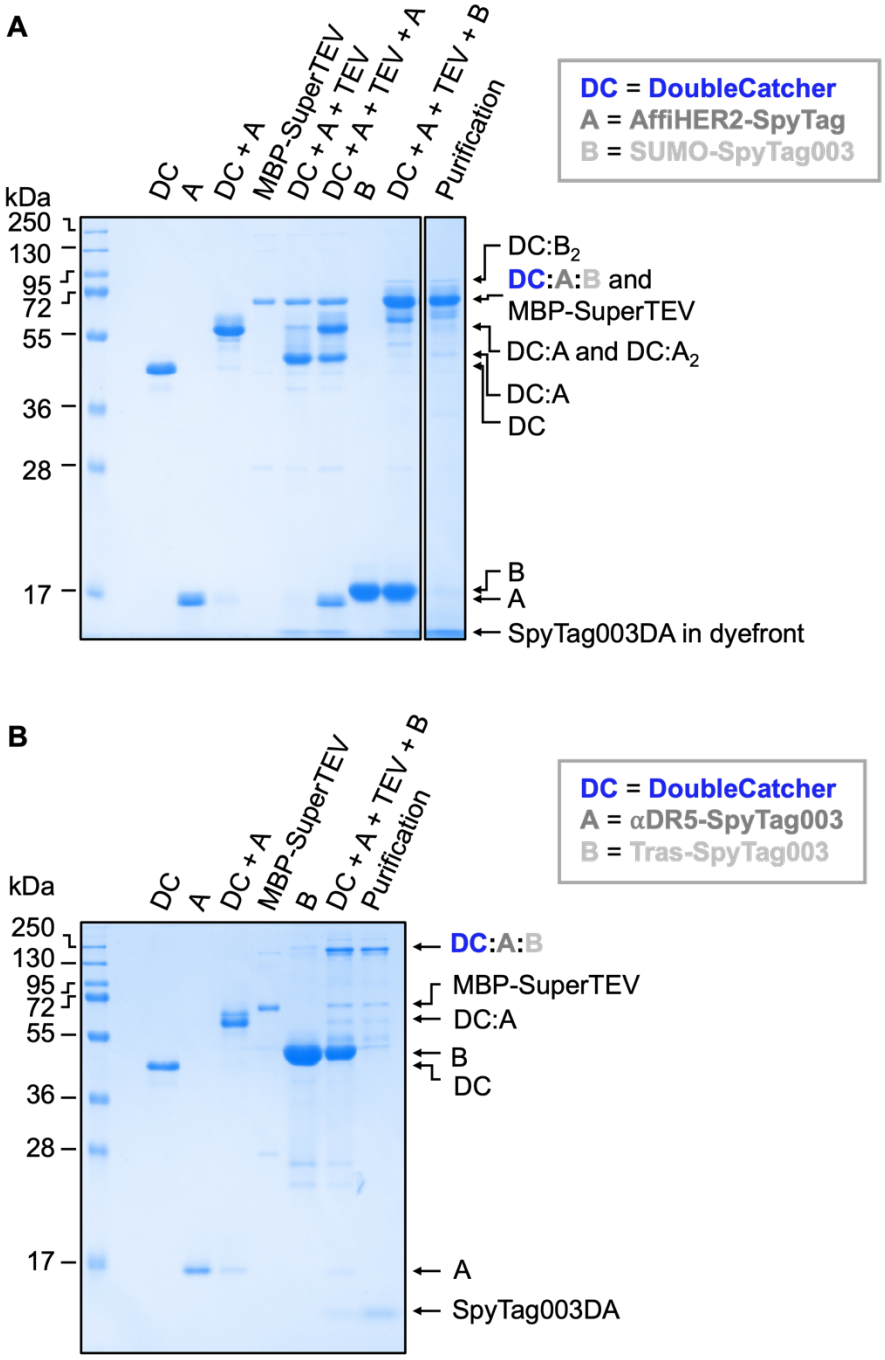


Figure 3.10. SpyMask protocol for one-pot combinatorial assembly of heterodimers is efficient with diverse pairs of Tagged proteins. The optimised SpyMask assembly pipeline was applied to assemble alternative combinations of SpyTag-linked proteins onto DoubleCatcher, to test whether the protocol is generalised. (**A**) AffiHER2-SpyTag (ligand A) and SUMO-SpyTag003 (ligand B) were conjugated onto DoubleCatcher (DC) according to the protocol in Fig. 3.7A, to produce the desired DC:A:B heterodimer with a purity of 88% (excluding TEV protease). (**B**) αDR5-SpyTag003 nanobody (ligand A) and Tras-SpyTag003 Fab (ligand B) were coupled onto the DoubleCatcher (DC) dimerisation scaffold to produce DC:A:B with 89% purity.

3.4 Discussion

For bispecific antibodies to function, they must bind and engage two targets simultaneously, often in a precise orientation for a precise duration. Bispecific antibody design thus becomes a multiparametric optimisation challenge: not only do the affinities, epitope specificities, and binder type of each parental binder within the bispecific require fine-tuning, so do the relative values of these parameters, the overall format architecture, and the flexibility of the linked binder domains. To date, the properties of parental antibodies/binders cannot be used to predict the properties of the bispecific that is produced upon their conjugation. Therefore, the quest to generate novel bispecific binders with desired mode of action and on-target activity has required the assembly and screening of hundreds-to-thousands of candidate bispecific variants (Geuijen et al., 2018; Kitazawa et al., 2012; Sampei et al., 2013). Existing combinatorial assembly platforms for the assembly of such matrices in high throughput are complicated by the need for the binders to be cloned and expressed in specialised formats (Dengl et al., 2020; Labrijn et al., 2013; Ren et al., 2021; Spiess et al., 2013).

In this Chapter, I describe the design and characterisation of a modular bispecific assembly platform, termed SpyMask, which exploits SpyCatcher/SpyTag bioconjugation technology. Unique from common bispecific antibody design strategies, the SpyMask platform enables the combinatorial dimerisation of antigen-binding building blocks which exist in a common format, namely fused to the SpyTag peptide (Antibody and Services, 2012; Keeble et al., 2017, 2019). The SpyTagged binders are coupled onto a dimerisation scaffold, termed DoubleCatcher, that harbours one reactive SpyCatcher003, and one with protease-activatable reactivity. With SpyMask, the need to produce each pair of binding proteins that you wish to assemble into their complementary formats is eliminated, but could greatly reduce the manufacturing burden of large-scale assemblies.

Inducible activation of SpyCatcher003 was achieved by fusing the non-covalent SpyTag003DA peptide to the Catcher's C-terminus via a TEV protease cleavage site. In Section 3.1.1, I determined that in the absence of TEV protease, the SpyTag003DA peptide mask within the Masked Catcher construct was shown to block > 95% of SpyCatcher003 reactivity with equimolar SpyTag003. The minimal reactivity was attributed to non-covalent dimer formation due to SpyTag003DA docking to an adjacent Catcher, rendering the SpyCatcher003 accessible for reaction. Section 3.2.3 discussed the observation that two of the five ColabFold-generated structural predictions for DoubleCatcher revealed SpyTag003DA to dock onto the C-terminal SpyCatcher003 in an inverted orientation, which was hypothesised to vastly reduce its affinity for the Catcher. As such, the peptide mask may be prone to intramolecular dissociation and intermolecular association. Thus, a series of DoubleCatcher variants were rationally designed to force the SpyTag003DA mask to dock onto SpyCatcher003 in the correct orientation. However, relative to the original DoubleCatcher construct, the improvement in masking activity of the strongest variants was negligible. It is important to note that structural predictions for DoubleCatcher using the more computationally powerful AlphaFold2 and AlphaFold3 servers (Abramson et al., 2024; Jumper et al., 2021), which were not accessible at the time, predict SpyTag003DA to dock in the correct orientation in all variants. Thus, the docking orientation is unlikely to be the direct cause of SpyTag003DA unbinding within Masked SpyCatcher003 and DoubleCatcher, which is instead simply due to the affinity of the peptide mask for SpyCatcher003.

As demonstrated in Section 3.3.2, depletion of MBP-superTEV from the reaction mixture was achieved using immobilised amylose. Analysis of the purified supernatant by SDS-PAGE/Coomassie followed by densitometry revealed depletion of MBP-superTEV to be 81%

efficient. TEV protease demonstrates highly sequence specific protease activity and has been repeatedly employed in mammalian synthetic biology (Fink and Jerala, 2022; Gray et al., 2010; Renna et al., 2022), so residual TEV protease is not a concern for therapeutic application of SpyMask-assembled bispecifics. However, MBP is known to stimulate maturation of dendritic cells (Fernandez et al., 2007), and has been shown to directly activate natural killer (NK) cells and T helper 1 (Th1) cells (Liu et al., 2017). As such, this immunostimulatory activity of MBP has been exploited for use as an adjuvant (Jie et al., 2018). Therefore, even trace amounts of MBP in the bispecific mixture may promote undesired immune activation. As MBP is large and MBP-superTEV is >800 times more dilute than the excess SpyTagged ligands being depleted from the complex reaction mixture simultaneously, amylose binding may be inefficient. Instead, purification of superTEV fused to a smaller glutathione S-transferase (GST)-tag by immobilised glutathione, or biotinylated superTEV by streptavidin-coated magnetic beads, may achieve more efficient TEV depletion. Alternatively, the second coupling step of the SpyMask protocol could be performed in the presence of bead-immobilised TEV protease (Miladi et al., 2012), thus eliminating the need to purify TEV from the final reaction mixture.

Finally, I applied the SpyMask protocol to multiple pairs of diverse SpyTag-linked binders (including a Fab, which possesses two chains and internal disulfide bonds that have the potential to complicate the reaction), to demonstrate efficient heterodimerisation using DoubleCatcher. Ideally, the SpyMask modular toolbox for combinatorial bispecific assembly developed in this chapter should permit any two SpyTag-linked ligands to be combined in a site-specific manner such that their orientation in the final heterodimeric molecule is controlled. The ability to assemble bispecifics in a one-pot reaction facilitates the scale-up of this assembly to 96-well plates or greater, so that larger matrices of bispecifics can be

assembled in parallel without the need for optimisation for each pair of binders. However, the largest ligand evaluated here for conjugation onto DoubleCatcher was the tandem MBP_X construct (85.4 kDa), so it cannot be assumed that dimerisation of larger ligands will be equally efficient. Many receptors require oligomer (> dimer) formation for activation of signalling (Heldin, 1995). As a leading example, the tumor necrosis factor (TNF) receptor superfamily requires trimerisation for activation (Locksley et al., 2001). Therefore, bispecific antibodies which aim to co-activate or modulate such receptor families may require pairing of multivalent ligands, such as elongated tandem binder repeats (Compte et al., 2018; Harwood et al., 2018). In such case, the size and shape of the ligands may sterically impede their stepwise conjugation onto DoubleCatcher, so it will be necessary to revalidate the reaction efficiency.

CHAPTER 4 – CONTROLLING HER2 DIMERISATION USING DOUBLECATCHER-ASSEMBLED ANTI-HER2 BISPECIFIC BINDERS

The work presented in Chapter 3 demonstrates the generalisability and tunability of DoubleCatcher for efficient assembly of bispecific antibodies using the SpyMask protocol. For SpyMask to be practical for use in higher-throughput bispecific discovery applications, assembly must be complemented with an activity screen of similar throughput. As a proof-of-concept, in this Chapter I generated a matrix of bispecific antibodies bridging different epitopes on the human epidermal growth factor receptor 2 (HER2) in individual wells of 96-well plates and screened the bispecifics for their effect on the metabolic activity of HER2-overexpressing breast cancer cells. HER2 has been extensively studied for its central role in pathogenesis of human breast, gastric, and ovarian cancers (Scholl et al., 2001). Deregulation of the HER2-encoding *ERBB2* gene through amplification, mutation, or post-transcriptional upregulation drives aberrant ligand-independent dimerisation with itself and other HER-family growth factor receptors (EGFR, HER3, and HER4), triggering constitutive proliferative and anti-apoptotic signalling (Lee et al., 2019).

HER2 signal transduction proceeds predominantly through the PI3K-Akt and Ras-MAPK signalling axes. However, characteristic of RTK signalling, the relative activity of each pathway is dependent on both ligand identity and cell type (Karl et al., 2020; Sweeney and Carraway, 2000; Wilson et al., 2009). Therefore, different ligands can exert distinct physiological outcomes, including proliferation, differentiation, cell survival, migration, invasion, adhesion, and apoptosis (Hsu and Hung, 2016; Yarden and Sliwkowski, 2001). For HER-family receptors, ligand bias has been ascribed to ligand-driven conformational changes which induce distinct phosphorylation signatures on the HER2 intracellular domain (Freed et al., 2017; Sweeney et al., 2000; Wilson et al., 2009). Considering 29 unique phosphorylation

sites on the HER2 intracellular domain have been reported (Hornbeck et al., 2015), many different phosphorylation patterns can arise. HER-family signalling bias has additionally been shown to reflect ligand-induced dimer strength and lifetime that determine signalling kinetics (Freed et al., 2017), or dimer identity (Macdonald-Obermann and Pike, 2014). The formation of HER-family heterodimers or homodimers is influenced by dimerisation preferences the relative expression of other HER-family receptors on HER2+ cells (Duneau et al., 2007; Kirouac et al., 2016). Although the signalling outcomes of native HER-family ligands are well-known, receptor tyrosine kinase signalling bias is yet to be exploited, enhanced, or tailored for personalised cancer therapies.

HER2 dimerisation is therefore an ideal mechanism to manipulate with structurally diverse bispecific binders, with an aim of fine-tuning the dimerisation geometry to influence downstream signalling (Brinkmann and Kontermann, 2017; Kast et al., 2021; Stüber et al., 2021). Indeed, recent single-molecule studies of HER2 receptors that were immobilised with DARPins, which were designed to cross-link different extracellular domains, revealed a binding geometry-dependence for inducing apoptosis (Stüber et al., 2021). A similar dependence on binding geometry was observed for Trastuzumab (Tras)-derived Fab dimers with altered relative orientations of their Fv regions and for Pertuzumab (Pert)-Tras bispecific molecules fused to the constant domains of the α/β T-cell receptor (TCR) (Scheer et al., 2012; Wu et al., 2015). In both cases, HER2-dependent signalling and cell proliferation was either promoted or inhibited depending on bispecific geometry. In DVD-Ig-format bispecific antibodies that incorporated Tras and Pert, both the orientation of the two variable domains and the linkers that connect them were shown to determine whether the bispecific induced apoptosis or cell cycle progression through specific disruption of HER2 heterodimer formation (Gu et al., 2014). To build upon these preliminary investigations, the work in this Chapter aims

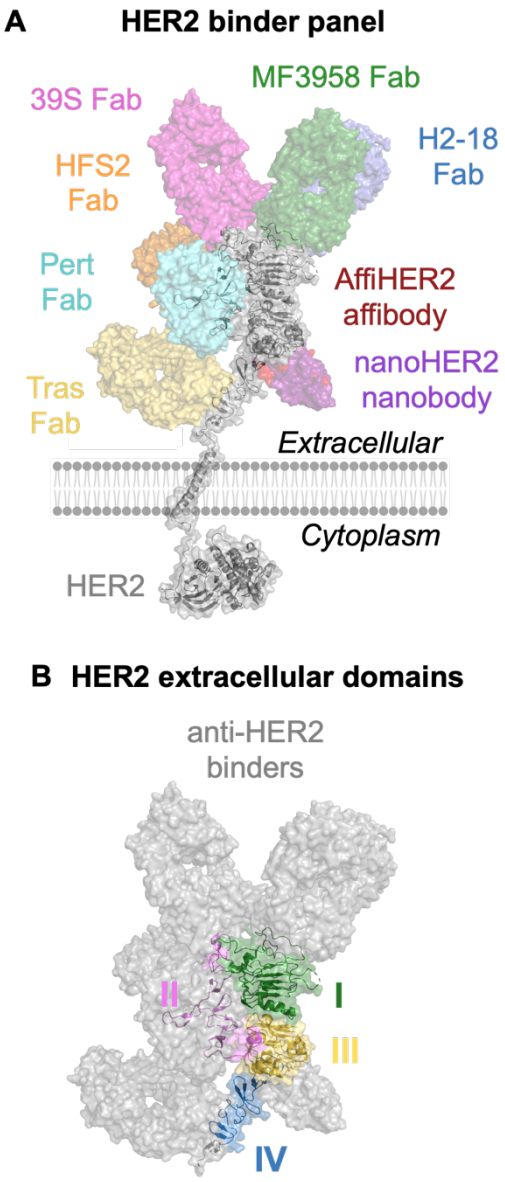
to broaden the HER2 homodimer geometries induced using biparatopic binder tools assembled by SpyMask, and screen for the consequence of these dimers on cancer cell proliferation. Bispecifics inducing HER2 heterodimers are then assembled and screened for their ability to influence cell proliferation, to demonstrate the broad range of applications of the SpyMask toolbox.

4.1 Identification and validation of panel of anti-HER2 binders targeting diverse epitopes on the HER2 extracellular domain

A phenomenon observed across the HER family of receptor tyrosine kinases is that not all ligand-induced dimer orientations have an equal ability to activate or inhibit the intracellular kinase domain (Jiang et al., 1999). Across the family, ligand binding to the receptor induces distinct structural changes in its extracellular domain to mediate the formation of symmetric or asymmetric dimers via extensive intermolecular interactions, predominantly between domain II of each receptor (Fig. 1.3) (Lemmon, 2009; Yarden and Schlessinger, 1987). Experimental and computational evidence further supports a mechanism whereby conformational changes to the extracellular domains are translated across the membrane by dictating the relative orientation of the transmembrane helices of the dimerised receptors (Arkhipov et al., 2013a; Moriki et al., 2001; Sinclair et al., 2018). While the exact mechanism of information transfer is still debated (Westerfield and Barrera, 2020), it is certain that the extracellular domain geometry mediates signalling propagation. The relative orientation of extracellular domains in HER2 dimers specifically has been attributed to differences in signalling output (Kast et al., 2021; Scheer et al., 2012; Sinclair et al., 2018). Thus, I sought to construct bispecifics that induce HER2 dimers in distinct orientations by bridging different epitopes on their extracellular domains. For this, a panel of anti-HER2 binding molecules that bound to unique epitopes on the four subdomains of the HER2 extracellular domain was identified.

4.1.1 Epitope analysis of panel of anti-HER2 binders

At least one protein binder (either an IgG-derived Fab or a recombinant nanobody or affibody) was identified from the literature for each of the four subdomains of the HER2 extracellular domain (ECD). The structures (experimentally determined or computationally predicted) of each selected binder in complex with the HER2 ECD are shown in Fig. 4.1A, with the ECD subdomains coloured in Fig 4.1B. The binding epitope of the Fabs Tras W102D, 39S, MF3958, H2-18, and Pert, have been determined previously and are summarised in Fig. 4.1C. Specifically, X-ray crystallography coupled with mutational studies validated the Tras epitope on HER2 to be subdomain IV (Cho et al., 2003; Lewis Phillips et al., 2022), and the Pert epitope on HER2 to be subdomain II (Franklin et al., 2004; Shin et al., 2019b). The 39S Fab epitope was validated to be subdomain II following the generation of human/mouse HER2 ECD chimeras, in which each subdomain of the human ECD was systematically replaced with its mouse counterpart (Oganesyan et al., 2018). The epitope of MF3958, subdomain I, was determined by crystallography together with alanine scanning of the binding interface (Geuijen et al., 2018). H2-18 was found to bind subdomain I by crystallography (Hu, S. et al., 2015). No such structural or mutational information exists for the HFS2 Fab and the nanoHER2 nanobody, and so their structures in complex with the HER2 ECD were modelled using AlphaFold-multimer (Evans et al., 2022; Jumper et al., 2021). For HFS2, 22 of the 25 highest-confidence structural predictions docked the Fab onto one common epitope on subdomain III, with the three outstanding models failing to predict the association of the Fab heavy chain with its light chain. In the case of nanoHER2, only three of the 25 predicted structures model a docking complex in which all three nanobody loops are interacting with the HER2 ECD. This nanoHER2 binding site lies at the C-terminus of subdomain III and is depicted in Fig. 4.1A.



C

HER2 Sub-domain	Binder	Epitope	Reference
I	MF3958	143–147, 160–181	(Geuijen et al., 2018)
	H2-18	112, 171-175, 185	(Hu et al., 2015)
II	HFS2	Unknown	(Salimi et al., 2018)
	39S	192–208	(Oganesyan et al., 2018)
	Pert	266–296, 298–333, 315–333	(Franklin et al., 2004)
III	AffiHER2	379, 395–401, 427–429, 485	(Eigenbrot et al., 2010)
	nanoHER2	Unknown	(Verheije, H. et al, 2013)
IV	Tras	557–561, 570–573, 593–603	(Jain et al., 2013)
	Tras NoLink	557–561, 570–573, 593–603	(Jain et al., 2013)

Figure 4.1. Panel of anti-HER2 binders spans epitopes across all four subdomains of the HER2 extracellular domain. (**A**) Epitopes of a panel of selected anti-HER2 binders span a broad surface area of the HER2 extracellular domain (ECD). The HER2 transmembrane domain and cytoplasmic juxtamembrane and kinase domains are shown, positioned in the plasma membrane to illustrate their relative positioning. Each binder is shown in a different colour bound to HER2. Docking structures are derived from crystal structures, except for HFS2 Fab and nanoHER2, which are based on AlphaFold2-multimer predictions of their docking sites on HER2 ECD. (**B**) For each subdomain (I-IV) of the HER2 ECD, at least one protein binder was identified. The HER2 ECD is shown coloured according to subdomain, with anti-HER2 binders from (A) overlaid in grey. (**C**) For each subdomain of the HER2 ECD, the selected binders are listed with their epitope listed. Here, epitope describes the residues that interact directly with the protein binder via hydrogen bonds, van der Waals, hydrophobic interactions, or ionic bonds.

Each binder was cloned with a C-terminal SpyTag003, except for AffiHER2 which was cloned previously by Tomohiko Nakamura (Howarth group) with a C-teminal SpyTag. All Fab binders were expressed in Expi293 cells, while the recombinant binder nanoHER2 was expressed in *E. coli* BL21, and AffiHER2 in *E. coli* T7 Express. Binders were purified by Ni-NTA, including a wash step with 0.1% (v/v) Triton X-114 to ensure the concentration of endotoxin from the protein samples was below 1 endotoxin unit/mL, as according to Limulus amebocyte lysate (LAL) Chromogenic Endotoxin Quantitation Kit (Thermo Fisher) (Aida and Pabst, 1990).

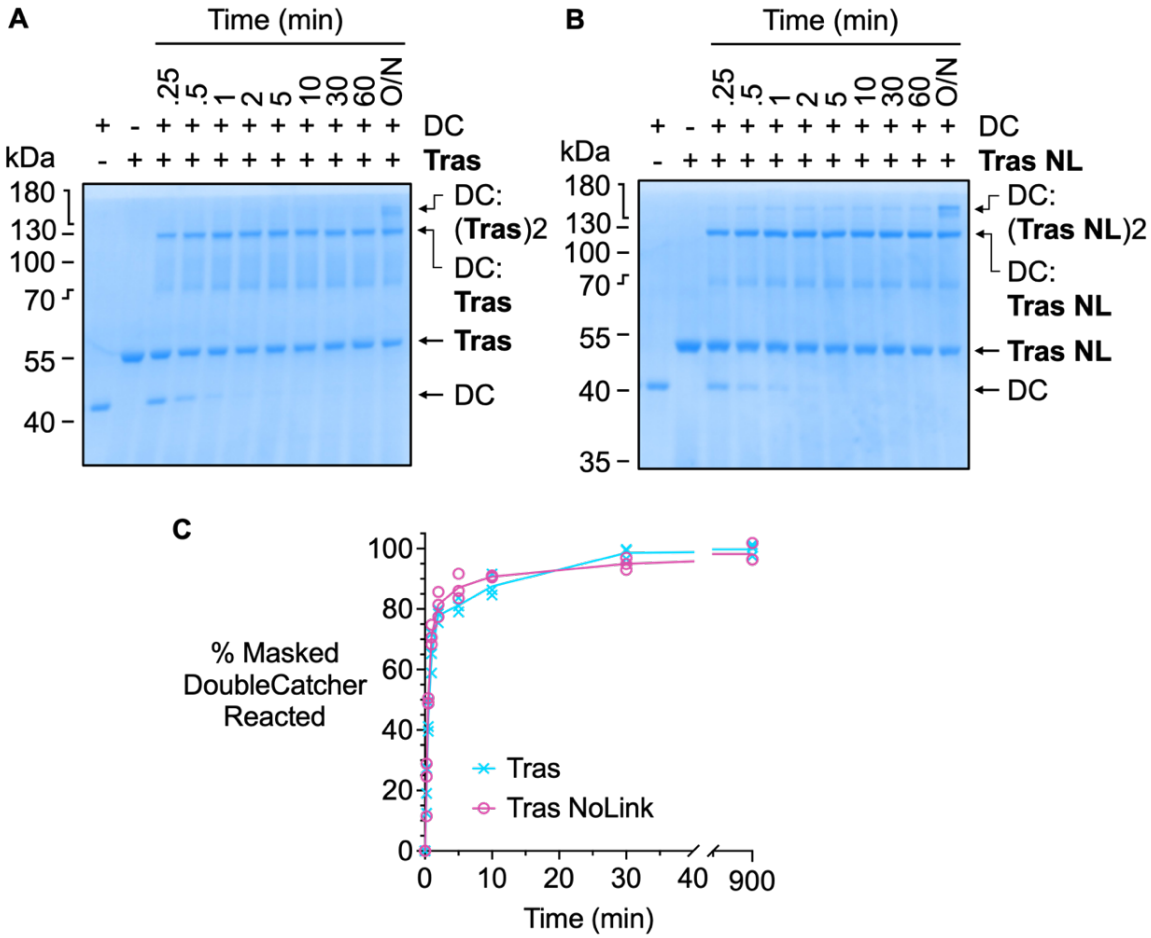


Figure 4.2. The reactivity of Tras Fab with DoubleCatcher is unaffected when the linker between the Fab and SpyTag003 is removed. The tripeptide linker connecting Tras Fab (Tras) and SpyTag003 was removed to generate Tras NoLink (Tras NL), to reduce the flexibility between the DoubleCatcher (DC) and the binder. The time-course of reaction between DoubleCatcher (2.5 µM) and either Tras (5 µM; **A**) or Tras NL (5 µM; **B**) in PBS pH 7.4 at 37 °C was analysed by SDS-PAGE with Commassie staining at the times indicted. Reactions were conducted in the absence of TEV protease to monitor the reactivity of the Fab with a single Catcher moiety of DoubleCatcher. (C) The reactivity of Tras or Tras NoLink with DoubleCatcher was quantified by densitometry. Each datapoint is shown (n = 3 independent reactions), with the line connecting the mean.

4.1.2 Validation of reactivity of Fab with truncated linker to SpyTag

When using a DoubleCatcher-assembled bispecific antibody to trap cell-surface proteins in a defined geometric arrangement, it is imperative that flexibility of the bispecific molecule is minimised. A bispecific constituting two SpyTagged binders that are conjugated onto DoubleCatcher possesses three positions of translational and rotational freedom: between each binder and its SpyTag, and between the two SpyCatcher003 moieties of DoubleCatcher. I initially tested the importance of Binder-SpyTag linker flexibility on activity, by including two variants of the same anti-HER2 binder in the panel for bispecific assembly: one with a GSG linker between Tras and the SpyTag003, and one with no linker (termed Tras NoLink). The NoLink variant was confirmed to react to 97% in 1 h in PBS pH 7.4 at 37 °C with DoubleCatcher, as determined by SDS-PAGE with densitometry (Fig. 4.2). The reaction efficiency of Tras NL is comparable to the linker-containing parental construct (99% in 1 h under equivalent reaction conditions; Fig. 4.2), confirming that reactivity is not impaired by removing the linker between the Fab and the reactive peptide.

4.1.3 Validating mass of anti-HER2 binders by mass spectrometry

Each purified anti-HER2 binder-SpyTag fusion was validated by intact protein mass spectrometry, to confirm the protein identity and the formation of the expected disulfide bonds. The observed and expected masses of each binder are displayed in Fig. 4.3A-I. The single disulfide bond expected to form for nanoHER2, which is llama in origin (Mendoza et al., 2020; Verheije et al., 2013), was observed in its mass spectrum (Fig. 4.3A). Each Fab is expected to form five disulfide bonds: two intramolecular disulfides within the heavy chain, two within the light chain, and one intermolecular disulfide bridging the C-termini of the heavy and light chains (Fig. 4.3C-H). The sequence for Pert Fab omits the heavy chain C-terminal pentapeptide extension EPKSC, encoding the IgG1 upper hinge region that enables the heavy-light inter-

chain disulfide bridge. In the assembly of multi-specific antibodies, the inter-chain disulfide bridge is desirable to avoid light chain mispairing during assembly (De Kruif et al., 2019). Therefore, only two disulfides are expected to form for each chain of the Pert Fab, with tight non-covalent interactions facilitating heavy-light chain pairing, as was observed in its mass spectrum (Fig. 4.3I). However, an unexpected +119 Da adduct was observed for the Pert light chain.

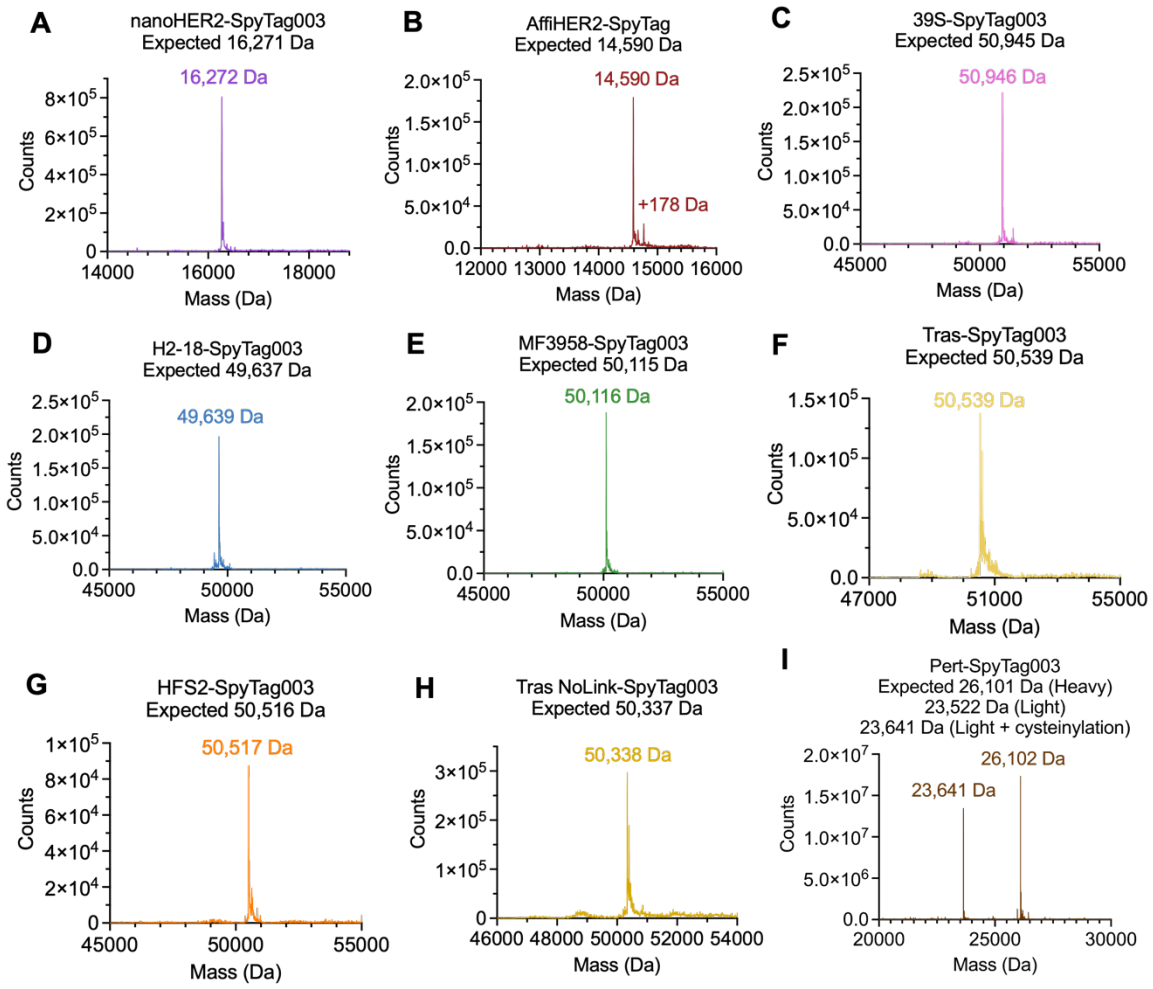


Figure 4.3. Mass spectrometry of HER2 binding proteins. Intact Electrospray Ionisation Mass Spectrometry of the SpyTagged anti-HER2 Fabs, affibody, and nanobody, described in Fig. 4.1 for use in the assembly of anti-HER2 bispecifics. The observed mass is indicated above the main peak. In (B), the minor +178 Da peak relates to gluconoylation (Geoghegan et al., 1999). In (I), since the hinge region is omitted from the Pert-SpyTag003 heavy chain sequence, there is no interchain disulfide bond in the Pert Fab, and so the heavy and light chains are two independent species. The +119 Da mass adduct observed for Pert-SpyTag003 light chain (of the kappa isotype) relates to cysteinylation, as previously observed on human IgG1 kappa light chains (Lim et al., 2001). The expected mass was calculated from ExPASy ProtParam. The Pert Fab heavy chain was reformatted to include the N-terminus of the hinge region.

The same mass adduct (+119 Da) has been identified on human IgG1 kappa light chains, the class of Pert Fab light chains, originally by the group of Costello (Lim et al., 2001) and by Gadgil *et al*. (Gadgil et al., 2006). The mass shift has been attributed to an S-cysteinylation at the C-terminal free cysteine – a post-translational modification that has a proposed role in regulating light chain stability without impacting binding affinity. Indeed, reduction of Pert-SpyTag003 Fab by incubation with DTT resulted in the loss of the 119 Da adduct from the expected mass (Fig. 4.4A). Upon insertion of the 'upper hinge' region to the C-terminus of the Pert heavy chain, expected formation of the heavy-light inter-chain disulfide bond was observed and again, the +119 Da adduct was not present (Fig. 4.4B), supporting the hypothesised post-translational modification of the free cysteine in the hinge-free Pert construct.

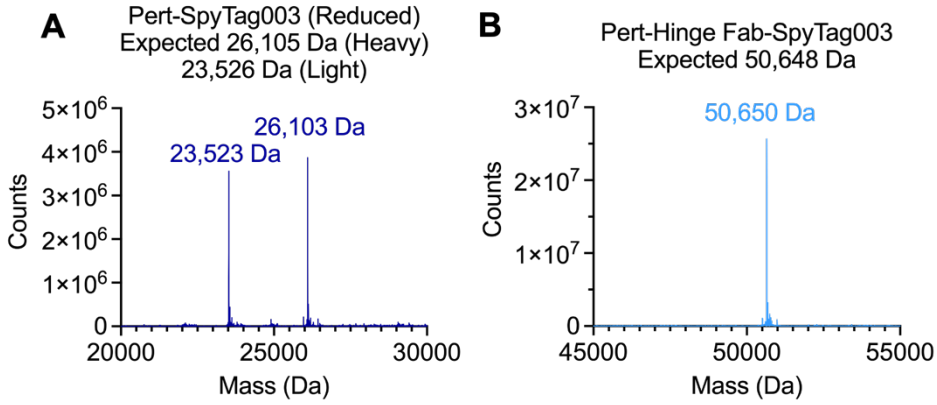


Figure 4.4. Without an upper-hinge region, the Pert-SpyTag003 Fab is post-translationally cysteinylated. (**A**) The +119 Da mass shift of the Pert-SpyTag003 Fab light chain is lost after treatment with 10 mM DTT, confirmed by mass spectrometry and consistent with the loss of a cysteinylation post-translational modification and the reduction of two intrachain disulfide bonds. (**B**) When Pert Fab-SpyTag003 is reformatted to contain the upper-hinge region at the C-terminus of its heavy chain, covalent heavy-light chain pairing and intramolecular disulfide bond formation is observed as expected. Accordingly, cysteinylation is not observed.

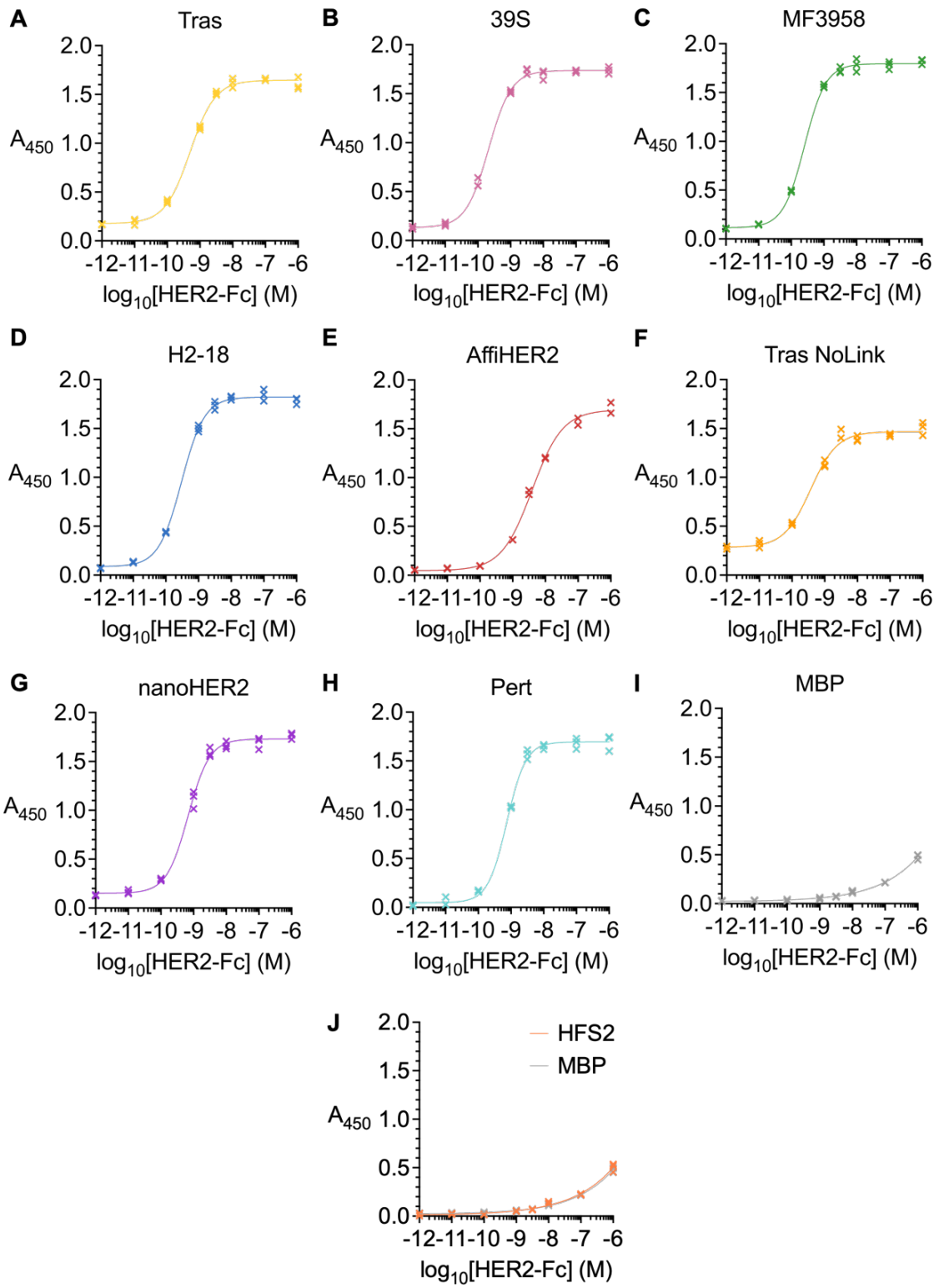


Figure 4.5. Validation of binder panel interaction with purified HER2 by ELISA. The binding activity of each anti-HER2 binder described in Fig. 4.1 to recombinant HER2 ECD-Fc was measured by ELISA. Wells were coated with purified SpyCatcher002-MBP, after which each 80 nM of each binder was added. Purified HER2 ECD-Fc was titrated into each well, before detection of binder-HER2 ECD Fc binding with anti-human IgG Fc-HRP and TMB substrate. As a negative control, 80 nM SpyTag003-MBP was conjugated to SpyCatcher002-MBP-coated wells instead of binder. Each triplicate data point is shown, with the line connecting the mean (n = 3). Background signal from SpyCatcher002-MBP-coated wells treated with buffer and anti-Fc HRP antibody alone was subtracted from all sample wells.

4.1.4 Validating binding activity of anti-HER2 binders on recombinant soluble HER2 extracellular domain by ELISA

Each anti-HER2 binder identified was re-formatted to display a terminal SpyTag peptide for conjugation to DoubleCatcher, so it was necessary to characterise specific binding to the HER2 ECD following expression and purification. First, the level of binding of each binder to the soluble HER2 ECD was quantified by an enzyme linked immunosorbent assay (ELISA). Here, 96-well plates were coated with 80 nM of SpyCatcher002-MBP and incubated with equimolar SpyTag-linked binder, or SpyTag003-linked MBP as a control. Recombinantly expressed HER2-Fc was titrated onto each well, before detection with a mouse anti-human IgG Fc antibody conjugated with HRP. Figure 4.5 displays the HER2-Fc titration curves for each individual SpyTag-fused binder annotated with the half-maximal effective concentration (EC_{50}) values of binding to HER2, or SpyTag003-MBP negative control.

For binders in Fig. 4.5A-H, strong binding to HER2 was measured. However, it was observed that the HFS2-SpyTag003 Fab had non-detectable binding HER2 ECD, with an ELISA titration profile comparable to that of a non-HER2 binding negative control, SpyTag003-MBP (Fig. 4.5J). The parental paper from which I obtained the variable sequences of the Fab was missing specific binding characterization (Salimi et al., 2018), and the use of this Fab has not been reported elsewhere. Therefore, the HFS2-SpyTag003 Fab was removed from the panel of binders to be used for assembly of anti-HER2 biparatopic binders.

4.1.5 Validating binding activity of anti-HER2 binders on HER2-overexpressing cells by flow cytometry

An important feature of the ELISA experimental setup is that the soluble recombinant HER2 ECD antigen was expressed fused to an IgG Fc domain, to facilitate cellular processing and

secretion from Expi293F expression cells (Lo et al., 1998). As the IgG Fc domain naturally forms covalent dimers via inter-chain disulfide bond formation between each hinge region, the HER2 ECD-Fc chimera is titrated as a dimer (Zizzari et al., 2011). Previous molecular dynamics simulations of HER2 dimerisation within a lipid bilayer predict the dimerisation interface in subdomain II to be maintained (Zhao et al., 2021). Therefore, whilst tight binding activity was still detected for the subdomain II-specific Fabs 39S (Fig. 4.5B) and Pert (Fig. 4.5H; which inhibits dimerisation of the HER2 ECD via domain II blockade (Franklin et al., 2004)), it is possible that the undetectable HFS2-HER2 binding by ELISA was due to steric occlusion of its epitope at the dimerisation interface.

Additionally, it was important for the ELISA binding data to be corroborated on cell-surface expressed HER2, on which bispecifics will be applied for subsequent phenotypical studies. Thus, each SpyTag-linked binder was reacted with SpyCatcher002-sfGFP, and their binding to HER2-overexpressing human adenocarcinoma SKBR3 cells was detected by flow cytometry (Fig. 4.6). As a control for background fluorescence, cells were treated with SpyCatcher002-sfGFP alone, or with SpyCatcher002-sfGFP conjugated to a nanobody targeting CD45, whose expression is restricted to haematopoietic cells (Trowbridge and Thomas, 1994).

In support of the ELISA data obtained for the HFS2-SpyTag003 Fab, HFS2 binding to HER2 on cells was also non-detectable above the background using flow cytometry (orange curve, Fig. 4.6). Pleasingly, the other binders identified for assembly into bispecifics were found to bind efficiently to SKBR3 cells. To test for specificity to HER2, the Pert-SpyTag003 variant possessing the upper hinge domain on its heavy chain was assessed by flow cytometry for binding to the HER2 negative cell line MDA-MB-468. As expected, there was no binding detected above the background fluorescence from the two negative control samples.

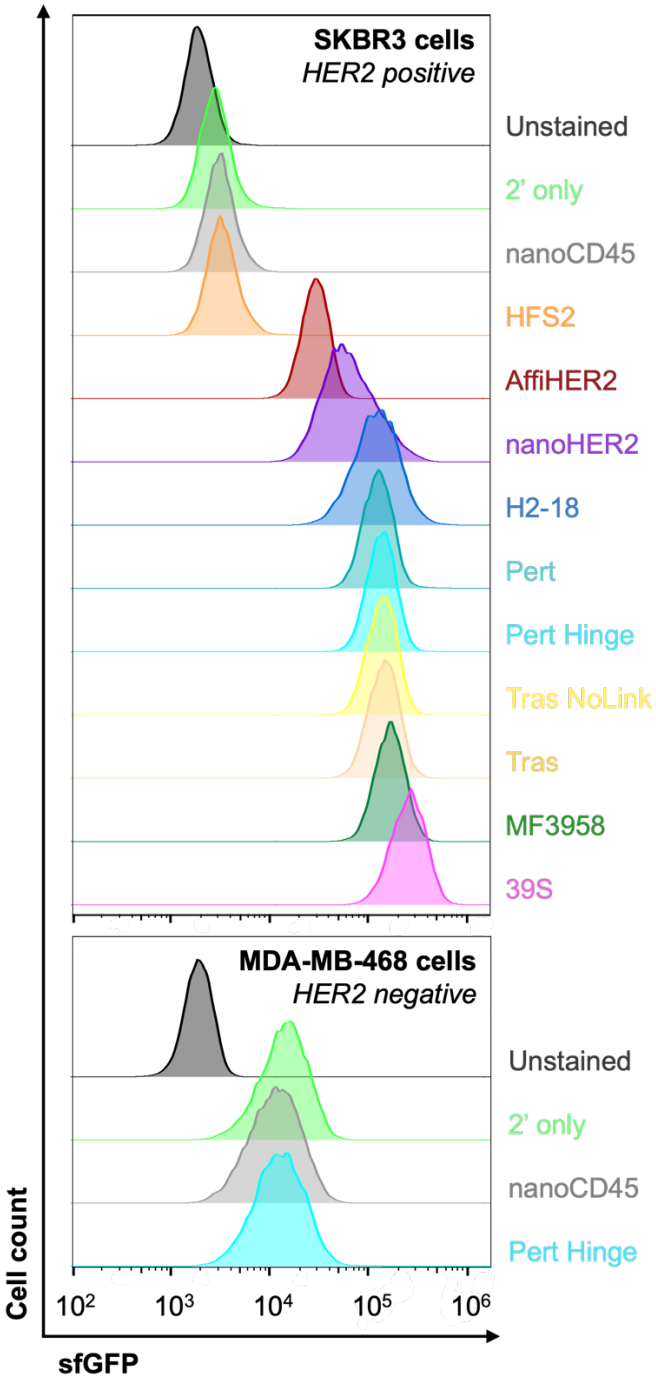


Figure 4.6. Validation of binder panel interaction with HER2 on cells by flow cytometry. Anti-HER2 binders pre-conjugated to SpyCatcher002-sfGFP (2 µM) were incubated with HER2-positive SKBR3 cells (top) or HER2-negative MDA-MB-468 cells (bottom) in HBS pH 7.2 + 10% (v/v) FBS for 30 min at 37 °C with 5% (v/v) CO_2 before detection of sfGFP fluorescence by flow cytometry. To detect background signal, cells were incubated with buffer only ('Unstained'), SpyCatcher002-sfGFP alone ('2' only'), or with the anti-CD45 binder nanoCD45 conjugated to SpyCatcher002-sfGFP. SKBR3 cells do not express CD45.

4.1.6 Elucidation of HER2 epitopes recognised by nanoHER2 by HER2:nanoHER2 complex prediction using AlphaFold2-multimer and competition ELISA

Of the validated binder molecules in the panel, the only binder whose binding epitope on HER2 ECD has not been fully characterised is nanoHER2, beyond the knowledge that its epitope is non-overlapping with that of Trastuzumab (Tras W102D) (Vaneycken et al., 2011). Thus, the 25 highest-confidence AlphaFold2-multimer docking structures for nanoHER2 with the HER2 ECD were scrutinised for their quality of binder-HER2 interaction (Evans et al., 2022; Jumper et al., 2021).

It is understood that the three variable loops within the variable regions of an antibody contribute to > 80% of all antigen-binding residues, with 94% of interacting residues residing in clear consensus regions of the antibody sequence (Kunik et al., 2012). Conversely, there is little such consensus between nanobody paratopes, with different combinations of variable loops and semi-conserved framework regions contributing to binding across a set of 156 unique nanobody:antigen co-crystal structures (Mitchell and Colwell, 2018a). While it is not impossible for the nanobody H3 loop alone to enable antigen binding (Rasmussen et al., 2011), two or more CDR loops were shown to contribute to antigen binding in at least 98% of the nanobody:antigen co-crystal structures analysed by Mitchell and Colwell, 2018a (Mitchell and Colwell, 2018a). Additional analysis of 90 non-redundant nanobody:antigen co-crystal structures revealed an average of 18.8 residues per paratope (Mitchell and Colwell, 2018b), but antigen binding has been achieved with a nanobody paratope as small as 4 interacting residues (Gordon et al., 2023), as observed in a more extensive analysis of 301 unique nanobody:antigen structures. Thus, I chose to filter the top 25-predicted docking structures for nanoHER2 and HER2 ECD by those with a paratope of at least 4 interacting residues, spanning at least two variable loops. NanoHER2 residues that interact with the HER2 ECD were identified using

Arpeggio (Jubb et al., 2017), where interactions include van der Waals, hydrophobic interactions, steric clashes, covalent bonds, and hydrogen bonds. Interestingly, the remaining docking structures shared a common epitope on the HER2 ECD, namely at the C-terminal end of subdomain III. A representative example of such filtered nanoHER2:HER2 ECD docking prediction is shown in Fig 4.7A, with the interacting residues highlighted in Fig 4.7B.

To confirm this epitope prediction, I performed a competitive ELISA, in which wells coated with immobilised nanoHER2 were incubated with soluble HER2 ECD-Fc that was pre-incubated with titrated amounts of a second, epitope-validated HER2 binder from the panel identified and characterised in Sections 4.1.1-4.1.5. The competitive ELISA setup is summarised in Fig. 4.7C. If the titrated binder has an overlapping epitope with nanoHER2, the binder will compete with nanoHER2 for HER2 ECD-Fc binding, thus reducing nanoHER2:HER2 binding, and the resulting signal measured by Fc detection. However, if the titrated binder binds HER2 at an epitope unique to that of nanoHER2, nanoHER2:HER2 ECD-Fc binding will be unimpeded, and the ELISA signal will not decrease. In agreement with the filtered AlphaFold2-multimer- predicted nanoHER2 epitope on subdomain III, the only anti-HER2 binder to compete with nanoHER2 for HER2 ECD-Fc binding was AffiHER2, which is the only binder in the panel to bind subdomain III. Thus, nanoHER2 was classified as a subdomain III binder in subsequent analyses.

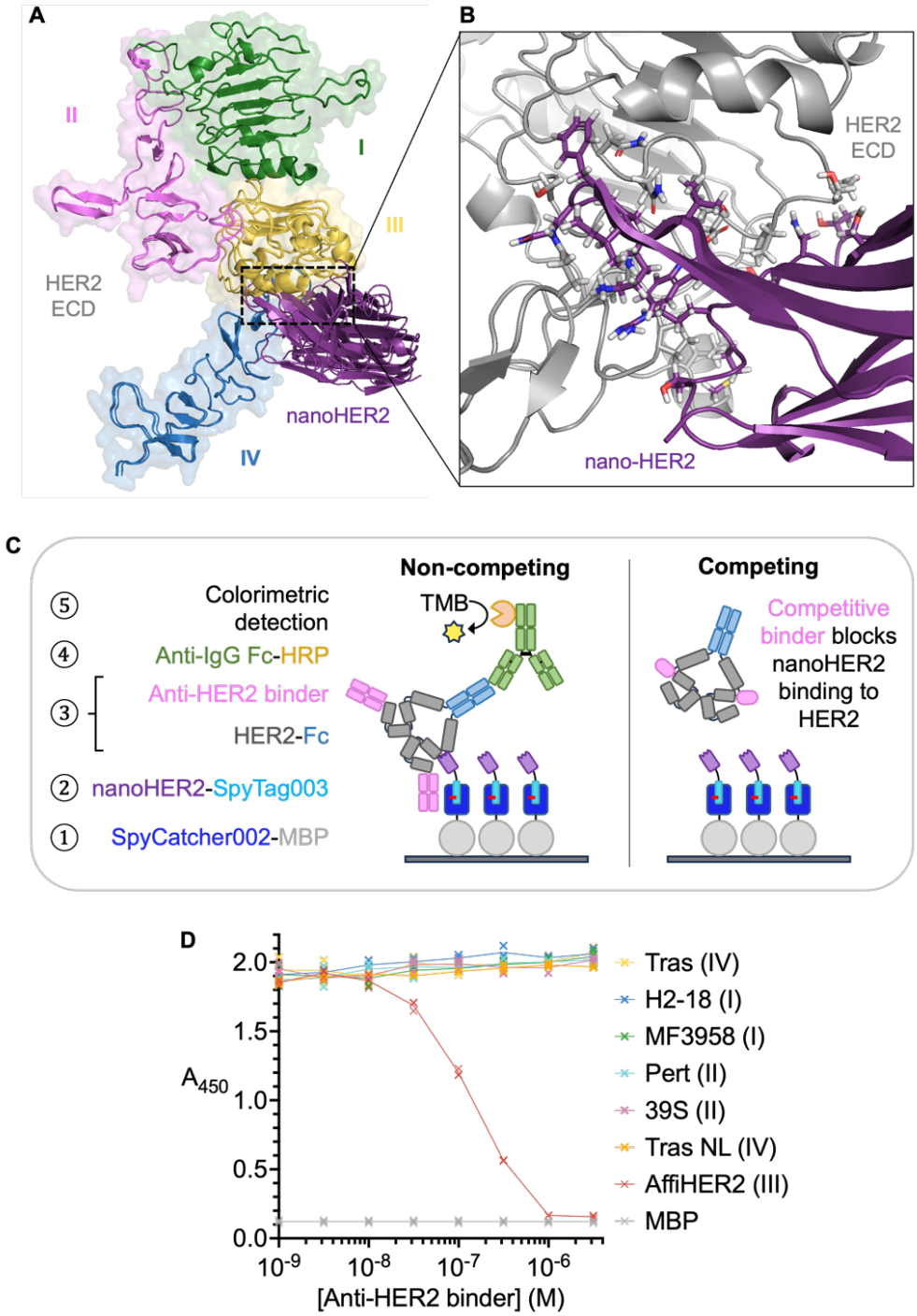


Figure 4.7. Elucidation of nanoHER2 binding epitope on HER2 by complex prediction and competitive ELISA. (**A**) AlphaFold-multimer-predicted docking of nanoHER2 to HER2 ECD. Docking structures are filtered by those which predict at least 4 interacting residues on nanoHER2, spanning at least two variable loops, to contribute to the interaction interface. HER2 ECD is presented in cartoon format with surface representation and coloured by subdomain, with filtered nanoHER2 docking structures represented in cartoon format and coloured purple. **(B)** The binding interface between the highest ranked nanoHER2 AlphaFold2 docking structure from (A) with HER2 ECD. Residues at the interface are shown in stick format. (**C**) To validate the predicting binding epitope of nanoHER2 on HER2 ECD, a competition ELISA was performed as outlined in the schematic. Numbers indicate the order of addition to the well. (**D**) Competition ELISA on nanoHER2 with HER2 ECD-Fc pre-incubated with the titrated amounts of each anti-HER2 binder as indicated. Triplicate points are shown with the line connecting the mean. MBP is a negative control where SpyCatcher002-MBP-coated wells were reacted with SpyTag003-MBP, instead of nanoHER2-SpyTag003.

4.2 Assembly of matrix of anti-HER2 biparatopic binders using DoubleCatcher

4.2.1 Validation of bispecific assembly by SDS-PAGE and mass spectrometry

To assemble a matrix of bispecifics that bridge every combination of HER2 ECD epitopes targeted by the selected panel of anti-HER2 binders, each binder was dimerised with itself or another binder using the optimised SpyMask protocol (Fig. 3.7A). Dimerisation reactions were conducted in parallel, in individual wells of a 96-well plate, to demonstrate that bispecifics can be assembled by SpyMask with similar throughput to their downstream screening assays. A subset of DoubleCatcher-assembled biparatopic molecules (at least one bispecific harboring an N-terminal Fab, nanobody, or affibody, and at least one bispecific harbouring a C-terminal Fab, nanobody, or affibody) were analysed by mass spectrometry to confirm their correct assembly and purity (Fig. 4.8). DoubleCatcher-assembled molecules that dimerised the same binder ('homodimers') within this subset were omitted from analysis by mass spectrometry, as the by-products from homodimeric assemblies are the same as the target molecule.

Pleasingly, mass spectrometry analysis of each representative biparatopic binder revealed the presence of a dominant peak that corresponded to the expected mass of the desired heterodimer within 5 Da, which is within acceptable error for intact protein UPLC-MS using Waters ethylene bridged hybrid amide columns (Li et al., 2023), such as the one used here. Expected masses were calculated using ExPASy ProtParam (Wilkins et al., 1999), and considered the loss of two water molecules (-36 Da) upon isopeptide bond formation to each SpyCatcher003 moiety of DoubleCatcher, as well as the loss of the N- and C-terminal peptides that flanked the two TEV recognition sites within the DoubleCatcher construct (-5,059 Da).

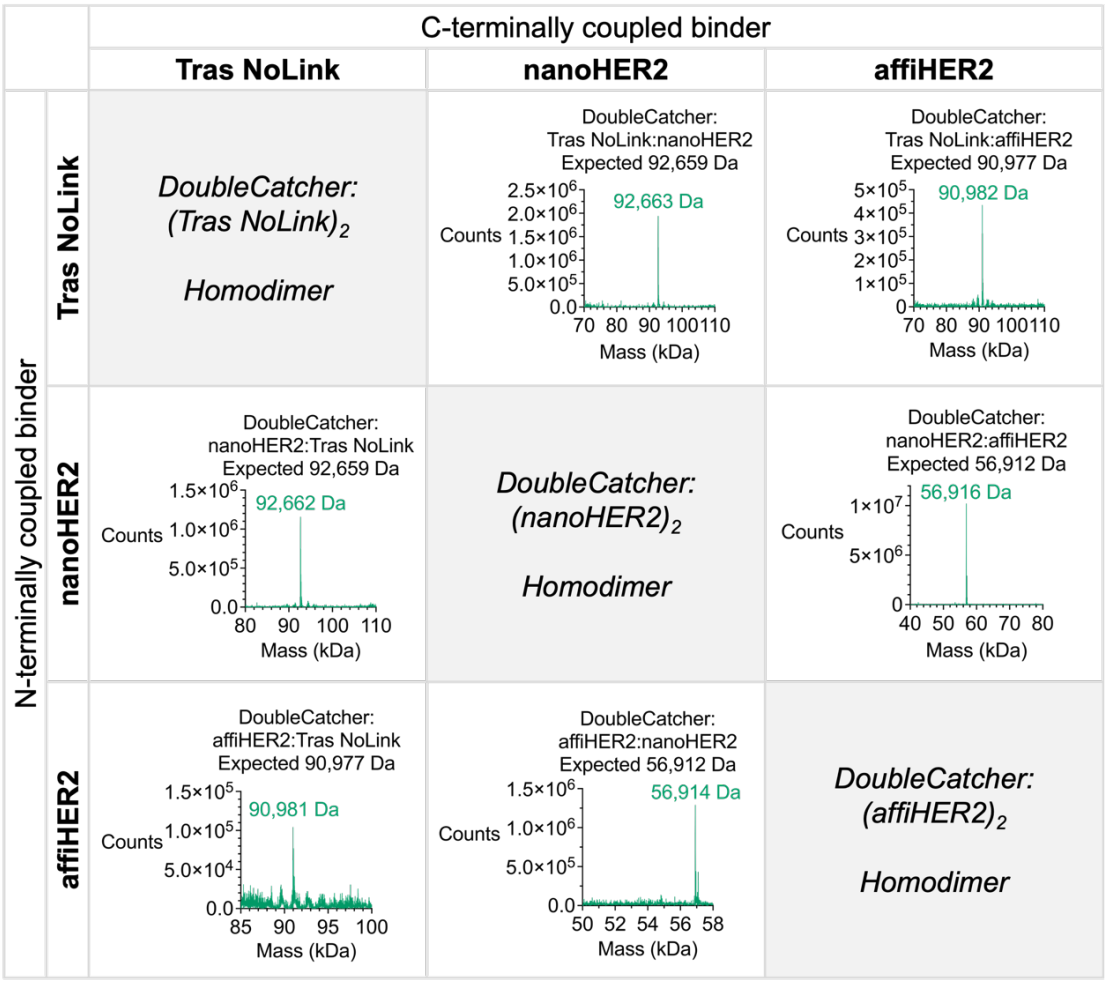


Figure 4.8. Purity of heterodimerisation by DoubleCatcher was validated by mass spectrometry. A subset of anti-HER2 binders (Tras NoLink Fab, nanoHER2 nanobody, and AffiHER2 affibody) were heterodimerised following the SpyMask protocol in each possible combination. For combinations which produce heterodimeric species, the identity of the heterodimer of the expected molecular weight was confirmed by Electrospray Ionisation Mass Spectrometry, presented within a grid. Only heterodimeric combinations were analysed, as on-target heterodimers can be distinguished from off-target homodimers. Rows indicate the binder at the N-terminus of DoubleCatcher within the bispecific, while columns indicate the binder at the C-terminus.

4.2.2 Effect on BT474 and SKBR3 cell proliferation using Resazurin assay

HER2 is an ideal model target for studying the effects of receptor dimerisation dynamics using combinatorially-assembled biparatopic binders, as the activation of HER2 results in signal transduction across multiple signalling axes, including PI3K-Akt, Ras-MAPK, phospholipase Cγ (PLCγ), and NF-κB (Merkhofer et al., 2010; Pan et al., 2024). With the activation of multiple signalling cascades that each demonstrate complex cross-talk with other transmembrane receptor signalling pathways, activation of HER2 can lead to a great diversity

of biological effects, depending on the cellular context and disease state (Huang et al., 2018; Pegram et al., 2023; Yarden and Sliwkowski, 2001; Zhang, 2021). Still, unique phenotypes can be elucidated from different signalling profiles. Specifically, the PI3K-Akt pathway in HER2-overexpressing cells is associated with cell survival (Brunet et al., 1999), while Ras-MAPK and PLCγ are more closely associated with cell proliferation (Yarden and Pines, 2012). Additionally, HER2-dependent NF-κB signalling has been shown to increase cell invasion, with no impact on cell proliferation (Merkhofer et al., 2010). Therefore, screening different phenotypes of HER2-overexpressing cells treated with HER2-modifiers can provide insight into both inhibition and biased activation of HER2. Here, the effect of the SpyMask-assembled matrix of anti-HER2 bispecifics and homodimers on metabolic activity of HER2-addicted BT474 or SKBR3 cells was quantified using the Resazurin assay (Stüber et al., 2021).

BT474 or SKBR3 cells were incubated with anti-HER2 assemblies (100 nM) for 96 h, after which the fold change in metabolic activity in treated cells was calculated relative to untreated cells (Fig. 4.9A: SKBR3, left; BT474, right). Interestingly, the different assemblies exhibited a range of potent antagonistic and agonistic activities. Therefore, binders with statistically significant activities were identified by two-way analysis of variance (ANOVA) with Dunnett's correction for multiple comparison at $\alpha = 0.05$. The triplicate data are presented as a bar chart for a representative set of bispecific binders (those assembled with Tras NL at the N-terminus) to highlight the typical error (Fig. 4.9B: SKBR3, left; BT474, right). Asterisks (*) above bars represent significant change in metabolic activity from untreated cells ($p \leq 0.05$ (*), $p \leq 0.001$ (***)). Cells were simultaneously treated with DoubleCatcher alone (100 nM) or MBP-superTEV (8.33 nM) alone as controls for background activity from SpyMask reagents (Fig. 4.9B). The top 5 bispecific binders with significant anti-proliferative or proliferative activity were titrated on SKBR3 cells, to reveal dose-dependent activity (Fig. 4.9C).

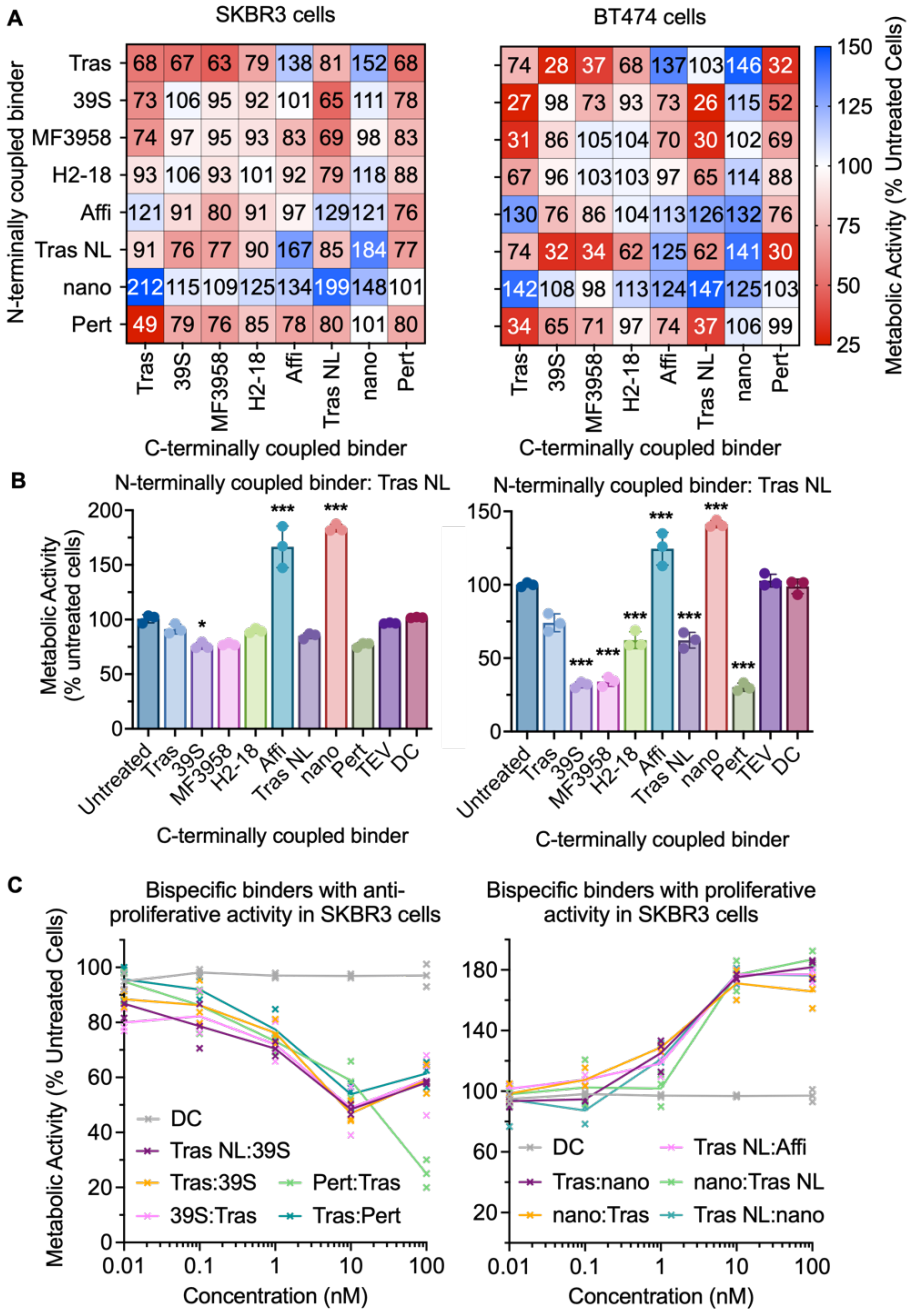


Figure 4.9. SpyMask-assembled anti-HER2 bispecific binders exhibit a range of pro- or anti-proliferative activities in HER2-positive cancer cells. (**A**) Anti-HER2 binders were dimerised by DoubleCatcher to generate a matrix of anti-HER2 biparatopic binder molecules. HER2-overexpressing SKBR3 (left) or BT474 (right) breast cancer cells were treated with each anti-HER2 bispecific (100 nM) for 96 h, after which cell metabolic activity was determined by the Resazurin assay. Cells were treated with DoubleCatcher alone as a negative control. The fold changes in metabolic activity of treated cells relative to untreated (media only) cells are represented as a heat map. (**B**) Representative triplicate data for SKBR3 cells (left) and BT474 cells (right) treated with bispecifics displaying an N-terminal Tras NoLink Fab are presented, with bars connecting the means ± 1 s.d.. For both cell types, the triplicate metabolic activities are also shown for cells treated with media only ('Untreated'), 8.33 nM MBP-superTEV alone ('TEV'), or 100 nM DoubleCatcher alone ('DC'). Statistical significance between untreated and treatment groups was analysed for each cell type by two-way analysis of variance (ANOVA) with Dunnett's correction for multiple comparison. Asterisks (*) above bars represent significant change in metabolic activity from untreated cells ($p \leq 0.05$ (*), $p \leq 0.001$ (***)). (**C**) Titration curves are presented for the top 5 bispecifics with significant anti-proliferative (left) or pro-proliferative (right) activity in SKBR3 cells. Triplicate data are shown with lines connecting the means.

While many binder combinations could not be predicted, there are several trends in the results that can be rationalised. Bispecific constructs displaying one or more domain II-binding arm (39S or Pert) consistently result in an anti-proliferative phenotype. As HER2 dimerisation is facilitated predominantly by interactions between domain II residues (Arkhipov et al., 2013a), it is likely that these bispecifics function by blocking HER2 dimerisation and activation. Conversely, bispecifics harbouring the small, domain III binders nanoHER2 (16 kDa) or AffiHER2 (15 kDa) – coupled to either the N- or the C-terminus of DoubleCatcher – display potent proliferative activity. Indeed, the bispecific constructs with significant agonistic activity in both SKBR3 (average metabolic activity of significant agonists = 168 ± 29% (mean ± 1 s.d., n = 8 significantly proliferative bispecifics) and BT474 cells (average metabolic activity of significant agonists = 127 ± 13% (mean ± 1 s.d., n = 16 significantly proliferative bispecifics), were all comprised of at least one of nanoHER2 or AffiHER2. Overall, bispecifics containing nanoHER2 or AffiHER2 at either terminus showed substantially higher metabolic activity than bispecifics without either constituent (120 ± 11% versus 82 ± 9.1% (SKBR3), and 111 ± 2.8% versus 66 ± 2.5% (BT474). Where agonistic activity of biparatopic anti-HER2 molecules has been observed previously (Gu et al., 2014; Kast et al., 2021; Scheer et al., 2012), it has been suggested to be a result of conformational changes in HER2 upon binding that favour homodimerisation over heterodimerisation, or from a shorter distance between antigen binding sites. Considering their small size, it is possible that DoubleCatchers coupled to either nanoHER2 or AffiHER2 can bridge HER2 molecules close enough for efficient association of their transmembrane helixes and activation by trans-phosphorylation of their intracellular C-terminal kinase domains.

Finally, the activity of bispecifics containing Tras were compared to equivalent binders that contained Tras NoLink in its place. Tras NoLink was included in the screen to test the effects

of removing the linker between a binder and SpyTag003, with the aim of minimising points of flexibility in the bispecific construct. Ultimate control over receptor bridging may only be achieved if the bridging molecule is rigid. Additionally, a rigid bridging scaffold would enable the scaffold architecture to be defined, providing structural information about the bridging interaction. Such information could be linked to the physiological outcomes of each bispecific to guide a mechanistic understanding of receptor signalling. Within the anti-HER2 binders screened in this study, the average difference in metabolic activity between cells treated with Tras-containing bispecifics, and cells treated with the equivalent bispecific instead containing Tras NL, was only 8%, with similar standard deviations. Considering the flexibility of the Gly/Ser linker that separates the two SpyCatcher003 moieties of DoubleCatcher, it is possible that a small reduction in the flexibility of Tras-SpyTag003 has little structural impact once assembled onto DoubleCatcher. Thus, further work to rigidify the DoubleCatcher scaffold is required to appreciate the effect of reduced flexibility of the bispecific molecule on its activity.

4.3 Bridging HER2 with other cell-surface receptors using SpyMask-assembled bispecifics

While HER2-HER2 dimerisation is a principal trigger of disease signalling in HER2-overexpressing cancers, it is known that HER2 heterodimerisation with EGFR and HER3 is favoured over homodimerisation (Baselga and Swain, 2009), owing to the high affinity of ligand-bound EGFR or HER3 for HER2. HER2 heterodimerisation with other HER-family receptors is consequently one route to acquired resistance to HER2 blockade therapy (Ritter et al., 2007). For this reason, many bispecific antibodies that simultaneously bind HER2 and EGFR/HER3 to inhibit heterodimerisation have been described (Geuijen et al., 2018), with effective anti-proliferative activities. However, bispecifics have not been applied to investigate the effects of tuning heterodimer geometry, despite subtle differences in the asymmetric dimers

that form upon heterodimerisation of HER2 with HER3 or EGFR bound to different ligands (Bai et al., 2023; Diwanji et al., 2021). I therefore selected affibodies targeting EGFR (Friedman, 2008; Friedman et al., 2007) or HER3 (Malm et al., 2013) that do not interfere with their dimerisation interface, to drive heterodimerisation with HER2.

Beyond oligomerisation within the HER-family of receptor tyrosine kinases (RTKs), promiscuous heterodimerisation of HER2 with non-HER-family RTKs is beginning to be appreciated (Kennedy et al., 2016, 2019). Biologically, a highly diverse HER2 interactome translates to an equally diverse array of adaptor proteins that can interact with the dimers to effect signalling. Therefore, promiscuous HER2 dimerisation can ensure signalling is sustained in many different disease or therapy-resistant states. One example of these alternative RTKs, platelet-derived growth factor receptor type beta (PDGFRβ) has been reported to confer resistance to anti-HER2 therapy when overexpressed on HER2-positive breast cancer cells, including SKBR3 and BT474 (Alexander et al., 2017). Thus, selective bridging of HER2 and PDGFRβ may provide insight into promiscuous heterodimerisation of HER2 (Kennedy et al., 2019). I therefore identified an affibody targeting PDGFRβ, AffiPDGFRβ, for bispecific assembly (Lindborg et al., 2011). On the other hand, heterodimerisation of HER2 with VEGFR2 does not emerge in response to anti-HER2 treatment (Kennedy et al., 2019), and thus bridging the two RTKs may provide insight into non-canonical signalling. An affibody against VEGFR2, AffiVEGFR2, was selected from the literature for screening (Frejd et al., 2016).

Bispecific binders can also be assembled using DoubleCatcher to target signalling crosstalk. One example in breast cancer cells is between HER-family receptor anti-apoptotic signalling and tumor necrosis factor α receptor (TNFR1)-mediated signalling following activation by its ligand, TNFα. Depending on the signal strength, TNFR1 signalling can either mediate cell

survival and proliferation or cell death (Mercogliano et al., 2020), the former of which is maintained in cancer signalling. However, TNFR1 has recently been shown to directly interact with and become phosphorylated by ligand-activated EGFR (Nam et al., 2024). Phosphorylation of TNFR1 results in inhibition of TNFR1-mediated NF-κB signalling pathway that leads to apoptotic cell death. A nanobody targeting TNFR1, nanoTNFR1 (Steeland et al., 2015), was therefore selected for the assembly of HER2×TNFR1 bispecifics to be screened for similar anti-proliferative activity.

Finally, I aimed to assemble a bispecific binder bridging HER2 with the cell-surface E3 ubiquitin ligase ring finger protein 43 (RNF43), which has been effectively recruited for the targeted degradation of receptors via the lysosomal pathway (Cotton et al., 2021; Marei et al., 2022; Rhee and Zhou, 2024; Siepe et al., 2023). An RNF43-binding Fab, αRNF43-90, was selected from a panel of anti-RNF43 binders that were reformatted into bispecific antibodies targeting the E3 ubiquitin ligase and an RTK (Agard et al., 2022). Importantly, for targeted protein degrading bispecifics, the kinetics of ubiquitin transfer to the target receptor to signal the receptor for degradation is influenced by the distance between binder arms of the bispecific, as well as binder orientation (Marei et al., 2022). Assembly of targeted protein degrading bispecifics in varied formats by SpyMask may therefore permit easy optimisation of format.

4.3.1 Validation of binders targeting alternative cell-surface receptors by mass spectrometry

As performed previously for the panel of anti-HER2 binders, binders against alternative cell-surface receptors were identified from the literature as described and cloned with a terminal SpyTag003. Binders AffiHER3, AffiEGFR, AffiPDGFRβ, AffiVEGFR2, and nanoTNFR1 were cloned with an N-terminal SnoopTagJr and a C-terminal SpyTag003 by Irsyad Khairil

Anuar (Howarth group). Each binder-SpyTag003 fusion was expressed in *E. coli* BL21, except for αRNF43-90 Fab which was expressed in Expi293, and purified by Ni-NTA, before analysis by intact protein mass spectrometry (Fig. 4.10A-F). The expected mass of each construct was confirmed, accounting for the formation of expected disulfide bonds in nanoTNFR1 and RNF43-90.

4.3.2 Effect on SKBR3 cell proliferation using Resazurin assay

Bispecifics were assembled to bridge HER2 to each of the alternative cell-surface receptors of interest. To do this, the HER2 ECD subdomain IV binder Tras was dimerised with each alternative receptor binder, using the SpyMask methodology. To test for the effect of ligand orientation on bispecific activity, each pair of binders was conjugated onto DoubleCatcher in both orientations, i.e. with Tras at either the N- or C-terminus of DoubleCatcher. As previously, HER2-overexpressing SKBR3 cells were treated with 100 nM of each bispecific for 96 h, after which the metabolic activity of the cells was calculated relative to untreated cells (Fig 4.11A, bispecifics with Tras at the N-terminus of DoubleCatcher; B, bispecifics with Tras at the C-terminus of DoubleCatcher). Binders with statistically significant activities were identified by two-way analysis of variance (ANOVA) with Dunnett's correction for multiple comparison at $\alpha = 0.05$. Asterisks (*) above bars represent significant change in metabolic activity from untreated cells ($p \leq 0.01$ (**), $p \leq 0.001$ (***)). To control for the activity of the free, monomeric substituents of each bispecific mixture, SKBR3 cells were treated with a 1:1 mixture of parental binder molecules (non-dimerised, 100 nM), DoubleCatcher alone (100 nM), or MBP-superTEV alone (8.33 nM). The change in metabolic activity of these control treatments from untreated cells was shown to be small and non-significant (Fig. 4.11C).

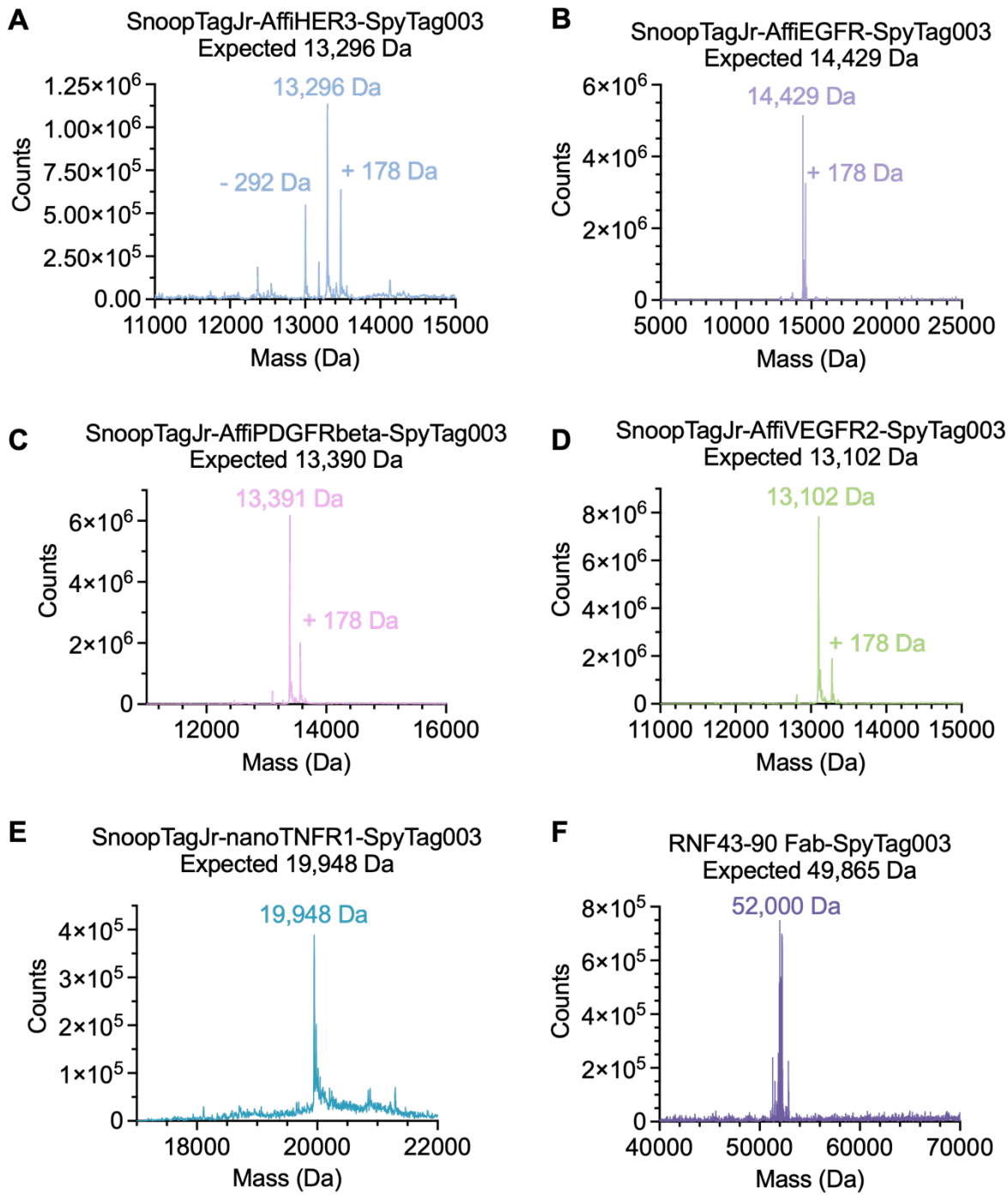


Figure 4.10. Mass spectrometry of binders targeting alternative receptors for bridging to HER2. Protein binders targeting non-HER2 cell-surface receptors were identified and cloned with an N-terminal SpyTag003. Their identity was validated by Electrospray Ionisation Mass Spectrometry. The observed masses for each major species are presented above the peak. The minor peaks in (A), (B), (C), and (D) at +178 Da relates to gluconoylation (Geoghegan et al., 1999). In (A), the loss of 292 Da corresponds to loss of YK in SpyTag003 peptide. In (F), laddering of +35 Da is observed between the expected molecular weight and beyond the major peak, corresponding to the attachment of individual chloride ions.

In section 4.3, the orientation of ligands in the anti-HER2 biparatopic binder influenced bispecific potency. A similar orientation dependence was observed for the HER2×HER3,

HER2×VEGFR2, and HER2×TNFR1 bispecifics assembled here, highlighting the importance of screening ligand orientation in bispecific synthesis. On the contrary, the HER2×EGFR bispecific displayed significant anti-proliferative activity (79.8 ± 6.7%) when Tras was conjugated to the N-terminus of DoubleCatcher, but significant pro-proliferative activity (117.1 ± 4.5%) when conjugated to DoubleCatcher's C-terminus (Fig. 4.11A, B). This suggests that, due to the asymmetry of the DoubleCatcher scaffold, only one orientation of the Tras-AffiEGFR dimer is able to bridge HER2 and EGFR sufficiently close to facilitate interaction of their juxtamembrane domains for activation.

It was expected that recruiting RNF43 E3 ubiquitin ligase to HER2 would result in lysosomal degradation of HER2, reduced HER2 signalling, and therefore reduced cell proliferation. However, neither version of the Tras-αRNF43-90 bispecific resulted in a significant reduction of metabolic activity in SKBR3 cells. This result may be explained by the low basal expression of RNF43 on SKBR3 cells and other breast tissue (Siepe et al., 2023). Instead, a more effective E3 ubiquitin ligase target may be RNF167, which is expressed 160-fold greater than RNF43 on SKBR3 cells (Pontén et al., 2008; Uhlen et al., 2017).

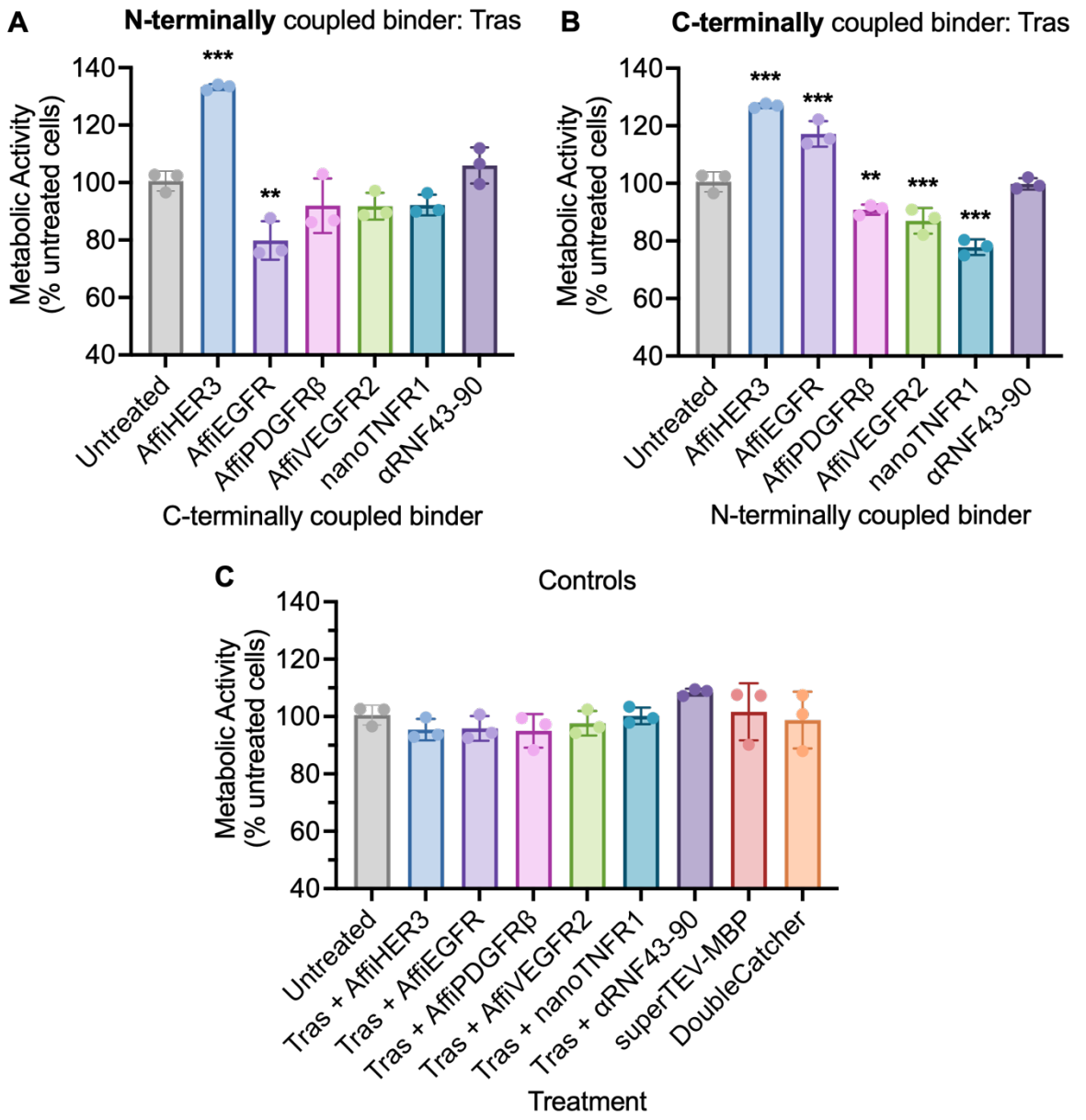


Figure 4.11. Orientation of binders in SpyMask-assembled bispecific binders influences activity and potency. Binders against HER3, EGFR, PDGFRβ, TNFR1, and RNF43 were coupled onto DoubleCatcher with the anti-HER2 Fab Tras conjugated to either the N- or C-terminal SpyCatcher003 moiety. SKBR3 cells were treated with each bispecific with Tras at the N-terminus (**A**) or C-terminus (**B**) at 100 nM for 96 h, after which cell metabolic activity was determined using the Resazurin assay. (**C**) To control for binder-alone activity, cells were treated with the combination of each parental binder with Tras (both at 100 nM) without conjugation to DoubleCatcher. Cells were also treated with MBP-superTEV or DoubleCatcher alone. Statistical significance between untreated and treatment groups was analysed by two-way analysis of variance (ANOVA) with Dunnett's correction for multiple comparison. Asterisks (*) above bars represent significant change in metabolic activity from untreated cells ($p \leq 0.01$ (**), $p \leq 0.001$ (***)).

4.4 Discussion

In this Chapter, the SpyMask protocol described in Chapter 3 was applied to the assembly of bispecific binders that bridge the oncoreceptor HER2 with itself or other receptors on the surface of cancer cells. There are two important features of HER2 signalling that make the receptor a suitable target for studying dimer geometry: first, HER2 requires dimerisation for activation, and second, HER2 activation results in the firing of multiple signalling pathways, with the extent of activation of each pathway dependant on the context of the HER2 dimer. Within the HER-family of receptors, different ligands induce different conformational changes in the receptor's extracellular domain (ECD), which are translated into distinct intracellular signals via unique coiled-coil geometries formed by the interacting receptor's transmembrane and juxtamembrane domains (Doerner et al., 2015; Mozumdar et al., 2020; Sinclair et al., 2018). The consequence of different coiled-coil structures ranges from preferences in effector protein recruitment to differential phosphorylation of the C-terminal tail (Sinclair et al., 2018; Wilson et al., 2009). Therefore, anti-HER2 bispecific molecules were designed to target an array of epitopes, to drive the formation of HER2 homo- or hetero-dimers with various contortions of the ECD.

Overall, DoubleCatcher proved to be a simple tool for the parallelised assembly of anti-HER2 bispecifics on a 96-well plate scale with high purity, as determined by intact protein mass spectrometry. Each bispecific was tested for its effect on the metabolic activity of HER2-overexpressing SKBR3 or BT484 breast cancer cells, revealing an unexpected array of pro- or anti-proliferative effects to confirm a mechanism for the bispecifics beyond HER2 blockade. Importantly, the activity of many bispecifics was sensitive to the orientation of binders in the bispecific – that is, the order in which binders were coupled onto DoubleCatcher. For these bispecifics, one binder orientation displayed enhanced potency over the alternative orientation,

mimicking what has been observed previously for biparatopic HER2 binders (Kast et al., 2021; Tamaskovic et al., 2016). While this supports the utility of DoubleCatcher as a tool for screening bispecifics in multiple formats, there were no pairs of HER2 biparatopic binders that displayed a switch in activity (i.e. from a potent agonist to a potent antagonist, or vice versa) when assembled in the opposite orientation, and only one combination of HER2/alternate receptor binders (Tras and affiEGFR) showed orientation dependent activity.

Anti-HER2 biparatopic antibodies also showed different potencies in SKBR3 cells relative to BT474 cells. Firstly, a higher number of bispecifics had significant proliferative activity in BT474 cells (16 constructs) than in SKBR3 cells (8 constructs). In SKBR3 and BT474 cells, there is differential total expression of HER2. Additionally, BT474 cells express HER2 to a greater extent (~2.8 x 10^6 copies per cell (Kamashev et al., 2022)) relative to SKBR3 cells (~1.2 x 10^6 copies per cell (Hendriks et al., 2013)). The higher potency of anti-proliferative bispecifics in the panel on BT474 cells may therefore reflect a greater ability to cluster HER2 at the cell surface in an inactive orientation, triggering internalisation and degradation (Oganesyan et al., 2018).

Secondly, the constructs with significant anti-proliferative activity relative to untreated control cells were more potent in BT474 cells (average metabolic activity of the ten most potent antagonists = 30.5 ± 2.6%) than in SKBR3 cells (average metabolic activity of the ten most potent antagonists = 67.2 ± 7.2%). Importantly, while both cell lines express HER3 to a similar level (1-1.2 x 10^6 copies per cell), SKBR3 expresses ~3-fold more EGFR (2.2 x 10^5 copies per cell) than BT474 (7 x 10^4 copies per cell) (Brockhoff et al., 2001). It is possible that while the screened bispecific assemblies control HER2 dimerisation, they do not prevent HER2 heterodimerisation. Notably, an established mechanism of HER2 resistance to blockade

therapy is through the upregulation of the metalloprotease ADAM17, which processes pro-HER family ligands into active HER ligands that drive ligand-dependent heterodimerisation (Gijsen et al., 2010). Indeed, while Trastuzumab effectively blocks ligand-independent heterodimer formation with HER2 (Junttila et al., 2009), the formation of HER2/EGFR dimers has been shown specifically in Trastuzumab-treated SKBR3 cells in the presence of EGF (Tamaskovic et al., 2016). Therefore, it is possible that the reduced potency of anti-proliferative bispecifics in SKBR3 cells is a result of compensatory ligand-driven HER2/EGFR signalling. Considering the morphogenesis of 3D culture is a process under the control of HER2 heterodimerisation, cell invasion assays would complement the metabolic activity assay used here to provide necessary insight into the homo- vs hetero-dimerisation formation after bispecific treatment. More importantly, fluctuations in signalling pathways should be investigated using multiplexed signalling assays, such as mass spectrometry (Whiteaker et al., 2021), high-content imaging (Bray et al., 2016), or a multi-orthogonal luciferase reporter assay (Sarrion-Perdigones et al., 2019), to identify correlations between signalling signatures and phenotypic changes.

A notable limitation of using DoubleCatcher as a scaffold for assembling biparatopic bispecifics is that the scaffold is inherently flexible. The maximal possible distance that could be spanned by the 9-residue Gly/Ser linker that separates the two SpyCatcher003 moieties of DoubleCatcher is ~30 Å, if assuming a β-strand extended conformation (Jost et al., 2013). When added to the length of each SpyCatcher003 protein (~40 Å), an estimate for the total distance bridging two Fabs is ~110 Å. The minimal distance between the C-terminus (to which SpyTag is linked) of any two pairs of binders in the panel employed in this study with non-overlapping epitopes/surfaces is ~90 Å (between binders Pert and MF3958). Therefore, it is likely that intramolecular cross linking of the HER2 ECD may be entropically favoured over

intermolecular HER2 crosslinking for a proportion of the binders assembled. While intramolecular crosslinking will still affect HER2 dimerisation and signalling by inhibiting dimer formation, it is not possible from this study alone to discern this basis of signalling changes from different dimer geometries. Furthermore, it is imperative that further protein engineering efforts to rigidify the DoubleCatcher scaffold are made, to build bispecifics with more defined, homogeneous architectures for precise bridging of their targets. These efforts will be discussed in Chapter 5.

CHAPTER 5 – DIVERSIFICATION OF THE SPYMASK PLATFORM

The last two decades of research driving bispecific antibody discovery has generated a multitude of bispecific formats (Guo et al., 2023). Increasingly, bispecific formats have been developed to be compatible with high-throughput switching of binder arms and downstream purification. However, seldom do such assembly protocols seek to optimise geometry – i.e., the distance and relative orientation of the paratopes with respect to one another. As the influence of receptor geometry on signal transduction becomes increasingly appreciated (Dickopf et al., 2020; Moraga et al., 2015), the importance of optimising bispecific architecture during discovery is being reconsidered. Recently, several encouraging methodologies have emerged that seek not only to vary binder identity, but also the spatial orientation of binders on the bispecific scaffold (Romei et al., 2024). Most of these examples rely on direct fusion of binder domains via varying linker types (Craig et al., 2012; Wu et al., 2017b; Yen et al., 2022), whose throughput has been impressively scaled via combinatorial DNA library synthesis and screening (Segaliny et al., 2023). However, library cloning, expression, and screening at the scale required to search sufficient format space is not possible for most research groups. Alternative approaches, such as fusion of binder domains to different termini of IgG heavy and light chains (Madsen et al., 2023), or modifications to IgG hinge regions (White et al., 2015; Yu et al., 2018), are important advances but are yet to be scaled.

This Chapter exploits the modularity of the SpyMask platform to engineer structural variants of DoubleCatcher for assembly of bispecific antibodies in different geometries. To probe the effects of bispecific geometry on biological systems, biparatopic bispecifics targeting HER2 homodimers, as described in the previous Chapter, were generated using multiple different DoubleCatcher architectures. While HER-family receptors are a prominent example of cell-surface molecules whose dimer geometries and kinetics influence the downstream signalling

pathway activation and cell fate (Freed et al., 2017), the importance of dimer architecture on signaling output has been appreciated for other receptor systems. Namely, dimer geometry-dependent signaling biases have been reported for other receptor tyrosine kinases, e.g. FGFR1 (Chan et al., 2023); cytokine receptors, e.g. EpoR (Mohan et al., 2019; Syed et al., 1998); and GPCRs, e.g. Bombesin BB_2 (Romantini et al., 2021). Beyond targeting native dimers, DoubleCatcher-assembled bispecifics with diverse geometries have the potential to be a valuable tool to study controlled bridging of novel pairs of surface proteins, for example linking disease-associated receptors with E3 ubiquitin ligases such as RNF43 to target the receptors for degradation (Marei et al., 2022). Indeed, the activity of bispecific molecules bridging RNF43 and IGF1R was shown to be sensitive to the distance between paratopes, as well as binder orientation (Marei et al., 2022).

Many antibody-like binders exist against the receptor classes that naturally bind and respond to protein ligands (including the receptor tyrosine kinase, cytokine receptor, and oestrogen receptor families). However, other dominant receptor classes (such as GPCRs and ion channels, which constitute the two largest classes of membrane proteins in the human genome (Overington et al., 2006)) are generally targeted with functional analogues of their native ligands, such as small molecules and peptides (Hutchings et al., 2019; Trkulja et al., 2021). Therefore, a combinatorial assessment of many different receptor combinations would require the efficient conjugation of numerous different classes of molecules. The seminal discovery and subsequent development of bioorthogonal bioconjugation technologies has facilitated site-specific modification of proteins with click chemistry reactive handles (Hoyt et al., 2019; McKay and Finn, 2014; Walsh et al., 2021). This way, antibodies and therapeutic proteins can be conjugated to one or more desired payload, such as drug effectors or fluorophores (Chudasama et al., 2016). Favourably, additions can be targeted to native protein

functionalities, such as thiol-maleimide crosslinking on cysteines (Marculescu et al., 2014), transglutaminase-catalysed transamidation of lysines (Haque et al., 2021), or disulfide rebridging reagents (Maruani et al., 2020). The primary application of these technologies is in homogeneous synthesis of antibody-drug conjugates (Oller-Salvia et al., 2018) or radiolabelled antibodies for molecular imaging and diagnostics (Rossin et al., 2010). Site-selective antibody modification with click chemistry modalities has also been successfully exploited for the bridging of two or more antibody-derived binders to generate multispecific antibodies (Szijj and Chudasama, 2021), as discussed in Chapter 3, although few examples of click-conjugated protein binders with alternative ligand types have been detailed (Ahn et al., 2021). Additionally, chemical bioconjugation techniques to bridge larger moieties (such as two antibodies, or antibody-carbohydrates) must overcome steric hindrance through careful linker and reaction optimisation to preserve respectable yields (Hull et al., 2014; Thoreau and Chudasama, 2022). Employing longer bridging linkers, such as PEG (Maruani et al., 2020), provides a solution, but control over linker rigidity and geometry then becomes the challenge.

Instead, this Chapter describes a methodology for chemically conjugating small molecule, oligonucleotide, and full-length IgG ligands with the SpyTag peptide, so that diverse ligand types can be heterodimerised using DoubleCatcher. Specifically, SpyTag was functionalized with click-chemistry-compatible or cysteine bridging reactive groups and the ligands possessed complementary, reactive chemical groups. This way, the need for genetic fusion and recombinant expression of SpyTag-fused ligands is removed. Therefore, the potential target combinations that can be explored by SpyMask-assembled bispecific molecules is greatly expanded.

5.1 Designing DoubleCatcher structural variants

As demonstrated in Chapter 4, the format of a bispecific antibody built using the SpyMask protocol can be influenced by the identity of the SpyTag003-linked binder and by the order in which the binders are coupled. While the shape, size, and flexibility of the bispecific molecule can be tuned by modifying the linker between a binder and its SpyTag peptide, these format parameters can also be determined by the DoubleCatcher module itself. Therefore, SpyMask can be used to assemble matrices of bispecific antibodies with six degrees of freedom, where both binder arms against the targets of interest, as well as the DoubleCatcher module, could be translationally and rotationally modified. When coupling each of these modules in different combinations, one can greatly amplify the bispecific format space that is being screened.

5.1.1 Tuning DoubleCatcher structure by varying linker

The first approach to modifying the architecture of DoubleCatcher is by varying the linker connecting the two SpyCatcher003 moieties. Linker engineering is a property that often requires optimisation in Fc-less bispecific antibodies (Labrijn et al., 2019; Schanzer et al., 2011), for example to improve bispecific solubility (Whitlow et al., 1993). To test the amenability of DoubleCatcher to linker modification, the flexible Gly/Ser linker separating the Catcher domains was substituted with the central helix from the *Bacillus stearothermophilus* ribosomal protein L9 (Kuhlman et al., 1997). The helix-containing DoubleCatcher variant was termed DoubleCatcher H-Lock (Fig. 5.1). In isolation, L9 retains 85% helicity at 1 °C in 10 mM 3-(N-morpholino)propanesulfonic acid (MOPS) pH 7.4, 68% helicity at 25 °C, and reduced yet detectible (18%) helicity at 85 °C (Kuhlman et al., 1997).

Despite the goal of increasing the distance between paratopes of DoubleCatcher-assembled bispecifics with the helical linker, the average distance between N_ζ of the reactive lysine residues of each SpyCatcher003 in the five lowest-energy AlphaFold2-predicted structures of

DoubleCatcher H-Lock (2.77 nm) was below that in the native DoubleCatcher structure (3.6 nm). Of these structures, the structural model with the lowest energy is presented in Fig. 5.1 and labelled. The relative orientation of the two SpyTag binding sites on DoubleCatcher are represented by cyan vectors, with arrows indicating C-N SpyTag directionality. Although the helical linker is longer and more rigid than the original Gly/Ser spacer, the inherent flexibility of the disordered SpyCatcher003 termini would explain why the SpyCatcher003 domains are still able to reside close to each other in DoubleCatcher H-Lock (Li et al., 2014).

5.1.2 Tuning DoubleCatcher structure by introducing intramolecular disulfide bonds

A second approach to modifying DoubleCatcher architecture that overcomes the inherent flexibility of the SpyCatcher003 termini is to engineer a covalent linkage between the two Catcher domains. Intramolecular covalent conjugation of therapeutics has been demonstrated previously in the site-specific multimerisation of nanobodies using non-canonical amino acids (Van Fossen et al., 2022), which are also commonly utilised for the structural stapling of peptide therapeutics (Lau et al., 2015), but have yet to be investigated controlling the architecture of bispecific antibodies. Instead, examples of inter-domain conjugation of native side chains have proven effective in defining the structure of bispecific antibodies, such as disulfide bond engineering in diabody-format bispecifics (Math et al., 2023), or chemical cross-linking of native lysine residues in engineered scFv-fusion bispecifics (Ueda et al., 2020). As the SpyCatcher/SpyTag system naturally lacks free cysteines or native disulfide bonds, it was hypothesised that efficient site-specific covalent linkage of the Catcher moieties within DoubleCatcher could be achieved by the introduction of a pair of cysteine residues: one cysteine per SpyCatcher003.

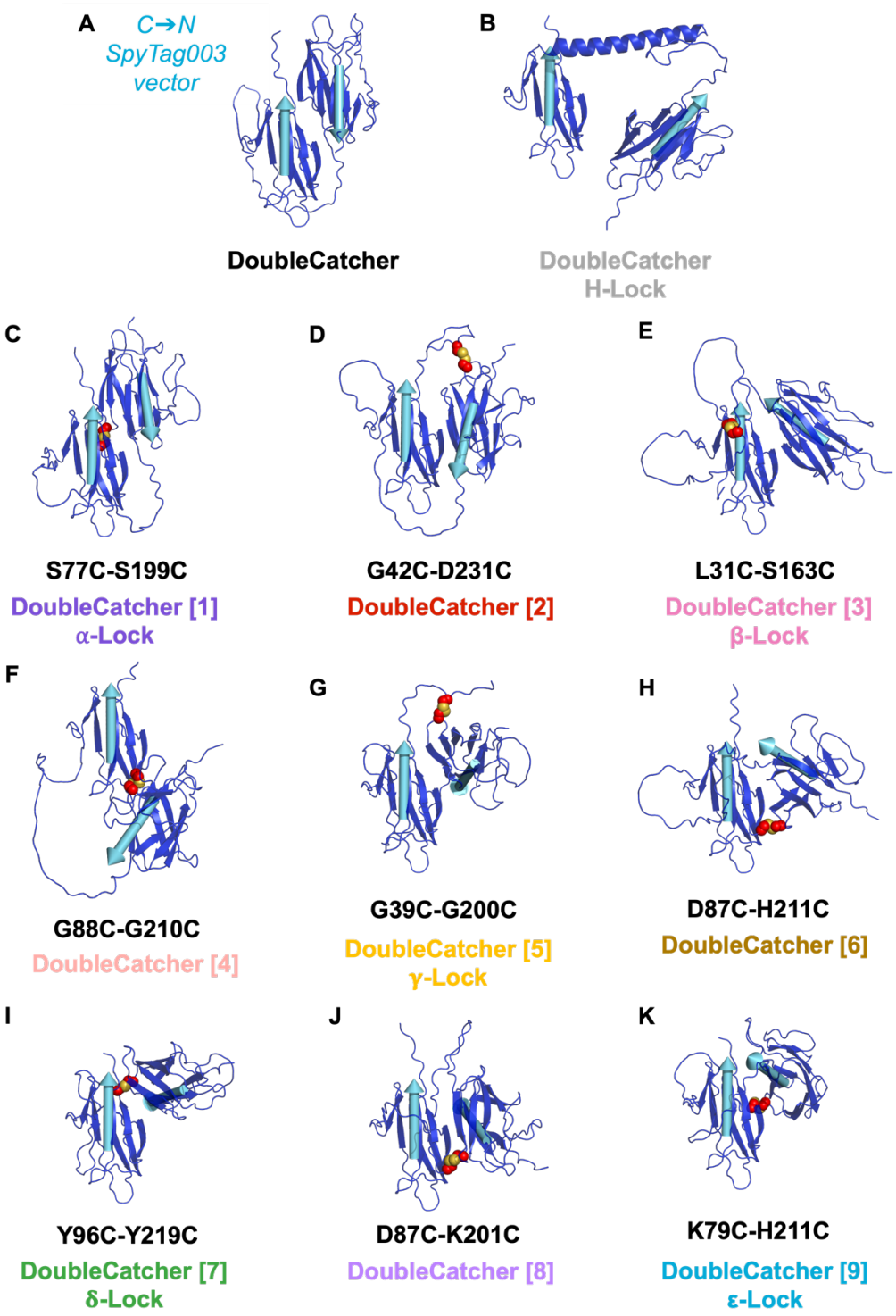


Figure 5.1. DoubleCatcher architecture can be modified. The reactive and caged SpyCatcher003 moieties in DoubleCatcher are separated by a flexible Gly/Ser linker. (**A**) The lowest energy AlphaFold3-predicted structure of DoubleCatcher is displayed, with DoubleCatcher in dark blue and the SpyTag-docking site represented by a cyan vector, whose arrow indicates the direction that a SpyTagged binder molecule would project. To generate DoubleCatcher H-lock, the flexible linker in DoubleCatcher was replaced with a stable α-helical linker (**B**). For the generation of DoubleCatcher disulfide-locked variants [1-9], pairs of cysteine substitution sites (one per SpyCatcher003 domain) with close proximity were rationally identified from the five highest-scoring AlphaFold2-predicted structures of DoubleCatcher (**C-K**). The engineered cysteine mutations are labelled according to DoubleCatcher numbering, and the resulting predicted disulfide bonds highlighted in sphere representation, coloured by atom.

To test this, nine pairs of residues (one residue from each SpyCatcher003) that reside in close proximity across the five highest-confidence AlphaFold2-predicted structures of DoubleCatcher were identified as sites for cysteine substitution, with the aim of engineering a SpyCatcher003-SpyCatcher003 intramolecular disulfide bond. Residues were selected for substitution if they resided in a loop and did not emerge during the evolution of SpyCatcher to SpyCatcher003 to contribute to high-affinity SpyTag003 binding (Keeble et al., 2019). The structures of each of the nine designed mutants were predicted using AlphaFold2, and later AlphaFold3 (Abramson et al., 2024), to assess their structures. In all cases, the disulfide bond was predicted to form as expected (Fig. 5.1), with minimal movement predicted between SpyCatcher003 domains across the top five lowest-predicted structures. For visual comparison, the highest-confidence predicted structures for each DoubleCatcher variant are displayed in Fig. 5.1, labelled with their cysteine substitution mutations and variant name (DoubleCatcher [1] – DoubleCatcher [9]). As for DoubleCatcher and DoubleCatcher H-lock, cyan vectors indicate SpyTag docking site and directionality, indicating where each binder would project in a bispecific molecule. All structures are aligned to the N-terminal SpyCatcher003 of the original DoubleCatcher construct (referred to as 'native DoubleCatcher' throughout).

5.1.3 Biophysical characterisation of DoubleCatcher structural variants

5.1.3.1 Monitoring intermolecular dimer formation by size-exclusion chromatography

Following expression in *E. coli* and purification by Ni-NTA, each DoubleCatcher variant was analysed by preparative-scale size-exclusion chromatography (SEC). Prior to running the DoubleCatcher samples, the SEC column was calibrated using 660 kDa to 1.35 kDa molecular weight protein standards (thyroglobulin, IgG, ovalbumin, myoglobin, and vitamin B12) (Bio-Rad), whose molecular weights are indicated at the appropriate elution volume in Fig. 5.2A

('M_W Markers', grey arrows). Each SEC chromatogram was normalised to the maximum $A_{280\ nm}$ of the main peak, coloured according to Fig. 5.1, and stacked above the SEC trace of native DoubleCatcher. The peak corresponding to the major species in each chromatogram is labelled with its apparent molecular weight, calibrated to the molecular weight protein standards.

First, SEC analysis of DoubleCatcher H-Lock revealed its apparent molecular weight to be 16.6 kDa larger than the original DoubleCatcher (Fig. 5.2A), while the ExPASy ProtParam tool calculates an increase of only 3.5 kDa. The increased apparent molecular weight supports the AlphaFold2-predicted role of the linker in increasing the distance between the SpyCatcher003 termini of DoubleCatcher, thus increasing the Stokes radius of the construct.

Second, the normalised SEC profiles of Ni-NTA-purified DoubleCatcher disulfide-lock variants presented one main peak corresponding to DoubleCatcher monomer ('Monomer' peak in Fig. 5.2A) and one minor peak corresponding to covalent DoubleCatcher dimer ('Dimer' peak in Fig. 5.2A), which arises due to incomplete intramolecular disulfide bond formation leaving free, reduced cysteines that are free to form disulfide bonds to adjacent DoubleCatcher molecules. The abundance of dimer relative to monomer varied between DoubleCatcher variant. SDS-PAGE analysis of the monomer peak of each double-cysteine mutant further revealed the monomer to exist as a mixture of oxidised and reduced species. The relative quantity of oxidised species, as a percentage of all monomer species, in each post-Ni-NTA DoubleCatcher disulfide lock sample was quantified by densitometry and presented below the gels in Fig. 5.2B-D. Incubation of DoubleCatcher double-cysteine monomer with 0.5 mM $CuSO_4$ (2 h, 25 °C; HEPES pH 7) was therefore required to drive oxidation to near completion (85-98%) prior to downstream analyses (Fig. 5.2B-D).

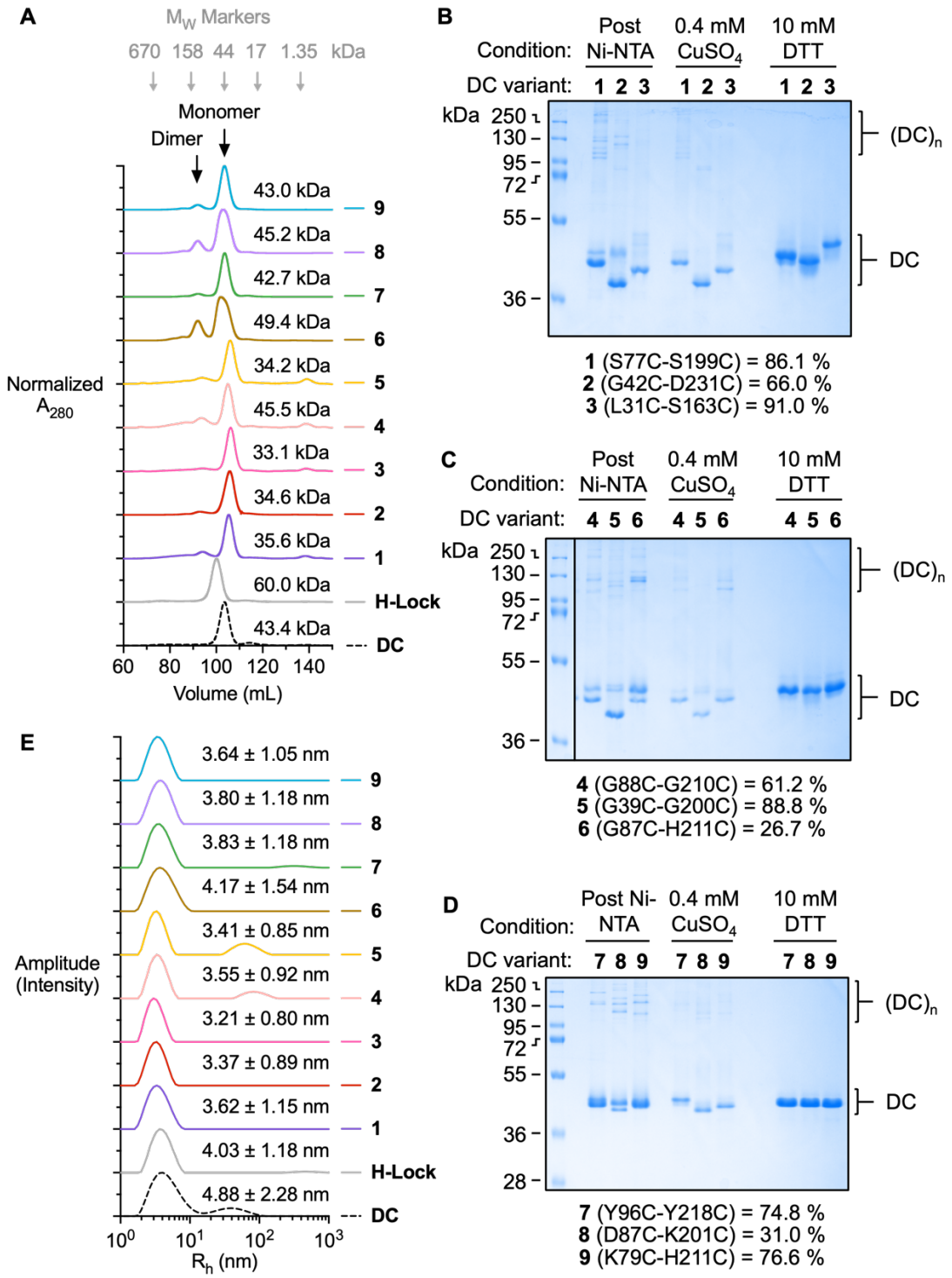


Figure 5.2. Analysis of the homogeneity of DoubleCatcher variants post-purification. The panel of 11 Ni-NTA-purified DoubleCatcher variants were analysed for intermolecular disulfide bond formation by size-exclusion chromatography (**A**). The chromatograms are normalised by $A_{280\ nm}$ and staggered from adjacent curves by y=1. The apparent M_W of each construct (labelled above each trace) was calculated by calibration with known M_W standards, whose elution volumes are indicated above the plot with grey arrows. (**B-D**) To quantify the extent of dimer formation and monomer oxidation in the DoubleCatcher double-cysteine variants, samples post Ni-NTA, post-oxidation with 0.4 mM $CuSO_4$, and post-reduction with 10 mM DTT were analysed by SDS-PAGE. (**E**) The homogeneity of the hydrodynamic radius (R_h) of each DoubleCatcher variant was determined by dynamic light scattering (DLS). Traces are normalised to the major peak and staggered by y=1. Mean R_h ± 1 s.d. (n = 10) of each variant is labelled above each trace.

5.1.3.2 Monitoring rigidity using dynamic light scattering

The overall flexibility of the DoubleCatcher disulfide-lock mutants, relative to native DoubleCatcher, were further analysed by dynamic light scattering (DLS) (Fig. 5.2E). The proteins' hydrodynamic radius (R_h), as determined by DLS, provides information on the average size of the macromolecule and the degree to which the size varies in the sample. The extent of dynamic changes to the macromolecular architecture of DoubleCatcher in solution, due to rearrangement of SpyCatcher003 domains, is expected to depend on the overall flexibility of the construct. For each variant, the peak attributed to the main species is labelled with the mean R_h ± 1 s.d. (n = 10). As expected, both the mean R_h and the mean s.d. of the double-cysteine mutants (3.6 ± 1.2 nm) were less than those for the cysteine-free variants (4.5 ± 1.7 nm), possibly due to a lower degree of flexibility within the architecture.

5.1.4 Validating reactivity of stable DoubleCatcher structural variants

To examine the effects of DoubleCatcher architecture on bispecific activity, DoubleCatcher H-Lock was selected for downstream investigation alongside five structurally distinct DoubleCatcher disulfide-lock variants. Amongst the nine variants designed and biophysically characterised, intramolecular disulfide bond formation was most efficient in DoubleCatcher variants [1], [3], [5], [7], and [9] (Fig. 5.2B-D), leading to reduced dimer formation or aggregation, higher yields post-SEC, and more complete oxidation following incubation with $CuSO_4$. These five DoubleCatcher variants were subsequently renamed: [1], α-Lock; [3], β-Lock; [5], γ-Lock; [7], *δ*-Lock; and [9], ε-Lock. The identities and oxidation states of the five selected DoubleCatcher disulfide-lock variants were confirmed by electrospray-ionisation mass spectrometry. As a representative example, DoubleCatcher α-Lock was analysed in its reduced state, following incubation with 10 mM DTT (Fig. 5.3A), and its oxidised state, following incubation with 0.5 mM $CuSO_4$ (Fig, 5.3B), demonstrating the -2 Da shift of the

main peak upon the oxidation of two cysteines to cystine. Each of the other variants were then analysed post-oxidation with $CuSO_4$ (Fig. 5.3C-F).

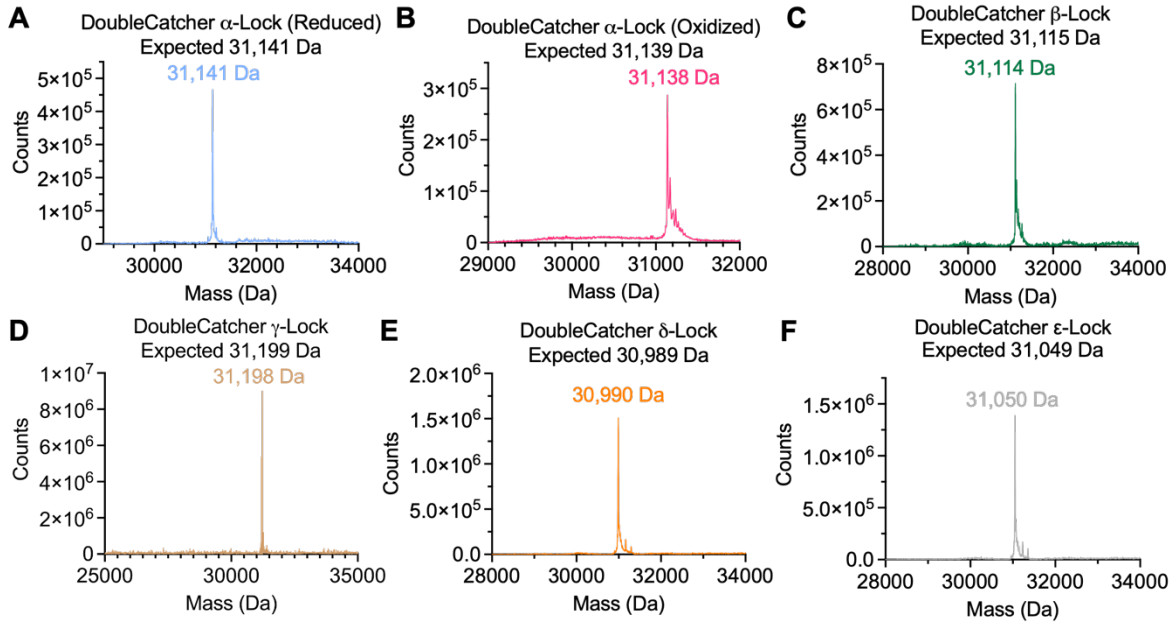


Figure 5.3. Complete oxidation of the five selected DoubleCatcher variants is confirmed by mass spectrometry. (**A-F**) The five DoubleCatcher disulfide-Lock variants that achieved the highest extent of intramolecular oxidation post-expression in *E. coli* were selected for further investigation. Intact protein Electrospray Ionization Mass Spectrometry was employed to validate their identity and monitor the intended disulfide bond formation.

The DoubleCatcher structural variants were then scrutinised for their stepwise reactivities with SpyTag-fused ligands. As employed in Section 4.2.1, intact protein mass spectrometry was applied to validate the bispecific products resulting from heterodimerisation of two anti-HER2 binders, nanoHER2-SpyTag003 and affiHER2-SpyTag, using each of the 7 DoubleCatcher variants following the SpyMask protocol. Pleasingly, bispecific products were observed at the expected molecular weights following assembly with each DoubleCatcher variant, with undetectable formation of undesired singly-saturated or homodimeric DoubleCatcher by-products (Fig. 5.4A-G). Considering assembly reactions with each variant were conducted in parallel in 96-well plate format, this experiment also supports the generalisability of the SpyMask protocol; reaction conditions do not need to be optimised following structural modifications of the DoubleCatcher module.

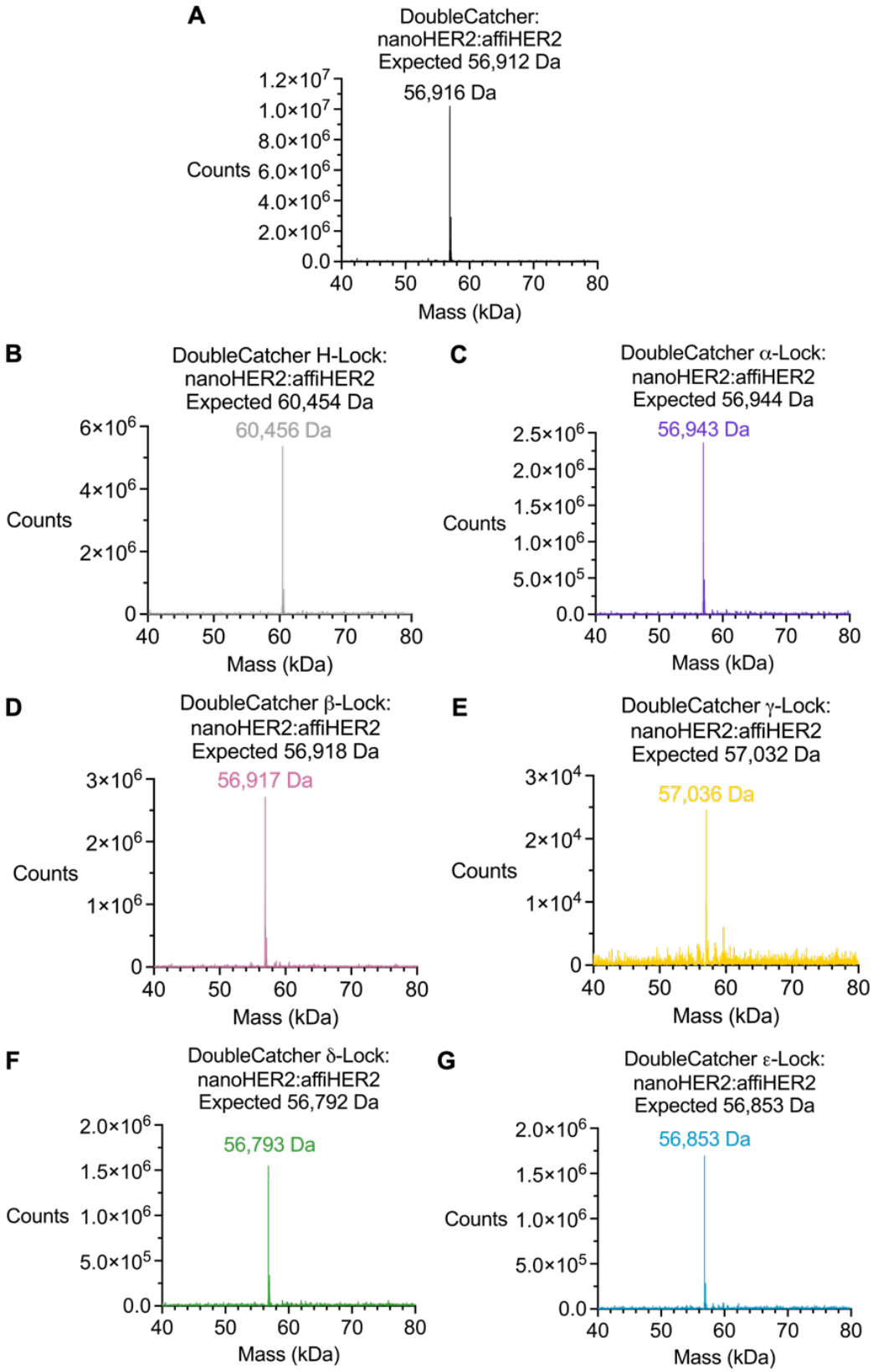


Figure 5.4. Heterodimerisation of nanoHER2 and affiHER2 with the panel of DoubleCatcher variants is validated by mass spectrometry. Bispecific binders were assembled with nanoHER2 at the N-terminus and affiHER2 at the C-terminus, using the full panel of DoubleCatcher variants. Purified bispecific molecules were analysed by Electrospray Ionization Mass Spectrometry, confirming the formation of the desired heterodimer (**A-G**).

5.1.5 Measuring the effect of DoubleCatcher architecture on activity of anti-HER2 bispecific antibodies

In agreement with the literature, it was observed in the previous Chapter that signalling downstream of bispecifc-induced HER2 dimerisation is responsive to differences in bispecific format. However, thus far, I have only explored the effects on cell metabolic activity of modifying the binder identity and orientation within the bispecific molecule. As these bispecifics were assembled with the native DoubleCatcher scaffold, whose flexible Gly/Ser linker possesses a substantial degree of flexibility, the distance and angle between the two paratopes is not fixed. While flexibility in a bispecific construct may be desirable when bridging targets across different cells (Wolf et al., 2005; Zoine et al., 2024), rigidity is preferrable in bispecifics that function to induce signalling or catalytically-active (or biased) target dimers (Segaliny et al., 2023; Wu et al., 2017b). First, rigid bispecific scaffolds permit control over the spatial orientation of their targets, and second, rigid bispecifics can provide information on the structure-function relationship of the target molecules.

Therefore, I sought to employ the set of characterised, structurally diverse DoubleCatcher scaffolds described in this section to study the sensitivity of HER2 signalling to dimer geometry. Using the SpyMask protocol, each of the seven DoubleCatcher variants were used to dimerise Tras NoLink, nanoHER2, and AffiHER2 in all possible combinations, to produce a set of small matrices of bispecifics with identical binder arms, but different DoubleCatcher architectures. The assembled bispecific binders were added to HER2-addicted SKBR3 cells (100 nM) for 96 h, after which the change in metabolic activity was calculated relative to untreated cells and grouped by dimerisation scaffold (Fig. 5.5A (top), B). As a control for the activity of the monomeric binders in combination, cells were treated with a mixture of the purified binders (100 nM) without DoubleCatcher added, (‘No DC’ matrix in Fig. 5.5A, top).

Simultaneously, cells were treated with purified DoubleCatcher variants alone (100 nM) to test for scaffold activity (Fig. 5.5A, bottom).

As observed in Fig. 4.9, the potency of a bispecific assembled with any given pair of anti-HER2 binders was shown to be dependent on binder orientation on the DoubleCatcher scaffold (Fig, 5.5). Interestingly, bispecific potency was additionally found to be sensitive to the DoubleCatcher scaffold. The effect of scaffold on potency was most pronounced for the nanoHER2-containing pro-proliferative DoubleCatcher β-lock bispecifics, which induced +25% greater mean proliferation in SKBR3 cells than the equivalent bispecifics assembled with native DoubleCatcher. In a similar example, the metabolic activity of Tras NoLink:Tras NoLink assembled with DoubleCatcher (85 ± 6.8%; mean (n = 3) ± 1 s.d.) was enhanced when dimerised with DoubleCatcher H-Lock (76 ± 2.5%), DoubleCatcher α-Lock (80 ± 3.9%), DoubleCatcher γ-Lock (80 ± 3.4%), DoubleCatcher δ-Lock (74 ± 4.9%), and DoubleCatcher ε-Lock (73 ± 4.3%). Improvements to bispecific potency is an important property that is screened for in therapeutic selection, and these data support a role for DoubleCatcher variation as well as binder arm orientation in the optimisation of a given bispecific.

However, it was most exciting to observe that the agonistic or antagonistic activity of some bispecifics was switched when its constituent binder arms were dimerised with a different DoubleCatcher scaffold. Notably, the bispecific AffiHER2:Tras NoLink showed mild agonistic activity on the native DoubleCatcher scaffold (113 ± 6.6% metabolic activity), yet the equivalent bispecific assembled using DoubleCatcher H-Lock exhibited strong antagonistic activity under the same conditions (83 ± 11.1%). An even more marked switch of bispecific activity was seen for Tras NoLink:AffiHER2 assembled in DoubleCatcher γ-Lock (79 ± 3.1%), relative to DoubleCatcher (128 ± 4.1%). Considering the predicted increase in rigidity of the

anti-HER2 bispecifics that have pronounced differences in their effect on cell proliferation, these findings reinforce the sensitivity of HER2 signalling to dimer geometry.

The proof-of-concept screen here accentuates the value of screening multiple formats in the assembly of bispecifics. However, from this screen alone, it is not possible to discern how changes to DoubleCatcher architecture alter the mechanics and biochemical properties of HER2 dimerisation. Such changes may include a preference for HER2 oligomerisation, which leads to arrest of receptor diffusion and compartmentalisation into membrane nanodomains (Stüber et al., 2021); differences in the distance between cross-linked HER2 molecules (Kast et al., 2021); differently distorted HER2 extracellular domains upon binding that influence the receptor's preference for homo/hetero-dimerisation (Gu et al., 2014); or altered bispecific-HER2 complex stoichiometries (Brack et al., 2014). Thus, further work on quantifying the structural parameters (distance and angle between SpyCatcher003 moieties, relative flexibility of the scaffold) is imperative to interpreting the phenotypical data fully, deciphering the mechanism of different binders, and improving our understanding of HER2-induced signalling. A protein-protein interaction tracking technique such as Bioluminescence Resonance Energy Transfer (BRET) may be employed to study homo- vs. hetero-dimer formation (Siddiqui et al., 2013), single-particle tracking analysis could be used to quantify changes in receptor diffusion kinetics (Freed et al., 2017), and nanoparticle-aided cryo-electron microscopy would enable us to gain insight into the conformational homogeneity, and thus rigidity, of different DoubleCatcher scaffolds (Ki et al., 2021).

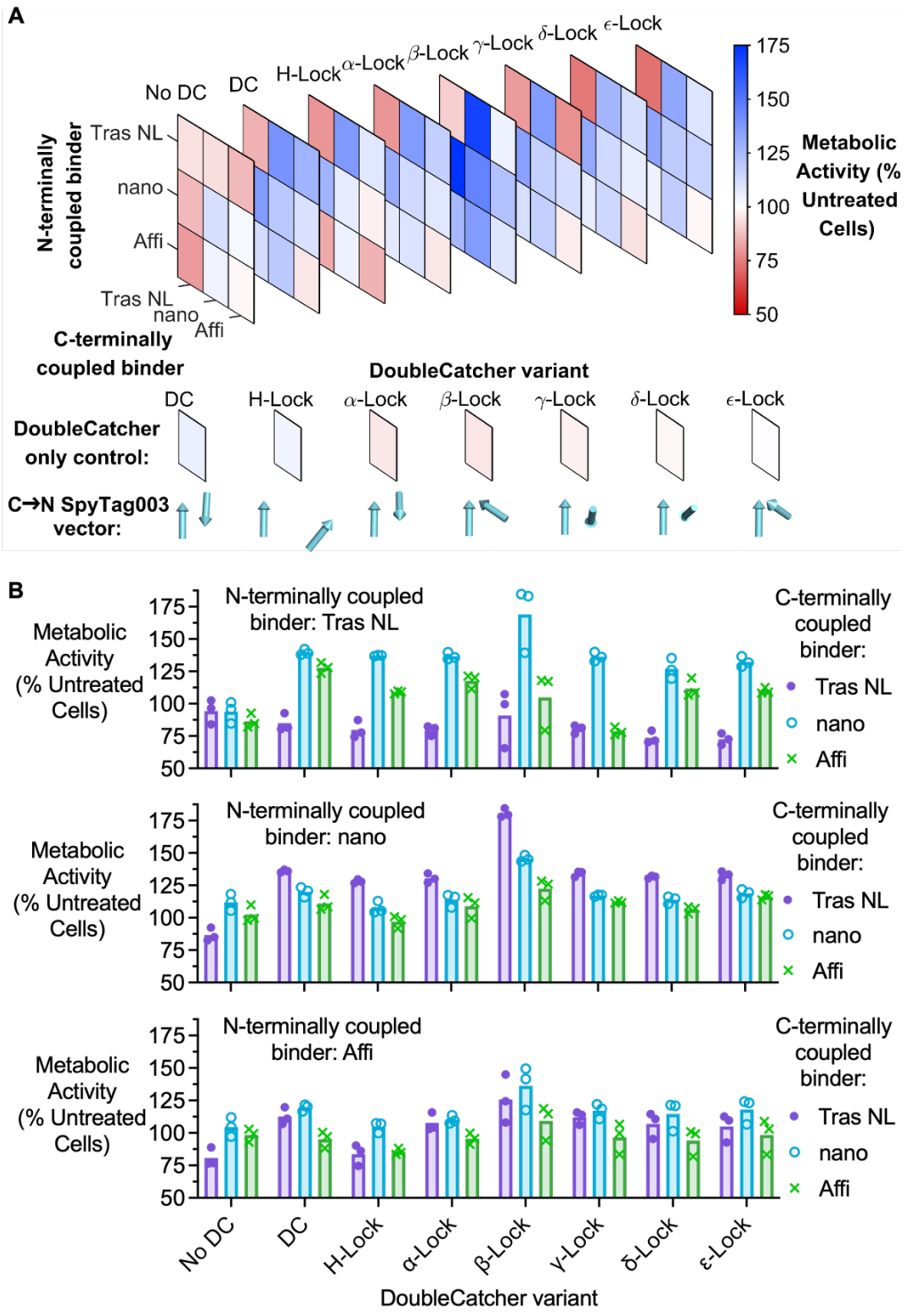


Figure 5.5. DoubleCatcher-heterodimerised anti-HER2 bispecific molecules harness a range of pro-proliferative and antiproliferative activities in HER2-positive cancer cells. (**A**) The set of selected DoubleCatcher variants were used to assemble equivalent matrices of bispecific antibodies from a subset of anti-HER2 binding molecules: the Tras NoLink Fab, nanoHER2 nanobody, and affiHER2 affibody. HER2-overexpressing SKBR3 cells were treated with each anti-HER2 bispecific (100 nM) for 96 h, after which cell metabolic activity was determined by the Resazurin assay. Cells were treated with each DoubleCatcher alone, or DoubleCatcher-free mixtures of binders, to control for the activity of the DoubleCatcher constituents. As in Fig. 5.1., cyan vectors representing SpyTag-binding groove and directionality are displayed for each DoubleCatcher variant to indicate their structural differences. (**B**) Triplicate metabolic activity data from (A) are presented as bar charts, grouped by N-terminally conjugated binder, with each point plotted and the bar indicating the mean.

5.2 Extending the serum half-life of DoubleCatcher

One commonly cited limitation of fragment-based bispecific antibodies is their rapid clearance, due to their smaller size and lack of FcRn-binding domains. A solution to this has been to fuse the bispecific molecule to IgG Fc-regions or human serum albumin (HuSA), plasma protein-binding domains, or polyethylene glycol (PEG) (Hutt et al., 2012; Müller et al., 2007). Therefore, to enhance the therapeutic potential of the SpyMask platform, I fused the DoubleCatcher to ABD035, a three-helix bundle protein engineered to bind HuSA with femtomolar affinity (Jonsson et al., 2008). Fusion of ABD035 to a 35 kDa endolysin therapeutic has previously been shown to increase the serum circulation half-life of the enzyme in mice by > 10 h (Seijsing et al., 2018). Previous attempts to directly engineer albumin binding domains to simultaneously bind albumin and a target of interest, such as HER2, were unsuccessful due to the steric limitations of a small three-helix bundle binding to both HuSA and a large receptor extracellular domain (Nilvebrant et al., 2014). To ensure sufficient separation of the albumin binding domain from the target binding domains on DoubleCatcher-conjugated binders, I chose to fuse ABD035 to the N-terminus of DoubleCatcher via a GSGESG hexapeptide linker (Fig. 5.6A).

Following expression of the ABD035-DoubleCatcher fusion in *E. coli* C41 cells and purification by Ni-NTA, I tested its ability to bind purified human serum albumin (HuSA) in solution by ELISA. Here, 80 nM SpyTag003-MBP was immobilised to 96-well plates and reacted with ABD035-DoubleCatcher in the absence of TEV protease. Wells were then treated with biotinylated HuSA (0.2 µg/mL; '+ HuSA' in Fig. 5.6B) (Sun et al., 2015), or with buffer alone ('- HuSA' in Fig. 5.6B), and HuSA binding was detected by the addition of streptavidin-horseradish peroxidase (HRP). As negative controls for HuSA binding, signal was monitored in wells without SpyTag003-MBP added ('No SpyTag003-MBP'), or in wells in which native

DoubleCatcher was reacted to immobilised SpyTag003-MBP instead of the ABD035-fusion ('DoubleCatcher'). ABD035-DoubleCatcher binding to HuSA was clearly detected, and specific to this DoubleCatcher variant.

Subsequently, mass spectrometry was employed to validate the ability of ABD035-DoubleCatcher (Fig. 5.6C) to heterodimerise two SpyTag-fused model proteins, SpyTag003-A (Fig. 5.6D) and SpyTag003-B (Fig 5.6E) by the SpyMask protocol. As intended, the ABD035-DoubleCatcher:A:B heterodimer was formed with the expected molecular weight, with undetectable formation of singly saturated DoubleCatcher or homodimeric by-product (Fig. 5.5F). Therefore, the ABD035-DoubleCatcher variant is suitable for use in the design of therapeutic bispecific molecules.

5.3 Chemical functionalisation of SpyTag for diversifying SpyMask ligands

The existing SpyMask approach dimerises protein-based binder molecules towards the target of interest, that can be recombinantly expressed as SpyTag fusions. While high-affinity synthetic or antibody-derived proteins can be readily raised against virtually all protein targets (Cao et al., 2022; Colwill et al., 2011; Dübel et al., 2010), identifying functional soluble protein agonist/antagonists that retain specificity have proven to be difficult for some classes of receptors. As a pertinent example, GPCRs possess low conformational conservation, display limited exposed extracellular epitopes, and have buried ligand-binding sites. Furthermore, signal transduction following ligand binding to GPCRs is propagated by conformational changes across multiple domains of the receptor, which must be mimicked by the therapeutic molecule to achieve the desired function (Cheng et al., 2023).

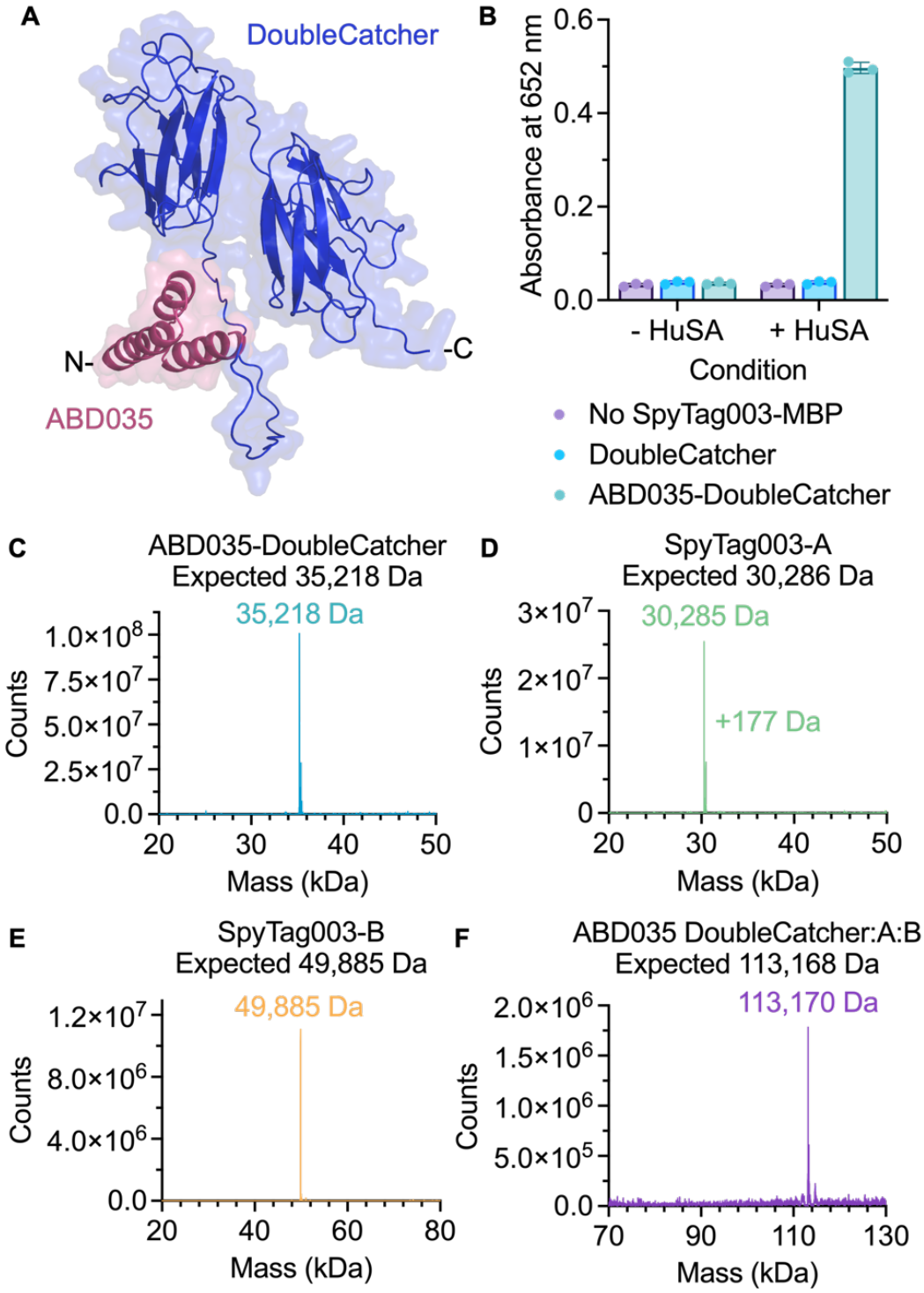


Figure 5.6. DoubleCatcher fused to the human serum albumin-binding protein ABD035 reacts efficiently with SpyTag-linked ligands to form bispecifics. To generate a variant of DoubleCatcher with prolonged serum-half life, the human serum albumin (HuSA)-binding three-helix bundle ABD035 was genetically fused to the N-terminus of DoubleCatcher. The AlphaFold3-predicted structure of the ABD035-DoubleCatcher variant is presented in (**A**), with DoubleCatcher in blue and ABD035 in magenta. (**B**) Specific binding of ABD035-DoubleCatcher to biotinylated HuSA was validated by ELISA, using streptavidin-horseradish peroxidase (HRP) to detect binding. Data shown are mean (n = 3) ± 1 s.d.. To ensure the function of ABD035-DoubleCatcher in bispecific assembly is retained, two SpyTag003-fused ligands (A and B) were conjugated onto the variant following the SpyMask protocol. The resulting ABD035-DoubleCatcher:A:B heterodimer was formed at the expected molecular weight, according to mass spectrometry analysis (**C-F**).

For this reason, whilst one-third to one-half of all approved drugs target GPCRs, only two GPCR-binding therapeutics are mAbs (Dolgin, 2018; Mullard, 2018). Therefore, the breadth of cell-surface targets that can be bridged by DoubleCatcher-based bispecific binders would be greatly expanded if the bispecifics incorporated non-protein-fragment-based ligands. Such ligands could include peptides, oligonucleotide aptamers, small molecules, full-length IgG antibodies, lipids, metabolites, lipids, and inorganic ions (Wu et al., 2017a; Yang et al., 2021a) The vision for expanding the SpyMask ligand toolbox with diversified SpyTagged ligands is outlined in the flow chart in Fig. 5.7. All compounds described in green were synthesised by Thomas Wharton and Sona Krajcovicova (David Spring group, University of Cambridge), and kindly gifted to me for the generation of ligands for bispecific assembly. Compounds coloured magenta are 'off-the-shelf' reagents that can be purchased from chemical suppliers, or in the case of small molecule ligands bearing amine groups, chemically modified to possess an azide functional group for downstream click chemistry reactions (Meng et al., 2019). The desired SpyTag-Ligand conjugates are shaded in blue and can be used directly in the assembly of bispecific compounds using DoubleCatcher, where multiplexed libraries of ligands can rapidly generate bispecifics that bridge diverse and unprecedented combinations of targets.

To start, automated peptide synthesis is used to synthesise SpyTag003 on Rink amide resin, as described previously (Lau et al., 2014). Directly following deprotection of the N-terminal fluorenylmethoxycarbonyl (Fmoc) protecting group with 5% 1,8-Diazabicyclo[5.4.0]undec-7-ene (DBU) in dichloromethane (DCM), the solid-phase peptide was reacted with 5-azidopentanoic acid to produce an N-terminal azide. Following washing of the resin, the synthesised peptide is cleaved from the resin using 10% trifluoroacetic acid (TFA) in DCM, according to standard protocols, yielding the SpyTag003 peptide with a C-terminal amide ('N_3-SpyTag003', Fig. 5.8A). This azide-functionalised SpyTag003 peptide is free to react with

small molecule ligands harbouring strained cycloalkynes, via copper-free strain-promoted azide–alkyne cycloaddition (SPAAC), or with linear alkyne-bearing ligands via copper-catalysed azide alkyne cycloaddition (CuAAC) (Krajcovicova et al., 2024).

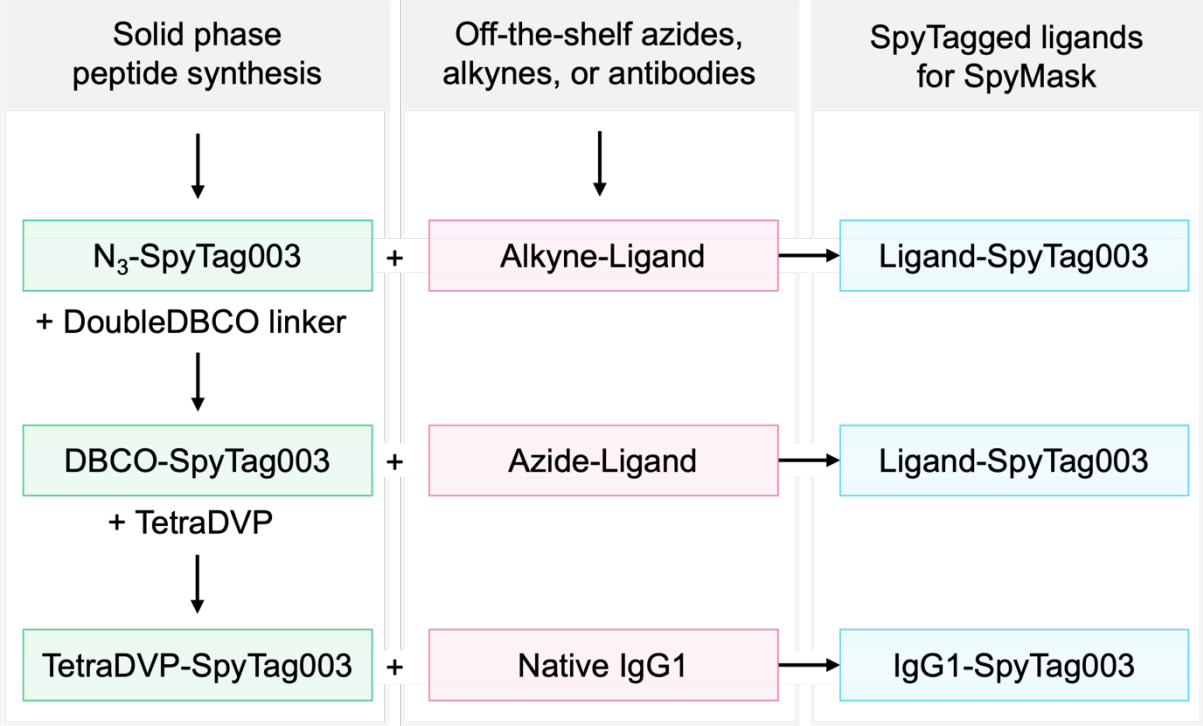


Figure 5.7. Diversification of the SpyMask-compatible ligand library. The vision to expand the set of ligands for conjugation onto DoubleCatcher, beyond recombinantly-expressed protein-SpyTag fusions, is presented as a flow chart. First, chemically functionalised SpyTag003 peptides, highlighted in green, are generated by automated solid-phase peptide synthesis followed by chemical modification. Each starting molecule can be then reacted with an off-the-shelf (or chemically modified) ligand, highlighted in magenta, by bioorthogonal reactions including strain-promoted azide-alkyne cycloaddition (SPAAC) and copper(I)-catalysed azide-alkyne cycloaddition (CuAAC), or disulfide re-bridging, to yield a covalently modified SpyTag-ligand. Abbreviations: DBCO = Dibenzocyclooctyne; TetraDVP = tetra-divinylpyrimidine.

For the generation of alkyne-functionalised SpyTag003 peptide, a tandem dibenzylcyclooctyne (DBCO) compound, termed Double-DBCO linker (Fig. 5.8B), was synthesised from the reaction of DBCO acid (2.2 eq.) with 2,2'-((oxybis(ethane-2,1-diyl))bis(oxy))bis(ethan-1-amine) (1 eq.) (Krajcovicova et al., 2024). Simple SPAAC reaction of N_3-SpyTag003 with one DBCO moiety of the Double-DBCO linker in equimolar amounts yielded the reactive DBCO-SpyTag003 peptide fusion (Fig. 5.8C), in only 1 h in DMSO, which can be equipped with any azide-bearing payload of interest.

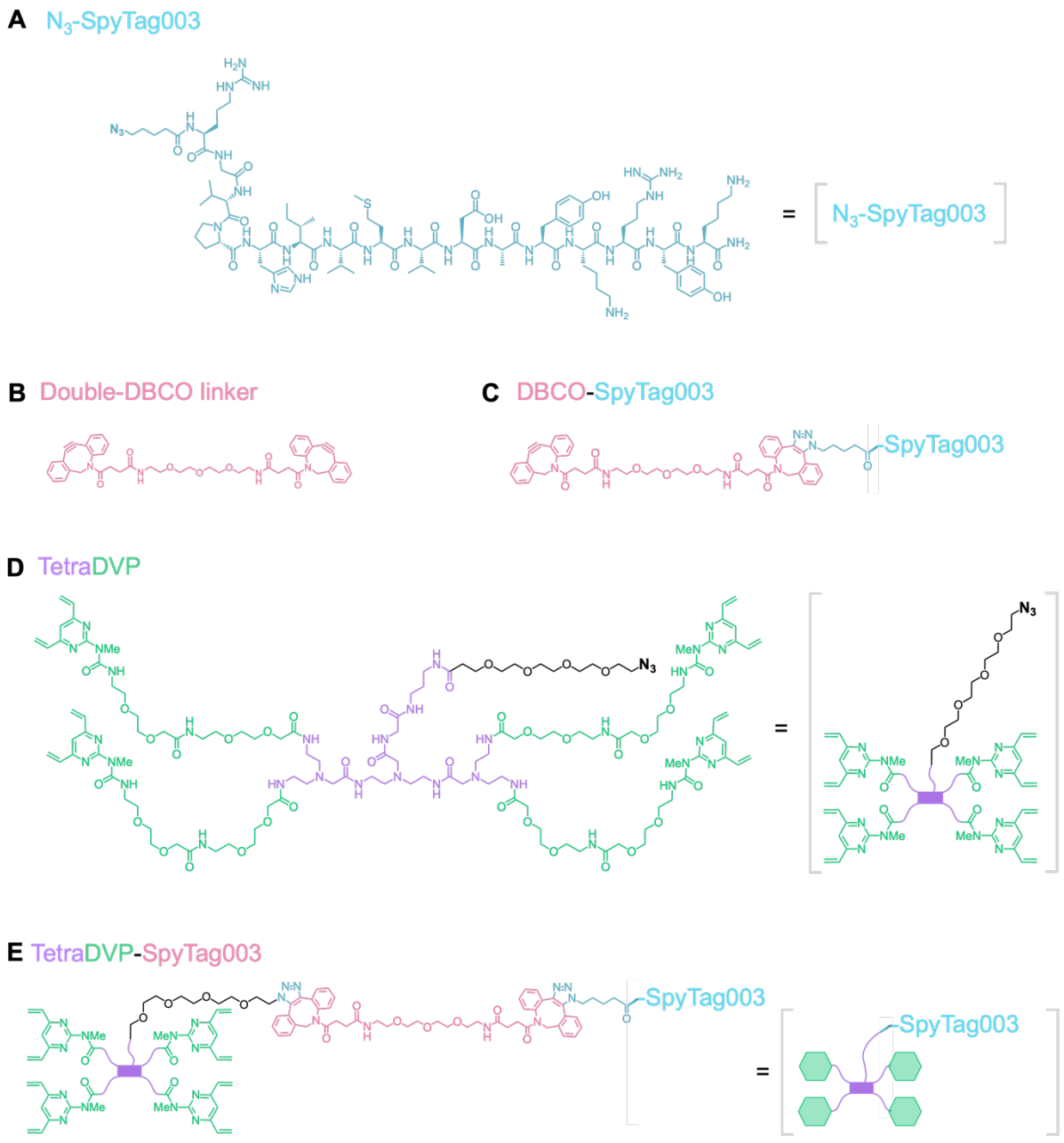


Figure 5.8. Chemical structures of functionalised SpyTag003 molecules. (**A-E**) The starting molecules in green in Fig. 5.7 were chemically synthesised and validated by the group of Prof. David Spring (University of Cambridge) and their chemical structures are shown. Structures are coloured according to chemical moiety, with N_3-SpyTag003 in cyan, Double-DBCO linker in magenta, elongated divinylpyrimidine (DVP) groups in green with their connecting linker backbone in purple and azido spacer in black. Molecules in grey brackets are simplified versions of the full structure, for ease of use in downstream representations. Compounds (A), (B), (D), and (E), were validated by mass spectrometry and analytical high-performance liquid chromatography (Krajcovicova et al., 2024).

Finally, SpyTag003 can be additionally decorated with the well-characterised disulfide re-bridging crosslinking reagent tetra-divinylpyrimidine (TetraDVP; Fig. 5.8D) (Dannheim et al., 2022; King et al., 2023; Krajcovicova et al., 2024), which bears four DVP groups that can each

react with two cysteine residues. Native IgG1 antibodies possess four interchain disulfide bonds: one between the CH1 region of each heavy chain and the CL domain of its associate light chain, and two between the two heavy chains, found within the hinge region (Fig. 5.11A, B). These interchain disulfide bonds can be selectively reduced using tris(2-carboxyethyl)phosphine hydrochloride (TCEP-HCl) for 1 hour at 37 °C, whilst leaving the intrachain disulfide bonds intact. Therefore, TetraDVP can act to bridge each of the four pairs of reduced cysteine residues that form the IgG1 interchain disulfide bonds (Fig. 5.11A, C). Importantly, the TetraDVP scaffold used here contains a central functional azide handle connected to the scaffold by a spacer (black, Fig. 5.8D), which has been optimised in length and flexibility to allow efficient bridging of the interchain disulfide bonds of IgG1 by TetraDVP even with a payload attached to the central azide (King et al., 2023; Krajcovicova et al., 2024). Here, the azide handle was reacted with the DBCO-SpyTag003 product by SPAAC in DMSO at 25 °C, resulting in full conversion to a TetraDVP-SpyTag003 conjugate (Fig. 5.8E). Thus, these chemical tools provide a route for the simple SpyTagging of off-the-shelf, full-length IgG1 antibody binders, expanding the number of bispecific combinations that can be explored using SpyMask. Beyond their application in bispecific antibody synthesis, SpyTag003-linked small molecules and full-length IgGs can also facilitate the assembly of dye-labelled antibodies, antibody-drug conjugates (ADCs) and bioconjugates with controlled and reliable payload-antibody ratios (Walsh et al., 2021).

5.4 Generation of SpyTag003-fused small molecule ligands

As a proof-of-concept for covalent conjugation of SpyTag003 to a commercially available ligand, I aimed to conjugate SpyTag to azide-functionalised oligonucleotides, which could be desirable for the assembly of bispecifics harbouring aptamer ligands, binders conjugated to DNA probes for imaging, or DNA-conjugated antibodies for multiplexed proteomics

applications (Gong et al., 2016; Hamada et al., 2023; Thomas et al., 2022). Oligonucleotides DNA-1 (5'-TCTTCATTACTAGAT-3') and DNA-2 (5'-AGAAGAAATGTTCTT-3') were first synthesized with a 5'-azide, and then incubated (each at 50 µM) with 5-fold excess DBCO-SpyTag003 (250 µM) at 37 °C for 16 h (reaction schematic outlined in Fig. 5.9A).

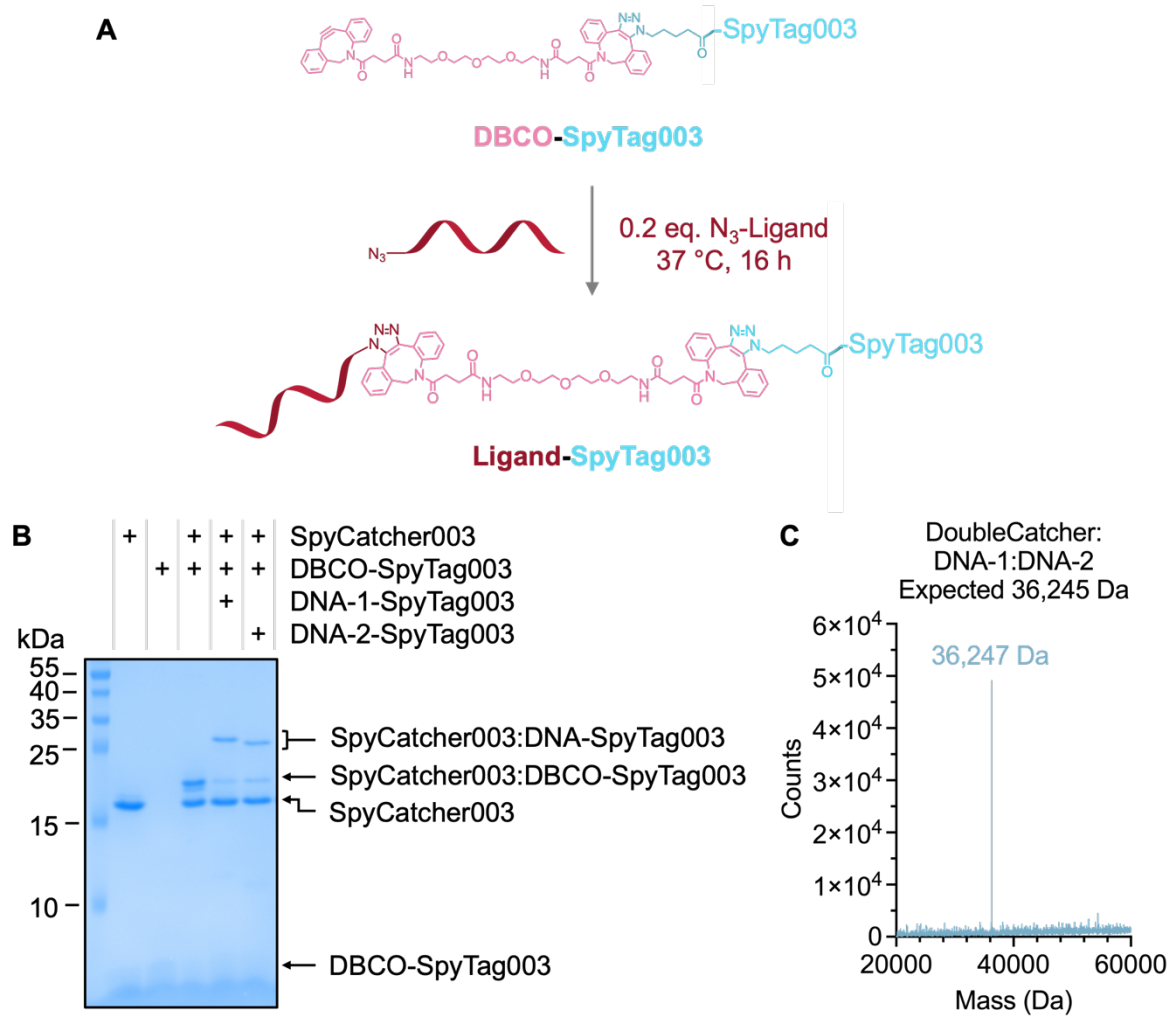


Figure 5.9. DBCO-SpyTag003 reacts with Azide-DNA to form SpyTagged DNA, which can be conjugated onto DoubleCatcher. DBCO-SpyTag003 can be used to covalently decorate azide-bearing ligands with the SpyTag003 peptide. As a representative example for this reaction, DBCO-SpyTag003 (250 µM) was reacted with one of two short DNA oligonucleotides synthesised with a 5' azide (N_3-DNA-1 or N_3-DNA-2; 250 µM) for 16 h at 37 °C, to yield a DNA oligonucleotide with a 3' SpyTag003. The formation of this product was monitored by incubating 2.5 µM of the reaction mixture with 5 µM SpyCatcher003, followed by SDS-PAGE analysis and Coomassie staining (**B**). After reaction with both DBCO-SpyTag003/azide-DNA reaction mixtures, a shift in the SpyCatcher003 band was observed, and this shift was greater than that for SpyCatcher003 plus DBCO-SpyTag003 alone, indicating the formation of DNA-SpyTag003. (**C**) Sequential conjugation of the two DNA-SpyTag003 ligands onto DoubleCatcher resulted in the formation of a DNA heterodimer at the expected molecular weight, as validated by mass spectrometry.

To remove excess, unreacted DBCO-SpyTag003, reaction mixtures were dialysed into PBS pH 7.4, for 4 h at 4 °C, using a 5 kDa molecular weight cutoff. To monitor the extent of reactivity, 2 μM of the reaction mixture was then incubated with 5 μM SpyCatcher003 for 2 h at 37 °C, and reaction products were visualised by SDS-PAGE (Fig. 5.9B). SpyCatcher003 was also incubated with 2 μM DBCO-SpyTag003 alone, to allow identification of the SpyCatcher003:DBCO-SpyTag003 band. A clear shift in SpyCatcher003 band was observed following its reaction with both DBCO-SpyTag003:N_3-DNA reactions, confirming the covalent conjugation of SpyTag003 to the DNA ligands. Therefore, the two DNA ligands were sequentially reacted with DoubleCatcher following the SpyMask protocol to assemble a bispecific molecule displaying two, unique DNA probes, which was identified by mass spectrometry at the correct molecular weight (Fig. 5.9C).

5.4.1 Stability of the DBCO-SpyTag003 reagent

It was interesting to observe that a five-fold molar excess of DBCO-SpyTag was required over Azide-DNA for near-complete conversion of DBCO-SpyTag to DNA-SpyTag, and the extent of product formation was greater than when the reaction was carried out with the Azide-DNA in 5-fold excess instead. This suggests that the absolute concentration of DBCO-SpyTag in solution was lower than the expected 2 mg/mL (708.5 μM). Directly after DBCO-SpyTag synthesis, the white solid was dissolved in DMSO and analysed by low-resolution mass spectrometry, to reveal the presence of the peptide at the expected molecular weight (2,823 Da) (Fig. 5.10A, C). However, the solution of DBCO-SpyTag in DMSO was aliquoted for storage at -80 °C for future use, and so the DBCO-SpyTag samples that were used for reaction with Azide-DNA were subjected to at least one freeze-thaw cycle.

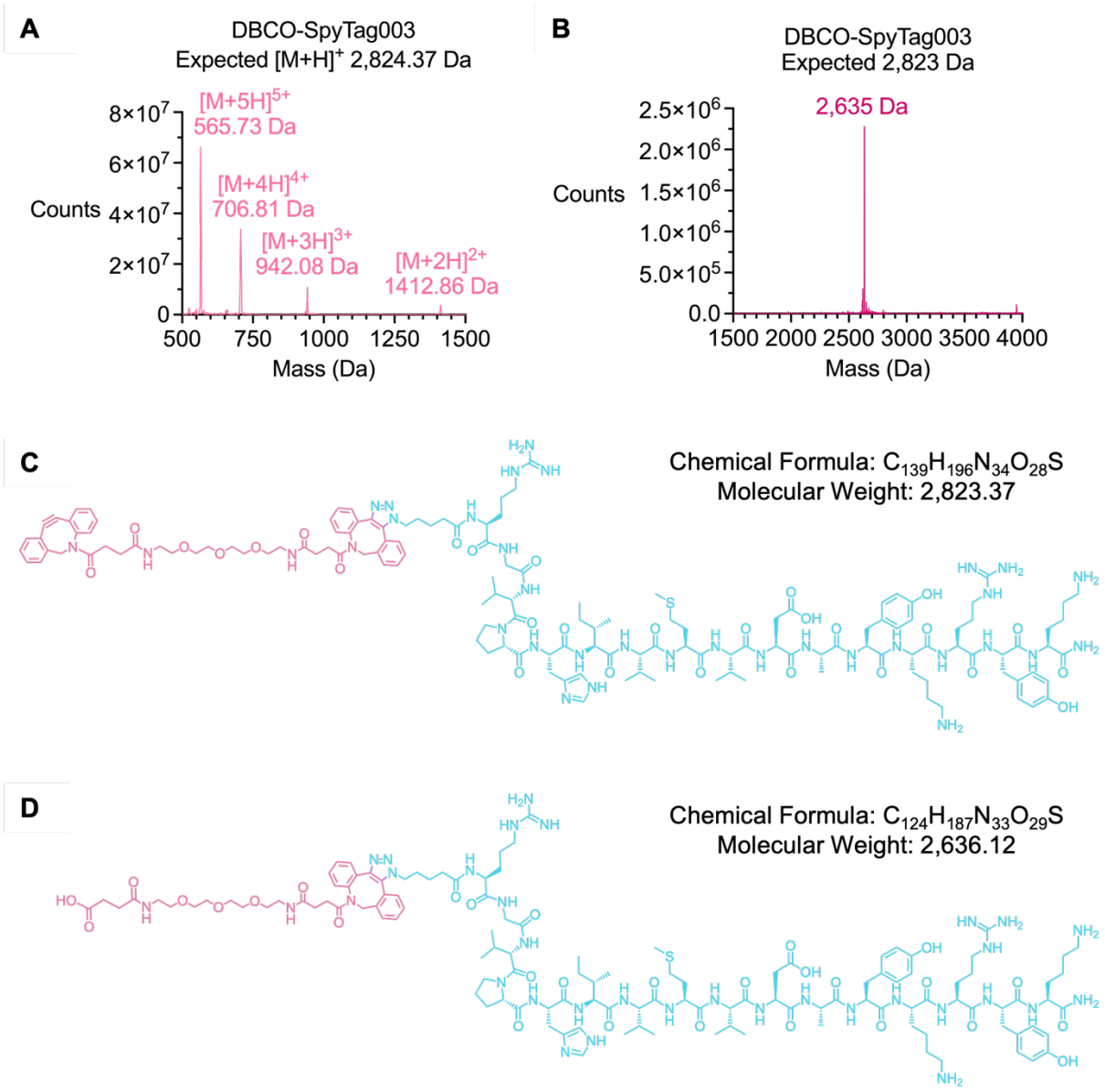


Figure 5.10. Degradation of DBCO-SpyTag003 after storage in DMSO. (**A**) Directly following chemical synthesis of DBCO-SpyTag003, low resolution mass spectrometry validated the identity of the peptide at the predicted molecular weight. (**B**) Storage of DBCO-SpyTag003 in DMSO at a concentration of 2 mg/mL at -80 °C for 3 months resulted in complete degradation of the reagent to a molecule of 2,635 Da. Analysis of the chemical structure of DBCO-SpyTag003 (**C**) allowed the degradation to be identified as the loss of the reactive DBCO group to leave a terminal carboxylic acid, which is unreactive to azides in PBS alone (**D**).

Subsequent analysis of an aliquot of DBCO-SpyTag in DMSO that had been stored for 3 months at -80 °C by high-resolution mass spectrometry revealed its complete conversion to a degradation product of 2,365 Da (Fig. 5.10B), which corresponds to the loss of the reactive DBCO unit from the double-DBCO linker (Fig. 5.10D). This DBCO-SpyTag degradation

product is unreactive to azides, thus reducing the concentration of reactive species in a sample where degradation has occurred. Therefore, DBCO-SpyTag should ideally be stored as a solid at -20 °C or below, under an inert environment, and resuspended directly before use.

5.5 Chemical coupling of IgG1 to TetraDVP-SpyTag003 using selective disulfide re-bridging

5.5.1 Validation of assembly by MS and SDS-PAGE

The conjugation of TetraDVP-SpyTag003 to the commercially available anti-HER2 IgG Trastuzumab was optimised by Thomas Wharton (Spring group, University of Cambridge), who discovered that three sequential 24-hour cycles of adding 10 equivalents of TCEP and 5 equivalents of TetraDVP-SpyTag003 to Trastuzumab reliably yielded the desired SpyTag-linked IgG. In fact, 97% conversion of Trastuzumab to SpyTag-linked product was realised by this methodology, as observed by hydrophobic interaction chromatography (Krajcovicova et al., 2024). The reaction was additionally monitored by SDS-PAGE (Fig. 5.11D) and intact mass spectrometry (Fig. 5.11E), to reveal the formation of two SpyTag-linked reaction products. As expected, the major product detected corresponds to the fully re-bridged form of Trastuzumab (‘SpyTag003-tDVP-Trastuzumab’), with two heavy chains (each 49,148 Da, oxidised), two light chains (each 23,438 Da, oxidised), and one TetraDVP-SpyTag003 linker (5,633 Da). The second, minor product, with a mass of 127,366 Da, corresponds to an incompletely re-bridged Trastuzumab product, comprised of two heavy chains and a single light chain covalently conjugated by one TetraDVP-SpyTag003 bridge. While this variant will still have one functional HER2-binding arm, it is important for future applications to note that the bispecific population will contain a small fraction of monovalent Trastuzumab, which is likely to possess different biological activity than a bispecific displaying a divalent Trastuzumab arm. Instead, purification of the final SpyTagged IgG by size-exclusion chromatography may be necessary before conjugation onto DoubleCatcher to ensure homogeneity of the final bispecific.

5.5.2 Confirmation of IgG-SpyTag003-SpyCatcher003 reactivity and specificity

Following synthesis of the SpyTag003-tDVP-Trastuzumab conjugate, it was important to validate its biological activity. Therefore, I reacted Trastuzumab-TetraDVP-SpyTag003 with three SpyCatcher-containing proteins, each representing a way in which SpyTag-conjugated IgG molecules could be functionalised. SpyCatcher003 alone can be site-specifically conjugated to fluorescent dyes for imaging (Alam et al., 2019); SpyCatcher002-MBP demonstrates the coupling of an IgG to a protein payload or enzyme (Keeble and Howarth, 2020), and DoubleCatcher presents a route for the synthesis of full-length IgG-containing bispecific antibodies by SpyMask. Thus, Trastuzumab-TetraDVP-SpyTag003 was mixed with a five-fold molar excess of each SpyCatcher-containing construct in PBS at 37 °C for 4 or 24 hours, and reconstitution of the SpyCatcher:SpyTag isopeptide bond was monitored by SDS-PAGE with Coomassie staining (Fig. 5.12A). A shift in molecular weight of each band attributing to re-bridged Trastuzumab was observed after incubation with all three Catcher-bearing constructs, with negligible unreacted SpyTag003-tDVP-Trastuzumab visible after 4 hours, and undetectable improvement after incubation 24 h. The molecular weight shift of the minor bands within the sample upon incubation with construct was identical to that for the major band, corroborating the finding from the mass spectrometry data for SpyTag003-tDVP-Trastuzumab that unmodified Trastuzumab is absent from the conjugated product reaction mixture.

To assess whether the SpyTagged Trastuzumab product retained strong and specific binding activity to HER2, we then conducted flow cytometric analysis of SpyTag003-tDVP-Trastuzumab on the HER2-positive breast cancer cell line SKBR3, using the HER2-negative breast cancer cell line MDA-MB-468 as a control for non-specific binding to the cell-surface

(Fig. 5.12B). SpyTag003-tDVP-Trastuzumab was reacted with SpyCatcher002-sfGFP before treatment of cells, so that binding to cells could be detected by sfGFP fluorescence. In this way, the binding activity of SpyCatcher-conjugated SpyTag003-tDVP-Trastuzumab is monitored, mimicking the format the functionalised antibody is intended to be used in as a therapeutic or detection tool. The anti-HER2 nanobody nanoHER2-SpyTag003 fusion, which was validated to bind specifically to the HER2 extracellular domain in Fig. 4.6, was used as a positive control for binding. We confirmed that SpyTag003-tDVP-Trastuzumab bound efficiently to SKBR3 cells, with more than a log-fold shift in fluorescence over background from the SpyCatcher002-sfGFP alone control, which was greater than the shift in signal for the nanoHER2-SpyTag003 control (Fig. 5.12B, top).

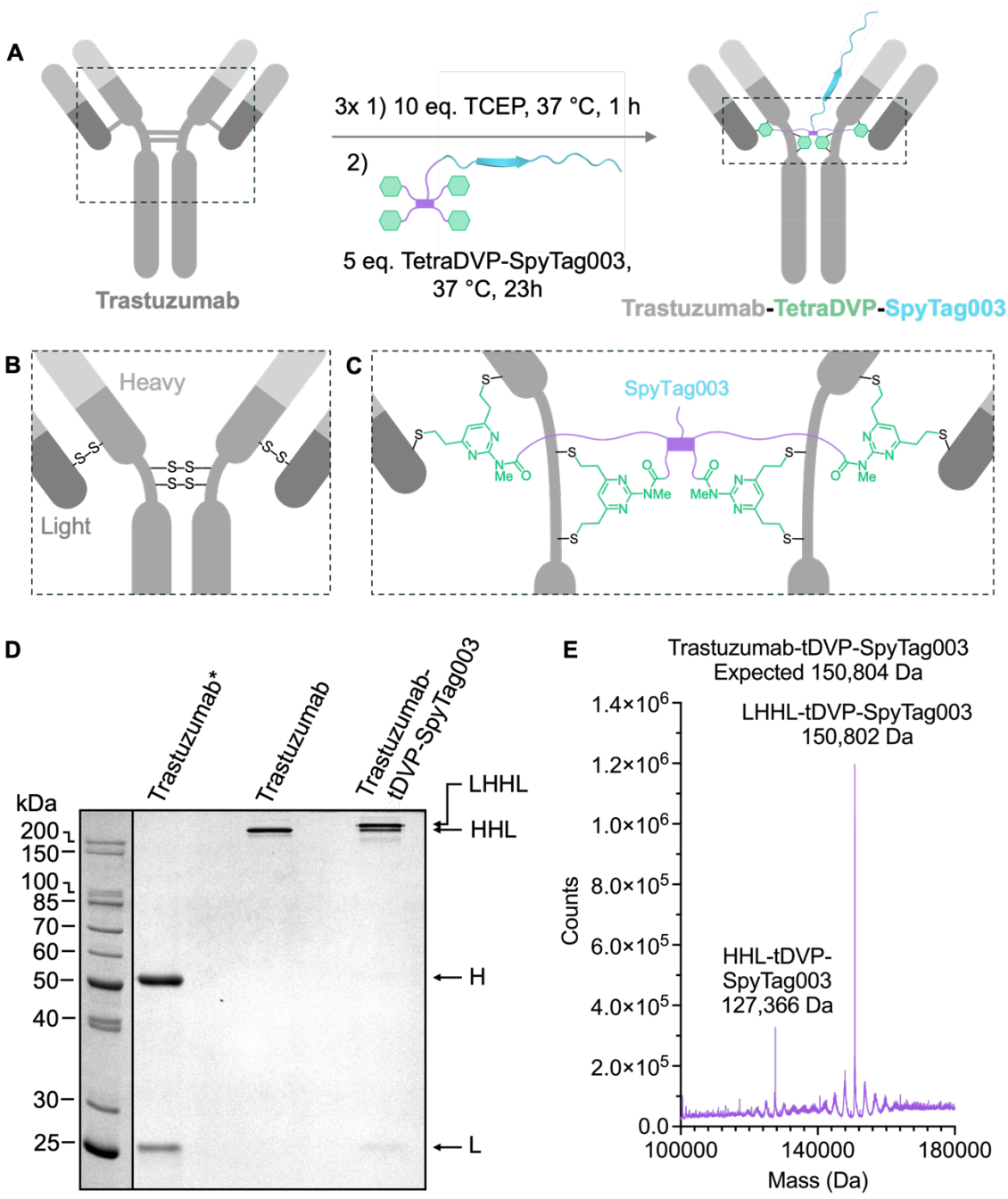


Figure 5.11. The off-the-shelf IgG1 antibody Trastuzumab is selectively re-bridged with TetraDVP-SpyTag003. (**A**) The commercially available anti-HER2 IgG1 molecule Trastuzumab was subjected to three sequential rounds of reduction by TCEP-HCl, followed by TetraDVP-SpyTag003 addition, over a 24 h period, to efficiently re-bridge all four pairs of cysteine residues that form inter-chain disulfide bonds in its structure and yield a covalently-linked Trastuzumab-TetraDVP-SpyTag003 conjugate. (**B**) A zoomed-in depiction of the four inter-chain (heavy:light chain) disulfide bonds in the Trastuzumab structure. (**C**) A zoomed-in representation of the pairs of cysteine residues shown in (B) re-bridged with the each DVP groups of TetraDVP. (**D**) The re-bridging reaction was monitored by SDS-PAGE, to reveal the formation of a major band at the expected molecular weight, and a slightly lighter minor band. Analysis of the reaction mixture by intact protein mass spectrometry revealed the major band to be the expected product constituting two light chains, two heavy chains, and a single TetraDVP-SpyTag003 group ('LHHL-tDVP-SpyTag003'), and the major band to be a re-bridged Trastuzumab variant lacking one light chain ('HHL-tDVP-SpyTag003'). The bands in (D) were labelled accordingly.

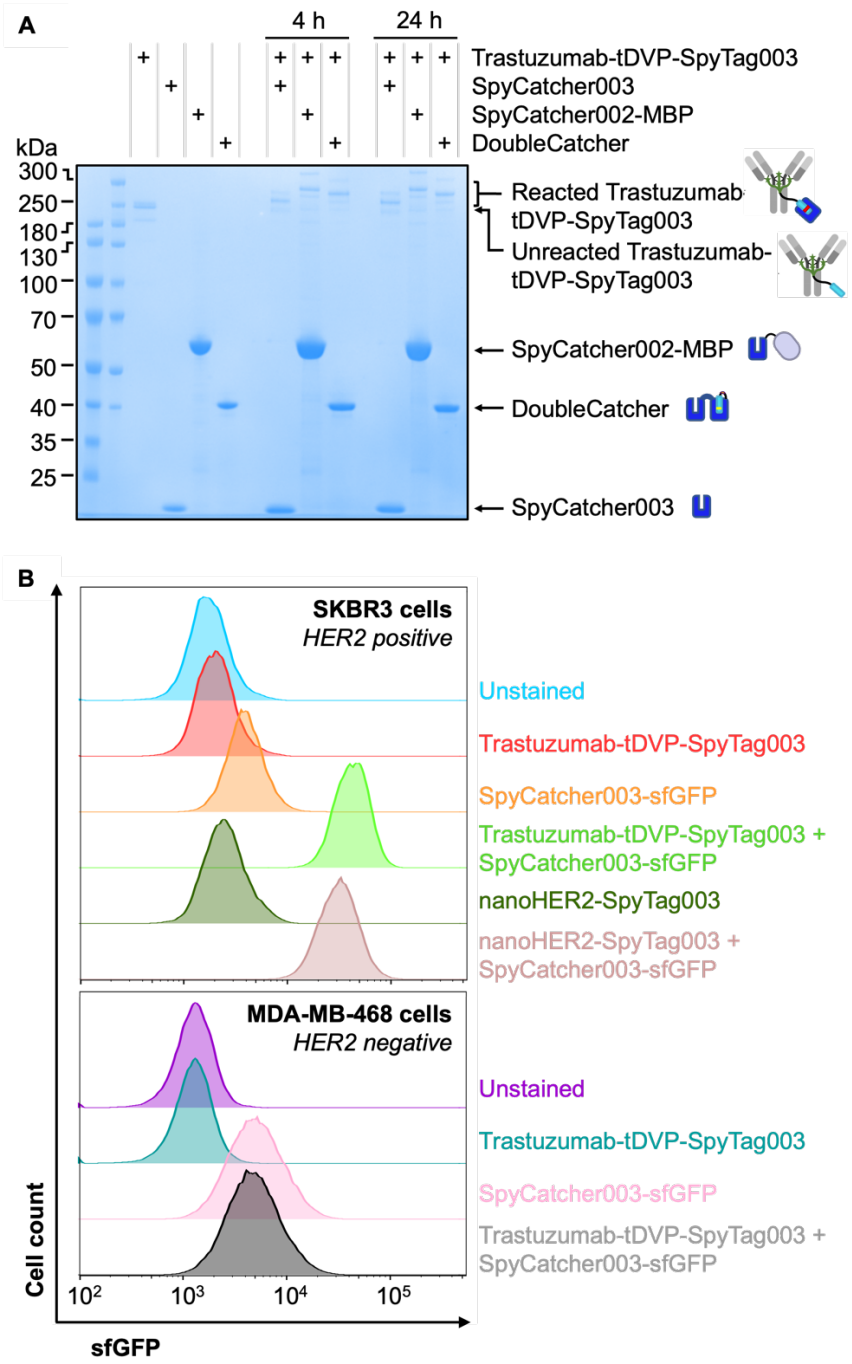


Figure 5.12. Evaluation of SpyCatcher-reactivity and HER2-binding activity of Trastuzumab-tDVP-SpyTag003. (**A**) 1 µM Trastuzumab-tDVP-SpyTag003 was incubated with 5 µM of either SpyCatcher003, SpyCatcher002-maltose binding protein (MBP), or DoubleCatcher, in PBS pH 7.4 at 37 °C for the time indicated. Reactivity of Trastuzumab-tDVP-SpyTag003 with each Catcher was monitored by SDS-PAGE followed by Coomassie staining. Cartoons represent reaction components, with SpyCatcher003 in dark blue, MBP in lilac, TetraDVP in green, SpyTag003 in cyan with D117A indicated in yellow, TEV cleavage site in orange, and Trastuzumab in grey. The SpyTag003:SpyCatcher003 isopeptide bond is shown in red. (**B**) Trastuzumab-tDVP-SpyTag003 pre-conjugated to SpyCatcher002-sfGFP (2 µM) was incubated with to HER2-positive SKBR3 cells (top) or HER2-negative MDA-MB-468 cells (bottom) in HBS pH 7.2 + 10% (v/v) FBS for 30 min at 37 °C with 5% (v/v) CO_2, prior to detection of sfGFP fluorescence by flow cytometry. The nanoHER2 nanobody, validated to bind HER2 in Fig. 4.6, was used as a positive control for binding. Cells incubated with either HER2-binder alone, SpyCatcher002-sfGFP alone, or buffer only were used to detect background signal.

Conversely, the signal detected from MDA-MB-468 cells treated with SpyTag003-tDVP-Trastuzumab:SpyCatcher002-sfGFP-treated was completely unshifted relative to that from MDA-MB-468 cells treated with SpyCatcher002-sfGFP alone (Fig. 5.12B, bottom), confirming the specificity of the construct for HER2. Together, these results confirm that the biological activities of both SpyTag and Trastuzumab remain intact upon their bioconjugation with TetraDVP, supporting the adoption of this chemical toolbox for the development of protein-antibody conjugates as multi-functionalised therapeutics or diagnostic tools, or for the facile synthesis of full-length IgG-bearing bispecific antibodies.

5.6 Discussion

This Chapter described the two-fold diversification of the previously described SpyMask platform. First, a series of structurally distinct DoubleCatcher scaffolds were designed to assemble bispecifics of varied shapes and sizes. Second, the SpyTag003 peptide was chemically decorated with a terminal azide, strained alkyne, or TetraDVP group, for the incorporation of a plethora of ligand classes into the SpyMask ligand library. The ability to tune the structure and reduce the conformational sampling of bispecific molecules has frequently been a requirement for the discovery of bispecifics with optimised activity. Furthermore, as the cell-surface interactome becomes increasingly annotated (Lin et al., 2024; Shilts and Wright, 2024), many new disease-associated protein-protein interactions to investigate will come to light that can be investigated for their druggability, providing that a generalised methodology for bispecific antibody assembly exists. An expanded SpyMask toolbox means that additional drug modalities can be investigated, such as bifunctional antibodies. Bifunctional antibodies are emerging with great potential to overcome limitations of monoclonal antibodies and even bispecific antibodies, such as the emergence of ligand-independent, sustained signalling from the target receptors (Fernandes et al., 2020), and include

targeted-protein degraders that exist as antibody-small molecule, antibody-glycan, or antibody-DNA fusions (Banik et al., 2020; Zhu et al., 2023).

Beyond its exploratory applications in combinatorially screening combinations of ligands against cell-surface targets, the diversified SpyMask toolbox can also be used to characterise or improve upon geometry-dependences in previously tested combinations of complex ligands. For example, to synthesise a T-cell engaging bispecific for prostate cancer, the prostate-specific membrane antigen (PSMA)-binding small molecule was conjugated to an anti-CD3 Fab (Kim et al., 2013). Conjugation was achieved by coupling the PSMA ligand to a series of different linkers with an aminooxy group at their termini, and expressing the anti-CD3 Fab with the unnatural amino acid *p*-acetyl phenylalanine, whose ketone reacts with the aminooxy group to form a moderately stable oxime bond. Interestingly, the length of the PSMA ligand-coupled linker was found to significantly affect the cytotoxic activity of the conjugate. In a second example, two bispecifics that bridged insulin-specific B cell receptors with the inhibitory receptor CD22, which is activated upon colocalisation with the B cell receptor, were screened for their ability to downregulate the activity of anti-insulin B cells that promote type 1 diabetes. The first bispecific was synthesised by conjugating alkyne-functionalised insulin with an azide-functionalised glycan that binds CD22, and the second by conjugating two insulin-azide molecules with two CD22 ligand-azides via a long-armed tetramer of PEG-alkyne (Apley et al., 2023). Interestingly, the simple fusion of one CD22 ligand with a single insulin peptide led to a significant reduction in B cell proliferation, while the bivalent variant failed to have any effect. While the difference in activity was postulated to be due to the increased valency of the bispecific driving receptor clustering, the differences in ligand lengths were neither explored nor commented on. Thus, further investigation with multiple DoubleCatcher scaffolds could provide insight into possible spatial requirements for the CD22-B cell receptor interaction.

Nevertheless, the incorporation of off-the-shelf IgG molecules in the SpyMask ligand set means that valency can also be explored. Previously, incorporation of off-the-shelf IgGs into bispecific antibodies has been described by fusing a small photoreactive antibody-binding domain to either SpyCatcher or SpyTag, which could be crosslinked onto IgG heavy chains under 385 nm light for 2 h, with subsequent conjugation of IgG-Catcher/Tag fusions to produce bispecific binders (Mei et al., 2022). While this elegant approach could enable the synthesis of large libraries of functionalised IgG ligands for combinatorial bispecific antibody assembly, the highest bispecific yield achieved by this method was only 40-50% and required SEC-purification of each bispecific assembly mixture. Considering the re-bridging of native IgGs with TetraDVP has been optimised to achieve 97% conversion, and < 10% of SpyTag-bearing Trastuzumab was detected by SDS-PAGE after incubation with five-fold excess DoubleCatcher for 4 h, the assembly of IgG-bearing bispecifics by SpyMask could result in comparable or higher bispecific yields than previously described methods.

Together, these efforts have equipped the SpyMask platform with the tools required to synthesise bispecific antibodies with varied geometries against many possible target pairs. Future work is aimed at building upon the preliminary anti-HER2 screen carried out here, to generate large, multiplexed libraries of bispecifics incorporating diverse classes of ligands, for the investigation of known or novel pairings at the cell surface.

CHAPTER 6 – SUMMARY AND GENERAL DISCUSSION

Modularity in bispecific binder assembly has long been pursued (Hofmann et al., 2020b), to facilitate simple and scalable synthesis of bispecifics exhibiting many different combinations of binder molecules. However, current approaches to plug-and-play assembly of bispecifics generally require binder constituents to be engineered in specialised, complementary formats that are not amenable to structural modification. Considering the increasingly evidenced importance of format on bispecific activity (Chen et al., 2021; Dickopf et al., 2020; Madsen et al., 2024), an ideal bispecific assembly platform would enable structural parameters to be screened in parallel with binder arm combinations.

Altogether, the work described in this Thesis establishes the design and application of a toolbox for bispecific assembly that facilitates the screening of multiple format parameters simultaneously. In summary, a tandem SpyCatcher003 construct, DoubleCatcher, was engineered to facilitate the site-specific, irreversible heterodimerisation of any two SpyTag(003)-fused antigen-binding ligands, according to a generalised, one-pot SpyMask protocol. Notably, both binder moieties exist in a common format, eliminating the need to reformat and reproduce each binder twice. Furthermore, I exemplified an approach for screening bispecifics in diverse geometries by engineering the architecture of the DoubleCatcher dimerisation module directly. To diversify the repertoire of target molecules accessible to SpyMask-assembled bispecifics, I introduced routes for the SpyTag-fusion of protein, peptide, small molecule, oligonucleotide, and full-length IgG ligands.

6.1 Resource requirements of SpyMask bispecific assembly

In Chapter 3, a generalised SpyMask protocol for the heterodimerisation of any two SpyTag-linked binding moieties using DoubleCatcher was devised. During optimisation of the

SpyMask methodology, I aimed to select conditions that favoured low complexity (minimum number of steps), high product yield (with low by-product formation), and high-throughput or automation compatibility (e.g. plate-based assembly). Considering an average bispecific purity of 90%, and a modest yield of 25 mg/L of DoubleCatcher from expression in *E. coli*, a single 1L expression would produce enough purified DoubleCatcher for bispecific assembly by SpyMask in roughly 22 96-well plates, assuming 300 µL of bispecific is produced at 1 µM, which would be sufficient for multiple cellular assays.

However, 22 96-well plates of bispecific assembly would require roughly 0.05 g of the first SpyTagged binder, and roughly 4 g of the second, assuming both binders are Fabs. Although each well will contain a different combination of binders, Fab expression in Expi293 cells typically did not exceed 10 mg/60 mL expression volume, which became limiting for some assembly reactions. Therefore, one feature of the SpyMask methodology that limits its economic viability for scaling up and industrial applications is the need for a five-fold molar excess of the second SpyTagged binder in Step 2 of the assembly reaction (Fig. 3.7A). As recently suggested by Hentrich et al., the excess of the second SpyTagged binder (B) required can be reduced if the residual, unreacted binder (A) from Step 1 is first removed by purification (Hentrich et al., 2024). For example, introducing a biotinylated cysteine to the cleavable Mask of DoubleCatcher would allow sequestration of DoubleCatcher:A by bead-streptavidin, and subsequent dissociation from the beads after the addition of TEV (Fig. 6.1). This way, there is no requirement for binder B to out-compete binder A for reaction with the unmasked C-terminal SpyCatcher003. However, cysteine modification of DoubleCatcher, subsequent biotinylation, and buffer exchange to remove excess biotin-labelling reagent would add 1-2 days to the reagent preparation steps. Furthermore, addition of a third free cysteine residue into the DoubleCatcher disulfide-Lock variants may result in incorrect disulfide bond formation.

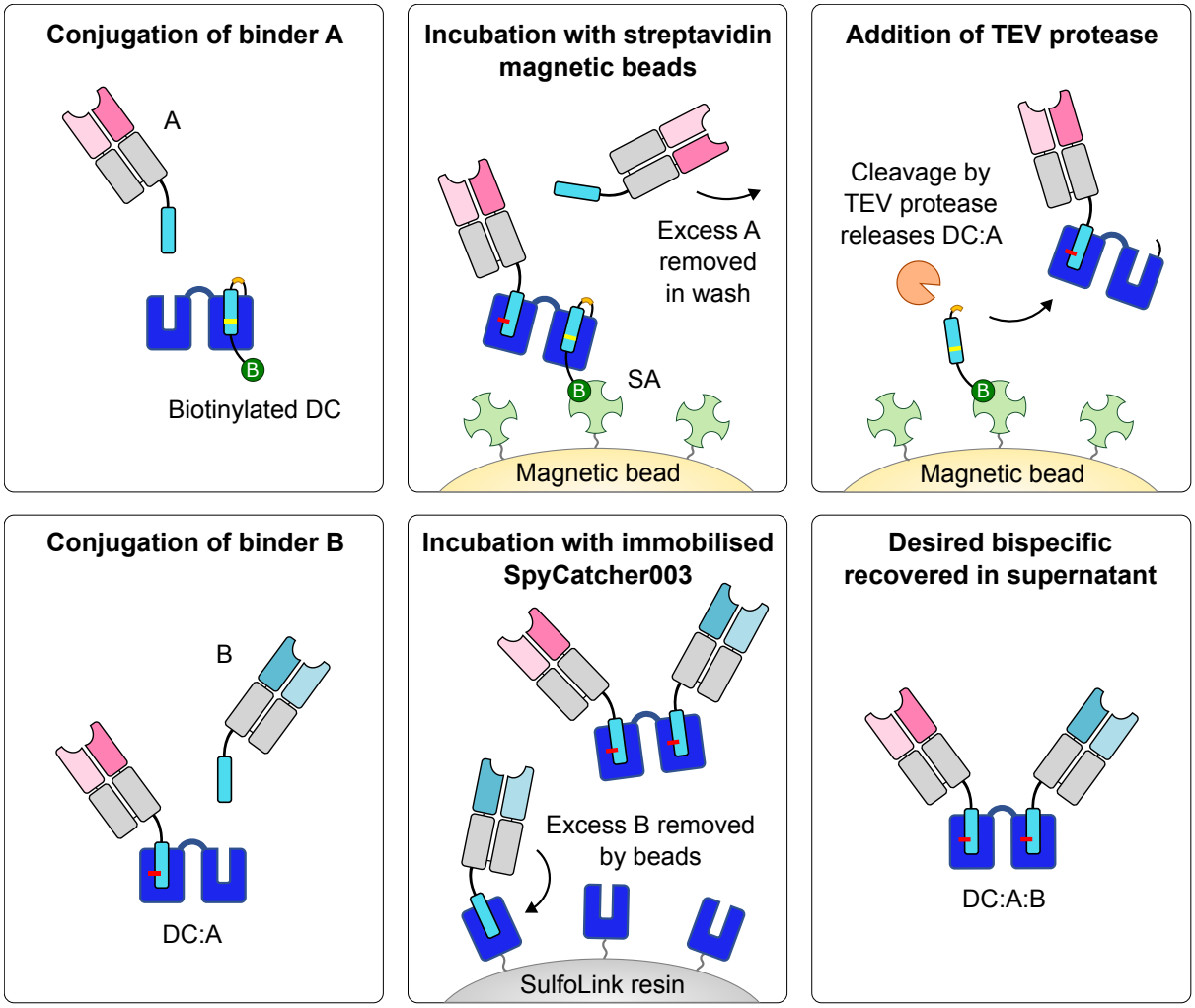


Figure 6.1. Bispecific antibody assembly by SpyMask with two-step purification. To minimise the amount of reagent required for SpyMask bispecific assembly, excess binder can be depleted from the reaction mixture after each conjugation step. First, C-terminally biotinylated DoubleCatcher (DC) is reacted with SpyTag-linked binder A (A). The desired product, DC:A, is then captured by streptavidin (SA)-coated magnetic beads, and excess A is removed in washes. Subsequent TEV cleavage of SpyTag003DA-Biotin from DoubleCatcher allows DC:A to be released from the beads, for reaction with SpyTagged binder B (B). Excess binder B is then sequestered by bead-immobilised SpyCatcher003, so that the desired bispecific molecule (DC:A:B) can be recovered in the supernatant.

Instead, *in vivo* biotinylation of DoubleCatcher could be achieved by co-expression of an DoubleCatcher-AviTag fusion with the *E. coli* biotin ligase BirA, followed by one-step purification by immobilised anti-AviTag antibodies to remove non-biotinylated protein from the Ni-NTA-purified expression mixture (Ashraf et al., 2004; Lu et al., 2024). However, the need for two-step purification during bispecific assembly will still increase the total reaction time, and was therefore intentionally avoided during the design of SpyMask.

A cost-efficient alternative to the current SpyMask strategy could be to use bead-immobilised non-covalent SpyTag-binding SpyCatcher003 S49C E77A V94I or SpyCatcher003 S49C S59T E77A variants in the final purification step, instead of covalent SpyCatcher003. As demonstrated in Fig. 3.8D, near-complete depletion of free SpyTag in solution can be achieved with the addition of sufficient resin (1 μL resin (1:1 slurry) per 1 μM free SpyTag). This way, the bound SpyTagged binders can be recovered from the resin by elution in 2.5 M imidazole in Tris-phosphate buffer (25 mM orthophosphoric acid adjusted to pH 7.0 with Tris base) (Khairil Anuar et al., 2019), which can then be buffer exchanged into PBS pH 7.4 and reused in bispecific assembly. If the purification step were to take place in resin-packed columns, such as in Empor 96-Well Filter plates (Merck; cat no. 66878-U), the resin could then simply be washed and reused in the next batch of bispecific assembly reactions.

6.2 Rigidity of SpyTag-linked binders

Throughout this Thesis, the importance of rigidity in a bispecific scaffold has been stated. Unlike IgG-based bispecific binders, which possess flexibility within the hinge region to allow free, independent rotation of the two Fab binding domains, flexibility within DoubleCatcher-assembled bispecifics originates within the DoubleCatcher scaffold itself, or within the junction between each binder and its SpyTag peptide. Approaches to minimise the rigidity within the scaffold (within the linker connecting the two SpyCatcher003 domains, and at the junctions where the linker termini meet each Catcher) are discussed in Section 6.3. However, assembly of SpyTag-fused binder moieties onto a rigid DoubleCatcher scaffold will still yield a bispecific molecule with rotation of binder domains around their SpyTag peptide, restricted only by the partial double-bond character of the peptide bond and potential steric hindrance within the bispecific structure. Ligand rotation may introduce structural heterogeneity into a bispecific sample. If bispecifcs with different structures induce different biological activities,

then such heterogeneous bispecific mixtures would reduce the desired potency of the bispecific.

In Chapter 4, as an initial approach to reduce SpyTag-binder flexibility, the GSG tripeptide linker connecting the anti-HER2 Fab Tras to SpyTag003 was deleted, to yield the Tras NoLink-SpyTag003 variant. This variant was shown to retain fast and complete reactivity with SpyCatcher003 and was assembled onto DoubleCatcher with the panel of other HER2-binding proteins to generate bispecifics. Interestingly, the activity of bispecifics assembled with Tras NoLink was very similar to the identical bispecifics that were assembled with Tras. The lack of discrimination between the activities of these two binders may be attributed to the use of the flexible DoubleCatcher scaffold; it is also possible that flexibility within the scaffold was not sufficiently reduced to cause biological differences. Therefore, AlphaFold3 was used to model structures of Tras-SpyTag003 and Tras NoLink-SpyTag003 in complex with SpyCatcher003. The top five predicted structures were aligned by the SpyCatcher003 domain to visualise predicted flexibility around the SpyTag003-binder hinge. Interestingly, in the Fab-SpyTag003:SpyCatcher003 complex, the Fab is predicted to dock onto SpyCatcher003 with the linker region forming a structured helix (highlighted in red, with the upper hinge region EPKSC in magenta) (Fig. 6.2A). However, the apparent structure within the flexible linker of Tras-SpyTag003 is likely due to the known phenomenon of AlphaFold3 spuriously favouring order within disordered regions, resulting in secondary structure ‘hallucinations’ (Abramson et al., 2024). Subsequent truncation of the linker to generate Tras NoLink-SpyTag003 resulted in substantial movement of the Tras Fab to be predicted, when in complex with SpyCatcher003 (Fig. 6.2B). The structural predictions reveal the residual flexibility to arise within the upper hinge region at the C-terminus of the Fab heavy chain (EPKSC), as expected (Roux et al., 1997; Zhang et al., 2015), and the positively-charged N-terminus of SpyTag003 (RGV), which is

predicted to enhance affinity with SpyCatcher003 by interacting favourably with the negatively-charged E20, E21, D22, and E95 (Keeble et al., 2019).

Ideally, truncation of the Fab hinge residues would be avoided, as the terminal cysteine is required for the formation of the sole intermolecular disulfide bond between the Fab heavy and light chains. To circumvent the deletion of the interchain disulfide bond, an alternative approach could be to replace the IgG1 constant heavy and light domains of the Fab with those of IgG2, whose intermolecular disulfide bond connects the C-terminus of the light chain and a cysteine proximal to the N-terminus of the heavy chain constant region (Yu et al., 2020). In this way, the hinge region can be omitted from the construct completely, without the worry of light-chain dissociation and mispairing with other Fabs on the bispecific. Structural modelling of SpyCatcher003 in complex with a variant of Tras Fab in which the constant heavy and light domains have been switched with the equivalent domains from the human IgG2a isotype suggested reduced movement of the Fab around its SpyTag003, as expected (Fig. 6.2C).

Otherwise, rigidity could be enhanced by truncating the flexible N-terminus of the SpyTag003 peptide, generating a sequence more similar to that of SpyTag002 (Keeble et al., 2017) (Fig. 6.2D). Enhanced rigidity by fusion to SpyTag003 ΔRGV could also be achieved with non-IgG derived binder scaffolds, including affibodies and nanobodies, but it would be necessary to test their expression, solubility, and reactivity with SpyCatcher003 before inclusion in a binder library for bispecific assembly. Indeed, reactivity of a nanobody variant fused to SpyTag003 ΔRGV with SpyCatcher003-sfGFP has been tested previously by Jamie Lam within the Howarth Group (data not shown), who found that the reaction proceeded to completion at a rate that was almost identical to the variant containing full-length SpyTag003 and a tripeptide linker between the nanobody and the tag.

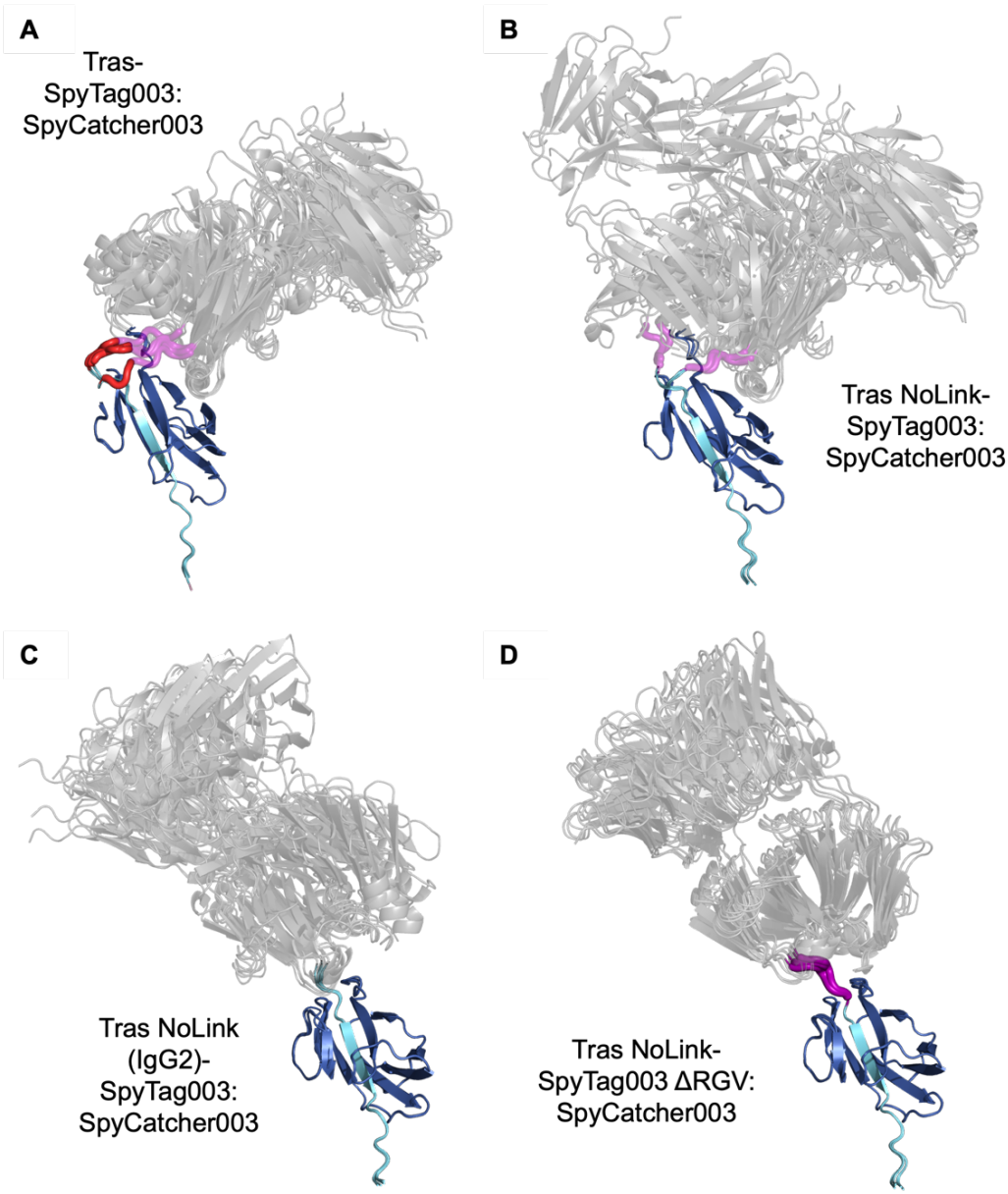


Figure 6.2. Minimising flexibility in the hinge connecting the anti-HER2 Fab Tras to SpyTag003. (**A**) The five highest-confidence AlphaFold3 predictions for the structure of the full-length Tras-SpyTag003 construct in complex with SpyCatcher003 are aligned by the SpyCatcher003 and overlaid. Structures are shown as cartoon representations and coloured by domain or motif. In this construct, SpyTag003 (cyan) is tethered to the upper hinge region ('EPKSC', magenta) C-terminus of the Fab heavy chain via a GSG tripeptide linker (red). The Tras Fab is in grey, and SpyCatcher003 is dark blue. (**B**) In Tras NoLink-SpyTag003, the Tag is fused directly to the C-terminal hinge of the Tras Fab. Unexpectedly, substantial movement of the Fab with respect to SpyCatcher003 is predicted, arising in the hinge region. Considering the hinge region contains the cysteine residue responsible for forming the intermolecular heavy chain-light chain disulfide bond within the Fab, its truncation should be avoided. Instead, the IgG1 constant heavy and constant light domains of the Tras Fab can be exchanged with those of the IgG2 isotype (**C**). In IgG2 Fabs, the intermolecular disulfide bond forms between the C-terminus of the light chain, but closer to the centre of the heavy chain, thus allowing direct fusion of SpyTag003 to the heavy chain without the need for the hinge sequence. (**D**) Alternatively, fusion of an N-terminally truncated SpyTag003 (ΔRGV) to the Tras Fab is predicted to sufficiently rigidify the Fab-Tag connection, without the need for isotype switching.

6.3 Rigidity of the DoubleCatcher scaffold

The ribosomal protein L9 from *Bacillus stearothermophilus* that was used to link SpyCatcher003 moieties in DoubleCatcher H-Lock in Chapter 5 is an example of a single α-helical domain (SAH). Unlike most structural helices, which are structurally stabilised by neighbouring residues in the protein tertiary structure, SAHs are stabilised by charged interactions between side chains within the helix, resulting in structural integrity and rigidity as an isolated helix (Swanson and Sivaramakrishnan, 2014). Such helices are expected to be found naturally in >150 human proteins, and have been extensively characterised in smooth muscle caldesmon (Bryan et al., 1989), myosin X (Ropars et al., 2016), and PDCD5 (Liu et al., 2005), which has informed the design of SAH-derived linkers with adjustable length and rigidity for fusion proteins (Collu et al., 2022; Ramšak et al., 2023).

However, investigation into the uses of single α-helical domains for rigid fusion of two protein domains into a fixed architecture revealed a requirement for direct fusion of the α-helical linker to existing terminal helices of proteins, to achieve a single, extended chimeric helix bridging the two domains (Collu et al., 2022; Kwon et al., 2020). In the case of SpyCatcher003, which contains no native helices in its secondary structure, the helix extension approach is not viable. An alternative approach for constructing rigid protein linkers with tuneable conformation employs computationally-designed helical repeat proteins, such as helix-turn-helix-turn repeats (Brunette et al., 2020), coiled-coil repeats (Huddy et al., 2024), leucine-rich repeats (Park et al., 2015), or ankyrin repeats (Kramer et al., 2010). *De novo* design of protein spacers would significantly expand the conformational space that can be explored by DoubleCatcher scaffolds, but their use is again limited. Like SAHs, for designed helical repeat proteins to rigidly connect two proteins, the bridged proteins must contain native helices to which the terminal helical repeat units can dock. Therefore, free rotation of the bridged proteins around

the linker is eliminated. Instead, it would be possible to engineer helical repeat protein scaffolds to contain terminal capping modules that have been computationally designed to simultaneously dock non-covalently to SpyCatcher003 and their neighbouring repeat protein unit (Cao et al., 2022).

Alternatively, analogous approaches to those described that instead exploit the β-sheets of SpyCatcher003 could be explored. For example, β-sheet motifs that possess one strand that geometrically matches an edge strand of SpyCatcher003 could be grafted onto both ends of small *de novo* αβ-protein scaffolds of tuneable shape and size (Lin et al., 2015; Sahtoe et al., 2021). This way, the resulting protein would dock to two SpyCatcher003 moieties with enhanced rigidity, essentially 'extending' a β sheet of SpyCatcher003 laterally. Whilst the longitudinal extension of one or more β strands is computationally possible (King et al., 2015), this approach would require substantial modification of the Catcher moieties themselves, increasing the possibility of detrimentally impacting Catcher-Tag reactivity.

6.4 Quantifying the architecture of different DoubleCatchers

The ability to reformat a DoubleCatcher-based bispecific into an alternative, clinically applicable format is contingent upon the knowledge of the precise structure and flexibility of the DoubleCatcher scaffold. Structural information is also imperative for DoubleCatcher to be used as research tool: different DoubleCatcher scaffolds can be applied as 'molecular callipers' to study how the geometry of native or novel pairings of molecules at the cell surface influences downstream signalling or phenotypic changes (Shaw et al., 2014). While the size exclusion chromatography and dynamic light scattering data obtained in Chapter 5 provide low resolution information on the relative sizes and structural heterogeneity of each of the DoubleCatcher variants generated, it is not possible to extract meaningful information about the distance and

angle between SpyCatcher003 domains within each scaffold. Therefore, it will be necessary to employ more sophisticated biophysical techniques to extract the structural parameters of DoubleCatcher.

First, the ability to conjugate oligonucleotide ligands to DoubleCatcher, as demonstrated in Chapter 5, enables the possibility of using single molecule fluorescence resonance energy transfer (FRET) to decipher distances between specific sites on the scaffold (Joshi et al., 2024). Specifically, two single-stranded DNA molecules with unique sequences can be synthesised. Both DNA strands should bear a 5' azide, and one should possess a 3' biotin. The DNA strands can then be chemically coupled to DBCO-SpyTag003 by SPAAC, and heterodimerised onto each DoubleCatcher scaffold. Following immobilisation of the DNA heterodimer onto a streptavidin-coated sample flow cell, single-stranded DNA-dye probes complementary to each of the two DoubleCatcher-conjugated DNA strands can be sequentially added to the flow cell. Importantly, each DNA-dye probe is each conjugated to a FRET-complementary dye, for example Cy3 and Cy5, so that the only FRET signal present in the sample is between the two Catcher domains of a single DoubleCatcher molecule. The FRET signal measured can then be converted into distances (with subangstrom accuracy within the 2–10 nm range (Joshi et al., 2024)). Additional modification of the linker domain separating the two SpyCatcher003 moieties, for example via maleimide-DBCO conjugation onto a free cysteine, can allow analysis of pairwise and triangulated FRET signals from three unique positions within DoubleCatcher (Joshi et al., 2024). This additional triangular distance information can therefore allow the angle between the two SpyCatcher003 groups to be calculated.

In cases where DoubleCatcher dimensions lie outside the dynamic FRET range, nanoparticle-aided cryo-electron microscopy (cryo-EM) could be used to measure the distance between two

particles positioned at individual sites on the DoubleCatcher scaffold (Ki et al., 2021). To avoid nanoparticle-induced alterations of the protein's structure after labelling, commercially available azide-linked gold nanoparticles can be obtained, for coupling with DBCO-SpyTag003 and conjugation onto DoubleCatcher, and nanoparticles can be coated with surfactant to mask their surface charge. Following the established protocol (Ki et al., 2021), this method allows calculation of the distance and angle between the two nanoparticles within a single molecule, as well as the distribution of these parameters. Therefore, flexibility within DoubleCatcher scaffolds can also be quantified.

Finally, low-resolution structural analysis of DoubleCatcher variants by small-angle X-ray scattering (SAXS) could provide information on their relative radii of gyration, maximum dimensions, and flexibility (Brunette et al., 2015; Hura et al., 2009; Rambo and Tainer, 2011), which can be used to map the position of ligands on a scaffold.

6.5 Discerning relationships between the structure and activity of bispecific-induced dimers

In Chapters 4 and 5, anti-HER2 bispecific binders were assembled using a series of binders with HER2 epitope diversity, and a panel of DoubleCatchers with structural diversity. Upon treatment of HER2-overexpressing cells with the bispecific variants, it was found that their activities were both diverse and unpredictable, emphasising the value of screening bispecifics in different formats during their discovery. Of particular interest was the observation that the activity of some pairs of binders on the cell proliferation was entirely switched (for example, from agonistic to antagonistic behaviour, or vice versa) when they were assembled on DoubleCatcher scaffolds with different geometries (Fig. 5.5). However, from metabolic activity assays alone, the structural or signalling differences that led to the phenotypic change

cannot be discerned. Therefore, a notable limitation of this study is the absence of data exploring the effects on signalling downstream of HER2 and other associated receptors. Future work on the existing panel of anti-HER2 bispecifics should therefore be focussed on high-throughput mechanistic investigations of their behaviour, and the assays established can be applied to the screening of SpyMask-assembled bispecific matrices in the future.

I will first consider methods to interrogate changes to the architecture or kinetics of bispecific-induced receptor-receptor interactions. Previously, the dimerisation kinetics of HER2 with other HER-family receptors have been analysed using a luciferase fragment complementation assay, in which complementary halves of a split luciferase protein are fused to the intracellular termini of the corresponding receptors (Macdonald-Obermann and Pike, 2014). Thus, upon receptor dimerisation, reconstitution of the split luciferase can be detected by measuring emitted light. Beneficially, luciferase-based assays require minimal sample preparation, and so luminometer measurements can take place at frequent time points, over extended periods of time. However, luciferase fragment complementation assays are limited to a single pair of receptors. Instead, bioluminescence resonance energy transfer (BRET), which monitors fluorescence emitted from a fluorescent protein when activated by a proximal luminescent donor, could be used (Siddiqui et al., 2013). Importantly, multiple BRET-compatible pairs of luciferases and fluorescent proteins have been identified, where a single luciferase can be paired with more than one fluorescent protein, or vice versa (Bacart et al., 2008; Breton et al., 2010). Therefore, different HER-family proteins could be labelled with proteins that have a common BRET partner, and this partner would be used to label HER2. By this approach, HER2 homo- or hetero-dimerisation preferences can be monitored following bispecific treatment.

Next, I will consider some state-of-the-art methods for the sensitive detection of fluctuations in multiple signalling pathways simultaneously, that would be compatible with a SpyMask assembly and screening pipeline. The first of such techniques is high-throughput, targeted mass spectrometry for the quantitative detection of the expression and phosphorylation of receptor tyrosine kinases and their associated effector proteins (Whiteaker et al., 2021). Advancements in the selective enrichment of complex cell lysis samples for target proteins of interest, automated data acquisition, and increased comprehensiveness of phosphoproteomics databases has allowed virtually any set of phosphoproteins to be studied from samples on a 96-well plate scale (Paulo and Schweppe, 2021). In cells treated with anti-HER2 bispecifics, high-throughput mass spectrometry could be used to map changes in the phosphorylation profile of the intracellular C-terminal tail of HER2 (Scheer et al., 2012), or quantify changes in the relative phosphorylation of proteins in the MAPK versus Akt signalling networks (Whiteaker et al., 2021).

Alternatively, the simultaneous monitoring of the activity of multiple different signalling pathways downstream of the HER2 receptor could be achieved by multiplexing spectrally unique luciferases. Specifically, recent work has described a single plasmid that encodes five luciferases, selected for their orthogonality, under the control of operator elements that report on either p53, TGF-β, NF-κβ, c-MYC, or MAPK/JNK signalling pathways (Sarrion-Perdigones et al., 2019, 2020). Subtle changes in the signalling pathways are therefore translated into subtle changes in luciferase expression, which can be measured with a single readout. Thus, for this study, fold-changes in luciferase expression before and after treatment with the panel of anti-HER2 bispecifics would aid our understanding of the relationship between HER2 signalling and phenotypic outcome.

Finally, transcriptomic analysis by single-cell RNA sequencing (scRNAseq) offers a cost-effective approach to quantifying changes in expression of pathway-related genes in response to bispecific treatment (Shin et al., 2019a). Gene enrichment analysis of transcriptomic datasets from untreated and bispecific-treated cells can enable signalling pathway-specific enrichment scores to be calculated (Hänzelmann et al., 2013), which can similarly be used to complement phenotypic data.

Significant advances in machine learning, multivariate statistics, and multiparametric image analysis techniques can now enable relationships between signalling changes at the molecular level and cell or population phenotypic changes to be understood on a large scale (Hughes et al., 2021; Mehrizi et al., 2023). Therefore, high-throughput phenotypic assays can be used to identify hits, which can then be paired with transcriptomic or signalling data to assign specific pathway alterations to particular phenotypes (Warchal et al., 2020). In addition to quantification of cell proliferation using Resazurin in 96-well plates, as performed in Chapters 4 and 5, cell migration assays can be performed in equal throughput (Luo et al., 2016).

The described physiological assays can also be complemented with high-content microscopy, which offers a more sophisticated approach for characterising phenotypic effects of drugs on diverse cell types (Bray et al., 2016; Heinrich et al., 2023). Specifically, imaging assays such as the Cell Painting assay multiplexes six unique fluorescent dyes, imaged in 5 different channels, that each stain a different organelle or cellular component. Cell Painting can allow over 70 features describing the morphology (area, symmetry, neighbouring contact area) and content of cells to be extracted simultaneously, on a 96-well plate scale or greater (Hughes et al., 2021).

Of course, the correct choice of phenotypic and signalling assay is pivotal to identification of successful pre-clinical candidates and remains a key challenge in drug discovery (Moffat et al., 2017). Unwanted hits may arise due to a lack of understanding of the activities of target receptors or disease mechanisms, heterogeneity in target activity, or signalling crosstalk. However, the high-throughput cellular assays proposed here can be modified to screen for transcriptomic or phenotypic changes in cells treated with non-HER2 targeting bispecifics in an unbiased manner.

6.6 Immunogenicity of the DoubleCatcher scaffold

The SpyMask platform is designed in for optimising two bispecific parameters – binder arm combinations (Chapter 3) and scaffold geometry (Chapter 5) – to identify binders or target combinations with potent activities or unique signalling signatures. In this way, these bispecifics can be used as a research tool to probe native dimerisation events at the cell surface or uncover novel target combinations that lead to clinically desired cell fates. However, a goal for this technology is to discover novel or improved bispecific drugs.

An underlying feature of SpyMask that may hinder its clinical application is the potential immunogenicity of the SpyCatcher/SpyTag pair (Liu et al., 2014), which are derived from *Streptococcus pyogenes*. The pre-existing antibody responses to SpyCatcher has been evaluated previously using ELISA, where it was found that anti-SpyCatcher:SpyTag antibodies were detected in 98% of sera from 53 healthy adults (Rahikainen et al., 2021). Whilst a 5.4-fold reduction in median antibody titre was observed in the same individuals against SpyCatcher003:SpyTag003, relative to the parental SpyCatcher:SpyTag complex, pre-existing antibody responses to the full SpyTag-bound DoubleCatcher scaffold are expected to be higher, particularly if the scaffolds contain bacterially derived or computationally designed linkers.

Upon recognition of exogenous proteins such as DoubleCatcher by antibodies, T cells, and antigen presenting cells, an immune response to the bispecific scaffold is activated. This immune response could lead to neutralisation of the drug, thus reducing the efficacy of the bispecific molecule as well as induce additional safety concerns (Sauna et al., 2018). Therefore, *in silico* prediction of MHC class II epitopes on DoubleCatcher using updated HLA peptide-binding databases and prediction algorithms (Vita et al., 2015), sensitive *in vitro* anti-drug antibody assays such as ELISA, and *ex vivo* CD4+ T cell activation assays on peripheral blood mononuclear cells (PBMCs) from healthy donors, such as flow cytometry or ELISpot (Arata et al., 2023), are required to improve our understanding of DoubleCatcher immunogenicity.

It is worth noting that there is currently no definitive threshold value of immunogenicity of a biologic that guarantees a successful clinical outcome; the impact of immunogenicity on therapeutic efficacy and cytotoxicity can depend on the drug's activity, pharmacokinetics, and patient populations or disease states. As such, multiple bacterially-derived therapeutic proteins continue to demonstrate promising results in clinical trials, notably affibodies (from protein A of *Staphylococcus*) (Klint et al., 2023), and a nanofitin (from Sac7d of *Sulfolobus acidocaldarius)* (Garlich et al., 2022).

Nevertheless, there are three possible approaches for the translation of a SpyMask-discovered bispecific into a format with reduced immunogenicity for the development of a clinical lead. First, it may be the case that the SpyMask platform is used to identify promising hits – specific pairs of binders or target combinations – which can then be reformatted into an immunoglobulin-like scaffold as a lead for clinical development (Jackman et al., 2010), or simplified by fusing the binder domains directly.

However, the second case describes a bispecific that has been discovered using a DoubleCatcher variant with fixed geometry or orientation, with desired activity that is lost when translated to the flexible DoubleCatcher scaffold or is assembled in the reverse orientation. It is likely in this case that direct fusion of the binder domains will likely not yield a functional bispecific. Instead, previous efforts to generate non-immunoglobulin like bispecifics with diverse architectures and low immunogenicity have exploited human-derived protein scaffolds to display binder domains. For example, amino acid randomisation of four of the five variable loops of the human tetranectin C-type lectin domain successfully produced trimeric Atrimer binders with specific, subnanomolar affinity for death receptor 4 (Allen et al., 2012). Similarly, insertion of Factor VIIa-binding peptides into the flexible mobile loop of human chaperonin 10 resulted in the generation of a stable heptamer which bound specifically to Factor VIIa with low nanomolar affinity (Alsultan et al., 2016). Alternatively, human oligomeric scaffolds including collagen X non-collagenous domain NC1 (trimer), human copper tolerance A protein (CutA; trimer), TNF or TNF-family members like TL1A or CD40L (trimers), or p53 (tetramer), have been described for use in displaying pairs of full-length binding proteins (one binder at each termini of the scaffold monomer), for the synthesis of bispecific antibodies with different structures and levels of multivalency (Khairil et al., 2022).

While multivalent bispecific binders could be synthesised using oligomeric protein scaffolds of different dimensions, DoubleCatcher-based bispecifics would require a monovalent scaffold. Indeed, several human-derived monomeric proteins or domains that are non-immunogenic, cysteine-free, and possess hypervariable loops that are amenable to modification, have been identified as acceptor scaffolds for binding peptide grafts (Binz et al., 2005; Kadonosono et al., 2020). Examples of these acceptor domains include the thermostable SH3 domain of the Src-family tyrosine-protein kinase Fyn (engineered to produce Fynomers)

(Silacci et al., 2014), or the fibronectin type III domain (to generate Adnectins) (Hackel et al., 2010); the Fyn- and fibronectin-derived scaffolds are of particular interest for synthesis of DoubleCatcher mimics as they contain multiple loops for binder insertion that reside on different faces of the protein structure.

Human γ-β-crystallin is another promising candidate for non-immunoglobulin binder protein design, with a highly rigid and conserved β sheet structure that contains a unique surface-exposed region which tolerates amino acid randomisation for the identification of rigid binders called Affilins (Ebersbach et al., 2007). However, randomisation or binder motif grafting into the hypervariable loops connecting the β strands of γ-β-crystallin is yet to be explored, yet this approach may yield rigid DoubleCatcher-like bispecific architectures. It would also be interesting to test whether the loops of these scaffolds would permit larger binder domain insertion for the generation of a wider variety of bispecific binders that structurally mimic a DoubleCatcher-assembled parental bispecific. Notably, current non-immunoglobulin scaffolds were intentionally selected for their small size and accessibility to chemical synthesis, even though most have been expressed to high yields in *E. coli* or Chinese hamster ovary (CHO) cells (Vazquez-Lombardi et al., 2015). As recombinant protein expression may be required for larger binding domain-scaffold fusions anyway, larger domains with more diverse architectures should continue to be investigated for use as binding protein scaffolds.

A substantial drawback of a DoubleCatcher bispecific reformatting approach is the requirement for the target-binding ability, activity, synthesis, and stability of the new bispecific to be re-characterised; even small changes in the relative affinities of the binding paratopes (for example, due to limitations in the size of the binding domain that can be grafted), or flexibility within the loops, may result in a bispecific with different activity. However, as structural

prediction tools continue to advance, it may become possible to design DoubleCatcher-free bispecifics that very closely mimic the parental DoubleCatcher-based binder.

The last case considers deimmunisation of the DoubleCatcher scaffold and SpyTag peptides themselves, so that an entirely deimmunised SpyMask toolbox can be developed for the assembly and screening of bispecific binders in a format that can be directly translated into pre-clinical studies (Scott et al., 2017). To abrogate binding and activation of B cells by the DoubleCatcher scaffold, binding epitopes may be shielded with chemical moieties, such as PEGylation (Turecek et al., 2016), but B cell epitopes are difficult to predict owing to their conformational nature and the incomplete knowledge of the diversity of the naïve B cell repertoire (Cantor et al., 2012). On the other hand, T cell epitopes can be 'deleted' from the DoubleCatcher scaffold by computationally predicting and mutating MHC Class II peptide epitopes from the construct using a tool such as MHCEpitopeEnergy within the Rosetta design suite (Yachnin et al., 2021). Computational T cell epitope deletion by mutation to immunologically 'silent' sequences is analogous to antibody humanisation (Boulianne et al., 1984; Morrison et al., 1984), but can instead be applied to any protein scaffold. However, deimmunisation of SpyCatcher003:SpyTag003 by substantial mutation to residues within MHC class II epitopes is likely to affect the reactivity of the protein:peptide pair and may require further rounds of evolution and design, as well as HLA peptide-binding validation, to restore its activity whilst maintaining low immunogenicity.

6.7 Concluding summary

An increasing number of proteins are expressed fused to SpyTag, for the purpose of purification (Keeble and Howarth, 2020; Khairil Anuar et al., 2019; Vester et al., 2022), multimerization (Brune and Howarth, 2018), or for downstream functional or biophysical assays, including

labelling antibodies with enzymes or probes (Hermanson, 1996; Keeble and Howarth, 2020). The launch of Bio-Rad's HuCAL recombinant Fab-SpyTag002 generation service has further increased the number of SpyTag-fused antigen binding molecules available to the research community that will be compatible SpyMask (Hentrich et al., 2021; Kellmann et al., 2023). Furthermore, substantial efforts are ongoing to explore interactions across the entire proteome using binders (Bausch-Fluck et al., 2018; Cao et al., 2022; Colwill et al., 2011; Dübel et al., 2010; Lin et al., 2024). As the arsenal of ligands expands, the number of possible combinatorial bispecific combinations becomes too vast to explore using conventional methods. Thus, SpyMask could be a valuable tool for the combinatorial assembly of thousands of binders simultaneously, to explore novel pairings and synergies within this interactome space.

Considering the central role of protein-protein interactions in all biological processes and the versatility of the SpyCatcher/SpyTag reactive pair, I anticipate diverse applications of the DoubleCatcher platform beyond signalling control using bispecifics. For example, DoubleCatcher could be employed to recruit stem cells for tissue repair (Cousens et al., 2009; Huang et al., 2019; Lum et al., 2006), or build enzyme networks for catalysis (Arkin et al., 2014; Maniaci and Ciulli, 2019).

BIBLIOGRAPHY

Abramson, J., Adler, J., Dunger, J., Evans, R., Green, T., Pritzel, A., Ronneberger, O., Willmore, L., Ballard, A.J., Bambrick, J., et al. (2024). Accurate structure prediction of biomolecular interactions with AlphaFold 3. Nature *630*, 493–500.

Aertgeerts, K., Skene, R., Yano, J., Sang, B.C., Zou, H., Snell, G., Jennings, A., Iwamoto, K., Habuka, N., Hirokawa, A., et al. (2011). Structural analysis of the mechanism of inhibition and allosteric activation of the kinase domain of HER2 protein. J. Biol. Chem. *286*, 18756–18765.

Agard, N.J., De Sousa E Melo, F., Li, J., Marei, H.M.G.M.F.E., Tsai, W.-T.K., De Sauvage, F.J., He, J., and Kee, Y.S. (2022). Multispecific Binding Protein Degrader Platform and Methods of Use.

Ahmed, F., Paul, M.D., and Hristova, K. (2020). The biophysical basis of receptor tyrosine kinase ligand functional selectivity: Trk-B case study. Biochem. J. *477*, 4515–4526.

Ahmed, F., Zapata-Mercado, E., Rahman, S., and Hristova, K. (2021). The Biased Ligands NGF and NT-3 Differentially Stabilize Trk-A Dimers. Biophys. J. *120*, 55–63.

Ahn, G., Banik, S.M., Miller, C.L., Riley, N.M., Cochran, J.R., and Bertozzi, C.R. (2021). LYTACs that engage the asialoglycoprotein receptor for targeted protein degradation. Nat. Chem. Biol. *17*, 937–946.

Aida, Y., and Pabst, M.J. (1990). Removal of endotoxin from protein solutions by phase separation using triton X-114. J. Immunol. Methods *132*, 191–195.

Akiba, H., Takayanagi, K., Kusano-Arai, O., Iwanari, H., Hamakubo, T., and Tsumoto, K. (2020). Generation of biparatopic antibody through two-step targeting of fragment antibodies on antigen using SpyTag and SpyCatcher. Biotechnol. Reports *25*, e00418.

Alam, M.K., El-Sayed, A., Barreto, K., Bernhard, W., Fonge, H., and Geyer, C.R. (2019). Site-Specific Fluorescent Labeling of Antibodies and Diabodies Using SpyTag/SpyCatcher System for In Vivo Optical Imaging. Mol. Imaging Biol. *21*, 54–66.

Alexander, P.B., Chen, R., Gong, C., Yuan, L., Jasper, J.S., Ding, Y., Markowitz, G.J., Yang, P., Xu, X., McDonnell, D.P., et al. (2017). Distinct receptor tyrosine kinase subsets mediate anti-HER2 drug resistance in breast cancer. J. Biol. Chem. *292*, 748–759.

Allen, J.E., Ferrini, R., Dicker, D.T., Batzer, G., Chen, E., Oltean, D.I., Lin, B., Renshaw, M.W., Kretz-Rommel, A., and El-Deiry, W.S. (2012). Targeting TRAIL death receptor 4 with trivalent DR4 atrimer complexes. Mol. Cancer Ther. *11*, 2087–2095.

Alsultan, A.M., Chin, D.Y., Howard, C.B., De Bakker, C.J., Jones, M.L., and Mahler, S.M. (2016). Beyond Antibodies: Development of a Novel Protein Scaffold Based on Human Chaperonin 10. Sci. Rep. *5*, 37348.

Alvarado, D., Klein, D.E., and Lemmon, M.A. (2009). ErbB2 resembles an autoinhibited invertebrate epidermal growth factor receptor. Nature *461*, 287–291.

Alvarez, B.H., Skokowa, J., Coles, M., Mir, P., Nasri, M., Maksymenko, K., Weidmann, L., Rogers, K.W., Welte, K., Lupas, A.N., et al. (2020). Design of novel granulopoietic proteins by topological rescaffolding. PLoS Biol. *18*, 1–26.

Andres, F., Schwill, M., Boersma, Y.L., and Plückthun, A. (2020). High-throughput generation of bispecific binding proteins by sortase a-mediated coupling for direct functional screening in cell culture. Mol. Cancer Ther. *19*, 1080–1088.

Antibody, T., and Services, C. (2012). TrailBlazer Antibody Custom Services.

Apley, K.D., Griffith, A.S., Downes, G.M., Ross, P., Farrell, M.P., Kendall, P., and Berkland, C.J. (2023). CD22L Conjugation to Insulin Attenuates Insulin-Specific B Cell Activation. Bioconjug. Chem. *34*, 2077–2088.

Arata, Y., Motoyama, S., Yano, M., Ikuno, T., Ito, S., Matsushita, T., Takeiri, A., Nishito, Y., Yabuki, N., Mizuno, H., et al. (2023). Rapid in vitro assessment of the immunogenicity potential of engineered antibody therapeutics through detection of CD4+ T cell interleukin-2 secretion. MAbs *15*, 2253570.

Arber, C., Young, M., and Barth, P. (2017). Reprogramming cellular functions with engineered membrane proteins. Curr. Opin. Biotechnol. *47*, 92–101.

Arkhipov, A., Shan, Y., Kim, E.T., Dror, R.O., and Shaw, D.E. (2013a). Her2 activation mechanism reflects evolutionary preservation of asymmetric ectodomain dimers in the human EGFR family. Elife *2013*, 1–14.

Arkhipov, A., Shan, Y., Das, R., Endres, N.F., Eastwood, M.P., Wemmer, D.E., Kuriyan, J., and Shaw, D.E. (2013b). Architecture and membrane interactions of the EGF receptor. Cell *152*, 557–569.

Arkin, M.R., Tang, Y., and Wells, J.A. (2014). Small-molecule inhibitors of protein-protein interactions: Progressing toward the reality. Chem. Biol. *21*, 1102–1114.

Ashraf, S.S., Benson, R.E., Payne, E.S., Halbleib, C.M., and Grøn, H. (2004). A novel multi-affinity tag system to produce high levels of soluble and biotinylated proteins in Escherichia coli. Protein Expr. Purif. *33*, 238–245.

Asor, R., and Kukura, P. (2022). Characterising biomolecular interactions and dynamics with mass photometry. Curr. Opin. Chem. Biol. *68*, 102132.

Bacart, J., Corbel, C., Jockers, R., Bach, S., and Couturier, C. (2008). The BRET technology and its application to screening assays. Biotechnol. J. *3*, 311–324.

Bai, X., Sun, P., Wang, X., Long, C., Liao, S., Dang, S., Zhuang, S., Du, Y., Zhang, X., Li, N., et al. (2023). Structure and dynamics of the EGFR/HER2 heterodimer. Cell Discov. *9*, 18.

Ballinger, M.D., and Wells, J.A. (1998). Will any dimer do? Nat. Struct. Biol. *5*, 938–940.

Banik, S.M., Pedram, K., Wisnovsky, S., Ahn, G., Riley, N.M., and Bertozzi, C.R. (2020). Lysosome-targeting chimaeras for degradation of extracellular proteins. Nature *584*, 291–297.

Barron, N., Dickgiesser, S., Fleischer, M., Bachmann, A.N., Klewinghaus, D., Hannewald, J., Ciesielski, E., Kusters, I., Hammann, T., Krause, V., et al. (2024). A Generic Approach for Miniaturized Unbiased High-Throughput Screens of Bispecific Antibodies and Biparatopic Antibody–Drug Conjugates. Int. J. Mol. Sci. *25*.

Baselga, J., and Swain, S.M. (2009). Novel anticancer targets: Revisiting ERBB2 and discovering ERBB3. Nat. Rev. Cancer *9*, 463–475.

Bausch-Fluck, D., Goldmann, U., Müller, S., van Oostrum, M., Müller, M., Schubert, O.T., and Wollscheid, B. (2018). The in silico human surfaceome. Proc. Natl. Acad. Sci. U. S. A. *115*, E10988–E10997.

Bhatta, P., Whale, K.D., Sawtell, A.K., Thompson, C.L., Rapecki, S.E., Cook, D.A., Twomey, B.M., Mennecozzi, M., Starkie, L.E., Barry, E.M.C., et al. (2021). Bispecific antibody target pair discovery by high-throughput phenotypic screening using in vitro

combinatorial Fab libraries. MAbs *13*.

Binz, H.K., Amstutz, P., and Plückthun, A. (2005). Engineering novel binding proteins from nonimmunoglobulin domains. Nat. Biotechnol. *23*, 1257–1268.

Bocharov, E. V., Mineev, K.S., Volynsky, P.E., Ermolyuk, Y.S., Tkach, E.N., Sobol, A.G., Chupin, V. V., Kirpichnikov, M.P., Efremov, R.G., and Arseniev, A.S. (2008). Spatial structure of the dimeric transmembrane domain of the growth factor receptor ErbB2 presumably corresponding to the receptor active state. J. Biol. Chem. *283*, 6950–6956.

Boulianne, G.L., Hozumi, N., and Shulman, M.J. (1984). Production of functional chimaeric mouse/human antibody. Nature *312*, 643–646.

Brack, S., Attinger-Toller, I., Schade, B., Mourlane, F., Klupsch, K., Woods, R., Hachemi, H., Von Der Bey, U., Koenig-Friedrich, S., Bertschinger, J., et al. (2014). A bispecific HER2-targeting fynomAb with superior antitumor activity and novel mode of action. Mol. Cancer Ther. *13*, 2030–2039.

Bragin, P.E., Mineev, K.S., Bocharova, O. V., Volynsky, P.E., Bocharov, E. V., and Arseniev, A.S. (2016). HER2 Transmembrane Domain Dimerization Coupled with Self-Association of Membrane-Embedded Cytoplasmic Juxtamembrane Regions. J. Mol. Biol. *428*, 52–61.

Bray, M.A., Singh, S., Han, H., Davis, C.T., Borgeson, B., Hartland, C., Kost-Alimova, M., Gustafsdottir, S.M., Gibson, C.C., and Carpenter, A.E. (2016). Cell Painting, a high-content image-based assay for morphological profiling using multiplexed fluorescent dyes. Nat. Protoc. *11*, 1757–1774.

Breton, B., Sauvageau, É., Zhou, J., Bonin, H., Le Gouill, C., and Bouvier, M. (2010). Multiplexing of multicolor bioluminescence resonance energy transfer. Biophys. J. *99*, 4037–4046.

Brinkmann, U., and Kontermann, R.E. (2017). The making of bispecific antibodies. MAbs *9*, 182–212.

Brockhoff, G., Schlegel, J., Heiß, P., Hofstaedter, F., and Knuechel, R. (2001). Epidermal growth factor receptor, c-erbB2 and c-erbB3 receptor interaction, and related cell cycle kinetics of SK-BR-3 and BT474 breast carcinoma cells. Cytometry *44*, 338–348.

Brune, K.D., and Howarth, M. (2018). New routes and opportunities for modular construction of particulate vaccines: Stick, click, and glue. Front. Immunol. *9*, 1432.

Brune, K.D., Buldun, C.M., Li, Y., Taylor, I.J., Brod, F., Biswas, S., and Howarth, M. (2017). Dual Plug-and-Display Synthetic Assembly Using Orthogonal Reactive Proteins for Twin Antigen Immunization. Bioconjug. Chem. *28*, 1544–1551.

Brunet, A., Bonni, A., Zigmond, M.J., Lin, M.Z., Juo, P., Hu, L.S., Anderson, M.J., Arden, K.C., Blenis, J., and Greenberg, M.E. (1999). Akt promotes cell survival by phosphorylating and inhibiting a forkhead transcription factor. Cell *96*, 857–868.

Brunette, T.J., Parmeggiani, F., Huang, P.S., Bhabha, G., Ekiert, D.C., Tsutakawa, S.E., Hura, G.L., Tainer, J.A., and Baker, D. (2015). Exploring the repeat protein universe through computational protein design. Nature *528*, 580–584.

Brunette, T.J., Bick, M.J., Hansen, J.M., Chow, C.M., Kollman, J.M., and Baker, D. (2020). Modular repeat protein sculpting using rigid helical junctions. Proc. Natl. Acad. Sci. U. S. A. *117*, 8870–8875.

Bruun, T.U.J., Andersson, A.M.C., Draper, S.J., and Howarth, M. (2018). Engineering a

Rugged Nanoscaffold to Enhance Plug-and-Display Vaccination. ACS Nano *12*, 8855–8866.

Bryan, J., Imai, M., Lee, R., Moore, P., Cook, R.G., and Lin, W.G. (1989). Cloning and expression of a smooth muscle caldesmon. J. Biol. Chem. *264*, 13873–13879.

Bryant, P., and Elofsson, A. (2023). Peptide binder design with inverse folding and protein structure prediction. Commun. Chem. *6*, 1–10.

Bryceson, Y.T., March, M.E., Ljunggren, H.G., and Long, E.O. (2006). Synergy among receptors on resting NK cells for the activation of natural cytotoxicity and cytokine secretion. Blood *107*, 159–166.

Burton, J., Siller-Farfán, J.A., Pettmann, J., Salzer, B., Kutuzov, M., van der Merwe, P.A., and Dushek, O. (2023). Inefficient exploitation of accessory receptors reduces the sensitivity of chimeric antigen receptors. Proc. Natl. Acad. Sci. U. S. A. *120*, 1–10.

Cantor, J.R., Panayiotou, V., Agnello, G., Georgiou, G., and Stone, E.M. (2012). Engineering reduced-immunogenicity enzymes for amino acid depletion therapy in cancer. In Methods in Enzymology, (Elsevier Inc.), pp. 291–319.

Cao, L., Coventry, B., Goreshnik, I., Huang, B., Sheffler, W., Park, J.S., Jude, K.M., Marković, I., Kadam, R.U., Verschueren, K.H.G., et al. (2022). Design of protein-binding proteins from the target structure alone. Nature *605*, 551–560.

Cao, Y., Liu, D., and Zhang, W. Bin (2017). Supercharging SpyCatcher toward an intrinsically disordered protein with stimuli-responsive chemical reactivity. Chem. Commun. *53*, 8830–8833.

Carlsson, J., Nordgren, H., Sjöström, J., Wester, K., Villman, K., Bengtsson, N.O., Ostenstad, B., Lundqvist, H., and Blomqvist, C. (2004). HER2 expression in breast cancer primary tumours and corresponding metastases. Original data and literature review. Br. J. Cancer *90*, 2344–2348.

Chames, P., Van Regenmortel, M., Weiss, E., and Baty, D. (2009). Therapeutic antibodies: Successes, limitations and hopes for the future. Br. J. Pharmacol. *157*, 220–233.

Chan, J., Chan, J., Shao, L., Stawicki, S.S., Pham, V.C., Akita, R.W., Hafner, M., Crocker, L., Yu, K., Koerber, J.T., et al. (2023). Systematic pharmacological analysis of agonistic and antagonistic fibroblast growth factor receptor 1 MAbs reveals a similar unique mode of action. J. Biol. Chem. *299*, 102729.

Che, S., Konno, H., and Makabe, K. (2024). SpyTag Peptide with Alkoxyl Aspartic Acids for pH-Dependent Activation of the SpyCatcher/Tag System. Bioconjug. Chem. *35*, 616–622.

Chen, W., Yang, F., Wang, C., Narula, J., Pascua, E., Ni, I., Ding, S., Deng, X., Chu, M.L.H., Pham, A., et al. (2021). One size does not fit all: navigating the multi-dimensional space to optimize T-cell engaging protein therapeutics. MAbs *13*, 1–18.

Cheng, L., Xia, F., Li, Z., Shen, C., Yang, Z., Hou, H., Sun, S., Feng, Y., Yong, X., Tian, X., et al. (2023). Structure, function and drug discovery of GPCR signaling. Mol. Biomed. *4*, 46.

Cho, H.S., Mason, K., Ramyar, K.X., Stanley, A.M., Gabelli, S.B., Denney, D.W., and Leahy, D.J. (2003). Structure of the extracellular region of HER2 alone and in complex with the Herceptin Fab. Nature *421*, 756–760.

Chudasama, V., Maruani, A., and Caddick, S. (2016). Recent advances in the construction of antibody-drug conjugates. Nat. Chem. *8*, 114–119.

Cochran, J.R. (2010). Engineered proteins pull double duty. Sci. Transl. Med. *2*, 1–5.

Collu, G., Bierig, T., Krebs, A.-S., Engilberge, S., Varma, N., Guixà-González, R., Sharpe, T., Deupi, X., Olieric, V., Poghosyan, E., et al. (2022). Chimeric single α-helical domains as rigid fusion protein connections for protein nanotechnology and structural biology. Structure *30*, 95-106.e7.

Colwill, K., Gräslund, S., Persson, H., Jarvik, N.E., Wyrzucki, A., Wojcik, J., Koide, A., Kossiakoff, A.A., Koide, S., Sidhu, S., et al. (2011). A roadmap to generate renewable protein binders to the human proteome. Nat. Methods *8*, 551–561.

Compte, M., Harwood, S.L., Muñoz, I.G., Navarro, R., Zonca, M., Perez-Chacon, G., Erce-Llamazares, A., Merino, N., Tapia-Galisteo, A., Cuesta, A.M., et al. (2018). A tumor-targeted trimeric 4-1BB-agonistic antibody induces potent anti-tumor immunity without systemic toxicity. Nat. Commun. *9*.

Correnti, C.E., Gewe, M.M., Mehlin, C., Bandaranayake, A.D., Johnsen, W.A., Rupert, P.B., Brusniak, M.Y., Clarke, M., Burke, S.E., De Van Der Schueren, W., et al. (2018). Screening, large-scale production and structure-based classification of cystine-dense peptides. Nat. Struct. Mol. Biol. *25*, 270–278.

Cotton, A.D., Nguyen, D.P., Gramespacher, J.A., Seiple, I.B., and Wells, J.A. (2021). Development of Antibody-Based PROTACs for the Degradation of the Cell-Surface Immune Checkpoint Protein PD-L1. J. Am. Chem. Soc. *143*, 593–598.

Couch, J.A., Yu, Y.J., Zhang, Y., Tarrant, J.M., Fuji, R.N., Meilandt, W.J., Solanoy, H., Tong, R.K., Hoyte, K., Luk, W., et al. (2013). Addressing safety liabilities of TfR bispecific antibodies that cross the blood-brain barrier. Sci. Transl. Med. *5*.

Cousens, L.P., Terry, F.E., and Falanga, V. (2009). New Applications for Bispecific Antibodies in Wound Healing (94.16). J. Immunol. *182*, 94.16-94.16.

Craig, R.B., Summa, C.M., Corti, M., and Pincus, S.H. (2012). Anti-HIV Double Variable Domain Immunoglobulins Binding Both gp41 and gp120 for Targeted Delivery of Immunoconjugates. PLoS One *7*, 1–13.

Dannheim, F.M., Walsh, S.J., Orozco, C.T., Hansen, A.H., Bargh, J.D., Jackson, S.E., Bond, N.J., Parker, J.S., Carroll, J.S., and Spring, D.R. (2022). All-in-one disulfide bridging enables the generation of antibody conjugates with modular cargo loading. Chem. Sci. *13*, 8781–8790.

Davenport, A.P., Scully, C.C.G., de Graaf, C., Brown, A.J.H., and Maguire, J.J. (2020). Advances in therapeutic peptides targeting G protein-coupled receptors. Nat. Rev. Drug Discov. *19*, 389–413.

Demaria, O., Cornen, S., Daëron, M., Morel, Y., Medzhitov, R., and Vivier, E. (2019). Harnessing innate immunity in cancer therapy. Nature *574*, 45–56.

Dengl, S., Mayer, K., Bormann, F., Duerr, H., Hoffmann, E., Nussbaum, B., Tischler, M., Wagner, M., Kuglstatter, A., Leibrock, L., et al. (2020). Format chain exchange (FORCE) for high-throughput generation of bispecific antibodies in combinatorial binder-format matrices. Nat. Commun. *11*, 4974.

Dent, P. (2002). Roles of Erbb family receptor tyrosine kinases and downstream signaling pathways in the control of cell growth and survival. Front. Biosci. *7*, d376-389.

Dickopf, S., Georges, G.J., and Brinkmann, U. (2020). Format and geometries matter: Structure-based design defines the functionality of bispecific antibodies. Comput. Struct. Biotechnol. J. *18*, 1221–1227.

Dillon, M., Yin, Y., Zhou, J., McCarty, L., Ellerman, D., Slaga, D., Junttila, T.T., Han, G., Sandoval, W., Ovacik, M.A., et al. (2017). Efficient production of bispecific IgG of different isotypes and species of origin in single mammalian cells. MAbs *9*, 213–230.

Diwanji, D., Trenker, R., Thaker, T.M., Wang, F., Agard, D.A., Verba, K.A., and Jura, N. (2021). Structures of the HER2–HER3–NRG1β complex reveal a dynamic dimer interface. Nature *600*, 339–343.

Doerner, A., Scheck, R., and Schepartz, A. (2015). Growth Factor Identity Is Encoded by Discrete Coiled-Coil Rotamers in the EGFR Juxtamembrane Region. Chem. Biol. *22*, 776–784.

Dolgin, E. (2018). First GPCR-directed antibody passes approval milestone. Nat. Rev. Drug Discov. *17*, 457–459.

Dong, J., Sereno, A., Aivazian, D., Langley, E., Miller, B.R., Snyder, W.B., Chan, E., Cantele, M., Morena, R., Joseph, I.B.J.K., et al. (2011). A stable IgG-Like bispecific antibody targeting the epidermal growth factor receptor and the type I insulin-like growth factor receptor demonstrates superior anti-tumor activity. MAbs *3*, 273–288.

Dovala, D., Sawyer, W.S., Rath, C.M., and Metzger, L.E. (2016). Rapid analysis of protein expression and solubility with the SpyTag-SpyCatcher system. Protein Expr. Purif. *117*, 44–51.

Dreier, T., Lorenczewski, G., Brandl, C., Hoffmann, P., Syring, U., Hanakam, F., Kufer, P., Riethmuller, G., Bargou, R., and Baeuerle, P.A. (2002). Extremely potent, rapid and costimulation-independent cytotoxic T-cell response against lymphoma cells catalyzed by a single-chain bispecific antibody. Int. J. Cancer *100*, 690–697.

Driscoll, C.L., Keeble, A.H., and Howarth, M.R. (2024). SpyMask enables combinatorial assembly of bispecific binders. Nat. Commun. *15*, 2403.

Dübel, S., Stoevesandt, O., Taussig, M.J., and Hust, M. (2010). Generating recombinant antibodies to the complete human proteome. Trends Biotechnol. *28*, 333–339.

Duneau, J.P., Vegh, A.P., and Sturgis, J.N. (2007). A dimerization hierarchy in the transmembrane domains of the HER receptor family. Biochemistry *46*, 2010–2019.

Ebersbach, H., Fiedler, E., Scheuermann, T., Fiedler, M., Stubbs, M.T., Reimann, C., Proetzel, G., Rudolph, R., and Fiedler, U. (2007). Affilin-Novel Binding Molecules Based on Human γ-B-Crystallin, an All β-Sheet Protein. J. Mol. Biol. *372*, 172–185.

Eden, E.R., White, I.J., Tsapara, A., and Futter, C.E. (2010). Membrane contacts between endosomes and ER provide sites for PTP1B-epidermal growth factor receptor interaction. Nat. Cell Biol. *12*, 267–272.

Edman, N.I., Phal, A., Redler, R.L., Schlichthaerle, T., Srivatsan, S.R., Ehnes, D.D., Etemadi, A., An, S.J., Favor, A., Li, Z., et al. (2024). Modulation of FGF pathway signaling and vascular differentiation using designed oligomeric assemblies. Cell *187*, 3726-3740.e43.

Eigenbrot, C., Ultsch, M., Dubnovitsky, A., Abrahmsén, L., and Härd, T. (2010). Structural basis for high-affinity HER2 receptor binding by an engineered protein. Proc. Natl. Acad. Sci. U. S. A. *107*, 15039–15044.

Elazar, A., Chandler, N.J., Davey, A.S., Weinstein, J.Y., Nguyen, J. V., Trenker, R., Cross, R.S., Jenkins, M.R., Call, M.J., Call, M.E., et al. (2022). De novo-designed transmembrane domains tune engineered receptor functions. Elife *11*, 1–29.

Evans, R., O'Neill, M., Pritzel, A., Antropova, N., Senior, A., Green, T., Žídek, A., Bates, R.,

Blackwell, S., Yim, J., et al. (2022). Protein complex prediction with AlphaFold-Multimer. BioRxiv 2021.10.04.463034.

Fawcett, C., Tickle, J.R., and Coles, C.H. (2024). Facilitating high throughput bispecific antibody production and potential applications within biopharmaceutical discovery workflows. MAbs *16*.

Feng, S.M., Sartor, C.I., Hunter, D., Zhou, H., Yang, X., Caskey, L.S., Dy, R., Muraoka-Cook, R.S., and Earp, H.S. (2007). The HER4 cytoplasmic domain, but not its C terminus, inhibits mammary cell proliferation. Mol. Endocrinol. *21*, 1861–1876.

Ferguson, K.M., Darling, P.J., Mohan, M.J., Macatee, T.L., and Lemmon, M.A. (2000). Extracellular domains drive homo- but not heterodimerization of erbB receptors. EMBO J. *19*, 4632–4643.

Fernandes, R.A., Su, L., Nishiga, Y., Ren, J., Bhuiyan, A.M., Cheng, N., Kuo, C.J., Picton, L.K., Ohtsuki, S., Majzner, R.G., et al. (2020). Immune receptor inhibition through enforced phosphatase recruitment (Springer US).

Fernandez, S., Palmer, D.R., Simmons, M., Sun, P., Bisbing, J., McClain, S., Mani, S., Burgess, T., Gunther, V., and Sun, W. (2007). Potential role for toll-like receptor 4 in mediating Escherichia coli maltose-binding protein activation of dendritic cells. Infect. Immun. *75*, 1359–1363.

Fink, T., and Jerala, R. (2022). Designed protease-based signaling networks. Curr. Opin. Chem. Biol. *68*, 102146.

Fischer, N., Elson, G., Magistrelli, G., Dheilly, E., Fouque, N., Laurendon, A., Gueneau, F., Ravn, U., Depoisier, J.F., Moine, V., et al. (2015). Exploiting light chains for the scalable generation and platform purification of native human bispecific IgG. Nat. Commun. *6*, 1–12.

Fleishman, S.J., Schlessinger, J., and Ben-Tal, N. (2002). A putative molecular-activation switch in the transmembrane domain of erbB2. Proc. Natl. Acad. Sci. U. S. A. *99*, 15937–15940.

Foley, E.D.B., Kushwah, M.S., Young, G., and Kukura, P. (2021). Mass photometry enables label-free tracking and mass measurement of single proteins on lipid bilayers. Nat. Methods *18*, 1247–1252.

Van Fossen, E.M., Bednar, R.M., Jana, S., Franklin, R., Beckman, J., Andrew Karplus, P., and Mehl, R.A. (2022). Nanobody assemblies with fully flexible topology enabled by genetically encoded tetrazine amino acids. Sci. Adv. *8*, 1–9.

Franklin, M.C., Carey, K.D., Vajdos, F.F., Leahy, D.J., De Vos, A.M., and Sliwkowski, M.X. (2004). Insights into ErbB signaling from the structure of the ErbB2-pertuzumab complex. Cancer Cell *5*, 317–328.

Freed, D.M., Bessman, N.J., Kiyatkin, A., Salazar-Cavazos, E., Byrne, P.O., Moore, J.O., Valley, C.C., Ferguson, K.M., Leahy, D.J., Lidke, D.S., et al. (2017). EGFR Ligands Differentially Stabilize Receptor Dimers to Specify Signaling Kinetics. Cell *171*, 683-695.e18.

Frejd, F., Klints, S., Ståhl, T., Löfblom, J., and Fleetwood, F. (2016). VEGFR-2 Binding Polypeptides. International Patent No. WO2016059068A1.

Friedman, M. (2008). Affibody molecules targeting the epidermal growth factor receptor for tumor imaging applications. Royal Institute of Technology.

Friedman, M., Nordberg, E., Höidén-Guthenberg, I., Brismar, H., Adams, G.P., Nilsson,

F.Y., Carlsson, J., and Ståhl, S. (2007). Phage display selection of Affibody molecules with specific binding to the extracellular domain of the epidermal growth factor receptor. Protein Eng. Des. Sel. *20*, 189–199.

Fudenberg, H.H., Drews, G., and Nisonoff, A. (1964). Serologic Demonstration of Dual Specificity of Rabbit Bivalent Hybrid. J. Exp. Med. *119*, 151–166.

Furtmann, N., Schneider, M., Spindler, N., Steinmann, B., Li, Z., Focken, I., Meyer, J., Dimova, D., Kroll, K., Leuschner, W.D., et al. (2021). An end-to-end automated platform process for high-throughput engineering of next-generation multi-specific antibody therapeutics. MAbs *13*.

Fuxe, K., Tarakanov, A., Romero Fernandez, W., Ferraro, L., Tanganelli, S., Filip, M., Agnati, L.F., Garriga, P., Diaz-Cabiale, Z., and Borroto-Escuela, D.O. (2014). Diversity and bias through receptor-receptor interactions in GPCR heteroreceptor complexes. Focus on examples from dopamine D2 receptor heteromerization. Front. Endocrinol. (Lausanne). *5*, 1–11.

Gadgil, H.S., Bondarenko, P. V., Pipes, G.D., Dillon, T.M., Banks, D., Abel, J., Kleemann, G.R., and Treuheit, M.J. (2006). Identification of cysteinylation of a free cysteine in the Fab region of a recombinant monoclonal IgG1 antibody using Lys-C limited proteolysis coupled with LC/MS analysis. Anal. Biochem. *355*, 165–174.

Galvez-Cancino, F., Simpson, A.P., Costoya, C., Matos, I., Qian, D., Peggs, K.S., Litchfield, K., and Quezada, S.A. (2024). Fcγ receptors and immunomodulatory antibodies in cancer. Nat. Rev. Cancer *24*, 51–71.

Garlich, J., Cinier, M., Chevrel, A., Perrocheau, A., Eyerman, D.J., Orme, M., Kitten, O., and Scheibler, L. (2022). Discovery of APL-1030, a Novel, High-Affinity Nanofitin Inhibitor of C3-Mediated Complement Activation. Biomolecules *12*.

Garrett, T.P.J., McKern, N.M., Lou, M., Elleman, T.C., Adams, T.E., Lovrecz, G.O., Zhu, H.J., Walker, F., Frenkel, M.J., Hoyne, P.A., et al. (2002). Crystal structure of a truncated epidermal growth factor receptor extracellular domain bound to transforming growth factor α. Cell *110*, 763–773.

Garrett, T.P.J., McKern, N.M., Lou, M., Elleman, T.C., Adams, T.E., Lovrecz, G.O., Kofler, M., Jorissen, R.N., Nice, E.C., Burgess, A.W., et al. (2003). The crystal structure of a truncated ErbB2 ectodomain reveals an active conformation, poised to interact with other ErbB receptors. Mol. Cell *11*, 495–505.

Gennaro, L.A., Kao, Y.-H., and Zhang, Y. (2014). Pertuzumab variants and evaluation thereof. US Patent No. US201403O8277A1.

Geoghegan, K.F., Dixon, H.B.F., Rosner, P.J., Hoth, L.R., Lanzetti, A.J., Borzilleri, K.A., Marr, E.S., Pezzullo, L.H., Martin, L.B., Lemotte, P.K., et al. (1999). Spontaneous α-N-6-phosphogluconoylation of a “His tag” in Escherichia coli: The cause of extra mass of 258 or 178 Da in fusion proteins. Anal. Biochem. *267*, 169–184.

Gera, N. (2022). The evolution of bispecific antibodies. Expert Opin. Biol. Ther. *22*, 945–949.

Geuijen, C.A.W., De Nardis, C., Maussang, D., Rovers, E., Gallenne, T., Hendriks, L.J.A., Visser, T., Nijhuis, R., Logtenberg, T., de Kruif, J., et al. (2018). Unbiased Combinatorial Screening Identifies a Bispecific IgG1 that Potently Inhibits HER3 Signaling via HER2-Guided Ligand Blockade. Cancer Cell *33*, 922-936.e10.

Ghosh, R., Narasanna, A., Wang, S.E., Liu, S., Chakrabarty, A., Balko, J.M., González-Angulo, A.M., Mills, G.B., Penuel, E., Winslow, J., et al. (2011). Trastuzumab has preferential activity against breast cancers driven by HER2 homodimers. Cancer Res. *71*, 1871–1882.

Gibson, D.G., Young, L., Chuang, R.Y., Venter, J.C., Hutchison, C.A., and Smith, H.O. (2009). Enzymatic assembly of DNA molecules up to several hundred kilobases. Nat. Methods *6*, 343–345.

Gijsen, M., King, P., Perera, T., Parker, P.J., Harris, A.L., Larijani, B., and Kong, A. (2010). HER2 phosphorylation is maintained by a PKB negative feedback loop in response to anti-HER2 herceptin in breast cancer. PLoS Biol. *8*, e1000563.

Glennie, M.J., McBride, H.M., Worth, A.T., and Stevenson, G.T. (1987). Preparation and performance of bispecific F(ab' gamma)2 antibody containing thioether-linked Fab' gamma fragments. J. Immunol. *139*, 2367–2375.

Gomez-Soler, M., Gehring, M.P., Lechtenberg, B.C., Zapata-Mercado, E., Ruelos, A., Matsumoto, M.W., Hristova, K., and Pasquale, E.B. (2022). Ligands with different dimeric configurations potently activate the EphA2 receptor and reveal its potential for biased signaling. IScience *25*, 103870.

Gong, D., Riley, T.P., Bzymek, K.P., Correia, A.R., Li, D., Spahr, C., Robinson, J.H., Case, R.B., Wang, Z., and Garces, F. (2021). Rational selection of building blocks for the assembly of bispecific antibodies. MAbs *13*.

Gong, H., Holcomb, I., Ooi, A., Wang, X., Majonis, D., Unger, M.A., and Ramakrishnan, R. (2016). Simple Method to Prepare Oligonucleotide-Conjugated Antibodies and Its Application in Multiplex Protein Detection in Single Cells. Bioconjug. Chem. *27*, 217–225.

Goodsell, D.S. (2022). HER2/neu and Trastuzumab. http://pdb101.rcsb.org/motm/268 (Accessed 1 April 2022).

Gordon, G.L., Capel, H.L., Guloglu, B., Richardson, E., Stafford, R.L., and Deane, C.M. (2023). A comparison of the binding sites of antibodies and single-domain antibodies. Front. Immunol. *14*, 1–18.

Graus-Porta, D., Beerli, R.R., Daly, J.M., and Hynes, N.E. (1997). ErbB-2, the preferred heterodimerization partner of all ErbB receptors, is a mediator of lateral signaling. EMBO J. *16*, 1647–1655.

Gray, D.C., Mahrus, S., and Wells, J.A. (2010). Activation of specific apoptotic caspases with an engineered small-molecule-activated protease. Cell *142*, 637–646.

Gu, J., Yang, J., Chang, Q., Lu, X., Wang, J., Chen, M., Ghayur, T., and Gu, J. (2014). Identification of anti-ErbB2 Dual Variable Domain Immunoglobulin (DVD-Ig^{TM}) proteins with unique activities. PLoS One *9*, e97292.

Guan, Y., Zhu, Q., Huang, D., Zhao, S., Jan Lo, L., and Peng, J. (2015). An equation to estimate the difference between theoretically predicted and SDS PAGE-displayed molecular weights for an acidic peptide. Sci. Rep. *5*, 1–11.

Gunasekaran, K., Pentony, M., Shen, M., Garrett, L., Forte, C., Woodward, A., Ng, S. Bin, Born, T., Retter, M., Manchulenko, K., et al. (2010). Enhancing antibody Fc heterodimer formation through electrostatic steering effects: Applications to bispecific molecules and monovalent IgG. J. Biol. Chem. *285*, 19637–19646.

Guo, X., Wu, Y., Xue, Y., Xie, N., and Shen, G. (2023). Revolutionizing cancer

immunotherapy: unleashing the potential of bispecific antibodies for targeted treatment. Front. Immunol. *14*, 1–33.

Hackel, B.J., Ackerman, M.E., Howland, S.W., and Wittrup, K.D. (2010). Stability and CDR Composition Biases Enrich Binder Functionality Landscapes. J. Mol. Biol. *401*, 84–96.

Hagan, R.M., Björnsson, R., McMahon, S.A., Schomburg, B., Braithwaite, V., Bühl, M., Naismith, J.H., and Schwarz-Linek, U. (2010). NMR spectroscopic and theoretical analysis of a spontaneously formed lys-asp isopeptide bond. Angew. Chemie - Int. Ed. *49*, 8421–8425.

Hamada, K., Hashimoto, T., Iwashita, R., Yamada, Y., Kikkawa, Y., and Nomizu, M. (2023). Development of a bispecific DNA-aptamer-based lysosome-targeting chimera for HER2 protein degradation. Cell Reports Phys. Sci. *4*, 101296.

Hänzelmann, S., Castelo, R., and Guinney, J. (2013). GSVA: Gene set variation analysis for microarray and RNA-Seq data. BMC Bioinformatics *14*.

Hao, C.H., Han, Q.H., Shan, Z.J., Hu, J.T., Zhang, N., and Zhang, X.P. (2015). Effects of different interchain linkers on biological activity of an anti-prostate cancer single-chain bispecific antibody. Theor. Biol. Med. Model. *12*, 1–10.

Haque, M., Forte, N., and Baker, J.R. (2021). Site-selective lysine conjugation methods and applications towards antibody-drug conjugates. Chem. Commun. *57*, 10689–10702.

Harada, Y., Sato, A., Araki, M., Matsumoto, S., Isaka, Y., Sagae, Y., Abe, T., Aoyagi, Y., Sueoka, E., Okuno, Y., et al. (2022). Integrated approach to functional analysis of an ERBB2 variant of unknown significance detected by a cancer gene panel test. Cell. Oncol. *45*, 121–134.

Hartman, Z., Zhao, H., and Agazie, Y.M. (2013). HER2 stabilizes EGFR and itself by altering autophosphorylation patterns in a manner that overcomes regulatory mechanisms and promotes proliferative and transformation signaling. Oncogene *32*, 4169–4180.

Hartzell, E.J., Terr, J., and Chen, W. (2021). Engineering a Blue Light Inducible SpyTag System (BLISS). J. Am. Chem. Soc. *143*, 8572–8577.

Harwood, S.L., Alvarez-Cienfuegos, A., Nuñez-Prado, N., Compte, M., Hernández-Pérez, S., Merino, N., Bonet, J., Navarro, R., Van Bergen en Henegouwen, P.M.P., Lykkemark, S., et al. (2018). ATTACK, a novel bispecific T cell-recruiting antibody with trivalent EGFR binding and monovalent CD3 binding for cancer immunotherapy. Oncoimmunology *7*.

Heinrich, L., Kumbier, K., Li, L., Altschuler, S.J., and Wu, L.F. (2023). Selection of Optimal Cell Lines for High-Content Phenotypic Screening. ACS Chem. Biol. *18*, 679–685.

Heldin, C.-H. (1995). Dimerization of cell surface receptors in signal transduction. Cell *80*, 213–223.

Hendriks, B.S., Klinz, S.G., Reynolds, J.G., Espelin, C.W., Gaddy, D.F., and Wickham, T.J. (2013). Impact of tumor HER2/ERBB2 expression level on HER2-targeted liposomal doxorubicin-mediated drug delivery: Multiple low-affinity interactions lead to a threshold effect. Mol. Cancer Ther. *12*, 1816–1828.

Hentrich, C., Kellmann, S.J., Putyrski, M., Cavada, M., Hanuschka, H., Knappik, A., and Ylera, F. (2021). Periplasmic expression of SpyTagged antibody fragments enables rapid modular antibody assembly. Cell Chem. Biol. *28*, 813-824.e6.

Hentrich, C., Putyrski, M., Hanuschka, H., Preis, W., Kellmann, S.-J., Wich, M., Cavada, M., Hanselka, S., Lelyveld, V.S., and Ylera, F. (2024). Engineered reversible inhibition of

SpyCatcher reactivity enables rapid generation of bispecific antibodies. Nat. Commun. *15*, 5939.

Hermanson, G.T. (1996). Antibody Modification and Conjugation. Bioconjugate Tech. 456–493.

Hofmann, T., Schmidt, J., Ciesielski, E., Becker, S., Rysiok, T., Schütte, M., Toleikis, L., Kolmar, H., and Doerner, A. (2020a). Intein mediated high throughput screening for bispecific antibodies. MAbs *12*, 1–15.

Hofmann, T., Krah, S., Sellmann, C., Zielonka, S., and Doerner, A. (2020b). Greatest hits—innovative technologies for high throughput identification of bispecific antibodies. Int. J. Mol. Sci. *21*, 1–17.

Holbro, T., Beerli, R.R., Maurer, F., Koziczak, M., Barbas, C.F., and Hynes, N.E. (2003). The ErbB2/ErbB3 heterodimer functions as an oncogenic unit: ErbB2 requires ErbB3 to drive breast tumor cell proliferation. Proc. Natl. Acad. Sci. U. S. A. *100*, 8933–8938.

Hornbeck, P. V., Zhang, B., Murray, B., Kornhauser, J.M., Latham, V., and Skrzypek, E. (2015). PhosphoSitePlus, 2014: Mutations, PTMs and recalibrations. Nucleic Acids Res. *43*, D512–D520.

Hoyt, E.A., Cal, P.M.S.D., Oliveira, B.L., and Bernardes, G.J.L. (2019). Contemporary approaches to site-selective protein modification. Nat. Rev. Chem. *3*, 147–171.

Hsu, J.L., and Hung, M.C. (2016). The role of HER2, EGFR, and other receptor tyrosine kinases in breast cancer. Cancer Metastasis Rev. *35*, 575–588.

Hu, S., Sun, Y., Meng, Y., Wang, X., Yang, W., Fu, W., Guo, H., Qian, W., Hou, S., Li, B., et al. (2015). Molecular architecture of the ErbB2 extracellular domain homodimer. Oncotarget *6*, 1695–1706.

Huang, B., Abedi, M., Ahn, G., Coventry, B., Sappington, I., Tang, C., Wang, R., Schlichthaerle, T., Zhang, J.Z., Wang, Y., et al. (2024). Designed endocytosis-inducing proteins degrade targets and amplify signals. Nature.

Huang, F., Shi, Q., Li, Y., Xu, L., Xu, C., Chen, F., Wang, H., Liao, H., Chang, Z., Liu, F., et al. (2018). HER2/EGFR–AKT signaling switches TGFb from inhibiting cell proliferation to promoting cell migration in breast cancer. Cancer Res. *78*, 6073–6085.

Huang, K., Li, Z., Su, T., Shen, D., Hu, S., and Cheng, K. (2019). Bispecific Antibody Therapy for Effective Cardiac Repair through Redirection of Endogenous Stem Cells. Adv. Ther. *2*, 1900009.

Huddy, T.F., Hsia, Y., Kibler, R.D., Xu, J., Bethel, N., Nagarajan, D., Redler, R., Leung, P.J.Y., Weidle, C., Courbet, A., et al. (2024). Blueprinting extendable nanomaterials with standardized protein blocks. Nature *627*, 898–904.

Hughes, R.E., Elliott, R.J.R., Dawson, J.C., and Carragher, N.O. (2021). High-content phenotypic and pathway profiling to advance drug discovery in diseases of unmet need. Cell Chem. Biol. *28*, 338–355.

Hull, E.A., Livanos, M., Miranda, E., Smith, M.E.B.B., Chester, K.A., and Baker, J.R. (2014). Homogeneous Bispecifics by Disulfide Bridging. Bioconjug. Chem. *25*, 1395–1401.

Hura, G.L., Menon, A.L., Hammel, M., Rambo, R.P., Poole, F.L., Tsutakawa, S.E., Jenney, F.E., Classen, S., Frankel, K.A., Hopkins, R.C., et al. (2009). Robust, high-throughput solution structural analyses by small angle X-ray scattering (SAXS). Nat. Methods *6*, 606–612.

Husain, B., and Ellerman, D. (2018). Expanding the Boundaries of Biotherapeutics with Bispecific Antibodies. BioDrugs *32*, 441–464.

Hutchings, C.J., Colussi, P., and Clark, T.G. (2019). Ion channels as therapeutic antibody targets. MAbs *11*, 265–296.

Hutt, M., Färber-Schwarz, A., Unverdorben, F., Richter, F., and Kontermann, R.E. (2012). Plasma half-life extension of small recombinant antibodies by fusion to immunoglobulin-binding domains. J. Biol. Chem. *287*, 4462–4469.

Hynes, N.E., and Lane, H.A. (2005). ERBB receptors and cancer: The complexity of targeted inhibitors. Nat. Rev. Cancer *5*, 341–354.

Jackman, J., Chen, Y., Huang, A., Moffat, B., Scheer, J.M., Leong, S.R., Lee, W.P., Zhang, J., Sharma, N., Lu, Y., et al. (2010). Development of a two-part strategy to identify a therapeutic human bispecific antibody that inhibits IgE receptor signaling. J. Biol. Chem. *285*, 20850–20859.

Jarantow, S.W., Bushey, B.S., Pardinas, J.R., Boakye, K., Lacy, E.R., Sanders, R., Sepulveda, M.A., Moores, S.L., and Chiu, M.L. (2015). Impact of cell-surface antigen expression on target engagement and function of an epidermal growth factor receptor x c-MET bispecific antibody. J. Biol. Chem. *290*, 24689–24704.

Jay, S.M., Kurtagic, E., Alvarez, L.M., De Picciotto, S., Sanchez, E., Hawkins, J.F., Prince, R.N., Guerrero, Y., Treasure, C.L., Lee, R.T., et al. (2011). Engineered bivalent ligands to bias ErbB receptor-mediated signaling and phenotypes. J. Biol. Chem. *286*, 27729–27740.

Jensen, M., Hansen, B., De Meyts, P., Schäffer, L., and Ursø, B. (2007). Activation of the insulin receptor by insulin and a synthetic peptide leads to divergent metabolic and mitogenic signaling and responses. J. Biol. Chem. *282*, 35179–35186.

Jiang, G., Den Hertog, J., Su, J., Noel, J., Sap, J., and Hunter, T. (1999). Dimerization inhibits the activity of receptor-like protein-tyrosine phosphatase-α. Nature *401*, 606–610.

Jie, J., Zhang, Y., Zhou, H., Zhai, X., Zhang, N., Yuan, H., Ni, W., and Tai, G. (2018). CpG ODN1826 as a promising mucin1-maltose-binding protein vaccine adjuvant induced DC maturation and enhanced antitumor immunity. Int. J. Mol. Sci. *19*, 1–17.

Jin, S., Sun, Y., Liang, X., Gu, X., Ning, J., Xu, Y., Chen, S., and Pan, L. (2022). Emerging new therapeutic antibody derivatives for cancer treatment. Signal Transduct. Target. Ther. *7*.

Jonsson, A., Dogan, J., Herne, N., Abrahmsén, L., and Nygren, P.Å. (2008). Engineering of a femtomolar affinity binding protein to human serum albumin. Protein Eng. Des. Sel. *21*, 515–527.

Joshi, B.S., de Lannoy, C., Howarth, M.R., Kim, S.H., and Joo, C. (2024). iMAX FRET (Information Maximized FRET) for Multipoint Single-Molecule Structural Analysis. Nano Lett. *24*, 8487–8494.

Joshi, K.K., Phung, W., Han, G., Yin, Y., Kim, I., Sandoval, W., and Carter, P.J. (2019). Elucidating heavy/light chain pairing preferences to facilitate the assembly of bispecific IgG in single cells. MAbs *11*, 1254–1265.

Jost, C., Schilling, J., Tamaskovic, R., Schwill, M., Honegger, A., and Plückthun, A. (2013). Structural basis for eliciting a cytotoxic effect in HER2-overexpressing cancer cells via binding to the extracellular domain of HER2. Structure *21*, 1979–1991.

Jubb, H.C., Higueruelo, A.P., Ochoa-Montaño, B., Pitt, W.R., Ascher, D.B., and Blundell, T.L. (2017). Arpeggio: A Web Server for Calculating and Visualising Interatomic

Interactions in Protein Structures. J. Mol. Biol. *429*, 365–371.

Jumper, J., Evans, R., Pritzel, A., Green, T., Figurnov, M., Ronneberger, O., Tunyasuvunakool, K., Bates, R., Žídek, A., Potapenko, A., et al. (2021). Highly accurate protein structure prediction with AlphaFold. Nature *596*, 583–589.

Junttila, T.T., Akita, R.W., Parsons, K., Fields, C., Lewis Phillips, G.D., Friedman, L.S., Sampath, D., and Sliwkowski, M.X. (2009). Ligand-Independent HER2/HER3/PI3K Complex Is Disrupted by Trastuzumab and Is Effectively Inhibited by the PI3K Inhibitor GDC-0941. Cancer Cell *15*, 429–440.

Junutula, J.R., Raab, H., Clark, S., Bhakta, S., Leipold, D.D., Weir, S., Chen, Y., Simpson, M., Tsai, S.P., Dennis, M.S., et al. (2008). Site-specific conjugation of a cytotoxic drug to an antibody improves the therapeutic index. Nat. Biotechnol. *26*, 925–932.

Kadonosono, T., Yimchuen, W., Ota, Y., See, K., Furuta, T., Shiozawa, T., Kitazawa, M., Goto, Y., Patil, A., Kuchimaru, T., et al. (2020). Design Strategy to Create Antibody Mimetics Harbouring Immobilised Complementarity Determining Region Peptides for Practical Use. Sci. Rep. *10*, 891.

Kamashev, D., Shaban, N., Suntsova, M., Raevskiy, M., Efimov, V., Moisseev, A., Sorokin, M., and Buzdin, A. (2022). Human Blood Serum Inhibits Ductal Carcinoma Cells BT474 Growth and Modulates Effect of HER2 Inhibition. Biomedicines *10*, 1914.

Kang, H.J., and Baker, E.N. (2011). Intramolecular isopeptide bonds: Protein crosslinks built for stress? Trends Biochem. Sci. *36*, 229–237.

Karl, K., Paul, M.D., Pasquale, E.B., and Hristova, K. (2020). Ligand bias in receptor tyrosine kinase signaling. J. Biol. Chem. *295*, 18494–18507.

Karpovsky, B., Titus, J.A., Stephany, D.A., and Segal, D.M. (1984). Production of target-specific effector cells using hetero-cross-linked aggregates containing anti-target cell and anti-Fcγ, receptor antibodies. J. Exp. Med. *160*, 1686–1701.

Kast, F., Schwill, M., Stüber, J.C., Pfundstein, S., Nagy-Davidescu, G., Rodríguez, J.M.M., Seehusen, F., Richter, C.P., Honegger, A., Hartmann, K.P., et al. (2021). Engineering an anti-HER2 biparatopic antibody with a multimodal mechanism of action. Nat. Commun. *12*, 3790.

Kaushansky, A., Gordus, A., Budnik, B.A., Lane, W.S., Rush, J., and MacBeath, G. (2008). System-wide Investigation of ErbB4 Reveals 19 Sites of Tyr Phosphorylation that Are Unusually Selective in Their Recruitment Properties. Chem. Biol. *15*, 808–817.

Keeble, A.H., and Howarth, M. (2020). Power to the protein: Enhancing and combining activities using the Spy toolbox. Chem. Sci. *11*, 7281–7291.

Keeble, A.H., Banerjee, A., Ferla, M.P., Reddington, S.C., Anuar, I.N.A.K., and Howarth, M. (2017). Evolving Accelerated Amidation by SpyTag/SpyCatcher to Analyze Membrane Dynamics. Angew. Chemie - Int. Ed. *56*, 16521–16525.

Keeble, A.H., Turkki, P., Stokes, S., Anuar, I.N.A.K., Rahikainen, R., Hytönen, V.P., and Howarth, M. (2019). Approaching infinite affinity through engineering of peptide-protein interaction. Proc. Natl. Acad. Sci. U. S. A. *116*, 26523–26533.

Keeble, A.H., Yadav, V.K., Ferla, M.P., Bauer, C.C., Chuntharpursat-Bon, E., Huang, J., Bon, R.S., and Howarth, M. (2022). DogCatcher allows loop-friendly protein-protein ligation. Cell Chem. Biol. *29*, 339-350.e10.

Keller, A., and Linko, V. (2020). Challenges and Perspectives of DNA Nanostructures in Biomedicine. Angew. Chemie - Int. Ed. *59*, 15818–15833.

Kellmann, S.J., Hentrich, C., Putyrski, M., Hanuschka, H., Cavada, M., Knappik, A., and Ylera, F. (2023). SpyDisplay: A versatile phage display selection system using SpyTag/SpyCatcher technology. MAbs *15*, 2003–2005.

Kennedy, S.P., Hastings, J.F., Han, J.Z.R., and Croucher, D.R. (2016). The under-appreciated promiscuity of the epidermal growth factor receptor family. Front. Cell Dev. Biol. *4*.

Kennedy, S.P., Han, J.Z.R., Portman, N., Nobis, M., Hastings, J.F., Murphy, K.J., Latham, S.L., Cadell, A.L., Miladinovic, D., Marriott, G.R., et al. (2019). Targeting promiscuous heterodimerization overcomes innate resistance to ERBB2 dimerization inhibitors in breast cancer. Breast Cancer Res. *21*, 43.

Khairil, I., Scheu, A.H.A., Dorgan, B., Nikov, G., Hoffmann, M.R., Brem, R., Wilson, J., and Chavez, A.O.J. (2022). Multivalent Proteins and Screening Methods (WIPO).

Khairil Anuar, I.N.A., Banerjee, A., Keeble, A.H., Carella, A., Nikov, G.I., and Howarth, M. (2019). Spy&Go purification of SpyTag-proteins using pseudo-SpyCatcher to access an oligomerization toolbox. Nat. Commun. *10*, 1734.

Khalili, H., Godwin, A., Choi, J.W., Lever, R., Khaw, P.T., and Brocchini, S. (2013). Fab-PEG-Fab as a potential antibody mimetic. Bioconjug. Chem. *24*, 1870–1882.

Ki, H., Jo, J., Kim, Y., Kim, T.W., Kim, C., Kim, Y., Kim, C.W., Muniyappan, S., Lee, S.J., Kim, Y., et al. (2021). Uncovering the Conformational Distribution of a Small Protein with Nanoparticle-Aided Cryo-Electron Microscopy Sampling. J. Phys. Chem. Lett. *12*, 6565–6573.

Kim, A.R., Ulirsch, J.C., Wilmes, S., Unal, E., Moraga, I., Karakukcu, M., Yuan, D., Kazerounian, S., Abdulhay, N.J., King, D.S., et al. (2017). Functional Selectivity in Cytokine Signaling Revealed Through a Pathogenic EPO Mutation. Cell *168*, 1053-1064.e15.

Kim, C.H., Axup, J.Y., Lawson, B.R., Yun, H., Tardif, V., Choi, S.H., Zhou, Q., Dubrovska, A., Biroc, S.L., Marsden, R., et al. (2013). Bispecific small molecule-antibody conjugate targeting prostate cancer. Proc. Natl. Acad. Sci. U. S. A. *110*, 17796–17801.

King, I.C., Gleixner, J., Doyle, L., Kuzin, A., Hunt, J.F., Xiao, R., Montelione, G.T., Stoddard, B.L., DiMaio, F., and Baker, D. (2015). Precise assembly of complex beta sheet topologies from de novo designed building blocks. Elife *4*, 3–11.

King, T.A., Walsh, S.J., Kapun, M., Wharton, T., Krajcovicova, S., Glossop, M.S., and Spring, D.R. (2023). Disulfide re-bridging reagents for single-payload antibody-drug conjugates. Chem. Commun. *59*, 9868–9871.

Kirouac, D.C., Du, J., Lahdenranta, J., Onsum, M.D., Nielsen, U.B., Schoeberl, B., and McDonagh, C.F. (2016). HER2+ Cancer Cell Dependence on PI3K vs. MAPK Signaling Axes Is Determined by Expression of EGFR, ERBB3 and CDKN1B. PLoS Comput. Biol. *12*, e1004827.

Kitazawa, T., Igawa, T., Sampei, Z., Muto, A., Kojima, T., Soeda, T., Yoshihashi, K., Okuyama-Nishida, Y., Saito, H., Tsunoda, H., et al. (2012). A bispecific antibody to factors IXa and X restores factor VIII hemostatic activity in a hemophilia A model. Nat. Med. *18*, 1570–1574.

Klein, C., Schaefer, W., Regula, J.T., Dumontet, C., Brinkmann, U., Bacac, M., and Umaña, P. (2019). Engineering therapeutic bispecific antibodies using CrossMab technology. Methods *154*, 21–31.

Klein, C., Brinkmann, U., Reichert, J.M., and Kontermann, R.E. (2024). The present and

future of bispecific antibodies for cancer therapy. Nat. Rev. Drug Discov. *23*, 301–319.

Klinger, M., Brandl, C., Zugmaier, G., Hijazi, Y., Bargou, R.C., Topp, M.S., Gökbuget, N., Neumann, S., Goebeler, M., Viardot, A., et al. (2012). Immunopharmacologic response of patients with B-lineage acute lymphoblastic leukemia to continuous infusion of T cell-engaging CD19/CD3-bispecific BiTE antibody blinatumomab. Blood *119*, 6226–6233.

Klint, S., Feldwisch, J., Gudmundsdotter, L., Dillner Bergstedt, K., Gunneriusson, E., Höidén Guthenberg, I., Wennborg, A., Nyborg, A.C., Kamboj, A.P., Peloso, P.M., et al. (2023). Izokibep: Preclinical development and first-in-human study of a novel IL-17A neutralizing Affibody molecule in patients with plaque psoriasis. MAbs *15*, 2209920.

Köhler, G., Milstein, C. (1975). Cultivos continuos de células fusionadas que secretan anticuerpos de especificidad predefinida. Nature *256*, 495–497.

Kolumam, G., Chen, M.Z., Tong, R., Zavala-Solorio, J., Kates, L., van Bruggen, N., Ross, J., Wyatt, S.K., Gandham, V.D., Carano, R.A.D., et al. (2015). Sustained Brown Fat Stimulation and Insulin Sensitization by a Humanized Bispecific Antibody Agonist for Fibroblast Growth Factor Receptor 1/βKlotho Complex. EBioMedicine *2*, 730–743.

Kontermann, R.E. (2012). Dual targeting strategies with bispecific antibodies. MAbs *4*, 182–197.

Kontermann, R.E., and Brinkmann, U. (2015). Bispecific antibodies. Drug Discov. Today *20*, 838–847.

Kortemme, T. (2024). De novo protein design—From new structures to programmable functions. Cell *187*, 526–544.

Kovacs, T., Zakany, F., and Nagy, P. (2022). It Takes More than Two to Tango: Complex, Hierarchal, and Membrane-Modulated Interactions in the Regulation of Receptor Tyrosine Kinases. Cancers (Basel). *14*, 1–31.

Krajcovicova, S., Wharton, T., Driscoll, C.L., King, T.A., Howarth, R., and Spring, D.R. (2024). All-At-Once Linkers for Single-Payload Bioconjugation to Native Antibodies. Submitted 1–10.

Kramer, M.A., Wetzel, S.K., Plückthun, A., Mittl, P.R.E., and Grütter, M.G. (2010). Structural determinants for improved stability of designed ankyrin repeat proteins with a redesigned C-Capping Module. J. Mol. Biol. *404*, 381–391.

Kreudenstein, T.S. Von, Escobar-Carbrera, E., Lario, P.I., D'Angelo, I., Brault, K., Kelly, J., Durocher, Y., Baardsnes, J., Jeremy Woods, R., Xie, M.H., et al. (2013). Improving biophysical properties of a bispecific antibody scaffold to aid developability: Quality by molecular design. MAbs *5*, 646–654.

Krishna, R., Wang, J., Ahern, W., Sturmfels, P., Venkatesh, P., Kalvet, I., Lee, G.R., Morey-Burrows, F.S., Anishchenko, I., Humphreys, I.R., et al. (2024). Generalized biomolecular modeling and design with RoseTTAFold All-Atom. Science (80-.). *384*.

De Kruif, C.A., Hendricks, L.J.A., Logtenberg, T., and Van Loo, P.F. (2019). Multivalent antibody (WIPO).

Kufareva, I., Gustavsson, M., Zheng, Y., Stephens, B.S., and Handel, T.M. (2017). What Do Structures Tell Us about Chemokine Receptor Function and Antagonism? Annu. Rev. Biophys. *46*, 175–198.

Kuhlman, B., Yang, H.Y., Boice, J.A., Fairman, R., and Raleigh, D.P. (1997). An exceptionally stable helix from the ribosomal protein L9: Implications for protein folding and

stability. J. Mol. Biol. *270*, 640–647.

Kunik, V., Peters, B., and Ofran, Y. (2012). Structural consensus among antibodies defines the antigen binding site. PLoS Comput. Biol. *8*.

Kwon, N.Y., Kim, Y., and Lee, J.O. (2020). The application of helix fusion methods in structural biology. Curr. Opin. Struct. Biol. *60*, 110–116.

Labrijn, A.F., Meesters, J.I., De Goeij, B.E.C.G., Van Den Bremer, E.T.J., Neijssen, J., Van Kampen, M.D., Strumane, K., Verploegen, S., Kundu, A., Gramer, M.J., et al. (2013). Efficient generation of stable bispecific IgG1 by controlled Fab-arm exchange. Proc. Natl. Acad. Sci. U. S. A. *110*, 5145–5150.

Labrijn, A.F., Janmaat, M.L., Reichert, J.M., and Parren, P.W.H.I. (2019). Bispecific antibodies: a mechanistic review of the pipeline. Nat. Rev. Drug Discov. *18*, 585–608.

Landau, M., Fleishman, S.J., and Ben-Tal, N. (2004). A putative mechanism for downregulation of the catalytic activity of the EGF receptor via direct contact between its kinase and C-terminal domains. Structure *12*, 2265–2275.

Lane, J.R., Donthamsetti, P., Shonberg, J., Draper-Joyce, C.J., Dentry, S., Michino, M., Shi, L., López, L., Scammells, P.J., Capuano, B., et al. (2014). A new mechanism of allostery in a G protein-coupled receptor dimer. Nat. Chem. Biol. *10*, 745–752.

Lau, Y.H., De Andrade, P., Sköld, N., McKenzie, G.J., Venkitaraman, A.R., Verma, C., Lane, D.P., and Spring, D.R. (2014). Investigating peptide sequence variations for "double-click" stapled p53 peptides. Org. Biomol. Chem. *12*, 4074–4077.

Lau, Y.H., De Andrade, P., Wu, Y., and Spring, D.R. (2015). Peptide stapling techniques based on different macrocyclisation chemistries. Chem. Soc. Rev. *44*, 91–102.

Law, S.M. (2020). Modevectors. https://pymolwiki.org/index.php/Modevectors (Accessed 2 February 2022).

Lee-Hoeflich, S.T., Crocker, L., Yao, E., Pham, T., Munroe, X., Hoeflich, K.P., Sliwkowski, M.X., and Stern, H.M. (2008). A central role for HER3 in HER2-amplified breast cancer: Implications for targeted therapy. Cancer Res. *68*, 5878–5887.

Lee, J., Franovic, A., Shiotsu, Y., Kim, S.T., Kim, K.M., Banks, K.C., Raymond, V.M., and Lanman, R.B. (2019). Detection of ErbB2 (HER2) gene amplification events in cell-free DNA and response to anti-HER2 agents in a large Asian cancer patient cohort. Front. Oncol. *9*, 1–10.

Lee, N.K., Zhang, Y., Su, Y., Bidlingmaier, S., Sherbenou, D.W., Ha, K.D., and Liu, B. (2018). Cell-type specific potent Wnt signaling blockade by bispecific antibody. Sci. Rep. *8*, 1–16.

Lemmon, M.A. (2009). Ligand-induced ErbB receptor dimerization. Exp. Cell Res. *315*, 638–648.

Van Lengerich, B., Agnew, C., Puchner, E.M., Huang, B., and Jura, N. (2017). EGF and NRG induce phosphorylation of HER3/ERBB3 by EGFR using distinct oligomeric mechanisms. Proc. Natl. Acad. Sci. U. S. A. *114*, E2836–E2845.

Lewis, S.M., Wu, X., Pustilnik, A., Sereno, A., Huang, F., Rick, H.L., Guntas, G., Leaver-Fay, A., Smith, E.M., Ho, C., et al. (2014). Generation of bispecific IgG antibodies by structure-based design of an orthogonal Fab interface. Nat. Biotechnol. *32*, 191–198.

Lewis Phillips, G., Guo, J., Kiefer, J.R., Proctor, W., Bumbaca Yadav, D., Dybdal, N., and

Shen, B.Q. (2022). Trastuzumab does not bind rat or mouse ErbB2/neu: implications for selection of non-clinical safety models for trastuzumab-based therapeutics. Breast Cancer Res. Treat. *191*, 303–317.

Li, A., Voleti, R., Lee, M., Gagoski, D., and Shah, N.H. (2023). High-throughput profiling of sequence recognition by tyrosine kinases and SH2 domains using bacterial peptide display. Elife *12*, 1–45.

Li, B., Xu, L., Pi, C., Yin, Y., Xie, K., Tao, F., Li, R., Gu, H., and Fang, J. (2018). CD89-mediated recruitment of macrophages via a bispecific antibody enhances anti-tumor efficacy. Oncoimmunology *7*, 1–9.

Li, L., Fierer, J.O., Rapoport, T.A., and Howarth, M. (2014). Structural analysis and optimization of the covalent association between SpyCatcher and a peptide tag. J. Mol. Biol. *426*, 309–317.

Liang, S.I., van Lengerich, B., Eichel, K., Cha, M., Patterson, D.M., Yoon, T.Y., von Zastrow, M., Jura, N., and Gartner, Z.J. (2018). Phosphorylated EGFR Dimers Are Not Sufficient to Activate Ras. Cell Rep. *22*, 2593–2600.

Lim, A., Wally, J., Walsh, M.T., Skinner, M., and Costello, C.E. (2001). Identification and location of a cysteinyl posttranslational modification in an amyloidogenic κ1 light chain protein by electrospray ionization and matrix-assisted laser desorption/ionization mass spectrometry. Anal. Biochem. *295*, 45–56.

Lin, Y.R., Koga, N., Tatsumi-Koga, R., Liu, G., Clouser, A.F., Montelione, G.T., Baker, D., and DeGrado, W.F. (2015). Control over overall shape and size in de novo designed proteins. Proc. Natl. Acad. Sci. U. S. A. *112*, E5478–E5485.

Lin, Z., Schaefer, K., Lui, I., Yao, Z., Fossati, A., Swaney, D.L., Palar, A., Sali, A., and Wells, J.A. (2024). Multiscale photocatalytic proximity labeling reveals cell surface neighbors on and between cells. Science *385*, eadl5763.

Lindborg, M., Cortez, E., Höidén-Guthenberg, I., Gunneriusson, E., Von Hage, E., Syud, F., Morrison, M., Abrahmsén, L., Herne, N., Pietras, K., et al. (2011). Engineered high-affinity affibody molecules targeting platelet-derived growth factor receptor β in vivo. J. Mol. Biol. *407*, 298–315.

Lindhofer, H., Mocikat, R., Steipe, B., and Thierfelder, S. (1995). Preferential species-restricted heavy/light chain pairing in rat/mouse quadromas. Implications for a single-step purification of bispecific antibodies. J. Immunol. *155*, 219–225.

Liu, X., and Ciulli, A. (2023). Proximity-Based Modalities for Biology and Medicine. ACS Cent. Sci. *9*, 1269–1284.

Liu, D., Yao, H., Chen, Y., Feng, Y., Chen, Y., and Wang, J. (2005). The N-terminal 26-residue fragment of human programmed cell death 5 protein can form a stable α-helix having unique electrostatic potential character. Biochem. J. *392*, 47–54.

Liu, G.M., Zhang, Y.X., Zhang, N.N., Ni, W.H., Jie, J., Jiang, L.N., and Tai, G.X. (2017). Escherichia coli maltose-binding protein (MBP) activates mouse Th1 through TLR2-mediated MyD88-dependent pathway and TLR4-mediated TRIF-dependent pathway. Int. Immunopharmacol. *50*, 338–344.

Liu, Z., Zhou, H., Wang, W., Tan, W., Fu, Y.X., and Zhu, M. (2014). A novel method for synthetic vaccine construction based on protein assembly. Sci. Rep. *4*, 7266.

Lo, K.M., Sudo, Y., Chen, J., Li, Y., Lan, Y., Kong, S.M., Chen, L., An, Q., and Gillies, S.D.

(1998). High level expression and secretion of Fc-X fusion proteins in mammalian cells. Protein Eng. *11*, 495–500.

Locksley, R.M., Killeen, N., and Lenardo, M.J. (2001). The TNF and TNF receptor superfamilies: Integrating mammalian biology. Cell *104*, 487–501.

Lorenczewski, G., Friedrich, M., Kischel, R., Dahlhoff, C., Anlahr, J., Balazs, M., Rock, D., Boyle, M.C., Goldstein, R., Coxon, A., et al. (2017). Generation of a Half-Life Extended Anti-CD19 BiTE® Antibody Construct Compatible with Once-Weekly Dosing for Treatment of CD19-Positive Malignancies. In Blood, (American Society of Hematology), p. 2815.

Lu, C., Bevers, J., Tyagi, T., To, H., Lin, M., Ti, S., Nakamura, G., Lin, W.Y., Chen, Y., Wu, Y., et al. (2024). AviTrap: A novel solution to achieve complete biotinylation. PLoS One *19*, 1–17.

Lu, D., Jimenez, X., Witte, L., and Zhu, Z. (2004). The effect of variable domain orientation and arrangement on the antigen-binding activity of a recombinant human bispecific diabody. Biochem. Biophys. Res. Commun. *318*, 507–513.

Lu, R.M., Hwang, Y.C., Liu, I.J., Lee, C.C., Tsai, H.Z., Li, H.J., and Wu, H.C. (2020). Development of therapeutic antibodies for the treatment of diseases. J. Biomed. Sci. *27*, 1–30.

Lucas, F.A.M., and Cristovam, S.N. (2016). HER2 testing in gastric cancer: An update. World J. Gastroenterol. *22*, 4619–4625.

Lum, L.G., Davol, P.A., and Lee, R.J. (2006). The new face of bispecific antibodies: Targeting cancer and much more. Exp. Hematol. *34*, 1–6.

Luo, C., Mo, M., Zhu, Y., Nie, Z., Long, L., and Li, Y. (2016). The microRNA-410 targets Fos-related antigen 1 and inhibits malignancy in breast cancer cells. Int. J. Clin. Exp. Med. *9*, 10374–10383.

Ma, J., Mo, Y., Tang, M., Shen, J., Qi, Y., Zhao, W., Huang, Y., Xu, Y., and Qian, C. (2021). Bispecific Antibodies: From Research to Clinical Application. Front. Immunol. *12*.

Macdonald-Obermann, J.L., and Pike, L.J. (2014). Different epidermal growth factor (EGF) receptor ligands show distinct kinetics and biased or partial agonism for homodimer and heterodimer formation. J. Biol. Chem. *289*, 26178–26188.

Macdonald-Obermann, J.L., Piwnica-Worms, D., and Pike, L.J. (2012). Mechanics of EGF receptor/ErbB2 kinase activation revealed by luciferase fragment complementation imaging. Proc. Natl. Acad. Sci. U. S. A. *109*, 137–142.

Mack, M., Riethmüller, G., and Kufer, P. (1995). A small bispecific antibody construct expressed as a functional single-chain molecule with high tumor cell cytotoxicity. Proc. Natl. Acad. Sci. U. S. A. *92*, 7021–7025.

Madsen, A. V., Kristensen, P., Buell, A.K., and Goletz, S. (2023). Generation of robust bispecific antibodies through fusion of single-domain antibodies on IgG scaffolds: a comprehensive comparison of formats. MAbs *15*, 2189432.

Madsen, A. V., Pedersen, L.E., Kristensen, P., and Goletz, S. (2024). Design and engineering of bispecific antibodies: insights and practical considerations. Front. Bioeng. Biotechnol. *12*, 1–13.

Malm, M., Kronqvist, N., Lindberg, H., Gudmundsdotter, L., Bass, T., Frejd, F.Y., Höidén-Guthenberg, I., Varasteh, Z., Orlova, A., Tolmachev, V., et al. (2013). Inhibiting HER3-Mediated Tumor Cell Growth with Affibody Molecules Engineered to Low Picomolar

Affinity by Position-Directed Error-Prone PCR-Like Diversification. PLoS One *8*, e62791.

Maniaci, C., and Ciulli, A. (2019). Bifunctional chemical probes inducing protein–protein interactions. Curr. Opin. Chem. Biol. *52*, 145–156.

Marculescu, C., Kossen, H., Morgan, R.E., Mayer, P., Fletcher, S.A., Tolner, B., Chester, K.A., Jones, L.H., and Baker, J.R. (2014). Aryloxymaleimides for cysteine modification, disulfide bridging and the dual functionalization of disulfide bonds. Chem. Commun. *50*, 7139–7142.

Marei, H., Tsai, W.-T.K., Kee, Y.-S., Ruiz, K., He, J., Cox, C., Sun, T., Penikalapati, S., Dwivedi, P., Choi, M., et al. (2022). Antibody targeting of E3 ubiquitin ligases for receptor degradation. Nature *610*, 182–189.

Maruani, A., Szijj, P.A., Bahou, C., Nogueira, J.C.F., Caddick, S., Baker, J.R., and Chudasama, V. (2020). A Plug-and-Play Approach for the de Novo Generation of Dually Functionalized Bispecifics. Bioconjug. Chem. *31*, 520–529.

Math, B.A., Waibl, F., Lamp, L.M., Fernández-Quintero, M.L., and Liedl, K.R. (2023). Cross-linking disulfide bonds govern solution structures of diabodies. Proteins Struct. Funct. Bioinforma. *91*, 1316–1328.

Mayes, P.A., Hance, K.W., and Hoos, A. (2018). The promise and challenges of immune agonist antibody development in cancer. Nat. Rev. Drug Discov. *17*, 509–527.

Mazor, Y., Oganesyan, V., Yang, C., Hansen, A., Wang, J., Liu, H., Sachsenmeier, K., Carlson, M., Gadre, D. V., Borrok, M.J., et al. (2015). Improving target cell specificity using a novel monovalent bispecific IgG design. MAbs *7*, 377–389.

McKay, C.S., and Finn, M.G. (2014). Click chemistry in complex mixtures: Bioorthogonal bioconjugation. Chem. Biol. *21*, 1075–1101.

Mehrizi, R., Mehrjou, A., Alegro, M., Zhao, Y., Carbone, B., Fishwick, C., Vappiani, J., Bi, J., Sanford, S., Keles, H., et al. (2023). Multi-omics Prediction from High-content Cellular Imaging with Deep Learning. ArXiv.

Mei, L., Zappala, F., and Tsourkas, A. (2022). Rapid Production of Bispecific Antibodies from Off-the-Shelf IgGs with High Yield and Purity. Bioconjug. Chem. *33*, 134–141.

Mendoza, M.N., Jian, M., King, M.T., and Brooks, C.L. (2020). Role of a noncanonical disulfide bond in the stability, affinity, and flexibility of a VHH specific for the Listeria virulence factor InlB. Protein Sci. *29*, 1004–1017.

Meng, G., Guo, T., Ma, T., Zhang, J., Shen, Y., Sharpless, K.B., and Dong, J. (2019). Modular click chemistry libraries for functional screens using a diazotizing reagent. Nature *574*, 86–89.

Merchant, A.M., Zhu, Z., Yuan, J.Q., Goddard, A., Adams, C.W., Presta, L.G., and Carter, P. (1998). An efficient route to human bispecific IgG. Nat. Biotechnol. *16*, 677–681.

Mercogliano, M.F., Bruni, S., Elizalde, P. V., and Schillaci, R. (2020). Tumor Necrosis Factor α Blockade: An Opportunity to Tackle Breast Cancer. Front. Oncol. *10*.

Merkhofer, E.C., Cogswell, P., and Baldwin, A.S. (2010). Her2 activates NF-κB and induces invasion through the canonical pathway involving IKKα. Oncogene *29*, 1238–1248.

Miao, Y., Gao, Q., Mao, M., Zhang, C., Yang, L., Yang, Y., and Han, D. (2021). Bispecific Aptamer Chimeras Enable Targeted Protein Degradation on Cell Membranes. Angew. Chemie - Int. Ed. *60*, 11267–11271.

Miladi, B., Marjou, A. El, Boeuf, G., Bouallagui, H., Dufour, F., Di Martino, P., and Elm'selmi, A. (2012). Oriented immobilization of the tobacco etch virus protease for the cleavage of fusion proteins. J. Biotechnol. *158*, 97–103.

Milstein, C., and Cuello, A.C. (1983). Hybrid hybridomas and their use in immunohistochemistry. Nature *305*, 537–540.

Mineev, K.S., Bocharov, E. V., Pustovalova, Y.E., Bocharova, O. V., Chupin, V. V., and Arseniev, A.S. (2010). Spatial Structure of the Transmembrane Domain Heterodimer of ErbB1 and ErbB2 Receptor Tyrosine Kinases. J. Mol. Biol. *400*, 231–243.

Mirdita, M., Schütze, K., Moriwaki, Y., Heo, L., Ovchinnikov, S., and Steinegger, M. (2022). ColabFold: making protein folding accessible to all. Nat. Methods *19*, 679–682.

Mitchell, L.S., and Colwell, L.J. (2018a). Analysis of nanobody paratopes reveals greater diversity than classical antibodies. Protein Eng. Des. Sel. *31*, 267–275.

Mitchell, L.S., and Colwell, L.J. (2018b). Comparative analysis of nanobody sequence and structure data. Proteins Struct. Funct. Bioinforma. *86*, 697–706.

Moasser, M.M. (2007). The oncogene HER2: Its signaling and transforming functions and its role in human cancer pathogenesis. Oncogene *26*, 6469–6487.

Moffat, J.G., Vincent, F., Lee, J.A., Eder, J., and Prunotto, M. (2017). Opportunities and challenges in phenotypic drug discovery: An industry perspective. Nat. Rev. Drug Discov. *16*, 531–543.

Mohan, K., Ueda, G., Kim, A.R., Jude, K.M., Fallas, J.A., Guo, Y., Hafer, M., Miao, Y., Saxton, R.A., Piehler, J., et al. (2019). Topological control of cytokine receptor signaling induces differential effects in hematopoiesis. Science (80-.). *364*, eaav7532.

Montagner, A., Yart, A., Dance, M., Perret, B., Salles, J.P., and Raynal, P. (2005). A novel role for Gab1 and SHP2 in epidermal growth factor-induced Ras activation. J. Biol. Chem. *280*, 5350–5360.

Moore, P.A., Zhang, W., Rainey, G.J., Burke, S., Li, H., Huang, L., Gorlatov, S., Veri, M.C., Aggarwal, S., Yang, Y., et al. (2011). Application of dual affinity retargeting molecules to achieve optimal redirected T-cell killing of B-cell lymphoma. Blood *117*, 4542–4551.

Moraga, I., Wernig, G., Wilmes, S., Gryshkova, V., Richter, C.P., Hong, W.-J., Sinha, R., Guo, F., Fabionar, H., Wehrman, T.S., et al. (2015). Tuning Cytokine Receptor Signaling by Re-orienting Dimer Geometry with Surrogate Ligands. Cell *160*, 1196–1208.

Moraga, I., Spangler, J.B., Mendoza, J.L., Gakovic, M., Wehrman, T.S., Krutzik, P., and Garcia, K.C. (2017). Synthekines are surrogate cytokine and growth factor agonists that compel signaling through non-natural receptor dimers. Elife *6*, 1–22.

Morgillo, F., and Lee, H.Y. (2005). Resistance to epidermal growth factor receptor-targeted therapy. Drug Resist. Updat. *8*, 298–310.

Moriki, T., Maruyama, H., and Maruyama, I.N. (2001). Activation of preformed EGF receptor dimers by ligand-induced rotation of the transmembrane domain. J. Mol. Biol. *311*, 1011–1026.

Morrison, S.L., Johnson, M.J., Herzenberg, L.A., and Oi, V.T. (1984). Chimeric human antibody molecules: Mouse antigen-binding domains with human constant region domains. Proc. Natl. Acad. Sci. U. S. A. *81*, 6851–6855.

Mozumdar, D., Doerner, A., Zhang, J.Y., Rafizadeh, D.N., and Schepartz, A. (2020).

Discrete Coiled Coil Rotamers Form within the EGFRvIII Juxtamembrane Domain. Biochemistry *59*, 3965–3972.

Mullard, A. (2018). FDA approves landmark RNAi drug. Nat. Rev. Drug Discov. *17*, 613–613.

Müller, D., Karle, A., Meißburger, B., Höfig, I., Stork, R., and Kontermann, R.E. (2007). Improved pharmacokinetics of recombinant bispecific antibody molecules by fusion to human serum albumin. J. Biol. Chem. *282*, 12650–12660.

Nam, Y.W., Shin, J.H., Kim, S., Hwang, C.H., Lee, C.S., Hwang, G., Kim, H.R., Roe, J.S., and Song, J. (2024). EGFR inhibits TNF-α-mediated pathway by phosphorylating TNFR1 at tyrosine 360 and 401. Cell Death Differ.

Nami, B., Maadi, H., and Wang, Z. (2018). Mechanisms underlying the action and synergism of trastuzumab and pertuzumab in targeting HER2-positive breast cancer. Cancers (Basel). *10*.

De Nardis, C., Hendriks, L.J.A., Poirier, E., Arvinte, T., Gros, P., Bakker, A.B.H., and De Kruif, J. (2017). A new approach for generating bispecific antibodies based on a common light chain format and the stable architecture of human immunoglobulin G1. J. Biol. Chem. *292*, 14706–14717.

Neijssen, J., Cardoso, R.M.F., Chevalier, K.M., Wiegman, L., Valerius, T., Anderson, G.M., Moores, S.L., Schuurman, J., Parren, P.W.H.I., Strohl, W.R., et al. (2021). Discovery of amivantamab (JNJ-61186372), a bispecific antibody targeting EGFR and MET. J. Biol. Chem. *296*, 100641.

Nesspor, T.C., Kinealy, K., Mazzanti, N., Diem, M.D., Boye, K., Hoffman, H., Springer, C., Sprenkle, J., Powers, G., Jiang, H., et al. (2020). High-Throughput Generation of Bipod (Fab × scFv) Bispecific Antibodies Exploits Differential Chain Expression and Affinity Capture. Sci. Rep. *10*, 1–10.

Nielsen, H., Tsirigos, K.D., Brunak, S., and von Heijne, G. (2019). A Brief History of Protein Sorting Prediction. Protein J. *38*, 200–216.

Nielsen, U.B., Adams, G.P., Weiner, L.M., and Marks, J.D. (2000). Targeting of bivalent anti-ErbB2 diabody antibody fragments to tumor cells is independent of the intrinsic antibody affinity. Cancer Res. *60*, 6434–6440.

Nilvebrant, J., Åstrand, M., Georgieva-Kotseva, M., Björnmalm, M., Löfblom, J., and Hober, S. (2014). Engineering of bispecific affinity proteins with high affinity for ERBB2 and adaptable binding to albumin. PLoS One *9*, e103094.

Nimmerjahn, F., Vidarsson, G., and Cragg, M.S. (2023). Effect of posttranslational modifications and subclass on IgG activity: from immunity to immunotherapy. Nat. Immunol. *24*, 1244–1255.

Nisonoff, A., Wissler, F.C., and Lipman, L.N. (1960). Properties of the major component of a peptic digest of rabbit antibody. Science (80-.). *132*, 1770–1771.

Nobles, K.N., Xiao, K., Ahn, S., Shukla, A.K., Lam, C.M., Rajagopal, S., Strachan, R.T., Huang, T.Y., Bressler, E.A., Hara, M.R., et al. (2011). Distinct phosphorylation sites on the β 2-adrenergic receptor establish a barcode that encodes differential functions of β-arrestin. Sci. Signal. *4*, 1–10.

Oganesyan, V., Peng, L., Bee, J.S., Li, J., Perry, S.R., Comer, F., Xu, L., Cook, K., Senthil, K., Clarke, L., et al. (2018). Structural insights into the mechanism of action of a biparatopic

anti-HER2 antibody. J. Biol. Chem. *293*, 8439–8448.

Ogiso, H., Ishitani, R., Nureki, O., Fukai, S., Yamanaka, M., Kim, J.H., Saito, K., Sakamoto, A., Inoue, M., Shirouzu, M., et al. (2002). Crystal structure of the complex of human epidermal growth factor and receptor extracellular domains. Cell *110*, 775–787.

Oke, M., Carter, L.G., Johnson, K.A., Liu, H., McMahon, S.A., Yan, X., Kerou, M., Weikart, N.D., Kadi, N., Sheikh, M.A., et al. (2010). The scottish structural proteomics facility: Targets, methods and outputs. J. Struct. Funct. Genomics *11*, 167–180.

Oller-Salvia, B., Kym, G., and Chin, J.W. (2018). Rapid and Efficient Generation of Stable Antibody–Drug Conjugates via an Encoded Cyclopropene and an Inverse-Electron-Demand Diels–Alder Reaction. Angew. Chemie - Int. Ed. *57*, 2831–2834.

Oslund, R.C., Holland, P.M., Lesley, S.A., and Fadeyi, O.O. (2024). Therapeutic potential of cis-targeting bispecific antibodies. Cell Chem. Biol. *31*, 1473–1489.

Overington, J.P., Al-Lazikani, B., and Hopkins, A.L. (2006). How many drug targets are there? Nat. Rev. Drug Discov. *5*, 993–996.

Pan, X., and Kortemme, T. (2021). Recent advances in de novo protein design: Principles, methods, and applications. J. Biol. Chem. *296*, 100558.

Pan, L., Li, J., Xu, Q., Gao, Z., Yang, M., Wu, X., and Li, X. (2024). HER2/PI3K/AKT pathway in HER2-positive breast cancer A review. Med. (United States) *103*, e38508.

Pance, K., Gramespacher, J.A., Byrnes, J.R., Salangsang, F., Serrano, J.A.C., Cotton, A.D., Steri, V., and Wells, J.A. (2023). Modular cytokine receptor-targeting chimeras for targeted degradation of cell surface and extracellular proteins. Nat. Biotechnol. *41*, 273–281.

Papaleo, E., Saladino, G., Lambrughi, M., Lindorff-Larsen, K., Gervasio, F.L., and Nussinov, R. (2016). The Role of Protein Loops and Linkers in Conformational Dynamics and Allostery. Chem. Rev. *116*, 6391–6423.

Pardridge, W.M. (2016). Re-engineering therapeutic antibodies for Alzheimer's disease as blood-brain barrier penetrating bi-specific antibodies. Expert Opin. Biol. Ther. *16*, 1455–1468.

Park, K., Shen, B.W., Parmeggiani, F., Huang, P.S., Stoddard, B.L., and Baker, D. (2015). Control of repeat-protein curvature by computational protein design. Nat. Struct. Mol. Biol. *22*, 167–174.

Park, S.H., Yin, P., Liu, Y., Reif, J.H., LaBean, T.H., and Yan, H. (2005). Programmable DNA Self-Assemblies for Nanoscale Organization of Ligands and Proteins. Nano Lett. *5*, 729–733.

Patke, S., Li, J., Wang, P., Slaga, D., Johnston, J., Bhakta, S., Panowski, S., Sun, L.L., Junttila, T., Scheer, J.M., et al. (2017). bisFabs: Tools for rapidly screening hybridoma IgGs for their activities as bispecific antibodies. MAbs *9*, 430–437.

Patterson, J.T., Isaacson, J., Kerwin, L., Atassi, G., Duggal, R., Bresson, D., Zhu, T., Zhou, H., Fu, Y., and Kaufmann, G.F. (2017a). PSMA-targeted bispecific Fab conjugates that engage T cells. Bioorganic Med. Chem. Lett. *27*, 5490–5495.

Patterson, J.T., Gros, E., Zhou, H., Atassi, G., Kerwin, L., Carmody, L., Zhu, T., Jones, B., Fu, Y., and Kaufmann, G.F. (2017b). Chemically generated IgG2 bispecific antibodies through disulfide bridging. Bioorganic Med. Chem. Lett. *27*, 3647–3652.

Paulo, J.A., and Schweppe, D.K. (2021). Advances in quantitative high-throughput

phosphoproteomics with sample multiplexing. Proteomics *21*, 139–148.

Pegram, M., Jackisch, C., and Johnston, S.R.D. (2023). Estrogen/HER2 receptor crosstalk in breast cancer: combination therapies to improve outcomes for patients with hormone receptor-positive/HER2-positive breast cancer. Npj Breast Cancer *9*, 45.

Perez, P., Hoffman, R.W., Shaw, S., Bluestone, J.A., and Segal, D.M. (1985). Specific targeting of cytotoxic T cells by anti-T3 linked to anti-target cell antibody. Nature *316*, 354–356.

Pontén, F., Jirström, K., and Uhlen, M. (2008). The Human Protein Atlas - A tool for pathology. J. Pathol. *216*, 387–393.

Qiao, Y., Qiu, Y., Ding, J., Luo, N., Wang, H., Ling, X., Sun, J., Wu, Z., Wang, Y., Liu, Y., et al. (2021). Cancer immune therapy with PD-1-dependent CD137 co-stimulation provides localized tumour killing without systemic toxicity. Nat. Commun. *12*, 1–12.

Rahikainen, R., Rijal, P., Tan, T.K., Wu, H., Andersson, A.C., Barrett, J.R., Bowden, T.A., Draper, S.J., Townsend, A.R., and Howarth, M. (2021). Overcoming Symmetry Mismatch in Vaccine Nanoassembly through Spontaneous Amidation. Angew. Chemie *133*, 325–334.

Rahikainen, R., Vester, S.K., Turkki, P., Janosko, C.P., Deiters, A., Hytönen, V.P., and Howarth, M. (2023). Visible Light-Induced Specific Protein Reaction Delineates Early Stages of Cell Adhesion. J. Am. Chem. Soc. *145*, 24459–24465.

Rajagopal, S., Rajagopal, K., and Lefkowitz, R.J. (2010). Teaching old receptors new tricks: Biasing seven-transmembrane receptors. Nat. Rev. Drug Discov. *9*, 373–386.

Rambo, R.P., and Tainer, J.A. (2011). Characterizing flexible and intrinsically unstructured biological macromolecules by SAS using the Porod-Debye law. Biopolymers *95*, 559–571.

Ramšak, M., Ramirez, D.A., Hough, L.E., Shirts, M.R., Vidmar, S., Eleršič Filipič, K., Anderluh, G., and Jerala, R. (2023). Programmable de novo designed coiled coil-mediated phase separation in mammalian cells. Nat. Commun. *14*, 1–15.

Rasmussen, S.G.F., Devree, B.T., Zou, Y., Kruse, A.C., Chung, K.Y., Kobilka, T.S., Thian, F.S., Chae, P.S., Pardon, E., Calinski, D., et al. (2011). Crystal structure of the β 2 adrenergic receptor-Gs protein complex. Nature *477*, 549–557.

Ren, T., Tan, Z., Ehamparanathan, V., Lewandowski, A., Ghose, S., and Li, Z.J. (2021). Antibody disulfide bond reduction and recovery during biopharmaceutical process development—A review. Biotechnol. Bioeng. *118*, 2829–2844.

Renna, P., Ripoli, C., Dagliyan, O., Pastore, F., Rinaudo, M., Re, A., Paciello, F., and Grassi, C. (2022). Engineering a switchable single-chain TEV protease to control protein maturation in living neurons. Bioeng. Transl. Med. *7*, 1–13.

Reyes-Alcaraz, A., Lee, Y.N., Yun, S., Hwang, J.I., and Seong, J.Y. (2018). Conformational signatures in β-arrestin2 reveal natural biased agonism at a G-protein-coupled receptor. Commun. Biol. *1*, 1–12.

Rhee, K., and Zhou, X. (2024). Two in one: the emerging concept of bifunctional antibodies. Curr. Opin. Biotechnol. *85*, 103050.

Ridgway, J.B.B., Presta, L.G., and Carter, P. (1996). "Knobs-into-holes" engineering of antibody C(H)3 domains for heavy chain heterodimerization. Protein Eng. *9*, 617–621.

Ritter, S.L., and Hall, R.A. (2009). Fine-tuning of GPCR activity by receptor-interacting proteins. Nat. Rev. Mol. Cell Biol. *10*, 819–830.

Ritter, C.A., Perez-Torres, M., Rinehart, C., Guix, M., Dugger, T., Engelman, J.A., and Arteaga, C.L. (2007). Human breast cancer cells selected for resistance to trastuzumab in vivo overexpress epidermal growth factor receptor and ErbB ligands and remain dependent on the ErbB receptor network. Clin. Cancer Res. *13*, 4909–4919.

Romantini, N., Alam, S., Dobitz, S., Spillmann, M., De Foresta, M., Schibli, R., Schertler, G.F.X., Wennemers, H., Deupi, X., Behe, M., et al. (2021). Exploring the signaling space of a GPCR using bivalent ligands with a rigid oligoproline backbone. Proc. Natl. Acad. Sci. U. S. A. *118*.

Romei, M.G., Leonard, B., Katz, Z.B., Le, D., Yang, Y., Day, E.S., Koo, C.W., Sharma, P., Bevers Iii, J., Kim, I., et al. (2024). i-shaped antibody engineering enables conformational tuning of biotherapeutic receptor agonists. Nat. Commun. *15*, 642.

Ropars, V., Yang, Z., Isabet, T., Blanc, F., Zhou, K., Lin, T., Liu, X., Hissier, P., Samazan, F., Amigues, B., et al. (2016). The myosin X motor is optimized for movement on actin bundles. Nat. Commun. *7*, 12456.

Roskoski, R. (2014). The ErbB/HER family of protein-tyrosine kinases and cancer. Pharmacol. Res. *79*, 34–74.

Rossin, R., Verkerk, P.R., Van Den Bosch, S.M., Vulders, R.C.M., Verel, I., Lub, J., and Robillard, M.S. (2010). In vivo chemistry for pretargeted tumor imaging in live mice. Angew. Chemie - Int. Ed. *49*, 3375–3378.

Roux, K.H., Strelets, L., and Michaelsen, T.E. (1997). Flexibility of human IgG subclasses. J. Immunol. *159*, 3372–3382.

Runcie, K., Budman, D.R., John, V., and Seetharamu, N. (2018). Bi-specific and tri-specific antibodies- the next big thing in solid tumor therapeutics. Mol. Med. *24*, 1–15.

Ruskowitz, E.R., Munoz-Robles, B.G., Strange, A.C., Butcher, C.H., Kurniawan, S., Filteau, J.R., and DeForest, C.A. (2023). Spatiotemporal functional assembly of split protein pairs through a light-activated SpyLigation. Nat. Chem. *15*, 694–704.

Sahtoe, D.D., Coscia, A., Mustafaoglu, N., Miller, L.M., Olal, D., Vulovic, I., Yu, T.Y., Goreshnik, I., Lin, Y.R., Clark, L., et al. (2021). Transferrin receptor targeting by de novo sheet extension. Proc. Natl. Acad. Sci. U. S. A. *118*, 1–8.

Salazar-Cavazos, E., Nitta, C.F., Mitra, E.D., Wilson, B.S., Lidke, K.A., Hlavacek, W.S., and Lidke, D.S. (2020). Multisite EGFR phosphorylation is regulated by adaptor protein abundances and dimer lifetimes. Mol. Biol. Cell *31*, 695–708.

Salimi, F., Forouzandeh Moghadam, M., and Rajabibazl, M. (2018). Development of a novel anti-HER2 scFv by ribosome display and in silico evaluation of its 3D structure and interaction with HER2, alone and after fusion to LAMP2B. Mol. Biol. Rep. *45*, 2247–2256.

Samna Soumana, O., Garnier, N., and Genest, M. (2008). Insight into the recognition patterns of the ErbB receptor family transmembrane domains: Heterodimerization models through molecular dynamics search. Eur. Biophys. J. *37*, 851–864.

Sampei, Z., Igawa, T., Soeda, T., Okuyama-Nishida, Y., Moriyama, C., Wakabayashi, T., Tanaka, E., Muto, A., Kojima, T., Kitazawa, T., et al. (2013). Identification and Multidimensional Optimization of an Asymmetric Bispecific IgG Antibody Mimicking the Function of Factor VIII Cofactor Activity. PLoS One *8*.

Sarrion-Perdigones, A., Chang, L., Gonzalez, Y., Gallego-Flores, T., Young, D.W., and Venken, K.J.T. (2019). Examining multiple cellular pathways at once using multiplex

hextuple luciferase assaying. Nat. Commun. *10*.

Sarrion-Perdigones, A., Gonzalez, Y., and Venken, K.J.T. (2020). Rapid and Efficient Synthetic Assembly of Multiplex Luciferase Reporter Plasmids for the Simultaneous Monitoring of Up to Six Cellular Signaling Pathways. Curr. Protoc. Mol. Biol. *131*.

Sauna, Z.E., Lagassé, D., Pedras-Vasconcelos, J., Golding, B., and Rosenberg, A.S. (2018). Evaluating and Mitigating the Immunogenicity of Therapeutic Proteins. Trends Biotechnol. *36*, 1068–1084.

Schaefer, W., Regula, J.T., Bähner, M., Schanzer, J., Croasdale, R., Dürr, H., Gassner, C., Georges, G., Kettenberger, H., Imhof-Jung, S., et al. (2011). Immunoglobulin domain crossover as a generic approach for the production of bispecific IgG antibodies. Proc. Natl. Acad. Sci. U. S. A. *108*, 11187–11192.

Schanzer, J., Jekle, A., Nezu, J., Lochner, A., Croasdale, R., Dioszegi, M., Zhang, J., Hoffmann, E., Dormeyer, W., Stracke, J., et al. (2011). Development of tetravalent, bispecific CCR5 antibodies with antiviral activity against CCR5 monoclonal antibody-resistant HIV-1 strains. Antimicrob. Agents Chemother. *55*, 2369–2378.

Scheck, R.A., Lowder, M.A., Appelbaum, J.S., and Schepartz, A. (2012). Bipartite tetracysteine display reveals allosteric control of ligand-specific EGFR activation. ACS Chem. Biol. *7*, 1367–1376.

Scheer, J.M., Sandoval, W., Elliott, J.M., Shao, L., Luis, E., Lewin-Koh, S.C., Schaefer, G., and Vandlen, R. (2012). Reorienting the Fab Domains of Trastuzumab Results in Potent HER2 Activators. PLoS One *7*, e51817.

Schlessinger, J. (2000). Cell signaling by receptor tyrosine kinases. Cell *103*, 211–225.

Scholl, S., Beuzeboc, P., and Pouillart, P. (2001). Targeting HER2 in other tumor types. Ann. Oncol. *12*, S81–S87.

Schram, A.M., Odintsov, I., Espinosa-Cotton, M., Khodos, I., Sisso, W.J., Mattar, M.S., Lui, A.J.W., Vojnic, M., Shameem, S.H., Chauhan, T., et al. (2022). Zenocutuzumab, a HER2xHER3 Bispecific Antibody, Is Effective Therapy for Tumors Driven by NRG1 Gene Rearrangements. Cancer Discov. *12*, 1233–1247.

Schumacher, F.F., Sanchania, V.A., Tolner, B., Wright, Z.V.F., Ryan, C.P., Smith, M.E.B., Ward, J.M., Caddick, S., Kay, C.W.M., Aeppli, G., et al. (2013). Homogeneous antibody fragment conjugation by disulfide bridging introduces "spinostics." Sci. Rep. *3*, 1–8.

Scott, M.J., Lee, J.A., Wake, M.S., Batt, K. V., Wattam, T.A., Hiles, I.D., Batuwangala, T.D., Ashman, C.I., and Steward, M. (2017). 'In-Format' screening of a novel bispecific antibody format reveals significant potency improvements relative to unformatted molecules. MAbs *9*, 85–93.

Segaliny, A.I., Jayaraman, J., Chen, X., Chong, J., Luxon, R., Fung, A., Fu, Q., Jiang, X., Rivera, R., Ma, X., et al. (2023). A high throughput bispecific antibody discovery pipeline. Commun. Biol. *6*, 380.

Seijsing, J., Sobieraj, A.M., Keller, N., Shen, Y., Zinkernagel, A.S., Loessner, M.J., and Schmelcher, M. (2018). Improved biodistribution and extended serum half-life of a bacteriophage endolysin by albumin binding domain fusion. Front. Microbiol. *9*, 1–9.

Seyedabadi, M., Ghahremani, M.H., and Albert, P.R. (2019). Biased signaling of G protein coupled receptors (GPCRs): Molecular determinants of GPCR/transducer selectivity and therapeutic potential. Pharmacol. Ther. *200*, 148–178.

Shatz, W., Chung, S., Li, B., Marshall, B., Tejada, M., Phung, W., Sandoval, W., Kelley, R.F., and Scheer, J.M. (2013). Knobs-into-holes antibody production in mammalian cell lines reveals that asymmetric afucosylation is sufficient for full antibody-dependent cellular cytotoxicity. MAbs *5*, 872–881.

Shatz, W., Ng, D., Dutina, G., Wong, A.W., Dunshee, D.R., Sonoda, J., Shen, A., and Scheer, J.M. (2016). An efficient route to bispecific antibody production using single-reactor mammalian co-culture. MAbs *8*, 1487–1497.

Shaw, A., Lundin, V., Petrova, E., Fördős, F., Benson, E., Al-Amin, A., Herland, A., Blokzijl, A., Högberg, B., and Teixeira, A.I. (2014). Spatial control of membrane receptor function using ligand nanocalipers. Nat. Methods *11*, 841–846.

Shilts, J., and Wright, G.J. (2024). Mapping the Human Cell Surface Interactome: A Key to Decode Cell-to-Cell Communication. Annu. Rev. Biomed. Data Sci.

Shin, D., Lee, W., Lee, J.H., and Bang, D. (2019a). Multiplexed single-cell RNA-seq via transient barcoding for simultaneous expression profiling of various drug perturbations. Sci. Adv. *5*, 1–10.

Shin, J.W., Kim, S., Ha, S., Choi, B., Kim, S., Im, S.A., Yoon, T.Y., and Chung, J. (2019b). The HER2 S310F mutant can form an active heterodimer with the EGFR, which can be inhibited by cetuximab but not by trastuzumab as well as pertuzumab. Biomolecules *9*, 629.

Siddiqui, S., Cong, W.N., Daimon, C.M., Martin, B., and Maudsley, S. (2013). BRET biosensor analysis of receptor tyrosine kinase functionality. Front. Endocrinol. (Lausanne). *4*, 1–11.

Siepe, D.H., Picton, L.K., and Garcia, K.C. (2023). Receptor Elimination by E3 Ubiquitin Ligase Recruitment (REULR): A Targeted Protein Degradation Toolbox. ACS Synth. Biol. *12*, 1081–1093.

Silacci, M., Baenziger-Tobler, N., Lembke, W., Zha, W., Batey, S., Bertschinger, J., and Grabulovski, D. (2014). Linker length matters, Fynomer-Fc fusion with an optimized linker displaying picomolar IL-17A inhibition potency. J. Biol. Chem. *289*, 14392–14398.

Sinclair, J.K.L., Walker, A.S., Doerner, A.E., and Schepartz, A. (2018). Mechanism of Allosteric Coupling into and through the Plasma Membrane by EGFR. Cell Chem. Biol. *25*, 857-870.e7.

Singh, D.R., Kanvinde, P., King, C., Pasquale, E.B., and Hristova, K. (2018). The EphA2 receptor is activated through induction of distinct, ligand-dependent oligomeric structures. Commun. Biol. *1*, 1–12.

Slamon, D.J., Clark, G.M., Wong, S.G., Levin, W.J., Ullrich, A., and McGuire, W.L. (1987). Human breast cancer: Correlation of relapse and survival with amplification of the HER-2/neu oncogene. Science (80-.). *235*, 182–191.

Smith, K.G.C., and Clatworthy, M.R. (2010). FcγRIIB in autoimmunity and infection: Evolutionary and therapeutic implications. Nat. Rev. Immunol. *10*, 328–343.

Smith, J.S., Lefkowitz, R.J., and Rajagopal, S. (2018). Biased signalling: From simple switches to allosteric microprocessors. Nat. Rev. Drug Discov. *17*, 243–260.

Spiess, C., Merchant, M., Huang, A., Zheng, Z., Yang, N.Y., Peng, J., Ellerman, D., Shatz, W., Reilly, D., Yansura, D.G., et al. (2013). Bispecific antibodies with natural architecture produced by co-culture of bacteria expressing two distinct half-antibodies. Nat. Biotechnol. *31*, 753–758.

Spiess, C., Zhai, Q., and Carter, P.J. (2015). Alternative molecular formats and therapeutic applications for bispecific antibodies. Mol. Immunol. *67*, 95–106.

Steeland, S., Puimège, L., Vandenbroucke, R.E., Van Hauwermeiren, F., Haustraete, J., Devoogdt, N., Hulpiau, P., Leroux-Roels, G., Laukens, D., Meuleman, P., et al. (2015). Generation and characterization of small single domain antibodies inhibiting human tumor necrosis factor receptor 1. J. Biol. Chem. *290*, 4022–4037.

Stüber, J.C., Richter, C.P., Bellón, J.S., Schwill, M., König, I., Schuler, B., Piehler, J., and Plückthun, A. (2021). Apoptosis-inducing anti-HER2 agents operate through oligomerization-induced receptor immobilization. Commun. Biol. *4*, 762.

Stutz, C., and Blein, S. (2020). A single mutation increases heavy-chain heterodimer assembly of bispecific antibodies by inducing structural disorder in one homodimer species. J. Biol. Chem. *295*, 9392–9408.

Sun, L., Shen, F., Qu, Y., and Liu, Z. (2023). Functional DNA as a Molecular Tool in Regulating Immunoreceptor-Ligand Interactions. JACS Au *3*, 1820–1834.

Sun, W., Zhang, H., Xie, W., Ma, L., Dang, Y., Liu, Y., Li, L., Qu, F., and Tan, W. (2024). Development of Integrin-Facilitated Bispecific Aptamer Chimeras for Membrane Protein Degradation. J. Am. Chem. Soc.

Sun, Y., Vandenbriele, C., Kauskot, A., Verhamme, P., Hoylaerts, M.F., and Wright, G.J. (2015). A human platelet receptor protein microarray identifies the high affinity immunoglobulin e receptor subunit α (FcεR1α) as an activating platelet endothelium aggregation receptor 1 (PEAR1) ligand. Mol. Cell. Proteomics *14*, 1265–1274.

Surowka, M., and Klein, C. (2024). A pivotal decade for bispecific antibodies? MAbs *16*, 1–9.

Swanson, C.J., and Sivaramakrishnan, S. (2014). Harnessing the unique structural properties of isolated α-helices. J. Biol. Chem. *289*, 25460–25467.

Sweeney, C., and Carraway, K.L. (2000). Ligand discrimination by ErbB receptors: Differential signaling through differential phosphorylation site usage. Oncogene *19*, 5568–5573.

Sweeney, C., Lai, C., Riese, D.J., Diamonti, A.J., Cantley, L.C., and Carraway, K.L. (2000). Ligand discrimination in signaling through an ErbB4 receptor homodimer. J. Biol. Chem. *275*, 19803–19807.

Syed, R.S., Reid, S.W., Li, C., Cheetham, J.C., Aoki, K.H., Liu, B., Zhan, H., Osslund, T.D., Chirino, A.J., Zhang, J., et al. (1998). Efficiency of signalling through cytokine receptors depends critically on receptor orientation. Nature *395*, 511–516.

Szijj, P., and Chudasama, V. (2021). The renaissance of chemically generated bispecific antibodies. Nat. Rev. Chem. *5*, 78–92.

Szijj, P.A., Bahou, C., and Chudasama, V. (2018). Minireview: Addressing the retro-Michael instability of maleimide bioconjugates. Drug Discov. Today Technol. *30*, 27–34.

Szijj, P.A., Gray, M.A., Ribi, M.K., Bahou, C., Nogueira, J.C.F., Bertozzi, C.R., and Chudasama, V. (2023). Chemical generation of checkpoint inhibitory T cell engagers for the treatment of cancer. Nat. Chem. *15*, 1636–1647.

de Taeye, S.W., Rispens, T., and Vidarsson, G. (2019). The ligands for human igG and their effector functions. Antibodies *8*, 30.

Tamaskovic, R., Schwill, M., Nagy-Davidescu, G., Jost, C., Schaefer, D.C., Verdurmen, W.P.R., Schaefer, J. V., Honegger, A., and Plückthun, A. (2016). Intermolecular biparatopic trapping of ErbB2 prevents compensatory activation of PI3K/AKT via RAS-p110 crosstalk. Nat. Commun. *7*, 1–18.

Tao, R.H., and Maruyama, I.N. (2008). All EGF(ErbB) receptors have preformed homo- and heterodimeric structures in living cells. J. Cell Sci. *121*, 3207–3217.

Thirumalai, D., Hyeon, C., Zhuravlev, P.I., and Lorimer, G.H. (2019). Symmetry, Rigidity, and Allosteric Signaling: From Monomeric Proteins to Molecular Machines. Chem. Rev. *119*, 6788–6821.

Thom, G., Hatcher, J., Hearn, A., Paterson, J., Rodrigo, N., Beljean, A., Gurrell, I., and Webster, C. (2018). Isolation of blood-brain barrier-crossing antibodies from a phage display library by competitive elution and their ability to penetrate the central nervous system. MAbs *10*, 304–314.

Thomas, B.J., Porciani, D., and Burke, D.H. (2022). Cancer immunomodulation using bispecific aptamers. Mol. Ther. Nucleic Acids *27*, 894–915.

Thoreau, F., and Chudasama, V. (2022). Enabling the next steps in cancer immunotherapy: from antibody-based bispecifics to multispecifics, with an evolving role for bioconjugation chemistry. RSC Chem. Biol. *3*, 140–169.

Thoreau, F., Szijj, P.A., Greene, M.K., Rochet, L.N.C., Thanasi, I.A., Blayney, J.K., Maruani, A., Baker, J.R., Scott, C.J., and Chudasama, V. (2023). Modular Chemical Construction of IgG-like Mono- and Bispecific Synthetic Antibodies (SynAbs). ACS Cent. Sci. *9*, 476–487.

Trkulja, C.L., Jungholm, O., Davidson, M., Jardemark, K., Marcus, M.M., Hägglund, J., Karlsson, A., Karlsson, R., Bruton, J., Ivarsson, N., et al. (2021). Rational antibody design for undruggable targets using kinetically controlled biomolecular probes. Sci. Adv. *7*, 1–15.

Trowbridge, I.S., and Thomas, M.L. (1994). CD45: An emerging role as a protein tyrosine phosphatase required for lymphocyte activation and development. Annu. Rev. Immunol. *12*, 85–116.

Turecek, P.L., Bossard, M.J., Schoetens, F., and Ivens, I.A. (2016). PEGylation of Biopharmaceuticals: A Review of Chemistry and Nonclinical Safety Information of Approved Drugs. J. Pharm. Sci. *105*, 460–475.

Tzahar, E., Waterman, H., Chen, X., Levkowitz, G., Karunagaran, D., Lavi, S., Ratzkin, B.J., and Yarden, Y. (1996). A Hierarchical Network of Interreceptor Interactions Determines Signal Transduction by Neu Differentiation Factor/Neuregulin and Epidermal Growth Factor. Mol. Cell. Biol. *16*, 5276–5287.

Ueda, A., Umetsu, M., Nakanishi, T., Hashikami, K., Nakazawa, H., Hattori, S., Asano, R., and Kumagai, I. (2020). Chemically crosslinked bispecific antibodies for cancer therapy: Breaking from the structural restrictions of the genetic fusion approach. Int. J. Mol. Sci. *21*, 711.

Uhlen, M., Zhang, C., Lee, S., Sjöstedt, E., Fagerberg, L., Bidkhori, G., Benfeitas, R., Arif, M., Liu, Z., Edfors, F., et al. (2017). A pathology atlas of the human cancer transcriptome. Science (80-.). *357*.

Ullrich, T., Pollmann, C., Ritter, M., Haaf, J., Aghaallaei, N., Tesakov, I., El-Riz, M., Maksymenko, K., Hatskovska, V., Kandabarau, S., et al. (2023). Tuning of granulopoietic

signaling by de novo designed agonists. BioRxiv 2023.11.25.568662.

Vaneycken, I., Devoogdt, N., Van Gassen, N., Vincke, C., Xavier, C., Wernery, U., Muyldermans, S., Lahoutte, T., and Caveliers, V. (2011). Preclinical screening of anti-HER2 nanobodies for molecular imaging of breast cancer. FASEB J. *25*, 2433–2446.

Vazquez-Lombardi, R., Phan, T.G., Zimmermann, C., Lowe, D., Jermutus, L., and Christ, D. (2015). Challenges and opportunities for non-antibody scaffold drugs. Drug Discov. Today *20*, 1271–1283.

Veggiani, G., Nakamura, T., Brenner, M.D., Gayet, R. V., Yan, J., Robinson, C. V., and Howarth, M. (2016). Programmable polyproteams built using twin peptide superglues. Proc. Natl. Acad. Sci. U. S. A. *113*, 1202–1207.

Verheije, H., Kijanka, M., Henegouwen, P.V.B.E., and Rottier, P. (2013). Bi-specific adapters. International Patent No. WO2013135655A1.

Veri, M.C., Burke, S., Huang, L., Li, H., Gorlatov, S., Tuaillon, N., Rainey, G.J., Ciccarone, V., Zhang, T., Shah, K., et al. (2010). Therapeutic control of B cell activation via recruitment of Fcγ receptor IIb (CD32B) inhibitory function with a novel bispecific antibody scaffold. Arthritis Rheum. *62*, 1933–1943.

Vester, S.K., Rahikainen, R., Khairil Anuar, I.N.A., Hills, R.A., Tan, T.K., and Howarth, M. (2022). SpySwitch enables pH- or heat-responsive capture and release for plug-and-display nanoassembly. Nat. Commun. *13*, 3714.

Vijayaraghavan, S., Lipfert, L., Chevalier, K., Bushey, B.S., Henley, B., Lenhart, R., Sendecki, J., Beqiri, M., Millar, H.J., Packman, K., et al. (2020). Amivantamab (JNJ-61186372), an Fc enhanced EGFR/cMet bispecific antibody, induces receptor downmodulation and antitumor activity by monocyte/macrophage trogocytosis. Mol. Cancer Ther. *19*, 2044–2056.

Vita, R., Overton, J.A., Greenbaum, J.A., Ponomarenko, J., Clark, J.D., Cantrell, J.R., Wheeler, D.K., Gabbard, J.L., Hix, D., Sette, A., et al. (2015). The immune epitope database (IEDB) 3.0. Nucleic Acids Res. *43*, D405–D412.

Walsh, S.J., Bargh, J.D., Dannheim, F.M., Hanby, A.R., Seki, H., Counsell, A.J., Ou, X., Fowler, E., Ashman, N., Takada, Y., et al. (2021). Site-selective modification strategies in antibody-drug conjugates. Chem. Soc. Rev. *50*, 1305–1353.

Wang, L., Liang, H., Sun, J., Liu, Y., Li, J., Li, J., Li, J., and Yang, H. (2019a). Bispecific Aptamer Induced Artificial Protein-Pairing: A Strategy for Selective Inhibition of Receptor Function. J. Am. Chem. Soc. *141*, 12673–12681.

Wang, M., Yang, D., Lu, Q., Liu, L., Cai, Z., Wang, Y., Wang, H.H., Wang, P., and Nie, Z. (2022). Spatially Reprogramed Receptor Organization to Switch Cell Behavior Using a DNA Origami-Templated Aptamer Nanoarray. Nano Lett. *22*, 8445–8454.

Wang, Q., Chen, Y., Park, J., Liu, X., Hu, Y., Wang, T., McFarland, K., and Betenbaugh, M.J. (2019b). Design and production of bispecific antibodies. Antibodies *8*, 43.

Wang, X., Mathieu, M., and Brezski, R.J. (2018). IgG Fc engineering to modulate antibody effector functions. Protein Cell *9*, 63–73.

Wang, Y., Prosen, D.E., Mei, L., Sullivan, J.C., Finney, M., and Vander Horn, P.B. (2004). A novel strategy to engineer DNA polymerases for enhanced processivity and improved performance in vitro. Nucleic Acids Res. *32*, 1197–1207.

Wang, Y., Xiong, Y., Song, L., He, S., Yao, F., Wu, Y., Shi, K., and He, L. (2023). Spatial

Control of Receptor Dimerization Using Programmable DNA Nanobridge. Biomacromolecules *24*, 3228–3236.

Warchal, S.J., Dawson, J.C., Shepherd, E., Munro, A.F., Hughes, R.E., Makda, A., and Carragher, N.O. (2020). High content phenotypic screening identifies serotonin receptor modulators with selective activity upon breast cancer cell cycle and cytokine signaling pathways. Bioorganic Med. Chem. *28*, 115209.

Wec, A.Z., Nyakatura, E.K., Herbert, A.S., Howell, K.A., Holtsberg, F.W., Bakken, R.R., Mittler, E., Christin, J.R., Shulenin, S., Jangra, R.K., et al. (2016). A "Trojan horse" bispecific-antibody strategy for broad protection against ebolaviruses. Science (80-.). *354*, 350–354.

Westerfield, J.M., and Barrera, F.N. (2020). Membrane receptor activation mechanisms and transmembrane peptide tools to elucidate them. J. Biol. Chem. *295*, 1792–1814.

White, A.L., Chan, H.T.C., French, R.R., Willoughby, J., Mockridge, C.I., Roghanian, A., Penfold, C.A., Booth, S.G., Dodhy, A., Polak, M.E., et al. (2015). Conformation of the human immunoglobulin G2 hinge imparts superagonistic properties to immunostimulatory anticancer antibodies. Cancer Cell *27*, 138–148.

Whiteaker, J.R., Sharma, K., Hoffman, M.A., Kuhn, E., Zhao, L., Cocco, A.R., Schoenherr, R.M., Kennedy, J.J., Voytovich, U., Lin, C., et al. (2021). Targeted mass-spectrometry-based assays enable multiplex quantification of receptor tyrosine kinase, MAP kinase, and AKT signaling. Cell Reports Methods *1*, 100015.

Whitlow, M., Bell, B.A., Feng, S.L., Filpula, D., Hardman, K.D., Hubert, S.L., Rollence, M.L., Wood, J.F., Schott, M.E., Milenic, D.E., et al. (1993). An improved linker for single-chain fv with reduced aggregation and enhanced proteolytic stability. Protein Eng. Des. Sel. *6*, 989–995.

Wilkins, M.R., Gasteiger, E., Bairoch, A., Sanchez, J.C., Williams, K.L., Appel, R.D., and Hochstrasser, D.F. (1999). Protein identification and analysis tools in the ExPASy server. Methods Mol. Biol. *112*, 531–552.

Wilson, K.J., Gilmore, J.L., Foley, J., Lemmon, M.A., and Riese, D.J. (2009). Functional selectivity of EGF family peptide growth factors: Implications for cancer. Pharmacol. Ther. *122*, 1–8.

Wolf, E., Hofmeister, R., Kufer, P., Schlereth, B., and Baeuerle, P.A. (2005). BiTEs: Bispecific antibody constructs with unique anti-tumor activity. Drug Discov. Today *10*, 1237–1244.

Wu, D., and Piszczek, G. (2020). Measuring the affinity of protein-protein interactions on a single-molecule level by mass photometry. Anal. Biochem. *592*, 113575.

Wu, D., and Piszczek, G. (2021). Standard protocol for mass photometry experiments. Eur. Biophys. J. *50*, 403–409.

Wu, F., Song, G., de Graaf, C., and Stevens, R.C. (2017a). Structure and Function of Peptide-Binding G Protein-Coupled Receptors. J. Mol. Biol. *429*, 2726–2745.

Wu, K., Bai, H., Chang, Y.T., Redler, R., McNally, K.E., Sheffler, W., Brunette, T.J., Hicks, D.R., Morgan, T.E., Stevens, T.J., et al. (2023). De novo design of modular peptide-binding proteins by superhelical matching. Nature *616*, 581–589.

Wu, W.H., Wei, J., and Zhang, W. Bin (2018). Controlling SpyTag/SpyCatcher Reactivity via Redox-Gated Conformational Restriction. ACS Macro Lett. *7*, 1388–1393.

Wu, X., Sereno, A.J., Huang, F., Zhang, K., Batt, M., Fitchett, J.R., He, D., Rick, H.L., Conner, E.M., and Demarest, S.J. (2015). Protein design of IgG/TCR chimeras for the co-expression of Fab-like moieties within bispecific antibodies. MAbs *7*, 364–376.

Wu, Y., Batyuk, A., Honegger, A., Brandl, F., Mittl, P.R.E., and Plückthun, A. (2017b). Rigidly connected multispecific artificial binders with adjustable geometries. Sci. Rep. *7*, 1–11.

Yachnin, B.J., Mulligan, V.K., Khare, S.D., and Bailey-Kellogg, C. (2021). MHCEpitopeEnergy, a Flexible Rosetta-Based Biotherapeutic Deimmunization Platform. J. Chem. Inf. Model. *61*, 2368–2382.

Yang, D., Zhou, Q., Labroska, V., Qin, S., Darbalaei, S., Wu, Y., Yuliantie, E., Xie, L., Tao, H., Cheng, J., et al. (2021a). G protein-coupled receptors: structure- and function-based drug discovery. Signal Transduct. Target. Ther. *6*.

Yang, L., Miao, Y., and Han, D. (2020). DNA Nanotechnology on Live Cell Membranes. Chem. Res. Chinese Univ. *36*, 203–210.

Yang, X., Zhao, L., Wang, Y., Ji, Y., Su, X.C., Ma, J.A., and Xuan, W. (2023). Constructing Photoactivatable Protein with Genetically Encoded Photocaged Glutamic Acid. Angew. Chemie - Int. Ed. *62*.

Yang, Y., Sanders, A.J., Dou, Q.P., Jiang, D.G., Li, A.X., and Jiang, W.G. (2021b). The Clinical and Theranostic Values of Activated Leukocyte Cell Adhesion Molecule (ALCAM)/CD166 in Human Solid Cancers. Cancers (Basel). *13*, 5187.

Yarden, Y., and Pines, G. (2012). The ERBB network: At last, cancer therapy meets systems biology. Nat. Rev. Cancer *12*, 553–563.

Yarden, Y., and Schlessinger, J. (1987). Epidermal Growth Factor Induces Rapid, Reversible Aggregation of the Purified Epidermal Growth Factor Receptor. Biochemistry *26*, 1443–1451.

Yarden, Y., and Sliwkowski, M.X. (2001). Untangling the ErbB signalling network. Nat. Rev. Mol. Cell Biol. *2*, 127–137.

Yen, M., Ren, J., Liu, Q., Glassman, C.R., Sheahan, T.P., Picton, L.K., Moreira, F.R., Rustagi, A., Jude, K.M., Zhao, X., et al. (2022). Facile discovery of surrogate cytokine agonists. Cell *185*, 1414-1430.e19.

Young, G., Hundt, N., Cole, D., Fineberg, A., Andrecka, J., Tyler, A., Olerinyova, A., Ansari, A., Marklund, E.G., Collier, M.P., et al. (2018). Quantitative mass imaging of single biological macromolecules. Science (80-.). *360*, 423–427.

Yu, X., Chan, H.T.C., Orr, C.M., Dadas, O., Booth, S.G., Dahal, L.N., Penfold, C.A., O'Brien, L., Mockridge, C.I., French, R.R., et al. (2018). Complex Interplay between Epitope Specificity and Isotype Dictates the Biological Activity of Anti-human CD40 Antibodies. Cancer Cell *33*, 664-675.e4.

Yu, X., Chan, H.T.C., Fisher, H., Penfold, C.A., Kim, J., Inzhelevskaya, T., Mockridge, C.I., French, R.R., Duriez, P.J., Douglas, L.R., et al. (2020). Isotype Switching Converts Anti-CD40 Antagonism to Agonism to Elicit Potent Antitumor Activity. Cancer Cell *37*, 850-866.e7.

Yu, X., Orr, C.M., Chan, H.T.C., James, S., Penfold, C.A., Kim, J., Inzhelevskaya, T., Mockridge, C.I., Cox, K.L., Essex, J.W., et al. (2023). Reducing affinity as a strategy to boost immunomodulatory antibody agonism. Nature *614*, 539–547.

Yu, Y.J., Zhang, Y., Kenrick, M., Hoyte, K., Luk, W., Lu, Y., Atwal, J., Elliott, J.M., Prabhu, S., Watts, R.J., et al. (2011). Boosting brain uptake of a therapeutic antibody by reducing its affinity for a transcytosis target. Sci. Transl. Med. *3*, 1–8.

Yumura, K., Akiba, H., Nagatoishi, S., Kusano-Arai, O., Iwanari, H., Hamakubo, T., and Tsumoto, K. (2017). Use of SpyTag/SpyCatcher to construct bispecific antibodies that target two epitopes of a single antigen. J. Biochem. *162*, 203–210.

Yunn, N.O., Kim, J., Ryu, S.H., and Cho, Y. (2023). A stepwise activation model for the insulin receptor. Exp. Mol. Med. *55*, 2147–2161.

Zakeri, B., Fierer, J.O., Celik, E., Chittock, E.C., Schwarz-Linek, U., Moy, V.T., and Howarth, M. (2012). Peptide tag forming a rapid covalent bond to a protein, through engineering a bacterial adhesin. Proc. Natl. Acad. Sci. U. S. A. *109*.

Zhang, Y. (2021). The root cause of drug resistance in HER2-positive breast cancer and the therapeutic approaches to overcoming the resistance. Pharmacol. Ther. *218*, 107677.

Zhang, D., Duque-Jimenez, J., Facchinetti, F., Brixi, G., Rhee, K., Feng, W.W., Jänne, P.A., and Zhou, X. (2024a). Transferrin receptor targeting chimeras for membrane protein degradation. Nature *2023*, 2023.08.10.552782.

Zhang, J.Z., Li, X., Liu, C., Jiang, H., Wu, K., and Baker, D. (2024b). De novo design of Ras isoform selective binders. BioRxiv 2024.08.29.610300.

Zhang, X., Gureasko, J., Shen, K., Cole, P.A., and Kuriyan, J. (2006). An Allosteric Mechanism for Activation of the Kinase Domain of Epidermal Growth Factor Receptor. Cell *125*, 1137–1149.

Zhang, X., Zhang, L., Tong, H., Peng, B., Rames, M.J., Zhang, S., and Ren, G. (2015). 3D Structural Fluctuation of IgG1 Antibody Revealed by Individual Particle Electron Tomography. Sci. Rep. *5*, 1–13.

Zhang, X., Yang, Y., Fan, D., and Xiong, D. (2017). The development of bispecific antibodies and their applications in tumor immune escape. Exp. Hematol. Oncol. *6*, 1–6.

Zhao, J., Mohan, N., Nussinov, R., Ma, B., and Wu, W.J. (2021). Trastuzumab blocks the receiver function of HER2 leading to the population shifts of HER2-containing homodimers and heterodimers. Antibodies *10*, 1–14.

Zheng, J., He, W., Li, J., Feng, X., Li, Y., Cheng, B., Zhou, Y., Li, M., Liu, K., Shao, X., et al. (2022). Bifunctional Compounds as Molecular Degraders for Integrin-Facilitated Targeted Protein Degradation. J. Am. Chem. Soc. *144*, 21831–21836.

Zheng, Y., Han, G.W., Abagyan, R., Wu, B., Stevens, R.C., Cherezov, V., Kufareva, I., and Handel, T.M. (2017). Structure of CC Chemokine Receptor 5 with a Potent Chemokine Antagonist Reveals Mechanisms of Chemokine Recognition and Molecular Mimicry by HIV. Immunity *46*, 1005-1017.e5.

Zhong, B., Su, X., Wen, M., Zuo, S., Hong, L., and Lin, J. (2022). ParaFold: Paralleling AlphaFold for Large-Scale Predictions. In ACM International Conference Proceeding Series, (New York, NY, USA: ACM), pp. 1–9.

Zhu, C., Wang, W., Wang, Y., Zhang, Y., and Li, J. (2023). Dendronized DNA Chimeras Harness Scavenger Receptors To Degrade Cell Membrane Proteins. Angew. Chemie - Int. Ed. *62*.

Zizzari, I.G., Veglia, F., Taurino, F., Rahimi, H., Quaglino, E., Belleudi, F., Riccardo, F., Antonilli, M., Napoletano, C., Bellati, F., et al. (2011). HER2-based recombinant immunogen

to target DCs through FcγRs for cancer immunotherapy. J. Mol. Med. *89*, 1231–1240.

Zografou-Barredo, N.A., Hallatt, A.J., Goujon-Ricci, J., and Cano, C. (2023). A beginner's guide to current synthetic linker strategies towards VHL-recruiting PROTACs. Bioorganic Med. Chem. *88–89*.

Zoine, J.T., Immadisetty, K., Ibanez-Vega, J., Moore, S.E., Nevitt, C., Thanekar, U., Tian, L., Karouni, A., Chockley, P.J., Arthur, B., et al. (2024). Peptide-scFv antigen recognition domains effectively confer CAR T cell multiantigen specificity. Cell Reports Med. *5*, 101422.